

Electronic Theses and Dissertations, 2004-2019

2014

Uncertainty treatment in performance based seismic assessment of typical bridge classes in United States

Mohammad Mehdizadeh
University of Central Florida

 Part of the [Civil Engineering Commons](#)
Find similar works at: <https://stars.library.ucf.edu/etd>
University of Central Florida Libraries <http://library.ucf.edu>

This Doctoral Dissertation (Open Access) is brought to you for free and open access by STARS. It has been accepted for inclusion in Electronic Theses and Dissertations, 2004-2019 by an authorized administrator of STARS. For more information, please contact STARS@ucf.edu.

STARS Citation

Mehdizadeh, Mohammad, "Uncertainty treatment in performance based seismic assessment of typical bridge classes in United States" (2014). *Electronic Theses and Dissertations, 2004-2019*. 4760.
<https://stars.library.ucf.edu/etd/4760>

UNCERTAINTY TREATMENT IN PERFORMANCE BASED SEISMIC ASSESSMENT OF
TYPICAL BRIDGE CLASSES IN UNITED STATES

by

MOHAMMAD MEHDIZADEH
B.S. Sharif University of Technology 2007
M.S. Sharif University of Technology 2010

A dissertation submitted in partial fulfilment of the requirements
for the degree of Doctor of Philosophy
in the Department of Civil, Environmental, and Construction Engineering
in the College of Engineering and Computer Science
at the University of Central Florida
Orlando, Florida

Spring Term
2014

Major Professor: Kevin Mackie

© 2014 Mohammad Mehdizadeh

ABSTRACT

Bridge networks are expensive and complex infrastructures and are essential components of today's transportation systems. Despite the advancement in computer aided modeling and increasing the computational power which is increasing the accessibility for developing the fragility curves of bridges, the complexity of the problem and uncertainties involved in fragility analysis of the bridge structures in addition to difficulties in validating the results obtained from the analysis requires precaution in utilization of the results as a decision making tool. The main focus of this research is to address, study and treatment of uncertainties incorporated in various steps of performance based assessments (PBA) of the bridge structures. In this research the uncertainties is divided into three main categories. First, the uncertainties that come from ground motions time and frequency content alteration because of scarcity of the recorded ground motions in the database. Second, uncertainties associated in the modeling and simulation procedure of PBA, and third uncertainties originated from simplistic approach and methods utilized in the conventional procedure of PBA of the structures. Legitimacy of the scaling of ground motions is studied using the response of several simple nonlinear systems to amplitude scaled ground motions suites. Bias in the response obtained compared to unscaled records for both as recorded and synthetic ground motions. Results from this section of the research show the amount of the bias is considerable and can significantly affect the outcome of PBA. The origin of the bias is investigated and consequently a new metric is proposed to predict the bias induced by ground motion scaling without nonlinear analysis. Results demonstrate that utilizing the predictor as a scaling parameter can significantly reduce the bias for various nonlinear structures. Therefore utilizing the new metric as the intensity measuring parameter of the ground motions is recommended in PBA. To address the uncertainties associated in the modeling and simulation, MSSS concrete girder bridge class were selected due to the frequency of the construction in USCS region and lack of seismic detailing. A large scale pa-

parameters screening study is performed using Plackett-Burman experimental design that considers a more complete group of parameters to decrease the computational expense of probabilistic study of the structures seismic response. Fragility analysis for MSSS bridge is performed and the effect of removing the lesser important parameters the probabilistic demand model was investigated. This study reveals parameters reduction based on screening study techniques can be utilized to increase efficiency in fragility analysis procedure without compromising the accuracy of the outcome. The results from this study also provides more direct information on parameter reduction for PBA as well as provide insight into where future investments into higher fidelity finite element and constitutive models should be targeted. Conventional simplistic PBA approach does not account for the fundamental correlation between demand and capacity models. A more comprehensive PBA approach is presented and fragility analysis is performed with implementation of a new formulation in the component fragility analysis for MSSS bridge class and the outcome is compared with the one from conventional procedure. The results shows the correlation between demand and capacity affects the outcome of PBA and the fragility functions variation is not negligible. Therefore using the presented approach is necessary when accuracy is needed.

This thesis is dedicated to my parents , Mina and Ali whom without their support this thesis could not have been written

ACKNOWLEDGMENTS

First and foremost, I would like to express my immense gratitude to my advisor Dr. Kevin Mackie for his continuous help, encouragement, and support. He has always been an excellent advisor and teacher which have been my influencer through all 4 years of Ph.D. program. I always admire his knowledge and appreciate his effort and guidance to achieve the objectives of the presented work. This dissertation would never have been made possible without him. I also would like to thank to Dr. Bryant Nielson whom was a tremendous help for essential part of this thesis. I would like to extend my gratitude to my Ph.D. committee members, DR. Necati Catbas, Yun Hae-Bum and Dr. Petros Xanthopoulo for their contributions, valuable suggestions and advices to improve the quality of the work. I am immensely grateful to my parents, Ali Mehdizadeh and Mina Tahmasbizadeh and my beloved sisters, Poroshat, who have always been a great source of motivation and support in every minute of my life. I would also like to take this opportunity to thank all of my friends especially Masoud Malekzadeh, Marzieh Ghasemi, Soroush Mokhtari, Amir Zavichi and Mehdi Noori for their sincere friendship and help during the past years.

TABLE OF CONTENTS

LIST OF FIGURES	xiii
LIST OF TABLES	xx
CHAPTER 1: INTRODUCTION	1
1.1 Performance based design and performance-based assessments	1
1.2 Uncertainty associated with performance-based assessment	4
1.3 Statement of the problem	4
1.4 Objective Statement	6
1.5 Research plan	8
CHAPTER 2: BACKGROUND STUDY	11
2.1 PBEE methodologies from code perspective	11
2.2 The Pacific Earthquake Engineering Methodology	12
2.2.1 Hazard analysis	14
2.2.2 Demand Model	15
2.2.3 Damage Model	16

2.2.4	Decision Model	17
2.3	Ground motion in central and eastern United States	17
2.3.1	Western United States earthquakes	18
2.3.2	Central and southern United States earthquakes	21
2.4	Synthetic ground motions	23
2.5	Ground motion scaling bias	24
2.6	Bridge inventory in Central, Southern and California states	25
2.6.1	CSUS State bridge classes	25
2.6.2	California State bridge classes	26
2.7	Performance-based design and performance-based assessments for highway bridges	31
2.7.1	Elastic Spectral Response	35
2.7.2	Non-Linear Static Analysis	35
2.7.3	N2 method	36
2.7.4	Non-Linear Time History Analysis	38
2.8	Uncertainty associated with performance-based assessment	39
 CHAPTER 3: SELECTION AND SCALING OF GROUND MOTIONS		 41
3.1	Introduction	41

3.1.1	Selection and scaling of ground motions	42
3.2	Method	45
3.2.1	Selection of ground motions	46
3.2.2	Nonlinear structural systems defined	49
3.2.3	General method for identification of bias in scaling	53
3.2.4	Spectrum matching and Average Spectral displacement method	55
3.3	Results	57
3.3.1	Bias ratio based on recorded ground motions	57
3.3.2	Spectrum matched records	61
3.3.3	Bias estimation based on SDI	62
3.3.4	Unbiased record selection methodology	65
3.3.5	Relation between SDI and velocity intensity parameters	68
3.3.6	Comparison between scaling based on SDI with existing scaling procedures	70
3.3.7	Bias ratio based on binning from synthetic earthquakes	71
3.4	Effect of bias on fragility analysis	73
3.5	Closure	76

CHAPTER 4: PARAMETER SCREENING FOR PERFORMANCE BASED ASSESSMENT

	ANALYSIS OF HIGHWAY BRIDGES	80
4.1	Introduction	80
4.2	Methodology	88
4.2.1	Selection of the bridge structure	89
4.2.2	Configuration of multi-span simply supported concrete girder bridge.	91
4.2.3	Nonlinear properties of MSSS Concrete Girder Bridge	93
4.2.3.1	Deck elements	94
4.2.3.2	Multi-column bent caps	95
4.2.3.3	Abutments	98
4.2.3.4	Impact elements	101
4.2.3.5	Fixed and expansion elastomeric bearing	103
4.2.3.6	Foundation	105
4.2.4	parameter screening analysis of the bridge structure	108
4.2.5	Selection of ground motions for screening study	112
4.2.6	Plackett-Burman design	116
4.2.7	ANOVA table and computation of p-values	118
4.2.8	Effect of the parameters screening on fragility analysis	120

4.3	Results	125
4.3.1	Parameters screening of the MSSS bridge seismic response	125
4.3.2	Fragility analysis of MSSS Bridge using parameters screening results . . .	141
4.4	Closure	153
CHAPTER 5: UNCERTAINTY TREATMENT FOR COMPONENT BRIDGE ELEMENTS		
	154
5.1	Introduction	154
5.2	Methodology	154
5.2.1	Uncertainty treatment of the fragility analysis	154
5.2.2	Description of the capacity model	161
5.2.3	Component fragility analysis of the MSSS concrete bridge column	162
5.3	Results	167
CHAPTER 6: CONCLUSIONS AND FUTURE WORKS		
6.1	Conclusions	174
6.2	Future works	181
APPENDIX A: ANOVA TABLES FOR DESIGN OF EXPERIMENT		
		183

APPENDIX B: VARIATION OF MSSS CONCRETE BRIDGE MONITORED PARAMETERS EFFECT WITH RESPECT TO GROUND MOTION INTENSITY	194
APPENDIX C: PDSM MODELS FOR MSSS CONCRETE BRIDGE COMPONENTS	204
APPENDIX D: FRAGILITY RESULTS OF MSSS CONCRETE GIRDER BRIDGE	213
APPENDIX E: EPISTEMIC UNCERTAINTY BOUNDS OF FRAGILITY FOR MSSS CONCRETE GIRDER BRIDGE	222
APPENDIX F: MEASUREMENT OF STATISTICAL SIGNIFICANTS OF NUMBER OF SAMPLES FOR DEMAND MODEL PARAMETERS	227
LIST OF REFERENCES	232

LIST OF FIGURES

1.1	Performance-based design diagram	3
2.1	Illustration of PEER framework	13
2.2	US seismic hazard as (PGA) with 10% probability of exceedence in 50 years (USGS website 2012 [44])	18
2.3	names of major fault systems in California State with slip rates greater than about 5 mm/yr (California Geological Survey 2012) [45]	20
2.4	Comparison of Attenuation Distances of Several Earthquakes in the Eastern and Western United States (USGS, 2002) [46]	23
2.5	Straight Cast-In-Place Post-Tensioned Box Girder, (Ketchum et al. (2004)) [31]	29
2.6	Straight Precast Pre-tensioned I Girder typical bridge. (Ketchum et al. (2004)) [31]	30
2.7	Fragility curves example (Nielson 2005) [30]	32
2.8	Pushover analysis (dash line) and equivalent SDOF force-displacement prop- erties. D_t and V are top floor deformation and shear at ground level for the MDOF structure, D^* and F_y^* are displacement and yielding displacement for SDOF equivalent system. (Peter Fajfar (2000) [56])	37

2.9	Elastic and inelastic demand for equivalent SDOF system versus capacity of the SDOF system. (Peter Fajfar (2000) [56])	37
2.10	Analytical Fragility Curve Generation (Nielson 2005 [30])	39
3.1	Properties of recorded ground motion record suite	47
3.2	Mean and mean $\pm\sigma$ displacement response spectrum	48
3.3	Nonlinear SDOF system behaviors	50
3.4	Percentage of ground motions inducing yielding observed for SDOF system with $F_y = 0.2 N$	51
3.5	Pushover curve of MDOF frame	52
3.6	Spectrum matched mean spectra for scaled bin one and un-scaled bin two, based on PGA binning	56
3.7	Relevance of SDI in capturing response of softening nonlinear systems	57
3.8	Computed bias ratio for the elasto-plastic system	58
3.9	Bias in bilinear system with 20% hardening based on Sd	60
3.10	Bias for frame based on CAV and Sd	61
3.11	Bias values using spectrum compatible bins	62
3.12	Computation of pseudo-bias values using linear spectral analysis only	64
3.13	Bias when binning based on SDI	66

3.14	Bias ratio for elasto-plastic systems using established scaling techniques . . .	71
3.15	Bias ratios for elasto-plastic system using synthetic ground motions.	72
3.16	Bias for elasto-plastic system for synthetic motions binned on SDI	73
3.17	Fragility estimate comparisons for a simple frame	75
4.1	MSSS Concrete Girder Bridge Configuration	92
4.2	Reinforcing layouts for concrete beam and bent cap	93
4.3	Reinforcing layouts for concrete beam and bent cap	94
4.4	schematic discretization of the multi-column bent cap	96
4.5	Abutment behavior in longitudinal direction	98
4.6	Nonlinear properties of the abutment in longitudinal direction	100
4.7	Nonlinear properties of the abutment in transverse direction	101
4.8	Modeling of impact elements for pounding between bridge deck elements . .	102
4.9	Analytical model of Impact between decks (Muthukumar, 2003)	102
4.10	Typical hysteretic behavior of impact element between decks	103
4.11	Typical nonlinear properties of the fixed elastomeric bearing	105
4.12	Typical nonlinear properties of the expansion elastomeric bearing.	106
4.13	Schematic and model properties view of the MSSS bridge deep foundation . .	107

4.14	MSSS bridge deep foundation unit layout	107
4.15	Typical horizontal behavior of nonlinear stiffness of deep foundation	108
4.16	Relationship between R_{rup} and Moment magnitude for the selected pairs of ground motions	115
4.17	Relationship between V_{S30} and Moment magnitude for the selected pairs of ground motions	115
4.18	Schematic uncertainty bounds of fragility curve	125
4.19	Variation of structure monitored responses versus SDI intensity of the earthquake in log-space	128
4.20	Effect of screening design parameters on abutments in longitudinal passive direction (in)	140
4.21	Bridge PSDMs for bridge columns curvature ductility	148
4.22	Variation of the demand model parameters to the number of samples	150
4.23	Fragility bounds of uncertainty of case2 and case 3	152
5.1	Effect of correlation between demand and capacity on the fragility curve	157
5.2	Schematic description of the two layers sampling technique for fragility analysis	160
5.3	Correlation elimination from the bar buckling model's dispersion	171
5.4	Variation of the demand and capacity model for different clusters in multi layers sampling	172

5.5	Improved fragility analysis	173
B.1	Effect of screening design parameters on fixed bearings in transverse direction (in)	195
B.2	Effect of screening design parameters on fixed bearings in longitudinal direction (in)	196
B.3	Effect of screening design parameters on expansion bearings in transverse direction (in)	197
B.4	Effect of screening design parameters on expansion bearings in longitudinal direction (in)	198
B.5	Effect of screening design parameters on curvature ductility of concrete columns in transverse direction	199
B.6	Effect of screening design parameters on curvature ductility of concrete columns in longitudinal direction	200
B.7	Effect of screening design parameters on abutments in transverse direction (in)	201
B.8	Effect of screening design parameters on abutments in longitudinal passive direction (in)	202
B.9	Effect of screening design parameters on abutments in longitudinal active direction (in)	203
C.1	Bridge component demand model for bridge columns	205

C.2	Bridge component demand model for fixed elastomeric bearing in longitudinal direction	206
C.3	Bridge component demand model for fixed elastomeric bearing in transverse direction	207
C.4	Bridge component demand model for expansion elastomeric bearing in longitudinal direction	208
C.5	Bridge component demand model for expansion elastomeric bearing in transverse direction	209
C.6	Bridge component demand model for abutments in active longitudinal direction	210
C.7	Bridge component demand model for abutments in passive longitudinal direction	211
C.8	Bridge component demand model for abutments in passive longitudinal direction	212
D.1	Bridge columns component fragility curves	214
D.2	Bridge component fragility curves for fixed elastomeric bearing in longitudinal direction	215
D.3	Bridge component fragility curves for fixed elastomeric bearing in transverse direction	216

D.4	Bridge component fragility curves for expansion elastomeric bearing in longitudinal direction	217
D.5	Bridge component fragility curves for expansion elastomeric bearing in transverse direction	218
D.6	Bridge component fragility curves for abutment in longitudinal active direction	219
D.7	Bridge component fragility curves for abutment in longitudinal passive direction	220
D.8	Bridge component fragility curves for abutment in transverse direction	221
E.1	Captured epistemic uncertainty in the fragility analysis for case 2	223
E.2	Captured epistemic uncertainty in the fragility analysis for case 2	224
E.3	Captured epistemic uncertainty in the fragility analysis for case 3	225
E.4	Captured epistemic uncertainty in the fragility analysis for case 3	226
F.1	Variation of the demand model parameters to the number of samples	228
F.2	Variation of the demand model parameters to the number of samples	229
F.3	Variation of the COV for the demand model parameters to the number of samples	230
F.4	Variation of the COV for the demand model parameters to the number of samples	231

LIST OF TABLES

2.1	Important earthquake events recorded in United States (USGS 2004) [43] . . .	22
2.2	Bridge types and Their Proportions (Nielson 2005) [30]	28
2.3	Damage Probability Matrix for Multi-Span Bridges (%) (Basoz and Kiremidjian [47]	34
3.1	Ground motion bin size used to assess different scale factors and intensity measures	54
3.2	Coefficients of determination for regression analysis of SDI versus other IMs for various periods of the structure	69
4.1	Sources of uncertainty in performance based seismic assessment of bridges .	84
4.2	Plackett-Burman design matrix for 8 parameters and 8 runs	87
4.3	Classification of bridge structures for CSUS region	90
4.4	Classification of bridge structures for California State	90
4.5	Typical deck stiffness and mass properties for MSSS concrete girder bridge .	95
4.6	typical parameters value for concrete and steel material	97
4.7	Definition and values for participant parameters in screening study	109
4.8	Selected pairs of ground motions for bridge parameter screening study	112

4.9	Plackett-Burman design matrix	117
4.10	Monitored response components of bridge structure	119
4.11	Sorted main effects and their correspondence p-values for deformation of abutments in longitudinal active direction	131
4.12	Sorted main effects and their correspondence p-values for deformation of abutments in longitudinal passive direction	132
4.13	Sorted main effects and their correspondence p-values for deformation of abutments in transverse direction	133
4.14	Sorted main effects and their correspondence p-values for curvature ductility of concrete columns in longitudinal direction	134
4.15	Sorted main effects and their correspondence p-values for curvature ductility of concrete columns in transverse direction	135
4.16	Sorted main effects and their correspondence p-values for deformation of expansion bearings in longitudinal direction	136
4.17	Sorted main effects and their correspondence p-values for deformation of expansion bearings in transverse direction	136
4.18	Sorted main effects and their correspondence p-values for deformation of fixed bearings in longitudinal direction	137
4.19	Sorted main effects and their correspondence p-values for deformation of fixed bearings in transverse direction	138

4.20	Significant Parameters for MSSS Concrete Girder Bridge	139
4.21	Fragility analysis parameter definition and parameters case participation . . .	142
4.22	Extensive and complete limit states for bridge components	144
4.23	Slight and moderate limit states for bridge components	145
4.24	Slight and moderate limit states for bridge components	147
4.25	PSDMs for MSSS Concrete Girder Bridge Components (Case 1)	150
4.26	PSDMs for MSSS Concrete Girder Bridge Components (Case 2)	151
4.27	PSDMs for MSSS Concrete Girder Bridge Components (Case 3)	151
5.1	Fragility analysis parameter definition and vector classification	165
5.2	Two levels sampling technique for bridge generation	168
A.1	ANOVA table for deformation of abutments in longitudinal active direction .	185
A.2	ANOVA table for Deformation of abutments in longitudinal passive direction	186
A.3	ANOVA table for Deformation of abutments in transverse direction	187
A.4	ANOVA table for Curvature ductility of concrete columns in longitudinal direction	188
A.5	ANOVA table for Curvature ductility of concrete columns in transverse di- rection	189

A.6	ANOVA table for Deformation of expansion bearings in longitudinal direction	190
A.7	ANOVA table for Deformation of expansion bearings in transverse direction	191
A.8	ANOVA table for Deformation of fixed bearings in longitudinal direction . .	192
A.9	ANOVA table for Deformation of fixed bearings in transverse direction . . .	193

CHAPTER 1: INTRODUCTION

This chapter contains the historical background, definition, and step-by-step procedure for performance-based design and performance-based assessment of structures. After the description of performance-based design and assessment, statement of the problem and objective of the research are included.

1.1 Performance based design and performance-based assessments

After the 1989 Loma Prieta and 1994 Northridge earthquakes, structural engineers in the United States began development of structural design procedures that would reduce the financial and other losses associated with earthquake damage. The results from aforementioned design today known as “performance-based design”. Attempts in developing seismic performance-based design have generalized conventional “load” and “resistance” terms with “demand” and “capacity” for design of structures.

Performance based earthquake engineering (PBEE) is design and assessment of a structure whose performance is in agreement with stakeholders (like owners, managers and governments) objectives and needs. Performance based design (PBD) is the implementation of PBEE methodology in design of structures. PBD consider the desired performance in the design procedure of the structures (FEMA-445 (2006) [53]). The performance-based seismic design process estimate how a building is likely to perform, given the potential hazard it might experience. In performance-based design, identifying and assessing the performance capability of a structure is a crucial part of the design process. First step for PBD is the selection of performance objectives. Each performance objective is a statement of the acceptable risk of occurring specific levels of damage, and the losses that might occur as a result of this damage, at a specified level of seismic hazard (FEMA 445

(2006) [53]). These losses can be related to structural damage, nonstructural damage, or both. They can be defined in the form of casualties, economic costs, and downtime (time out of service) resulting from the damage perceived by the structure. In case of bridge structures, losses are corresponding to potential damage to bridge structures and indirect effects of post-event transportation network closure, such as indirect economic losses, business disruption, or inhibition of emergency response efforts. Methods for estimating losses are discussed in more detail later in background study. Stakeholders must define the risk of a hazard events they can sustain, and might define the acceptable level of performance but may not directly participate in the design process. Once the performance objectives are defined, a series of simulations (analyses of building response to loading) are performed to estimate the probable performance of the building under various design scenario events. If the performance meets or exceeds the performance objectives, the design is complete. If not, the design needed to be revised in an iterative process until the performance objectives are met.

Figure 1.1 shows the performance-based design flowchart. The third step of the flowchart is performance-based assessment of the structure. When the performance objectives have been selected and a preliminary design developed, the next step is assessment of the performance capability of the design to determine whether or not it meets the selected performance objectives. There are certain steps needed to be taken for assessing the performance of the structure. These steps are listed as following:

- Characterization of the ground motion hazard.
- Analysis of the structure to determine the probable response and the intensity of ground motion transmitted to supported nonstructural components as a function of ground shaking intensity.
- Determination of the probable damage to the structure at various levels of response.

- Determination of the probable damage to nonstructural components as a function of structural and nonstructural response
- Determination of the potential for casualty, capital and occupancy losses as a function of structural and nonstructural damage.
- Computation of the expected future losses as a function of intensity, structural and nonstructural response, and related damage.

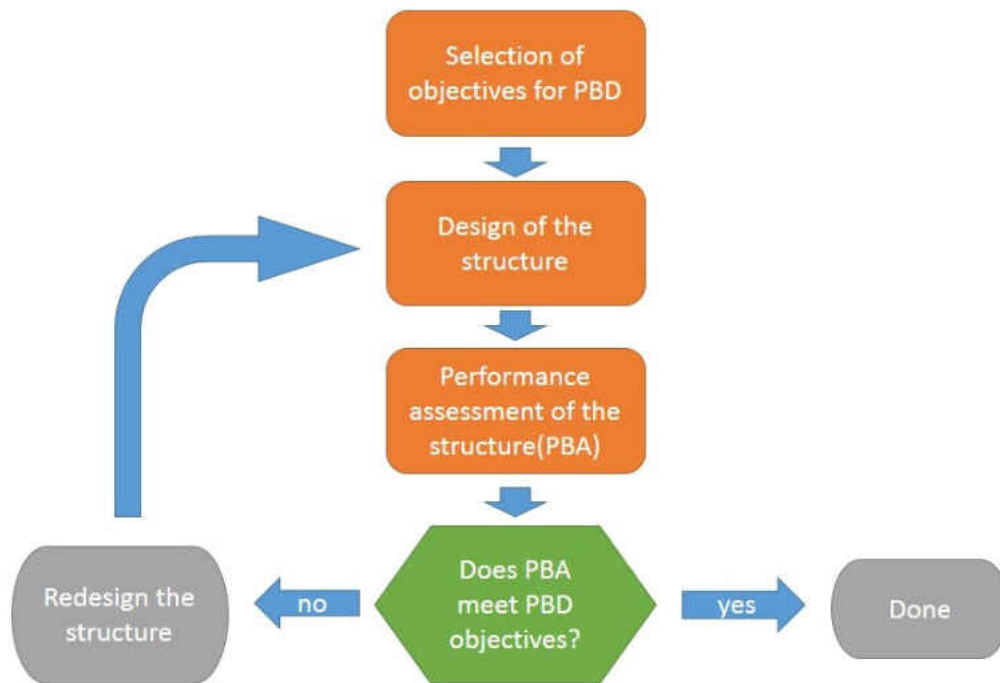


Figure 1.1: Performance-based design diagram

1.2 Uncertainty associated with performance-based assessment

Engineering problems, including reliability analysis, seismic performance-based assessment, risk and decision problems, are being solved using a model universe. These models contain the set of physical and probabilistic sub-models. The mathematical model may contain uncertain quantities, also the sub-models are imperfect and inherent the model uncertainties. Therefore, an important part of solving the problem is consideration of these uncertainties in analytical modeling of the structures. While there can be many sources of uncertainty, in the modeling, uncertainties can be categorized as either aleatory or epistemic. The word aleatory derives from the Latin *alea*, which means the rolling of dice. Thus, an aleatoric uncertainty is one that is assumed to be the actual randomness of a phenomenon. The word epistemic derives from the Greek (*episteme*), which means knowledge. Thus, an epistemic uncertainty is one that is caused by lack of knowledge (or data). In engineering most of the problems involve both types of uncertainties. In the modeling, sometimes it may be difficult to determine whether a particular uncertainty is aleatory or the epistemic. It is the job of the model builder to make the distinction and address these uncertainties in the mathematical realization of the model.

1.3 Statement of the problem

By looking at the process of PBA of bridges, a long list of parameters defining the capacity and demand domains can be recognized. The results from the analysis rely on the accuracy of input parameters incorporated in the procedure. Uncertainty in the inputs can result in uncertainty or error in the output results. Accuracy in the input becomes more important when measurement of probability for extremely rare incidents are expected. For extreme rare incidents (very low probability incidents) a small error in the input can result in a change in the order of magnitude of the output

probability of incident. For example error in modeling the uncertainty of soil stiffness properties might change the probability of failure of the structure from 10^{-4} ($\beta=4$) to 10^{-5} ($\beta=5$), whereas the risk associated with these reliability results are very different in nature. Therefore including the uncertainties associated with parameters is an important step in PBA of structures. Previous attempts tried to address and include the uncertainties associated with the input parameters for PBA of structures; however incorporating all of these sources in the analysis, if not impossible, is computationally very expensive.

In addition, another issue discerned in PBA procedure the assumption of uncoupled uncertainties associated with demand and capacity of the structure. One of the most well-known method for PBA of the structures are based on the reliability methods. Based on this method, component fragility function is derived with assumption of statistical independency of log-normally distributed demand and capacity models . In reality the demand and capacity of the structure are correlated and consequently the parameters that are used to define the bridge and bridge seismic response will affect the damage states in component fragility curve analysis. Therefore basic assumptions used in driving the PBA formulations are not valid and using those equation cannot fully capture the uncertainties associated with component fragility analysis.

Another drawback for extensive use of PBEE by engineers is scarcity of recorded ground motions that closely match the site characteristics and have the target intensity of interest. The reason is quantifying earthquake demands is dependent on existence of previously recorded ground motions as well as the site characteristics of hazard region. Limitations in the existing ground motion database force engineers to scale real records. However, scaling of ground motions creates the concern of whether a record that has been scaled to target intensity has the same effect on the structure compared to a record that is naturally at the target intensity.

1.4 Objective Statement

The objective of this research is to address the major sources of error in PBA procedure of the bridge structures and present integrated methods to eliminate or improve these uncertainties. Recognition of the source of the errors and improvement of the PBA procedure for highway bridges can be divided into three categories:

1. Errors rooted in parameters included in PBA procedure:

For an accurate response assessment of the highway bridges various parameters participate in the PBA procedure needed to be recognized and uncertainty associated with each one needed to be considered in the model. Incorporating all of the sources of uncertainty in the PBA analysis if not impossible is computationally very expensive. To overcome this obstacle only the important parameters can be included in probabilistic PBA approach and the rest of the parameters can be treated as deterministic values (mean value can be assigned to the parameters). Therefore a method needed to be utilized to rate the importance of these parameters with respect to the response of the bridge structure. Despite the efforts have been made in the past using one of the sensitivity analysis techniques to acquire the importance of the parameters, only simplistic approach which did not incorporate all the parameters in the sensitivity analysis have been utilized. Therefore more comprehensive study on the sources of the uncertainty and their influence on the response of the bridge structure needed to be performed. Also the influence of the reduction of number of parameters on the fragility analysis needed to be evaluated to validate the procedure of elimination of lesser important parameters in fragility analysis of the highway bridges.

2. Errors rooted in method utilized in PBA of highway bridges:

Up to date for derivation of fragility curves for highway bridges, PEER PBA methodology

have been adopted with the assumption of independence of demand and capacity. Even when the correlation between demand and capacity needed to be considered, the correlation coefficient was implemented in the fragility function using a simplistic approach. A rigorous solution which fully consider the dependence of demand and capacity have not been presented in the literature before. Therefore a revised PEER PBA methodology with capability of consideration of correlation between demand and capacity needed to be introduced.

3. Errors originated from ground motions scaling:

Scarcity of ground motions naturally at the target intensity of interest pushed researchers to scale the ground motions. Despite the attempts that have been made previously, no comprehensive study can be found in the literature that considers a variety of methods of scaling, SDOF and MDOF system parameters, and addresses the fundamental reasons corresponding to scaling-induced bias for response of nonlinear systems. Specifically, it may be widely believed that bias is attributable to period elongation of nonlinear systems not captured in the scaling method however a study that quantify the dependency of the bias to period elongation is lacking. The lack of such a comprehensive study is rooted in the complexity and variability in the nature of ground motions, nonlinear system response, and their interaction. The objective of this section of the research is to quantify ground motion record amplitude scaling bias induced in nonlinear structural response statistics. For this purpose, a comprehensive study was performed using different types of nonlinear SDOF systems and various well-known intensity measuring parameters (IMs) for ground motion amplitude scaling. Given that such bias has been observed previously, not only is the bias quantified, a method to minimize the bias is proposed and a new intensity measuring parameter is introduced for bias minimization. It is shown that the new parameter can be used to minimize bias from amplitude scaling as well as the prediction of the magnitude of bias in nonlinear response using only linear response analyses. The effect of scaling bias and the proposed bias reduction

techniques are illustrated using fragility analysis results.

1.5 Research plan

Performance based assessment is the core requirement for performance-based design procedure and fragility curves are one of the most important outcome of performance-based assessment. Damages in the highway bridge network are associated with direct and indirect loss. Bridge damage fragility curves are conditional probability of exceeding a level of direct or indirect bridge damage for given a level of seismic hazard. As mentioned before the objective of this research is to reduce the uncertainty in performance-based assessment for highway bridges. The three types of uncertainties are mentioned in section 1.4. For seismic PBA for highway bridges, first a suit of ground motions needed to be selected that closely represent the site seismic characteristics. In many sites, the scarcity of high intensity earthquake events force the engineers to use scaling algorithms for generating higher intensity accelerograms from low intensity ground motion accelerations. Previous studies showed that scaling procedure can cause bias in results obtained from response analysis of nonlinear structures. The response analysis of structure is an important step in seismic PBA procedure therefore bias induced from ground motion scaling can affect fragility curve analysis results for highway bridges. The first goal of this research is to reduce or even eliminate the ground motion scaling bias by studying the nature of the bias induced by scaling procedure. Chapter 3 is consisted of comprehensive study for ground motion selection bias reduction techniques. In chapter 3 the effect of scaling procedures on the response of nonlinear systems was studied. It needed to be determined whether ground motion record amplitude scaling produces biased nonlinear structural response statistics and if so, how the biased can be minimized. For this purpose a comprehensive study was performed using different types of nonlinear SDOF and MDOF systems and various well-known intensity measuring parameters for amplitude scaling. In

addition to recorded ground motions, synthetically simulated ground motions was employed to identify a similar amplitude-scaling bias and to allow for generation of a larger catalog of high intensity records for comparison to unscaled ground motions. Using the synthetic ground motions also forms the basis of future efforts to identify the characteristics of ground motions that cause bias after amplitude scaling of records. Dependency of bias associated with scaling for different types of nonlinear systems, amount of scaling, and methods for selection of bins was studied. Based on the biased nonlinear response statistics observed for various IMs, A new IM was defined to minimize the bias induce from amplitude scaling and reduce the bias values obtained from nonlinear structure response. Also the effect of bias on fragility analysis was studied.

Many analytical methods have been used to obtain fragility curves but a comprehensive study that can track the sources of uncertainties and minimize its consequence over the outcome of analysis is lacking. After finding the optimized bias reduction technique for fragility analysis ground motion selection, in chapter 4, aleatory and epistemic uncertainties in the procedure of fragility assessment for highway bridges was considered. Theoretically all the parameters in analysis can be assumed as variables with a properly assigned probability distribution. The problem here would be the limitation in computational performance of todays computers. The number of the sample needed to perform the analysis increases exponentially with number of uncertain parameters. For instance adding 3 parameters with 10 intervals for each parameter can increase the computational time required for PBSA up to 1000 times. To optimize the computational time, a combination of sampling along with parameter screening techniques is taken into the account. The outcome of this part of the research was finding the parameters that are the main sources of variability in the response of nonlinear bridge structure .Having obtained these parameters, the effect of exclusion of lesser important parameters in probabilistic demand analysis for fragility curve development was studied.

California benchmark bridges that share the same characteristics and are owned, operated, and

maintained by California department of transportation (Caltrans) as well as central and southern United States (CSUS) bridges were identified from national bridge inventory (NBI) database for bridge selection propose. To be consistent with previous studies and having a common basis for finite element modeling of elements and bridge system, MSSS concrete girder bridge which its seismic performance was assessed in previous fragility studies was selected. A screening study was performed on all the parameters that could be included in the FEM model of the structure and the important parameters were selected as the outcome of the screening analysis. Consequently fragility analysis for three cases was performed to capture the effect of exclusion of lesser important parameters from the probabilistic model.

In chapter 5 correlation between demand and capacity in performance based assessment of structures was studied. An alternate formulation for obtaining the probability of failure was derived that can measure the correlation between the component demand and capacity parameters in the analysis and in the derivation of the fragility curves function. To assess the formulation, A capacity model for bridge concrete column has been adopted and to be compatible with the proposed formulation, fragility curves were obtained using multi-layer sampling technique. Comparison between conventional and the proposed formulation shows the effect of neglecting correlation in the outcome of fragility analysis as well as PBA of the structures.

CHAPTER 2: BACKGROUND STUDY

2.1 PBEE methodologies from code perspective

Recommended Lateral Force Requirements and Commentary (SEAOC, 1999) and the FEMA-356 (ASCE, 2002) national rehabilitation guidelines are early attempts to implement Performance-based seismic design for buildings in the United States. They use discrete performance levels (damage states), from minor damage to structural collapse and consequently utilize methods to relate these damage states to response of the structure (i.e. inter-story drift or internal member forces) ATC 14 (1987) and FEMA 273 (1997) [2] represented major addressed evaluating the seismic hazards for existing buildings. ATC 14 created the concept of screening buildings for potential deficiencies. FEMA 273 employed “displacement-based” methodologies for evaluating the demand and capacity of the structure. Following the publication of both ATC 14 and FEMA 273, the Federal Emergency Management Agency (FEMA) began to support efforts to transition those documents from guidelines into national standards. FEMA 178, 1992; FEMA 310, 1998; and FEMA 356, 2000 [3] are FEMA’s attempts for transition from previous guidelines to national standards. Later displacement based analysis procedures from FEMA 273 were simplified in FEMA 310. ASCE 31-03 Seismic Evaluation of Existing Buildings in 2003 and then in 2006 with ASCE 41-06 Seismic Rehabilitation of Existing Buildings are product of continual attempts for standardization of PBEE for buildings.

These methodologies had significant influence on U.S. engineering design and retrofit of structures and also have been used to upgrade the performance of existing structures. After using the performance-based methodology for seismic design some attempts has been made to adopt the same methodology for other design conditions such as wind, snow, fire and blast.

2.2 The Pacific Earthquake Engineering Methodology

The Pacific Earthquake Engineering Research Center (PEER) is a multi-institutional research and education center with headquarters at the University of California, Berkeley. Investigators from over 20 universities, several consulting companies, plus researchers at various State and Federal government agencies contribute to research programs focused on performance-based earthquake engineering in disciplines including structural and geotechnical engineering, geology/seismology, lifelines, transportation, risk management, and public policy (www.peer.berkeley.edu). One of the main responsibility of PEER Center is the development of a performance-based earthquake engineering (PBEE) methodology in order to provide a unified approach to the seismic risk assessment (Cornell and Krawinkler, 2000) [32]. Performance objectives are defined as a probability of exceeding a threshold value for decision variables (DV) given the seismic hazard conditions applied to the structure. Instead of directly evaluating the DVs values given hazard condition, PEER framework divided the problem into different intermediate probabilistic model. This approach can decrease the complexity of the problem and also makes it easier to trace the sources of uncertainties incorporated in each intermediate model.

Damage measures (DMs), engineering demand parameters (EDPs), and seismic hazard intensity measures (IMs) are intermediate variables defined in PEER framework. DVs usually evaluate repair cost, downtime, repair time, and loss of life and functionality of the structure. DMs are multilevel thresholds for the EDPs also known as damage states. EDPs include displacements, drifts, strains, curvatures, moments, and residual deformations. IMs also usually assumed to be peak ground acceleration (PGA), peak ground velocity (PGV) or first spectral acceleration $S_a(T1)$ for the first mode of vibration of the structure. From PEER framework the fragility evaluation

(probability of exceeding a decision limit state) can be defined as following:

$$P(DV > dv^{ls}) = \int \int G(dv^{ls}|dm)dG(dm|edp)dG(edp|im)d(im) \quad (2.1)$$

The $G(X|Y)$ denotes the cumulative distribution function of variable X conditioned on variable Y. Also lower case variables (dv, dm, edp, im) are individual realization of variables (DV, DM, EDP, IM). Also mean annual frequency of exceedance of a decision variable can be found as following:

$$\nu(dv^{ls}) = \int \int G(dv^{ls}|dm)dG(dm|edp)dG(edp|im)dv(im) \quad (2.2)$$

Where $\nu(x)$ expresses the mean annual frequency of exceeding variable x . The figure bellow illustrate the PEER PBEE framework.

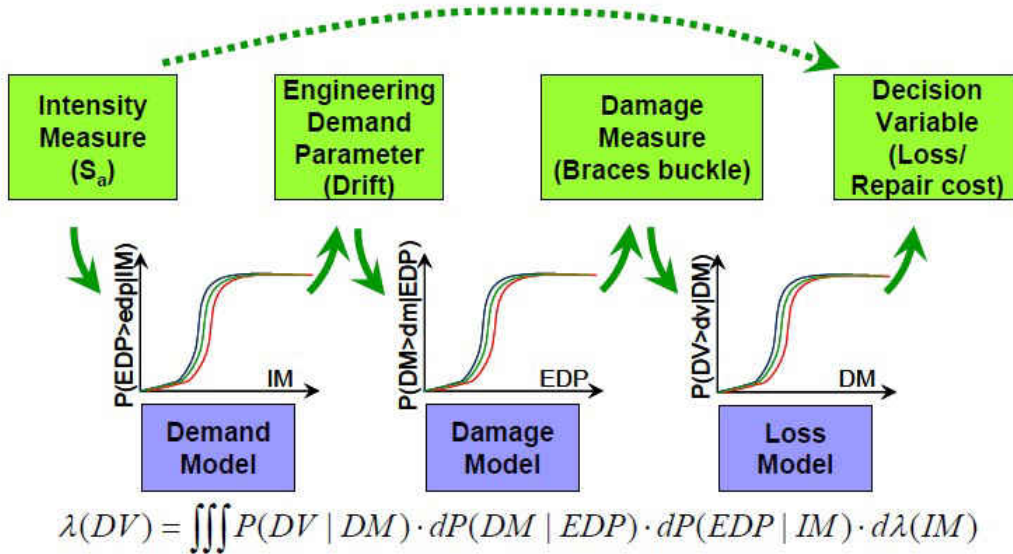


Figure 2.1: Illustration of PEER framework

Hazard model, Demand model, Damage model and Decision model analysis are essential for obtaining the conditional CDF functions incorporated in Equation 2.2. A brief description of each model is described in the following sections.

2.2.1 Hazard analysis

The first step for seismic PBA of a structure is ground motion hazard characterization. The assessment begins with definition of a ground motion Intensity Measure (IM). In hazard analysis the frequency which the intensity of a ground motion is exceeded annually is calculated. The main output of hazard analysis is seismic hazard curve that shows the relation of IM and its mean annual frequency MAF, (i.e., $\lambda(IM)$). The IM could be scalar (i.e., $Sa(T_1)$) or a vector (e.g. combination of $Sa(T_1)$ and peak ground acceleration, PGA). Usually $Sa(T_1)$ have been used as IM for simplicity and effectiveness. Baker and Cornell (2005) proved advantages of using vector of IMs in describing ground motion characteristics and predicting the response of structure. Hazard analysis can be performed deterministically or probabilistically. In deterministic seismic hazard analysis (DSHA) the ground motion hazard is evaluated based on specific seismic scenario. Probabilistic seismic hazard analysis first proposed by Cornell at 1968 and after that become conventional tool for seismic hazard assessment. It incorporates uncertainties in location, size and occurrence rate of earthquakes in the estimation of seismic hazard. The outcome of PSHA is expressed in MAF of IM (i.e. $\lambda(IM)$). For example if $Sa(T_1)$ is used as an IM, the hazard curve obtained from PSHA shows the relation between $Sa(T_1)$ and $\lambda(Sa(T_1))$ (the MAF in $Sa(T_1)$).

Seismic hazard curve for California State and CSUS region can be obtained from USGS website and in most cases there is no need for additional the PSHA analysis.

2.2.2 Demand Model

The demand model describes the probabilistic effect of ground motions on a structure response in terms of engineering demand parameters (EDPs) for a certain level of intensity measure variable. A relation between IMs and EDPs can be obtained using the response values of the structure for each of the ground motions in the selected suite. There are various procedures for obtaining a demand model. The “cloud” or direct (Shome and Cornell, 1999) [34] method which attempts to represent the site seismicity through selection of many ground motions. Cloud analysis method do not use any scaling procedure on the ground motions therefore, the demand model can directly be obtained from IM-EBD data. The incremental dynamic analysis (IDA) method in which the intensity of a selected ground motion records is scaled to predefined minimum to maximum values using a certain increments and for each intensity level the maximum EBD parameters can be obtained from the response analysis (Vamvatsikos and Cornell, 2002 [36]). The stripe method that scales all ground motions to the few intensity levels which is a special case of IDA. Regardless of the method used to obtain the demand model, for most of the studies these assumptions have been used to obtain probabilistic demand model. - The EDP data are assumed to have a lognormal distribution when conditioned on IM - The conditional mean of EDP given IM is linear in log space - Conditional dispersion of EDP given IM is constant.

Using the above assumptions demand models can be obtained by Equation 2.3 in log space or Equation 2.4 in linear space. Parameters A , B , and dispersion $\beta_{EBP|IM}$ can be computed using regression analysis.

$$\ln(\widehat{EDP}) = A + B \ln(IM) \quad (2.3)$$

$$\widehat{EDP} = aIM^b \quad (2.4)$$

For equation 2.3 several issues can be recognized when applied to structures with highly nonlinear behaviors including global instability or collapse (Jalayer (2003); Krawinkler and Ibarra (2003); Baker and Cornell (2005)) [37], [39], [17] and some modification in the above formulation is suggested (Mackie and Stojadinovic, 2003) [41].

2.2.3 *Damage Model*

The damage model describes the probabilistic damage state of a structure using damage measures (DMs) for a given a value of engineering demand parameters (EDPs). In fact DMs assumed to be a function of EBDs. Examples of damage states for reinforced concrete columns include cracking, spalling, and transverse reinforcement fracture. Damage models can be obtained from experimental tests that measure capacity of structural components in term of demand loads. Analytical approach using finite element reliability analysis also can be taken into the account or they can be obtained using suggested capacities of structural components included in standard design codes. Usually relation between EDP and DM assumed as a power-law relationship however this relationship is not accurate for high values region of EDP's such as collapse condition. The following equation showing the power low equation described above:

$$\ln(\widehat{DM}) = C + D \ln(EDP) \quad (2.5)$$

2.2.4 Decision Model

Decision model employ mathematical equations to explain the relation between decision variable (DV) and damage measures (DM). Decision variables are losses that can be measured in terms of cost, reduction in functionality or interruption due to damage, repair time, loss of life and etc. Decision models can be developed and examined using data from professional surveys and opinion, repair data from post-earthquake reconstruction, construction cost estimation and data collected during past earthquakes. Various concerns such as relation between component level and system level repair cost, correlation between component decision models and using continuous versus discrete DMs and DVs needed to be incorporated in derivation of the damage model that increase the complexity of the problem. Decision values usually assumed to be binary .As an example a bridge may be categorized as either open or closed or level of functionality can be expressed as a four discrete levels. If DM and DV chosen as continuous variables, decision model can be expressed as following:

$$\ln(\widehat{DV}) = E + F \ln(DM) \quad (2.6)$$

2.3 Ground motion in central and eastern United States

Based on the USGS hazard map there are two major region with high seismic activity in United States. UCSC region and States near the west coast. This section describes the previous seismic activities in CSUS and west coast region.

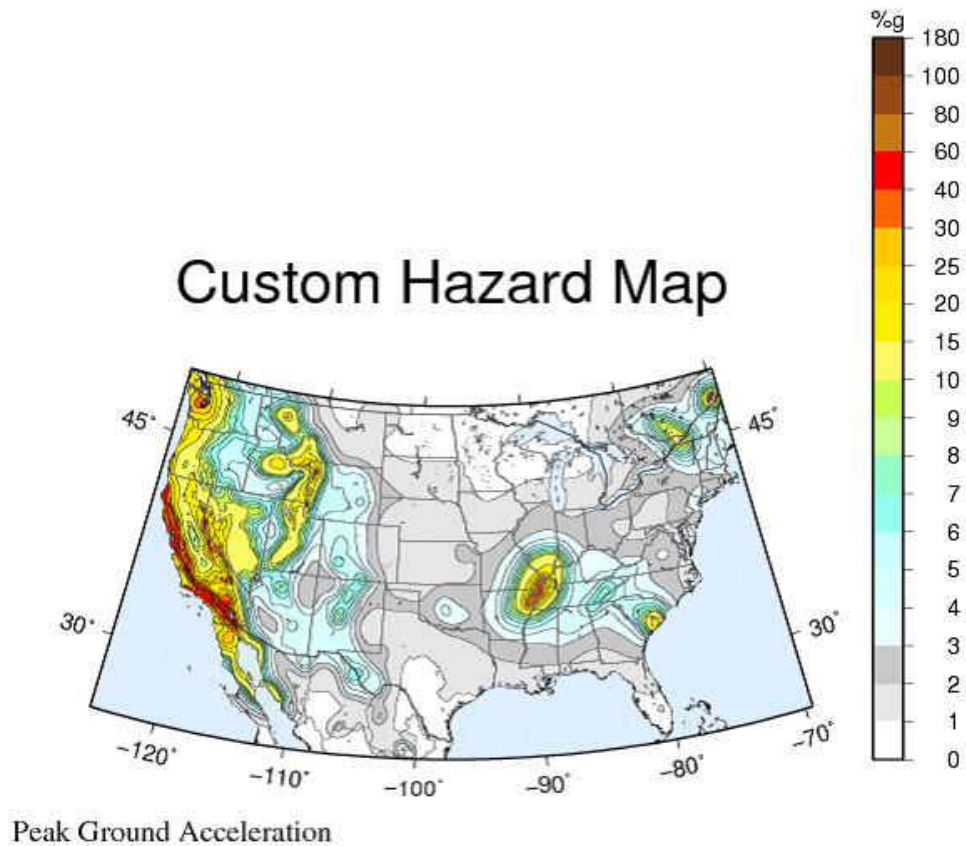


Figure 2.2: US seismic hazard as (PGA) with 10% probability of exceedence in 50 years (USGS website 2012 [44])

2.3.1 Western United States earthquakes

Seismic hazard in California is high .Based on historical data considerable number of large earthquakes have occurred in this region. Many of these earthquakes occurred within about 50 km of the San Andreas Fault. In the 1812 Wrightwood earthquake, $M \sim 7$; 1838 San Francisco peninsula earthquake ($M \sim 7.1/2$) 1857 Fort Tejon earthquake ($M \sim 7.9$) 1868 Hayward earthquake($M \sim 7$) 1906 San Francisco earthquake($M \sim 7.9$) and the 1989 Loma Prieta earthquake($M:7.0$) are

examples of large earthquakes with moment magnitude $M > 7$ that have occurred near the San Andreas Fault Zone. Broad San Andreas Fault system has strike slip fault mechanism.

in the 1872 Owens Valley earthquake($M \sim 7.6$), 1952 Kern County earthquake ($M \sim 7.5$), 1971 San Fernando earthquake ($M:6.7$), 1992 Landers earthquake ($M:7.4$) and the 1994 Northridge earthquake ($M:6.7$) happened far from San Andreas Fault Zone.1983 Coalinga earthquake ($M:6.5$) 1987 Whittier Narrows earthquake ($M:5.9$) and the 1994 Northridge earthquake are some examples of earthquakes happened based on reverse fault mechanism.

California State experience every 2 to 3 years earthquakes with magnitude $M > 6$. The loss estimation from these large earthquakes was several billions of dollars in damage (i.e. 1906 San Francisco earthquake, 1933 Long Beach earthquake- ($M:6.2$), 1971 San Fernando earthquake, 1989 Loma Prieta earthquake, and 1994 Northridge earthquake).Figure 2.3 shows the major faults in California State.

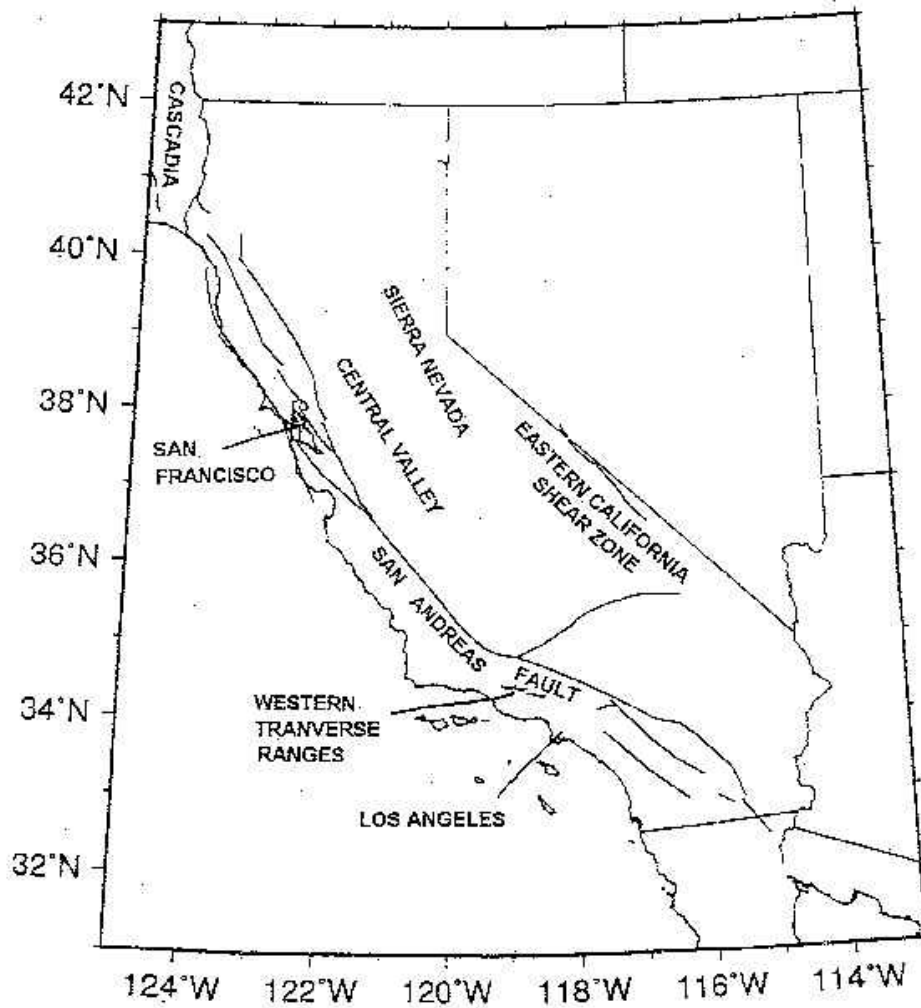


Figure 2.3: names of major fault systems in California State with slip rates greater than about 5 mm/yr (California Geological Survey 2012) [45]

2.3.2 Central and southern United States earthquakes

In the winter of 1811-1812 several large earthquakes rocked the Central and Southeastern United States (CSUS) originating from the Missouri/Tennessee region. Later that same century, in 1886, another large earthquake that originated in South Carolina rocked the region once again. These earthquakes, can illustrate the existence of seismic hazard and the associated seismic risk that exists in this part of the United States. The earthquakes of 1811-1812, which is known as the New Madrid earthquakes, were consisted of three large earthquakes and hundreds of moderate earthquakes in a six month period of time. One of the main shocks occurred on December 16, 1811 with an estimated moment magnitude of 8.1. The other two occurred on January 23, 1812 and March 15, 1812 with moment magnitudes of 7.8 and 8.0 respectively (USGS, 2004) [43]. It should be noted that the estimates for these earthquakes range from 7.2 to 8.7. Based on the magnitudes published by the United States Geological Survey, two of these earthquakes rank in the top ten largest earthquakes in the United States. The loss incurred from these earthquakes was not significant because the region was underdeveloped at the time. Seismic hazard is defined as the potential that the region has of experiencing a certain level of ground shaking intensity. Given the seismic nature of the CSUS, it has been classified as a moderate seismic zone because the earthquakes in this region are infrequent.

Table 2.1: Important earthquake events recorded in United States (USGS 2004) [43]

No.	Location	Magnitude (Mw)	Date
1	Prince William Sound, AK	9.2	3-Mar-64
2	Andreanof Islands, AK	9.1	3-Mar-57
3	Rat Islands, AK	8.7	Feb 4, 1965
4	East of Shumagin Islands, AK	8.2	10-Nov-38
5	New Madrid, MO	8.1	Dec 16, 1811
6	Yakutat Bay, AK	8.0	Sep 10, 1899
7	Andreanof Islands, AK	8.0	May 7, 1986
8	New Madrid, MO	8.0	Feb 7, 1812
9	Near Cape Yakataga, AK	7.9	Sep 4, 1899
10	Fort Tejon, CA	7.9	Jan 9, 1857

The geological characteristics of CSUS region is different compared to those in the west. The soil layer profile for eastern part of US is consisted of hard intact rock with soft sediments overlaying layers which result in large attenuation distance. Figure 2.4 compares the attenuation distances of several earthquakes in the East with several earthquakes in the West. It can be seen that the attenuation distances in the East are much longer and therefore the affected areas are much larger.

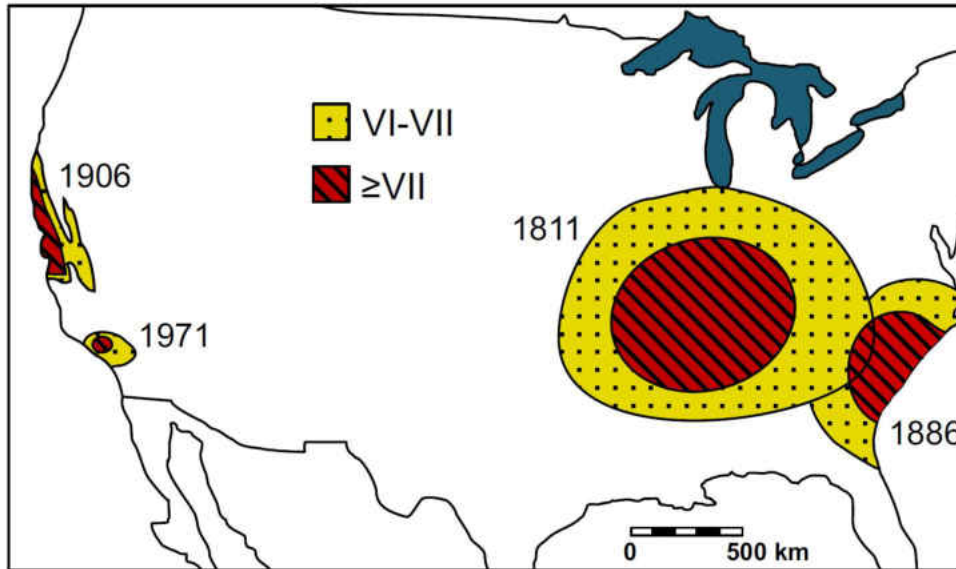


Figure 2.4: Comparison of Attenuation Distances of Several Earthquakes in the Eastern and Western United States (USGS, 2002) [46]

2.4 Synthetic ground motions

Synthetic earthquake ground motions have been used when appropriate recorded ground motions are not available. Many types of synthetic ground motion models have been developed in the past years and many are still under development. These models can be classified in three categories (Douglas and Aochi, 2008) [18]) 1) seismological models of site rupture mechanism and wave propagation, 2) parameterized stochastic models fitted to previously recorded ground motions, and 3) hybrid models employing a combination of first and second method elements. Seismological and hybrid models did not see widespread adoption in practice because they require extensive computation and thorough knowledge of the site characteristics, source, and wave path, which vary significantly by region (Rezaeian and Der Kiureghian, 2010) [20]. In the stochastic method

proposed by (Rezaeian and Der Kiureghian 2012) [21] ensembles of horizontal ground motion components with correlated parameters for specified earthquake and site characteristics can generated. The ground acceleration process is described as the response of a linear filter with time varying parameters to white-noise excitation. The filter response is normalized by its standard deviation and is multiplied by a deterministic time-modulating function. While modulation of the process in time introduces temporal nonstationarity, variation of filter parameters provides spectral nonstationarity. The method generates orthogonal lateral components of ground motions by determination of the correlation between the parameters obtained from predictive equations developed for model parameters of each component.

2.5 Ground motion scaling bias

Different methods have been utilized to overcome this obstacle. Scaling the ground motions, using synthetic earthquakes or combination of both methods have been taken into account. A variety of scaling methods such as amplitude scaling, amplitude and linear scaling for spectral acceleration for first period of structure $S_a(T_1)$ (Shome et al., 1998) [5], linear scaling of S_a over period range (Hancock, et al., 2008) [8] and scaling using spectrum matching (Hancock et al., 2006) [9] have been used previously.

Shome et al. (1998) [9] addressed the illegitimacy of scaling more directly whereas Sewell (1989) [11], Iervolino and Cornell (2005) [12] and Baker (2005) [13] indirectly addressed the bias induced by scaling. According to Luco and Bazzurro (2004) these studies had little impact on engineering practice because the conclusions are limited by statistical concepts and findings. In more recent studies, Luco and Bazzurro (2004; 2007) [14] ,[6], investigated the bias associated with scaling in the median nonlinear structural drift response for a target S_a , and conclude records with the same value of $S_a(T_1)$ structure should be considered in selection of records to avoid bias in the median

response.

Huang et al. (2011) [15] used four different scaling procedures including geometric-mean scaling, spectrum matching, Sa (T1) scaling, and distribution-scaling to quantify bias induced in the spectral shape and median Sa, as well as dispersion in nonlinear responses of the structures. Epsilon ϵ has significant correlation with Sa (Baker and Cornell, 2005) [17] and was considered a predicting parameter for legitimacy of scaling for each individual record based on Sa. The study by Huang et al. (2011) [15] was limited by the scaling based on Sa, and the conclusions are limited to first-mode-dominated buildings with minor to moderate inelastic deformation.

2.6 Bridge inventory in Central, Southern and California states

To perform the performance-based seismic assessment for various classes of highway bridges its essential to have complete understanding of the bridge inventory in each region. The types and characteristics of bridges may vary based on the time they have been constructed or the location of the site thus the focus at this section should be dedicated to finding classes of bridge that are representative of all bridges in various regions. Technically for each bridge its possible to develop fragility curve analysis but this approach is computationally very intense and time consuming. Therefore only the frequent classes of bridges are can be considered for this study to reduce the cost of computation. It worth mentioning that finding of this research are not limited to the selected bridge class and can be applied to any type of bridge structures in various regions.

2.6.1 CSUS State bridge classes

Table 2.2 show the possible bridge structure types and their population in (central and southern United States) CSUS area as they are listed in the NBI database.

Each class of bridge listed in the above Table 2.2 share the same characteristics based on the construction material and the methods used in their design and construction. Based on (Nielson 2005 [30]) the important parameters in bridge class statistics study are listed below

- Number of spans
- Maximum span length
- Deck width
- Vertical under clearance (Infer column height)
- Skew angle
- Year Built/Rebuilt
- Deck condition rating
- Superstructure condition rating
- Substructure condition rating

2.6.2 California State bridge classes

Reviewing recent state highway bridge construction in California, it appears that four structure types are (Ketchum et al. (2004) [31]):

- Post-tensioned cast-in-situ concrete box girders on monolithic piers
- Pre-tensioned pre-cast concrete I-girders on bearings supported by piers
- Concrete slabs on pile extensions

- Steel plate girders on bearings supported by piers.

The concrete box girder and concrete I girder bridges are most prevalent. The steel plate girder type has been recently used in high-ground-motion areas with special alignment and/or constructability constraints. Other types are occasionally used. It also appears that the following foundation types are dominant for these bridge types:

- H-piles,
- Precast concrete piles,
- Steel pipe piles
- CIDH shafts

Also cast-in-place box girders and precast I/bulb tee girders make up over 90% of new bridge construction in California therefore cast-in-place post-tensioned box girders and precast pre-tensioned I girder types of bridges can be good representative of bridge classes exist in California State .Figure 2.5 and Figure 2.6 show schematic view for two most frequently constructed California Bridges.

Table 2.2: Bridge types and Their Proportions (Nielson 2005) [30]

Name	Abbreviation	Number	Percentage
Multi-Span Continuous Concrete Girder	MSC Concrete	10,638	6.5%
Multi-Span Continuous Steel Girder	MSC Steel	21,625	13.2%
Multi-Span Continuous Slab	MSC Slab	5,955	3.6%
Multi-Span Continuous Concrete Box Girder	MSC Concrete-Box	916	0.6%
Multi-Span Simply Supported Concrete Girder	MSSS Concrete	30,923	18.9%
Multi-Span Simply Supported Steel Girder	MSSS Steel	18,477	11.3%
Multi-Span Simply Supported Slab MSSS Slab	9,981	6.1%	
Multi-Span Simply Supported Concrete Box Girder	MSSS Concrete-Box	4,909	3.0%
Single-Span Concrete Girder	SS Concrete	22,793	13.9%
Single-Span Steel Girder	SS Steel	18,281	11.2%
Other		18,945	11.7%
Total		163,433	100%

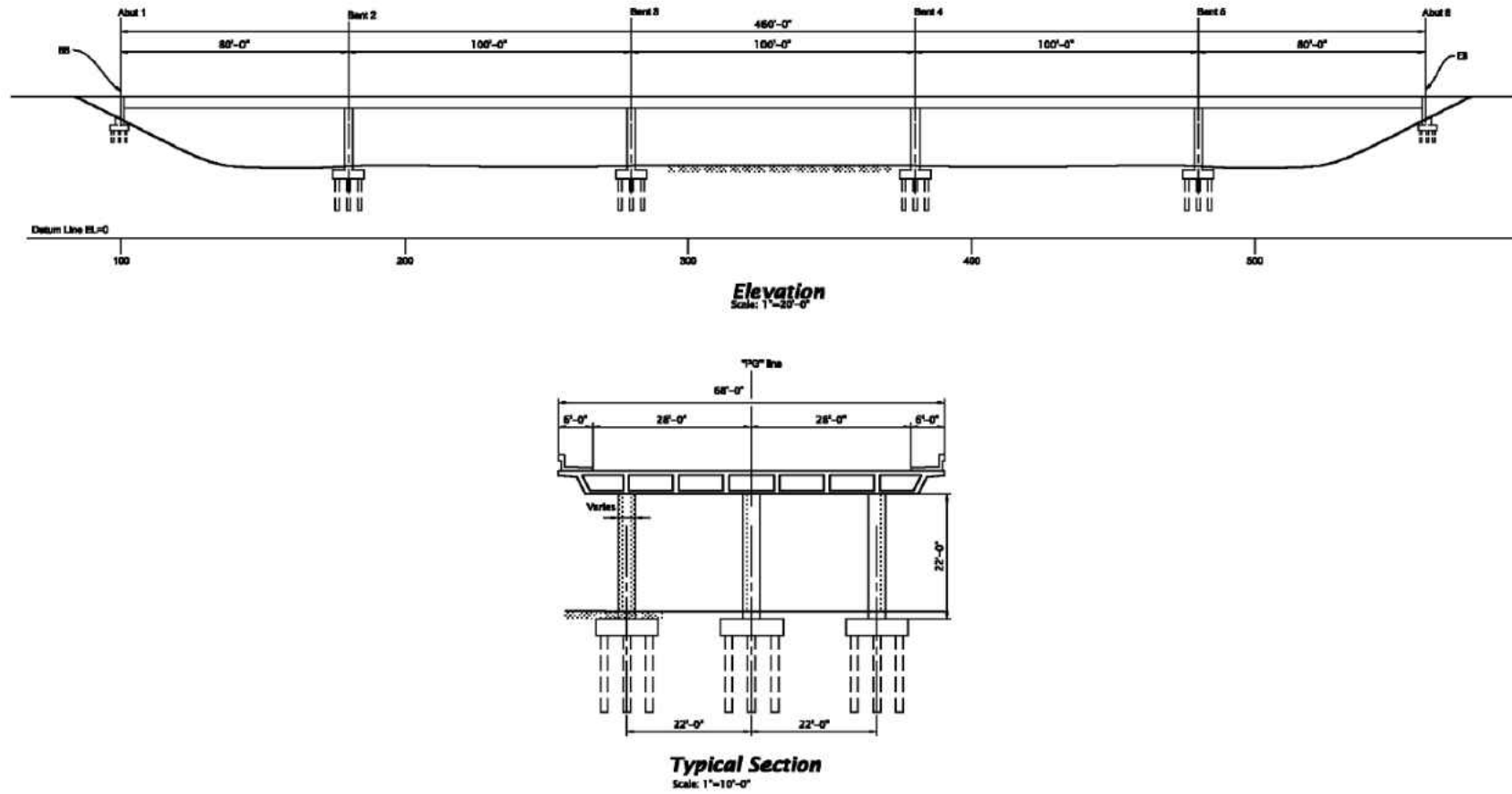
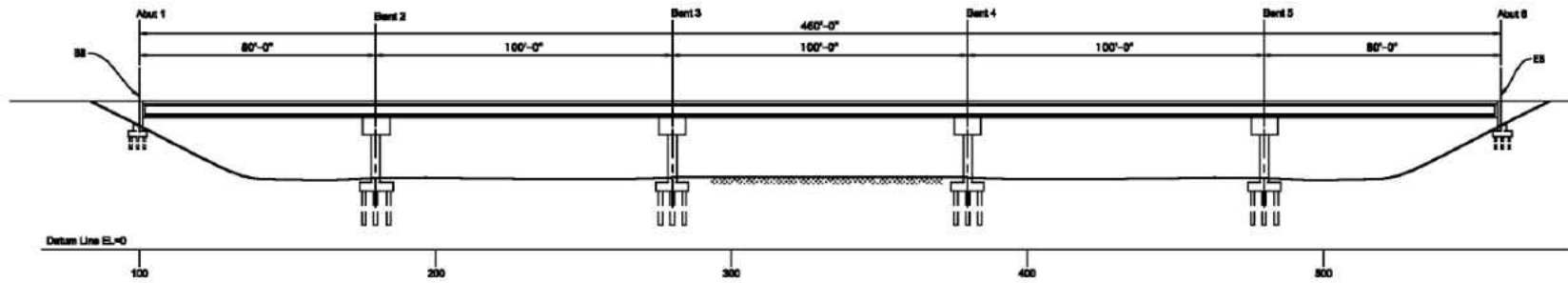
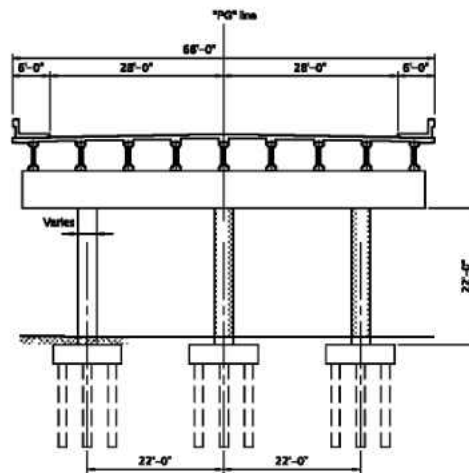


Figure 2.5: Straight Cast-In-Place Post-Tensioned Box Girder, (Ketchum et al. (2004)) [31]



Elevation
Scale: 1"=20'-0"



Typical Section
Scale: 1"=10'-0"

Figure 2.6: Straight Precast Pre-tensioned I Girder typical bridge. (Ketchum et al. (2004)) [31]

2.7 Performance-based design and performance-based assessments for highway bridges

As mentioned before performance-based design is an iterative procedure. However previous attempts have been made to substitute alternative straightforward methodology that uses closed form solutions instead of iterative methods (Mackie KR, Stojadinovi (2007), [61, 62]), utilizing such methodologies are still in doubt for design of complex structures. There are certain considerations needed to be taken into account for each step PBA to assure the final design meets the stakeholders required performance therefore PBD is more of a multidisciplinary procedure that demands for integration knowlage of structural engineers as well as financial, social, and environmental considerations and also employment of decision-making tools. This research only focus on the estimation of structure seismic performance (PBA). The outcome of PBA is a graph called Fragility curve or vulnerability curve. Fragility function is a probabilistic tool used to estimate the damage likely to occur during a seismic event. It estimates the probability of meeting or exceeding some limit state (LS) for a specific intensity of seismic excitation (IM). Figure 2.7 is an example of a fragility curves for a structure. For this example the minor damage, moderate damage, major damage and total collapse of the structure limit states can be seen with different colors on the figure. The horizontal axis is showing the intensity of the ground motion (IM) and the vertical axis is showing the mean probability of exceeding one of the damage states.

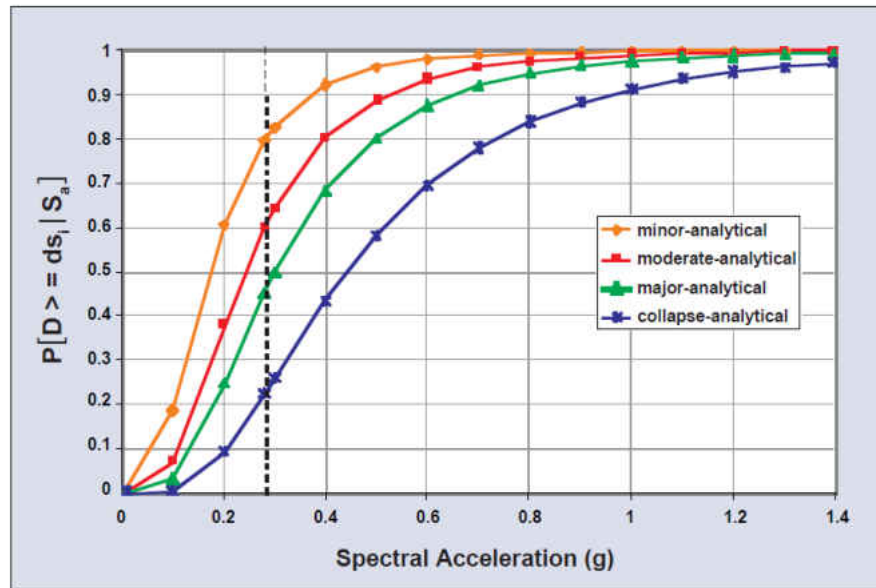


Figure 2.7: Fragility curves example (Nielson 2005) [30]

Different methodologies have been used for determining the structural fragility curves. One method is using the judgments of experts in structural inspection field and use their opinions to determine whether or not the structure is exceeded one of the indicated limit states. This method is called expert based fragility function. One of the examples of this kind of fragility function is the report included in ATC-25 which is based on the questionnaires answered by 4 experts evaluating the probability of the bridge being in one of the limit states. This methodology is not very accurate and a lot of uncertainties arising from the judgment of limited numbers of experts, language uncertainty in questionnaires and lack of description of the structure type and etc. are associated with it. The second type of fragility curves are Empirical fragility functions. For this type of fragility curves, a post-earthquake assessment needed to be performed to assess the damage state associated with the bridges. For each bridge the intensity of the ground motion applied to the structure and caused the structure to reach a damage state needed to be obtained from the historical data.

This can be found by using a shake map that geographically defines the ground motion in terms of some intensity measures, such as peak ground acceleration (PGA). Table 2.3 is an example of a damage frequency matrix that was assembled by Basoz and Kiremidjian (1997) [47] for all multi-span bridges damaged during the 1994 Northridge earthquake. Acquired information can be used in many number of ways. Basoz and Kiremidjian (1997) [47] used a logistic regression analysis to generate the fragility curves. Shinozuka et al. (2000) [48] recommended using the Maximum Likelihood method in conjunction with hypothesis and goodness-of-fit tests to estimate the two parameters of lognormal probability distribution while Der Kiureghian (2002) [49] used a Bayesian approach and the Likelihood function to obtain fragility curves. There are some limitations associated with this method. First it's hard to get statistically sufficient results for obtaining the fragility curves. Second the limit states assigned to each bridge is dependent on the judgment of individual inspectors. Also it's hard to obtain a reputable Shakemaps noting that the Shakemaps are different based on the method utilized for their generation.

Table 2.3: Damage Probability Matrix for Multi-Span Bridges (%) (Basoz and Kiremidjian [47])

		USGS Peak Ground Acceleration(g)						
Observed	Damage	0.15-0.2	0.2-0.3	0.3-0.4	0.4-0.5	0.5-0.6	0.6-0.7	0.7-0.8
None		98.5	92.3	86.2	66	37	55.6	81
Minor		1	2.8	9.2	4.3	22.2	14.8	9.5
Moderate		0.5	2.8	4.6	19.2	22.2	18.5	4.8
Major		0	2.1	0	10.6	18.5	11.1	4.8
Collapse		0	0	0	0	0	0	0

		USGS Peak Ground Acceleration(g)						
Observed	Damage	0.8-0.9	0.9-1.0	1.0-1.1	1.1-1.2	1.2-1.3	1.3-1.4	
None		3	1.00069	2.6688	2.0833	0	4.17	
Minor		0	0.70972	0.2924	2.0833	0	0	
Moderate		0.6667	1.00069	0.8778	0	0	0	
Major		0.1667	1.29167	0	0	0	0	
Collapse		0.3333	0.12847	0.2924	0	0	0	

The third type of method used by researchers is analytical fragility curves method. When historical damage data of bridge structure due to past earthquake events are not available, analytical fragility curves must be used to assess the performance of highway bridges. Many researchers adopted different methodologies for finding analytical fragility curves. Probability of exceeding each limit states P_i can be described as following:

$$P_i = P(D - C_i \geq 0) \quad (2.7)$$

Where i is indicator of i_{th} limit state, D is the demand of the structure given the ground motion intensity and C_i is the capacity of the structure for the indicated limit state. There are various methods for assessment of the demand of the bridge structures. Below is the summary of these methods:

2.7.1 Elastic Spectral Response

In this method demand on the bridges was determined by performing an elastic spectral analysis of the bridge models using a computer program. Yu et al. (1991) [50] illustrated the use of this approach for assessment of seismic vulnerability of highway bridges in Kentucky. Later Jernigan and Hwang (2002) [51] further developed this method to provide this method for practicing engineering. However this method is simplistic and cannot capture the nonlinearity associated with highly complex systems like bridges.

2.7.2 Non-Linear Static Analysis

This method is a non-linear static procedure and is commonly called the Capacity-Spectrum method. The basic methodology uses a converted non-linear static pushover curve in concert with a reduced response spectrum. The same methodology was adopted in the generation of seismic bridge fragility analysis of HAZUS (FEMA, 2003) (1999) [52]. Mander and Basoz (1999) [54] used this methodology to create seismic fragility curves for standard classes of bridges across the United States. Shinozuka et al. (2000) [48] used this methodology on a three-span continuous concrete girder bridge in the Memphis, TN area.

2.7.3 N2 method

N2 is simple non-linear method used for calculation of structures during earthquakes. It combines multi degree pushover analysis with spectrum analysis of equivalent single degree of freedom (SDOF) system. It is formulated in acceleration-displacement format, which is suitable for visual overview of basic variables that account for seismic response of the structure. N2 method can be considered combination of pushover analysis and spectrum analysis. It previously have been used for MDOF frame structures rather than bridges however the applicability of method have been extended to bridge structures (Fajfar et. al. (1989) [55]). Inelastic demanded spectrum is obtained from elastic spectrum. Seismic load (demand) in N2 method is defined in the shape of elastic acceleration spectrum Figure 2.8. For better visualization seismic demand in N2 method is defined as elastic spectrum in acceleration-displacement format. Here is a very brief description of the N2 method described in (Peter Fajfar (2000),[56]). The Relevant equations required to perform the procedure can be find in (Peter Fajfar (2000) [56]). Equivalent SDOF elastoplastic model needed to be chosen for the MDOF structure. Pushover analysis on the structure needed to be performed and the parameters of SDOF system (equivalent pre-yielding period, yielding displacement and force) needed to be obtained from the results of pushover analysis.

The capacity diagram can be obtained using base shear, conversion factor from MDOF to SDOF equivalent system and equivalent mass of the structure. The demand and capacity are presented in acceleration-displacement (AD) graph. For a given demand acceleration, elastic spectra can be obtained. Also for a certain constant μ (ductility) value, the nonlinear AD spectra can be computed. The μ value itself can be obtained using AD elastic spectrum and $R_{\mu} - \mu - T$ well-known equations for SDOF elasto-plastic systems.

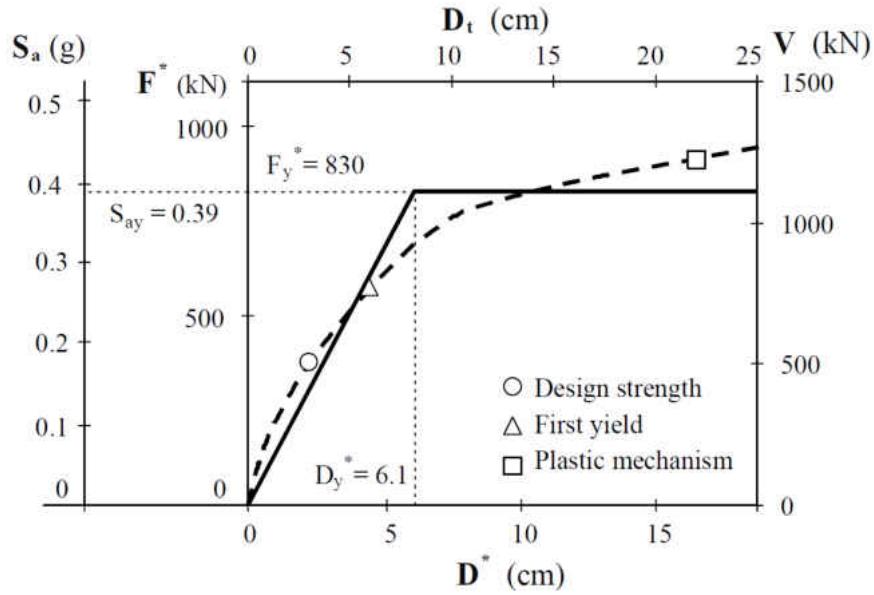


Figure 2.8: Pushover analysis (dash line) and equivalent SDOF force-displacement properties. D_t and V are top floor deformation and shear at ground level for the MDOF structure, D^* and F_y^* are displacement and yielding displacement for SDOF equivalent system. (Peter Fajfar (2000) [56])

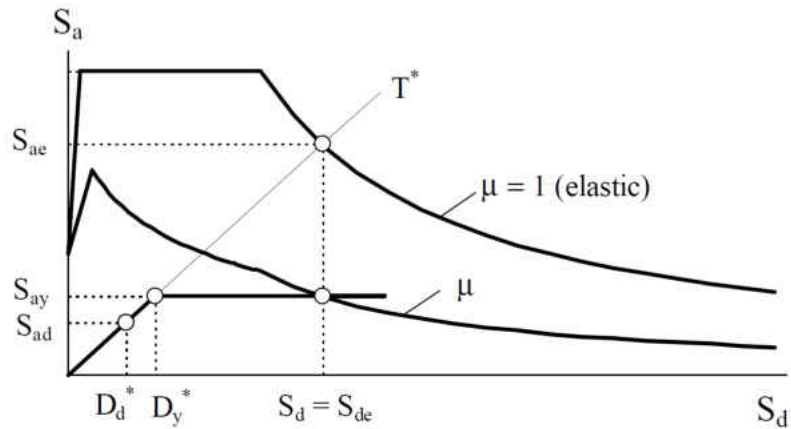


Figure 2.9: Elastic and inelastic demand for equivalent SDOF system versus capacity of the SDOF system. (Peter Fajfar (2000) [56])

The intersection of demand inelastic spectrum and capacity (S_d) in Figure 2.9 is the demand of the equivalent SDOF system. Consequently the demand for SDOF system needed to be converted to MDOF top node deformation (D_t). Pushover analysis is performed for MDOF system until it reaches the D_t deformation. Note that D_t represents the mean value of the applied earthquake loading. The performance of MDOF structure can be obtained by comparing seismic demand (pushover analysis until D_t value) with the capacity of the structure.

2.7.4 Non-Linear Time History Analysis

Non-linear time history approach is the most reliable methodology available for generating seismic fragility curves (Shinozuka et al., 2000 [48]). The general methodology used by researchers can be seen in figure 2.10, although there is a slight variation between the nonlinear time history analysis methods that researchers utilized for obtaining the demand model of the structure. For obtaining the demand of the structure sampling techniques are used by most of the researchers. Cornell et al. (2002) [57] utilized a methodology using regression analysis to generate a probabilistic seismic demand model for structures. The same approach adopted by Mackie and Stojadinovic (2001) [58] to generate probabilistic seismic demand models for typical California over-pass bridges. (Bignell et al., 2004; Choi et al., 2004 [64, 65]) also used regression analysis over the seismic response of the structure for finding the demand parameters. Logistic regression analysis of the response simulation (Hwang and Huo, 1998 [66]) and the Maximum Likelihood Method (MLE) to model the column responses to the chosen earthquake intensity measure (Shinozuka et al., (2003) [59]). On the other side the capacity or limit states of the bridge can be described using experimental or analytical approaches. Static pushover, adaptive pushover and incremental dynamic analyses are some examples of analytical techniques. These evaluation of the capacity model can be performed using a sampling technique (Vamvatsikos and Cornell, 2002 [36]) or a first order reliability method (FORM) (Mackie and Stojadinovic, 2004 [42]). Figure 2.10 shows the

step by step procedure of performance-based assessment of bridge structure taken from (Nielson 2005 [30]).

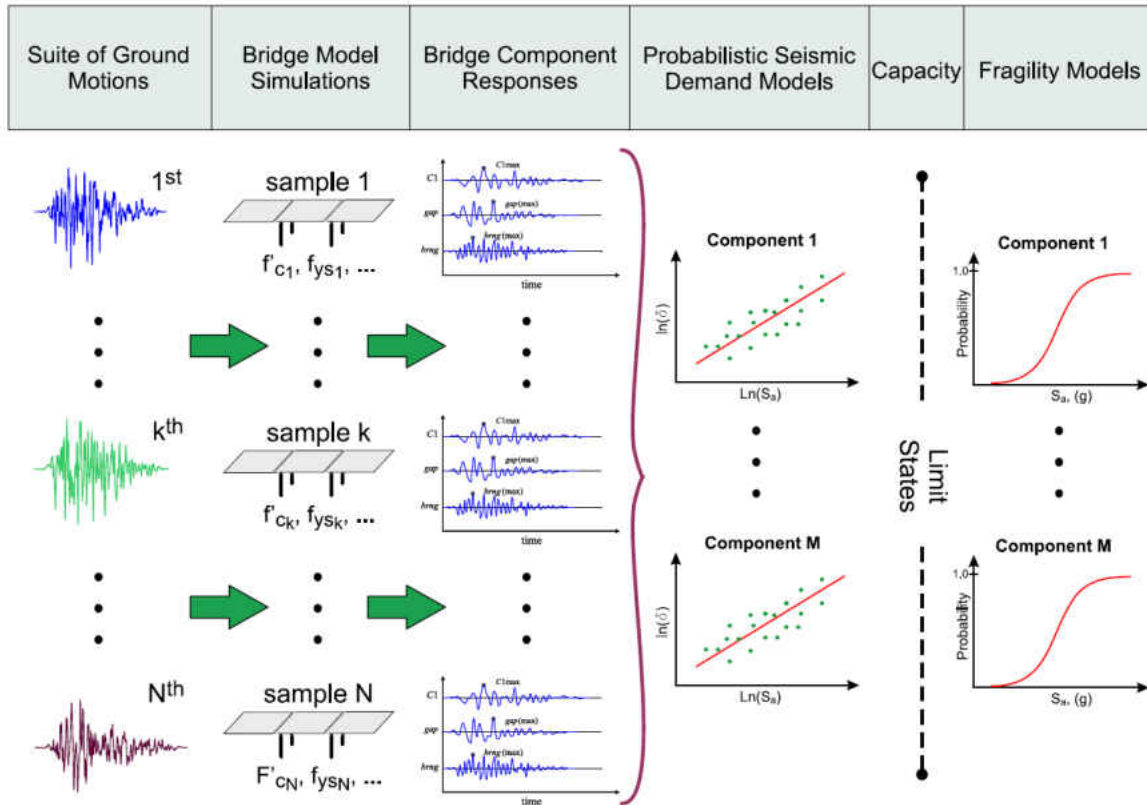


Figure 2.10: Analytical Fragility Curve Generation (Nielson 2005 [30])

2.8 Uncertainty associated with performance-based assessment

There are various sources of uncertainty can be realized in each step of performance-based assessment of the structures. Hazard analysis, measuring the demand of the structure for different levels of hazard, measuring structural damage associated with various level of demand and the cost associated with each level of damage and etc. are some examples of these sources of uncertain-

ties. Each PBA step involves various parameters and assumptions that are origin of uncertainties. Nielson has investigated some of the epistemic uncertainties in performance-based assessment of nonlinear bridges. He utilized design of experiment (DOE) methodology to screen the parameters that should be treated as probabilistic in the bridge analytical model. Mackie et al. (2011) [60] have investigated the effect of aleatory uncertainties in ground motions randomness incident angle in addition to the epistemic uncertainties that come from randomness in modeling and material properties. In their research, three cases that represent different categories of uncertainties were investigated to illustrate the effect of aleatory and epistemic uncertainties on the fragility curves results. For the first case they applied a simulation-based approach to capture the correlation between random quantities used in Latin hypercube sampling at the demand stage and the damage state definitions. The second case uncouples the demand and damage stages by considering only the non-damage-state-dependent uncertainties in the demand stage. Finally, the third case considers the previously uncoupled method of Mackie and Stojadinovic (2007) [61, 62] where all epistemic uncertainties enter only during the damage stage. The results from their research conclude that between the uncertainty classes considered, aleatory uncertainties originated from randomness of the ground motions are the most influential uncertainty.

CHAPTER 3: SELECTION AND SCALING OF GROUND MOTIONS

3.1 Introduction

Probabilistic seismic assessment of structural response is typically performed to quantify response levels under ground motions representative of different probabilities of exceedance and site/scenario characteristics. It is also used to evaluate fragility or vulnerability that arises when comparing the response to acceptance criteria or limit states (possibly defined in terms of probabilistic “capacities”). Studies that quantify seismic response and utilize the results for design, damage, decision, or risk purposes are commonly referred to as performance-based earthquake engineering (PBEE). Fragility curves are one of the key PBEE tools for quantifying performance and are typically used in risk assessment. Therefore, they directly impact decision making for infrastructure management, such as retrofit prioritization, resilient planning for redundancy, improvement of emergency response based on a-priori performance predictions, and comparison of different design alternatives in a performance-based design context.

To perform seismic response analysis (SRA) for the purposes of probabilistic response assessment or fragility analysis, a catalog of ground motions is required that covers a range of intensities relevant to generate response near the limit being considered. Usually a single scalar intensity measuring parameter is selected to describe the ground motions and the corresponding correlation with both structural response and probabilistic seismic hazard analysis (PSHA). The problem is that either there are not enough historical recorded motions of substantial intensity (i.e., central and eastern US), or the structure is stronger than currently recorded motions can significantly excite into the inelastic range.

3.1.1 Selection and scaling of ground motions

Common solutions to the lack of high intensity ground motion records are to modify existing motions (amplitude or frequency) or to generate synthetic motions. A variety of scaling methods such as amplitude scaling, amplitude and linear scaling for spectral acceleration (Sa) at the first structural period Sa (T_1) [5], linear scaling of Sa over a period range [8], and scaling using spectrum matching [9] have been used previously. In amplitude scaling of the ground motions, engineers seek a suite of ground motions with similar site characteristic as the site of the structure under consideration, or ground motions that minimize the difference with some target elastic spectrum at multiple periods (a good review of some of the common methods is contained in [4]). Consequently each record may be scaled to multiple target intensities to preserve the proportionate distribution of the intensity measure (IM) of interest.

Synthetic earthquake ground motions have been used when appropriate recorded ground motions are not available. Many types of synthetic ground motion models have been developed in the past years and many are still under development. These models can be classified in three categories [18]: 1) seismological models of site rupture mechanism and wave propagation, 2) parameterized stochastic models fitted to previously recorded ground motions, and 3) hybrid models employing a combination of first and second method elements. Seismological and hybrid models did not see widespread adoption in practice because they require extensive computation and thorough knowledge of the site characteristics, source, and wave path, which vary significantly by region [20].

Scaling of ground motions has raised significant concerns over whether a record that has been scaled to a target intensity has the same effect on the structure compared to a record that is naturally at the target intensity. Or more specifically, little consensus exists on what scale factor would be considered appropriate or inappropriate for amplitude scaling. Grigoriu demonstrated

using random processes [7] that amplitude scaling produces ground motion processes with different probability content, with differences quantified by skewness and kurtosis. He also studied the probability content of both linear and nonlinear oscillator responses with similar results.

Previous numerical studies show that scaling of ground motions can cause bias in response of nonlinear structures. Shome et al. [5] addressed the illegitimacy of scaling more directly whereas Sewell [11], Iervolino and Cornell [12] and Baker [13] indirectly addressed the bias induced by scaling. According to Luco and Bazzurro [14] these studies had little impact on engineering practice because the conclusions are limited by statistical concepts and findings.

In more recent studies, Luco and Bazzurro [14, 20] investigated the bias associated with scaling in the median nonlinear structural drift response for a target S_a , and conclude that records with the same value of $S_a(T_1)$ should be considered in the selection of records to avoid bias in the median response. According to their studies, period elongation of the nonlinear system is an important factor that causes bias in the scaling procedure of ground motions. They investigated different periods and strengths (for computing bias), but the justification for the cause was limited to a single case where ground motions were selected that matched the target spectra most closely. Numerous other methods exist in the literature for selection and scaling of ground motions. Many of these were investigated in parallel as applied to response history analysis of buildings [23], with similar conclusions to the previous studies regarding importance of spectral shape. The Bias in ground motion scaling has also been observed to add significant amount of uncertainty to fragility analysis results [16], a topic explored directly at the end of this research.

Two previous studies implicitly used the method studied in this research to guarantee that the mean inelastic responses are the same. Watson-Lamprey and Abrahamson [10] proposed a method for selection that allows amplitude scaling limits much higher than would be appropriate for limiting bias if randomly selected motions were used. They use a simple nonlinear model as a proxy to

guarantee that the mean inelastic response under scaling matches some target (Newmark displacements were used). The target displacement surface of Shantz [19] is also a similar approach in that the selected motions and scale factors are based on inelastic response of nonlinear SDOF oscillators. The Shantz procedure works by modifying the elastic S_d based on the normalized inelastic displacement demand, which has parallels with considering response in different periods for the inelastic system.

Huang et al. [15] used four different scaling procedures including geometric-mean scaling, spectrum matching, $S_a(T_1)$ scaling, and distribution-scaling to quantify bias induced in the spectral shape and median S_a , as well as dispersion in nonlinear responses of the structures. The study by Huang et al. [15] was limited by the scaling based on S_a , and the conclusions are limited to first-mode-dominated buildings with minor to moderate inelastic deformation. Epsilon (ϵ) has significant correlation with S_a [13] and has been considered a predicting parameter for structural response and bias. It is defined as the number of standard deviations by which an observed logarithmic spectral acceleration differs from the mean logarithmic spectral acceleration of a ground-motion prediction (attenuation) equation. When using S_a as an intensity measuring parameter of ground motion records with negative epsilons tends to have more intensity on other periods compared to records with positive epsilons. As a result, scaling the records with negative epsilon values can induce positive bias in nonlinear response of the structure. Epsilon values can not be used as an intensity measuring parameter in record selection strategies because they are being measured relative to an attenuation function. However, ϵ can explain and predict bias induced by amplitude scaling to some extent.

The conditional mean spectrum (CMS) is commonly accepted as more representative of response of structures to ground motions than the uniform hazard spectra (UHS). The CMS [24] is constructed by modifying the attenuated median spectrum with a term that includes the ϵ and S_a at a target period (the conditional information). A correlation function for ϵ at different periods based

on ϵ at the target allow computation of the CMS at periods other than the anchor point. A generalization of the approach for other intensity measuring parameters has also been proposed [26]. Recent requirements in ASCE 7-16 require selection of ground motions that match the CMS between $0.2T_1$ to $2.0T_1$, which is also a requirement for matching records in EC8 (in consideration of nonlinear response of buildings with both higher modes and softening). There is anecdotal evidence to suggest that selecting motions in this manner does not result in biased response of nonlinear systems [24, 23], a result that will be quantified directly in this research. Several software tools are emerging (e.g., Rexel [27]) to select motions that match target spectra and additional causal parameters.

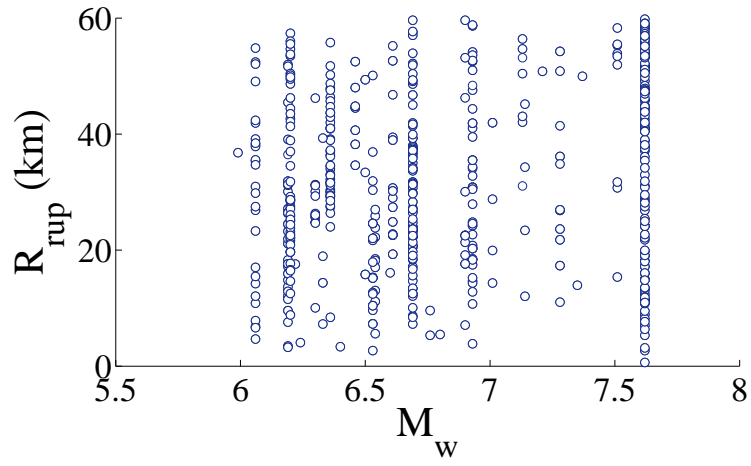
3.2 Method

Dependency of bias associated with amplitude scaling for three different types of nonlinear systems, amount of scaling, and methods for selection of bins were studied. Bias is quantified using the bias ratio presented in this section, which is a measure of the mean nonlinear response bias, as well as the impact on the fragility assessment. The three simple structures, selected to be representative of commonly used forms of structural nonlinearities, were subjected to excitation by two general suites of ground motions - one recorded and one synthetic - to check the consistency of findings. To check the influence of scaling on the bias, comparisons must be made between structural response when no scaling is used and structural response when scaling is used. These comparisons are made for typical scaling parameters that are used to measure ground motion intensities. Based on the biased nonlinear response statistics observed for various IMs, a new intensity parameter (called SDI) was utilized to minimize the bias induced from amplitude scaling. It is then demonstrated that the bias in nonlinear response can be quantified directly using simple linear analysis and SDI. Finally, the bias estimates utilizing some common scaling procedures from the

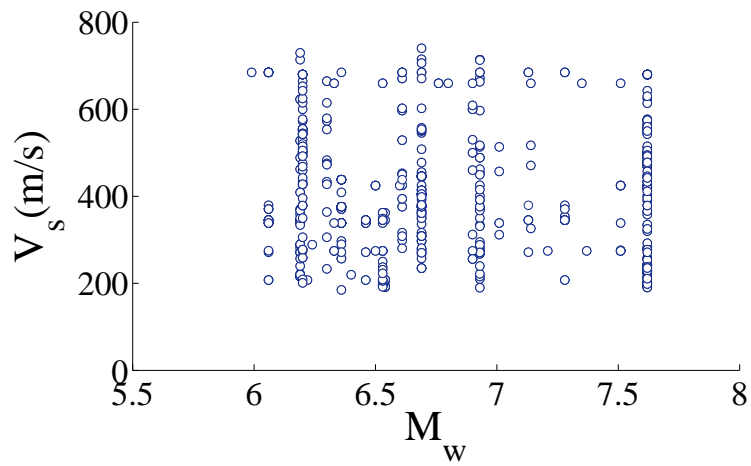
literature are computed and compared to that obtained using SDI.

3.2.1 Selection of ground motions

For this study, two suites of ground motions were assembled - one of recorded ground motions and one of synthetic ground motions. The first suite consists of many recorded earthquakes which were selected from the Pacific Earthquake Engineering Research (PEER) Ground Motion Database [29]. Records were identified from different sites based on parameters that represent basic engineering or seismological characteristics: M_w , R_{rup} and $V_{S,30}$, where M_w is the moment magnitude of the earthquake, R_{rup} is the shortest distance from the recording location to the rupture area, and $V_{S,30}$ is the shear wave velocity of the top 30 meters of the site soil. For this study, earthquakes with M_w greater than 6.0 were selected to ensure larger magnitude events that are more likely to cause nonlinear response. Similarly, far field records with R_{rup} greater than 60 km were not considered. No lower limit was placed on R_{rup} , so records that exhibited near fault characteristics, such as pulse and fling, had to be explicitly removed from the suite of records. The $V_{S,30}$ of the records selected was limited to the range of 180 m/s to 760 m/s to be consistent with USGS soil types C and D. After considering these constraints, a suite of 566 ground motions was identified. Neglecting the vertical components of these records, the two horizontal orthogonal time history components were treated separately. This provided 1132 time histories which could be used for analysis purposes. To give an overall understanding of the recorded motion suite, Figures 3.1(a) and 3.1(b) show the scatter plots for M_w versus R_{rup} and M_w versus $V_{S,30}$, respectively. An idea of spectral content and variability is provided in the displacement response spectrum of Figure 3.2.



(a) Distribution of M versus R_{rup}



(b) Distribution of M versus $V_{S,30}$

Figure 3.1: Properties of recorded ground motion record suite

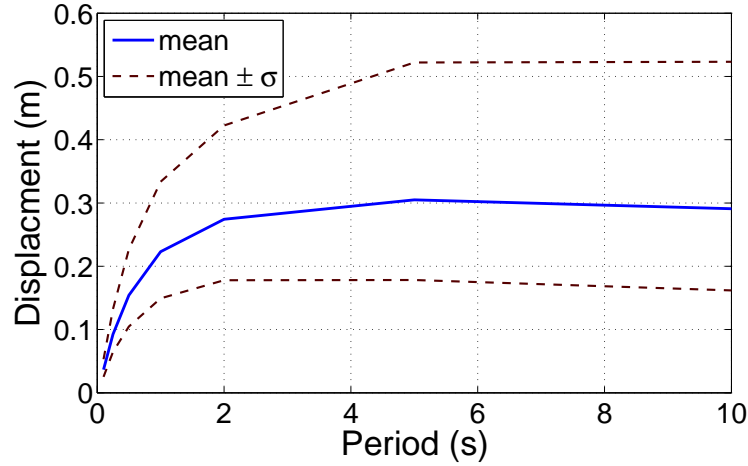


Figure 3.2: Mean and mean $\pm \sigma$ displacement response spectrum

A suite of synthetic ground motions was also assembled to serve as a comparison with the findings from the as-recorded ground motions. The stochastic synthetic motion generating procedure of Rezaeian and Der Kiureghian [21] was utilized for generating the synthetic ground motions. Earthquake site characteristics are used as the input parameters for simulating an ensemble of records, and only M_w , $V_{S,30}$, R_{rup} , and fault type are required input parameters. The ground acceleration process is described as the response of a linear filter with time varying parameters to white-noise excitation. The filter response is normalized by its standard deviation and is multiplied by a deterministic time-modulating function. While modulation of the process in time introduces temporal nonstationarity, variation of filter parameters provides spectral nonstationarity. The method generates orthogonal lateral components of ground motions by determination of the correlation between the parameters obtained from predictive equations developed for model parameters of each component.

The use of only earthquake site characteristics as input to the model allows for the parameters of the as-recorded motions to serve as the input parameters for synthetic ground motion generation as

well. Therefore, a suite of synthetic ground motions which are nominally similar to the real ground motion suite can be generated. A total number of 566 pairs (1132 records) of ground motions were generated using the same site characteristics of the as-recorded earthquakes. Inspection of the intensity parameters of each individual record led to removal of 4 records due to their large value for Arias Intensity ($I_A \geq 40$ m/s).

3.2.2 *Nonlinear structural systems defined*

For this study three different nonlinear system types were considered. The first system is a simple nonlinear system that exhibits elastic-perfectly plastic response in a single dynamic degree of freedom (SDOF) - see Figure 3.3(a). The SDOF oscillator has a mass of 1 kg and includes 5% equivalent viscous damping. Characteristics of this nonlinear system are presented using pre-yielding stiffness (K) and yielding strength of the system (F_y). Pre-yielding stiffness also determines the initial period of the oscillator ($T = 2\pi\sqrt{mass/K}$). The yielding strength is the only parameter that differentiates this system from linear systems. The model unloads and reloads along the same initial stiffness.

Three common approaches for selecting the properties of SDOF nonlinear systems are to set F_y (yielding strength) to be constant, set the force reduction factor, R , as a constant, or to set the ductility factor, μ , as a constant. Based on [25] and similar studies, the relationships between R and μ are known for each period of the structure for the mean response of a nonlinear system. In this study, to prevent a mixed scaling method for the amplitude scaling of ground motions, a constant F_y approach was adopted. Bias induced by amplitude scaling will have the same trend for these different approaches (constant R and μ) due to the correlation between R , μ , and T . However, one should acknowledge that the actual magnitude of the bias will be different depending on which approach is adopted.

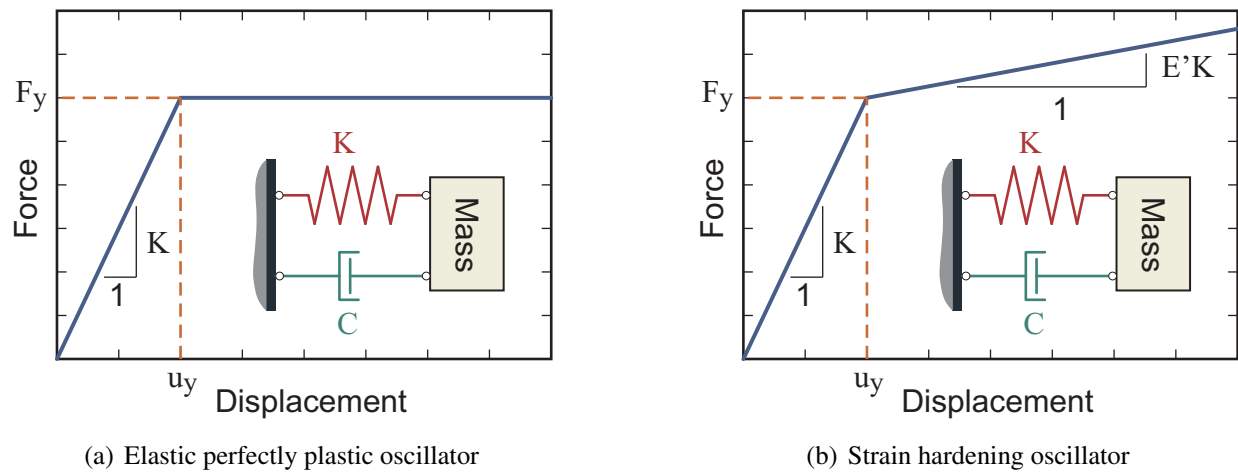


Figure 3.3: Nonlinear SDOF system behaviors

The yield strength of the nonlinear system was chosen as $F_y = 0.2$ N by experimentation to ensure that the system will enter the nonlinear state for most of the ground motion records which were considered. This seemingly low yield strength occurs only because of the small mass which was used (1 kg) to build the SDOF system. Selecting this value of F_y resulted in yielding for 82.7% of SDOF systems with periods between 0.1 to 5 sec. This is considered to be an acceptable threshold. Figure 3.4 shows the percentage of as-recorded ground motions that cause yielding for a SDOF system with $F_y = 0.2$ N based on period. Naturally, as the period lengthens, the structures become less influenced by the typical ground motions as is clearly seen.

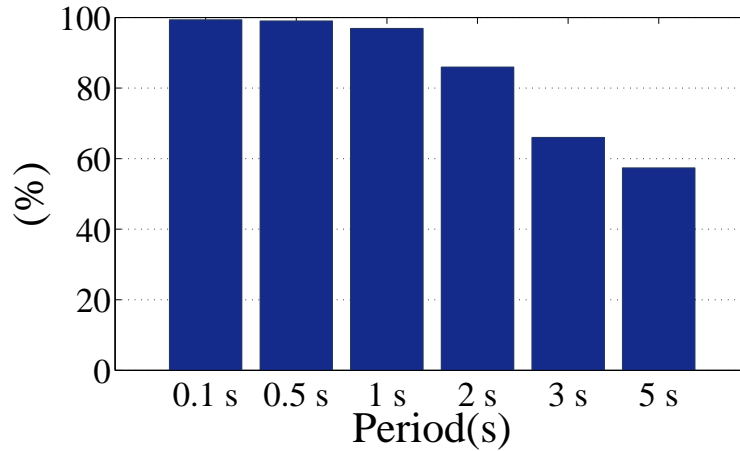


Figure 3.4: Percentage of ground motions inducing yielding observed for SDOF system with $F_y = 0.2 \text{ N}$

The second nonlinear system considered, shown in Figure 3.3(b), is similar to the first system in that it is a bilinear SDOF system. However, it has a post-yield hardening ratio (E') equal to either 0.01 or 0.2. The yielding strength (F_y) of the bilinear SDOF system was the same value as that for the elastic-perfectly plastic SDOF systems.

For consideration of more complex nonlinear response, a third type of nonlinear system was introduced. A reinforced concrete frame with nonlinear properties for both reinforcing steel and concrete was modeled as a two-dimensional MDOF dynamic system as shown in Figure 3.5. Ground motions were imposed on this frame in the horizontal direction. The MDOF system consists of a pin-supported frame with two columns and one beam. The frame was not intended to directly represent an as-built case, but rather an MDOF extension to the previous two systems by incorporating more complex nonlinearities in the cross section. The frame is symmetric and the properties of the vertical members are identical. The height of the column was assumed to be 7.3 m and the width of the frame span was 10.9 m. Horizontal and vertical lumped masses were assigned to the top nodes of the frame (top node of each column). The flexural stiffness of the beam was assumed

to be large (20 times) relative to elastic column stiffness to simulate a shear type building. The joint connection between the elements was assumed to be rigid. Due to the rigidity of the beam, the system behaves approximately as a SDOF system, and is therefore not intended to highlight effect of higher modes on amplitude scaling.

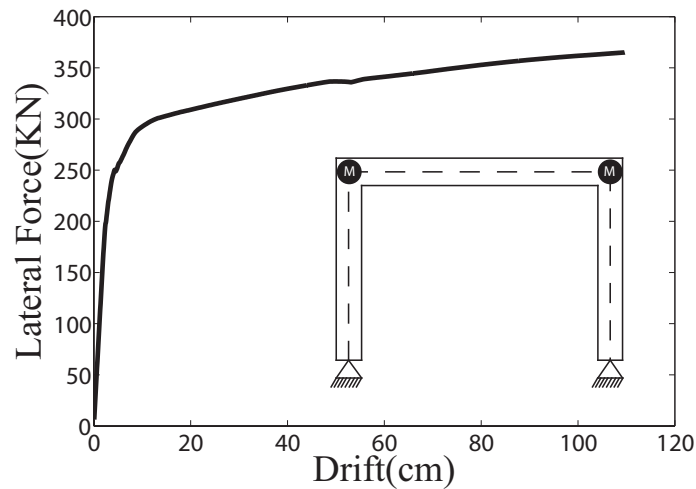


Figure 3.5: Pushover curve of MDOF frame

The OpenSees software was used for modeling and nonlinear dynamic analysis of this frame. Non-linear fiber-based beam-column elements were used with discrete concrete and steel constitutive relationships. The columns are circular with a radius of 60 cm. A longitudinal reinforcement ratio of 0.2% was selected with a concrete cover of 3 cm. Although it appears to be low, the level of reinforcement was selected to once again ensure that inelastic response occurred for most of the ground motions. Figure 3.5 shows the pushover curve for this frame. The horizontal axis is lateral displacement of the top joints of the columns and the vertical axis is the overall base shear in the frame. The mass of the structure was selected to assure the the pre-yielding period of the frame was equal to one second. This was based on the pre-yielding stiffness obtained from pushover analysis.

3.2.3 General method for identification of bias in scaling

To quantify bias in nonlinear response, a comparison between scaled and un-scaled ground motion responses was conducted. This comparison is performed initially for four typical scaling parameters. The scaling parameters selected, also called intensity measures (IMs), are: peak ground acceleration (PGA), peak ground velocity (PGV), cumulative absolute velocity (CAV), and elastic spectral displacement with 5% equivalent viscous damping (Sd), respectively.

For any of the four intensity measures, two bins of ground motions were assembled for each scale factor investigated. Bin one contains records that should be scaled by the target scale factor to match the intensity of the records in bin two - where bin two will serve as the control in the comparison study. The bins were constructed by selecting ground motions from the overall suite of 1132 motions. The i^{th} record in bin one was selected such that if the amplitude is scaled by the target scale factor of interest, its *IM* magnitude matches the *IM* magnitude of the i^{th} record in bin two. As an example, if binning is done with respect to PGA and a target scale factor of two, the PGA of the i^{th} record in bin two should be two times greater than the PGA of the i^{th} record in bin one (within a nominal tolerance). The only exception for this procedure is binning based on Sd values. For selection of the records for each bin based on Sd, the variation of the elastic response of the structure with a change in the system period was also accounted for.

Bin selection was repeated for scale factors of ranging from 0.1 to 10 for each different type of nonlinear system. The nonlinear systems were selected with elastic periods varying from $T = 0.1$ to 5 sec. Remember that each bin is a subset of the original 1132 ground motions which means that each of the two bins cannot technically have more than 1132 ground motions if each ground motion is allowed to appear in both bins. Realistically, the two bins will have a number far less than this since bin size is dependent upon the number of available ground motion pairs that could describe a certain scale factor. Indeed, the farther a scale factor is from 1.0, the fewer ground

motion pairs can be found to capture that scale factor. Table 3.1 provides a summary of the bin sizes which were able to be used for a given IM and a given scale factor.

Table 3.1: Ground motion bin size used to assess different scale factors and intensity measures

IM parameters	Scaling factor						
	0.1	0.5	1.5	2	3	5	10
PGA	134	506	578	506	388	255	134
PGV	161	528	571	528	422	292	161
CAV	102	505	576	505	389	231	101
Sd($T = 0.1$ s)	155	520	581	520	416	286	154
Sd($T = 0.5$ s)	169	554	605	554	426	309	161
Sd($T = 1$ s)	170	516	572	516	422	314	172
Sd($T = 2$ s)	196	540	605	540	453	347	195
Sd($T = 5$ s)	314	571	587	571	511	427	312

The maximum displacement response, u , of each system was tracked for each case shown in Table 3.1. Bias values can be quantified using different metrics, one metric is known as the mean of the ratios, the other one is the ratio of means. However both of these metrics are biased predictors (point estimates) themselves, the former having the tendency of being affected by big ratios and the later one having the tendency of being affected by the high intensity ground motions. The ratio of means was selected for presentation in this research as by observation of the data it produces smoother response. The bias induced by amplitude scaling is computed by taking the mean displacement response from bin one (the scaled bin) and dividing it by the mean displacement response from bin two (the un-scaled bin). This computation is mathematically carried out using Equation 3.1 where the first subscript is the bin number and the second subscript is the ground

motion number. Remember that once bin one is scaled, the IM values in both bin one and bin two should be identical. Thus, this computed ratio should be 1.0 if no bias exists. When the bias value is greater than one it is considered to be a positive bias and when it is less than one it is considered to be a negative bias.

$$\text{bias} = \frac{\sum_{i=1}^n u_{1,i}}{\sum_{i=1}^n u_{2,i}} \quad (3.1)$$

3.2.4 *Spectrum matching and Average Spectral displacement method*

The effect of period elongation on the response of nonlinear systems and its role in the perceived bias due to scaling is a necessary component of this study. The spectral displacement matching method was utilized to facilitate this investigation. The amplitude and frequency content of each record in the scaled bin were modified so that the resulting spectral displacement matched that of the paired record in bin two. The RASCAL method was used as the spectrum matching scheme [67] over a range of periods between 0 and 5 seconds. Figure 3.6 shows an example of the mean spectrum of bins one and two after the applying spectrum matching technique. The bias values were then quantified using these spectrum matched ground motions (i.e., bin two) and compared to the non-spectrally altered ground motions (i.e., bin one).

Stiffness degradation and post yielding stiffness in nonlinear structures can change the predominant response period of the structure. For SDOF nonlinear systems, the average period of vibration for the oscillator can be obtained from a response history frequency analysis. Assuming an average nonlinear period (or some secant period) for the SDOF systems, the maximum displacement of two records with similar spectral characteristics should be equal. Bias values induced by amplitude scaling were computed using the method proposed in Section 3.2.3. Comparison between the results obtained from spectrally matched with originally selected bins can illustrate the extent of the relation between bias values and period elongation.

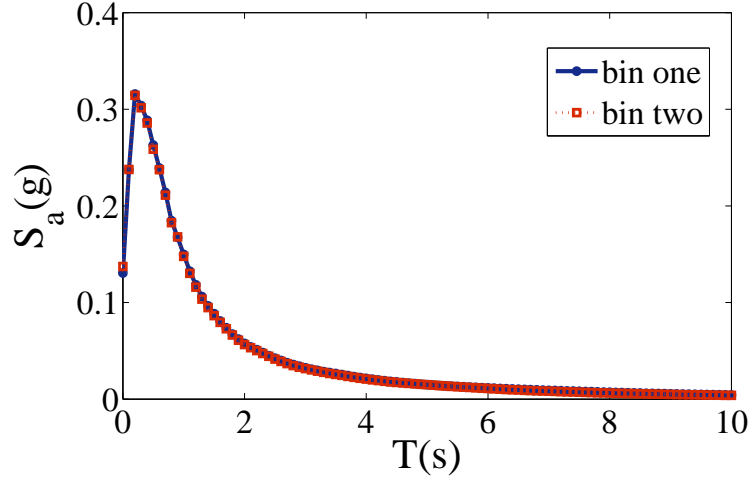


Figure 3.6: Spectrum matched mean spectra for scaled bin one and un-scaled bin two, based on PGA binning

To capture the effect of stiffness degradation and the resulting period elongation on the response of nonlinear systems, a new IM is utilized and denoted as the spectral displacement intensity (SDI). The definition of this parameter is a generalization of the original Housner Intensity [33]. Kadas [35] essentially proposed an SDI-like parameter (which they named I_A , but is not the same as Arias intensity), but defined in terms of S_a instead of S_d . However, they went on to normalize the parameter by the structural yield acceleration and weight periods further from the fundamental period; therefore, the SDI in this research is more general for any oscillator and does not require as many inputs. Assuming that the initial period and the period elongation are equal to T_i and δT , respectively, SDI can be computed using Equation 3.2.

$$SDI = \frac{A}{\delta T} \quad (3.2)$$

where A is the area under the spectral displacement curve over the period range of $[T_i, T_i + \delta T]$. SDI and S_d are both representative of the intensity of the ground motion. Figure 3.7 illustrates the

quantification of SDI values for several response spectra. The superiority of SDI over S_d is due to the consideration of spectral intensity at several periods, unlike S_d which is a single point estimate of the intensity of the ground motion. A single point estimation of the ground motion intensity may be sufficient for a linear system but the nature of nonlinear systems and their stiffness degradation properties demand a more descriptive estimate, as has been used by previous researchers [15].

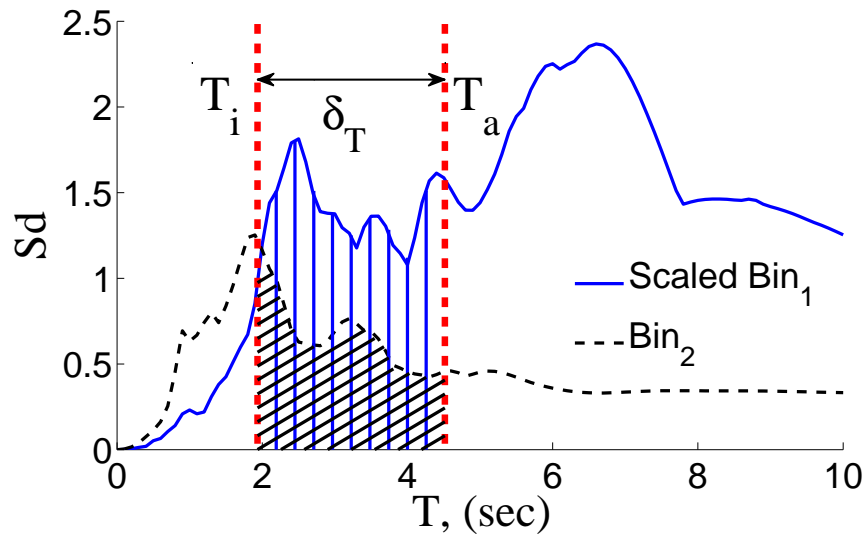


Figure 3.7: Relevance of SDI in capturing response of softening nonlinear systems

3.3 Results

3.3.1 Bias ratio based on recorded ground motions

The bias ratios for the elasto-plastic system is first examined. The bias ratio for all the considered scale factors, IMs, and structural periods for this structure are computed using Equation 3.1. Figure 3.8 shows the computed bias ratios when the recorded ground motions are used. The horizontal axis of these plots is the target scale factor, which can be defined as the ratio of intensity of bin two

compared to the unscaled bin one. The vertical axis is the bias ratio defined by the Equation 3.1. At a scale factor of one, the bias ratio is assumed to be unity which implies no bias. The different lines on these figures indicate bias for SDOF systems with different periods but the same yielding strength.

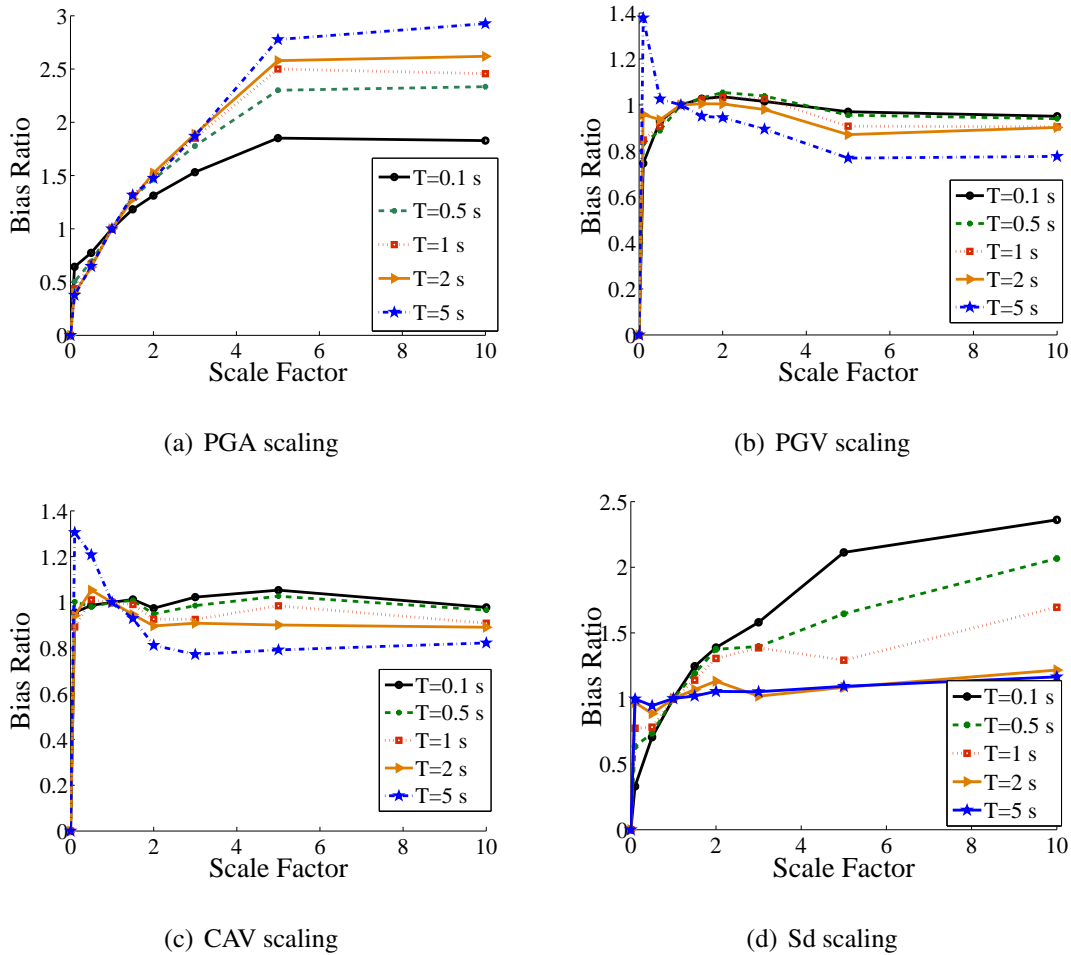


Figure 3.8: Computed bias ratio for the elasto-plastic system

Figure 3.8(a) shows the computed bias when scaling is done on the PGA. The general trend in this figure shows a significant bias which increases with scale factor for all structural periods - producing bias ratios in the range of 1.5 to 3.0. PGA is generally considered a good predictor of

response of short period systems. Thus, the bias tends to increase with increase of period of the SDOF nonlinear system. This also indicates, however, that a portion of the bias for larger periods is actually indicative of the mapping between PGA and an IM specific to the structural period, e.g., $S_d(T_1)$, as well as the bias induced from scaling alone.

Figures 3.8(b) and 3.8(c) illustrate the bias ratio values for different scale factors and scaling based on PGV and CAV. These graphs show that scaling based on both of these IMs lead to much smaller observed bias as compared with PGA. When $T = 5$ sec for a scale factor of 0.1 the bias does tend to spike. not as severely as for PGA but still produces a bias in the 30% - 40% range. Thus, except for the system with long period (5 sec), when the scale factor varies between two to ten, the bias ratio is nominally equal to one. This is especially true when one compares these results to the PGA results - see Figure 3.8(a). This phenomenon is explored in more detail later.

Figure 3.8(d) shows the bias associated with scaling based on S_d . Between all of the intensity measures considered in this study, S_d is the only variable that incorporates both the intensity of the record and (elastic) characteristics of the structure. This figure demonstrates that systems with smaller periods tend to have more bias for different scale factors, while for softer systems, the bias ratio is close to unity. Long period structures tend to behave close to linear structures especially for low intensity ground motions; therefore, the bias values for $T = 3$ sec and $T = 5$ sec are close to one. Results for binning based on S_d also show smaller bias compared to binning based on PGA, because, as mentioned above, there is no bias sourced from the mapping of the intensity parameter to a spectral value.

To investigate the effect of post-yielding behavior of the oscillator on bias, several bilinear oscillator results are also presented. In Figure 3.9, the results for a bilinear system with a 20% stiffness hardening ratio are presented. Similar to bias values for the elasto-plastic systems scaled on S_d , the bias values are significant for long periods. However, for short periods, the bias ratio values

are negligible. A comparison between Figure 3.9 and Figure 3.8(d) shows the numerical bias magnitudes for the 20% bilinear system are less than the elasto-plastic counterparts. This observation can be explained by the characteristics of the oscillator: the average period of response in the bilinear system is closer to the linear period as compared to an elasto-plastic oscillator with the same period and yielding force. This means that the response of a bilinear system tends toward a linear system as the stiffness hardening ratio tends to 100%. Conversely, as the stiffness hardening ratio tends toward 0%, then results converge to the elasto-plastic case in Figure 3.8(d). Therefore, the bias results for the oscillator with 1% stiffness hardening ratio are not presented here.

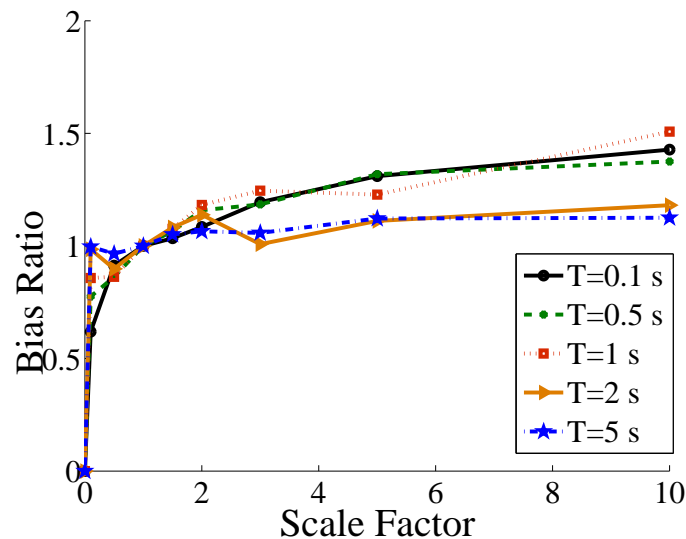


Figure 3.9: Bias in bilinear system with 20% hardening based on Sd

Bias values for the MDOF frame were calculated with the same bins that were used for the SDOF systems which had a period equal to one. Only CAV and Sd were considered for scaling. Figure 3.10 shows the calculated bias values for the frame based on Sd and CAV for as-recorded ground motions. Similarities can be observed by comparing frame results and SDOF system results presented in Figures 3.8 and 3.10. Clearly, bias exists for the MDOF system based on both metrics.

However, the magnitude of the bias when scaling is based on S_d is similar to the values corresponding to a bilinear oscillator having a stiffness hardening ratio comparable to the hardening exhibited by the frame (Figure 3.5). Binning based on CAV appears to minimize the bias which is consistent with the trends observed in the SDOF systems. In fact, the frame responds in primarily a single dynamic degree of freedom, so this finding is not totally unexpected. Possible implications of bias estimation in MDOF systems with widely separated periods is discussed in the conclusions.

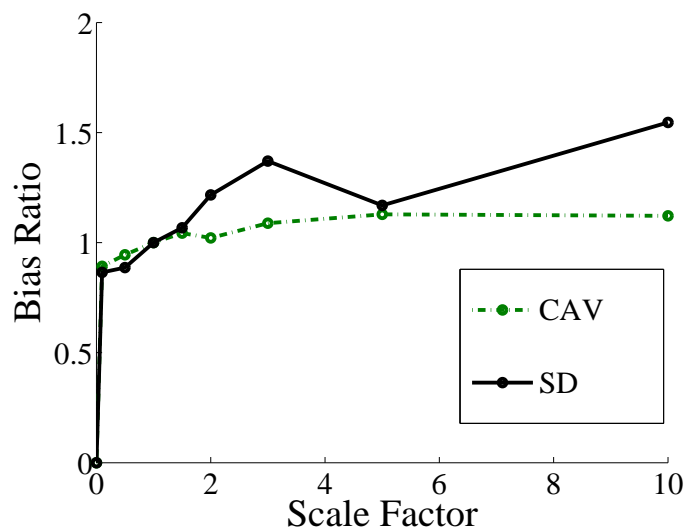


Figure 3.10: Bias for frame based on CAV and S_d

3.3.2 Spectrum matched records

The method described in Section 3.2.1 was used to match the spectral displacement of each pair of records in bin one and bin two. The same bins used in Section 3.3.1 were used here for comparison purposes. Figure 3.11 shows the variation of the existing bias both before and after implementation of the spectrum matching technique previously described. The first two curves show the bias for the SDOF and MDOF structure - each with a pre-yielding period of 1 second. The scaling was based on S_d but the motions were spectrally modified. The other two curves show the results for

the same structures but without using the modified ground motions. These results illustrate that the spectral content of records in bin one and bin two have a considerable effect on the bias induced by amplitude scaling. Using spectrally-matched records between bin one and bin two can reduce (and basically eliminate) this bias. The reason for this is rooted in the period elongation of the nonlinear system. This is where the maximum displacement can be approximated using multi-point estimates of the spectral shape over the elongation range, as is commonly performed when selecting S_a or ϵ at more than one period or using spectrum matching in the codes.

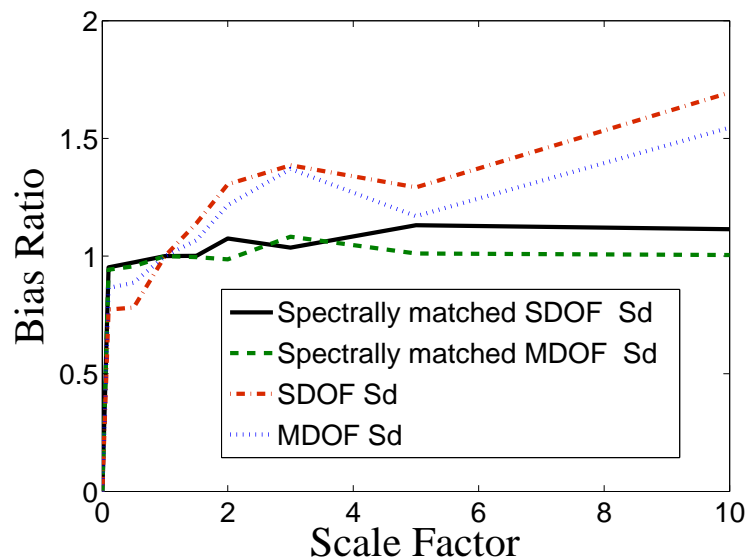


Figure 3.11: Bias values using spectrum compatible bins

3.3.3 Bias estimation based on SDI

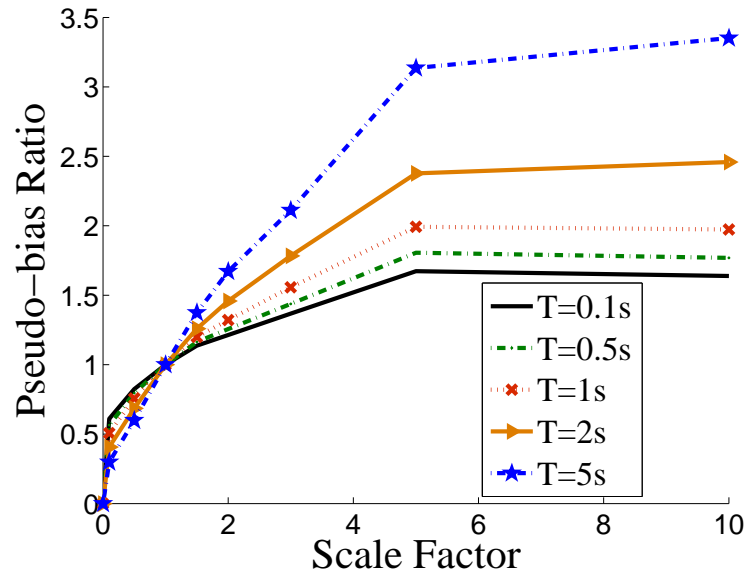
In this section, the SDI parameter was employed to predict the bias caused by amplitude scaling of the initial four IMs. The hypothesis is that if SDI is a good representation of the the intensity of a record applied to nonlinear systems, it should be able to measure and and closely estimate the actual bias caused by amplitude scaling relative to other IMs. For this purpose, the SDI values

for records in each bin were calculated and then the bias values were examined. In Equation 3.1, the ratio of the mean maximum nonlinear displacements was replaced by ratio of the mean SDI values to estimate what is coined the “pseudo” bias. This procedure was repeated for various scale factors and various IMs. Period elongation for computing SDI values was assumed to be 2 sec. The important implication of this hypothesis is that if it is true then the bias induced from record scaling in nonlinear systems can easily be computed using only linear elastic analysis.

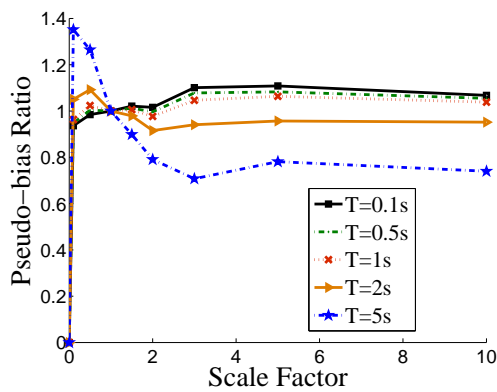
Figure 3.12 shows the regenerated bias graphs using the ratio of the SDI values instead of the maximum nonlinear displacement. In Figure 3.12(a) records were binned and scaled based on their PGA values and then their SDI values were computed and used to calculate the pseudo-bias as previously explained. Comparison of Figure 3.12(a) with the actual bias graph of Figure 3.8(a) shows that a close relation exists for both bias magnitudes and trends between these graphs. For example, for a period of 5 sec and a scale factor of 10, the actual computed bias is 2.92 where the pseudo bias is 3.35. This is less than a 15% error in this estimate. In both graphs one may observe and steady increase in bias as both the period and the scale factor increases. Figures 3.12(b) and 3.12(c) can be compared to Figures 3.8(b) and 3.8(c), respectively for the IMs of CAV and Sd. These demonstrate similar findings where the SDI estimate produces a slightly larger deviation from 1.0 than does the actual estimate.

This comparison shows that SDI values can be a good estimator for the mean of the maximum nonlinear response of the structure subjected to a suite of ground motions and can adequately predict the bias values induced by any amplitude scaling of the ground motions. This is a more efficient approach than the response analysis method described in section 3.2.3. The observed differences between the actual bias values and the pseudo bias values is due to the period elongation value estimate that was chosen for computing SDI. For all the graphs in this section, the period elongation was assumed to be 2 seconds for simplicity as previously explained. In reality this value varies based on the ground motion, scale factor, and nonlinear systems characteristics. The

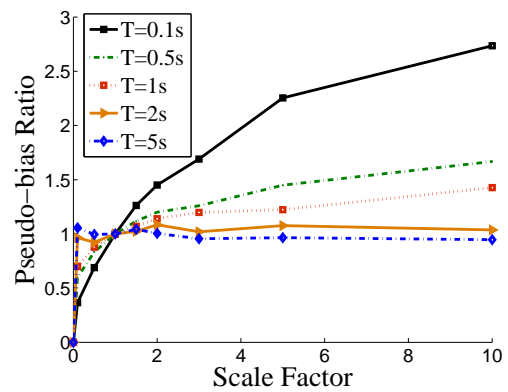
accuracy of this prediction can be improved with employment of nonlinear response analysis for the estimation of period elongation related to various nonlinear systems, scale factors and the IM used for binning. However, one must consider the increase in the time and effort required to recover the approximate 15% error that is currently observed.



(a) Using SDI values for PGA scaling



(b) Using SDI values for CAV scaling

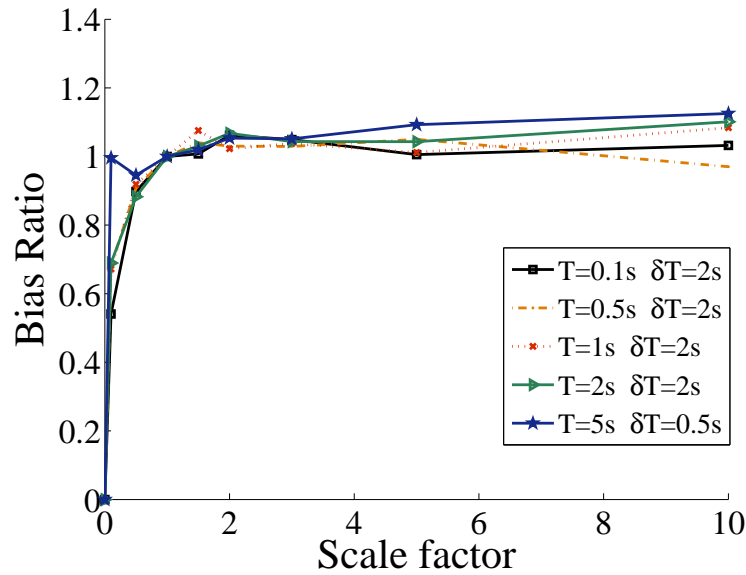


(c) Using SDI values for Sd scaling

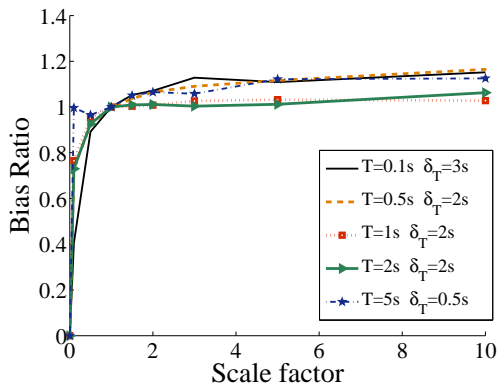
Figure 3.12: Computation of pseudo-bias values using linear spectral analysis only

3.3.4 Unbiased record selection methodology

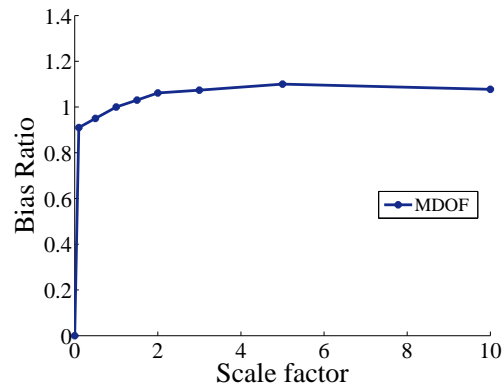
Results from section 3.3.1 show that a substantial bias in nonlinear response exists when amplitude scaling ground motions. This bias can be reasonably estimated indirectly without nonlinear analysis of the structure by using the method introduced in section 3.3.3. Here, an additional step is taken to use SDI as the IM parameter for binning to minimize the bias induced by the amplitude scaling of ground motions. The same binning method described in section 3.3.2 was utilized. The period elongation values were selected from the nonlinear response analysis and captured the fact that systems with less stiffness exhibit smaller levels of period elongation. Figure 3.13 shows the bias graph when binning based on SDI for SDOF system with elasto-plastic nonlinear characteristics. The properties of the system are defined in section 3.2.2.



(a) elasto-plastic nonlinear system



(b) bilinear system with 20% stiffness hardening ratio



(c) Frame with $T = 1s$, $\delta T = 1s$

Figure 3.13: Bias when binning based on SDI

In all figures shown, the bias values for different scale factors and pre-yielding periods (T) are close to one; 1.13 is the maximum value for the bias obtained for scale factor equal to 10 and for a system with $T = 5$ sec. Comparing Figure 3.13(a) to Figures 3.8(a) and 3.8(c) shows that using

SDI values for binning selection can significantly reduce the bias which exists with these other IMs. For example, the maximum bias obtained for a scale factor of 10 for the SDOF elasto-plastic systems were 2.93 and 2.36 for binning based on PGA and Sd respectively. Compare these levels of bias with the 1.13 obtained when binning was done using SDI.

Figure 3.13(b) shows the bias graph obtained for the SDOF bilinear systems having 20% stiffness hardening and for binning based on SDI. The maximum value of bias shown in this figure is 1.16 and belongs to scale factor 10 and $T = 0.5$ s. The bias for this same set of parameters is 1.37 when binning is done using Sd. Overall, comparing Figure 3.13(b) with Figure 3.9 clearly shows that binning based on SDI values can markedly reduce the bias related to amplitude scaling of ground motions used with systems having bilinear stiffness characteristics as compared to binning based on Sd values.

Figure 3.13(c) shows the bias values related to the MDOF system described in section 3.2.2. Binning is based on SDI values for $T=1$ sec corresponding to the first mode of vibration for the structure. The maximum bias corresponds to the scale factor 5 which is 1.09. Comparison between results for originally recorded ground motions in Figures 3.10 and 3.13(c) shows that using SDI IMs in binning procedure can reduce bias values for MDOF system considerably. This maximum bias value (1.09) is less than those seen when binning is based on Sd (1.55) and CAV (1.13).

In all three aforementioned cases, using SDI in the binning procedure reduced the bias values but did not eliminate the bias altogether. The reason lies in the difficulty of obtaining the true period elongation of the nonlinear system. In addition to the maximum deformation, the number of hysteretic cycles, and absorbed hysteretic energy within the cycles of vibration need to be considered. This elongation also varies based on the ground motion characteristics, initial period of the system, scale factor, and yield force of the system. An average period elongation for each point on the bias graph could be obtained by applying all the ground motions inside each bin to the system

and using response analysis techniques. However, one should note that this average period varies over the duration of the vibration and therefore no unique definition exists for the average period of the vibration. Alternative methods are to use approximate formulations [59] based on the target ductility and/or the secant period, or empirical relationships fitted to parametric data [59].

3.3.5 Relation between SDI and velocity intensity parameters

Comparison of Figures 3.8(b) and 3.8(c) with Figure 3.13(a) shows that binning based on SDI is not the only approach to reducing the bias. One may note that binning based on CAV and PGV can lead to reduced bias levels for the nonlinear response of structures. CAV and PGV binning show a negative bias for scale factors more than 1 and positive bias for scale factors less than 1. This trend is just opposite for binning based on SDI. Linear regression analysis was utilized for various system periods to investigate the linear dependency between each IM and SDI. The coefficient of determination R^2 values were obtained to demonstrate this linear dependency, shown in Table 3.2. The period elongation for nonlinear SDOF systems was assumed to be 2 sec here to ensure that a consistent comparison was made; however, even for assumed elongation less than 2 sec, similar results were obtained for the R^2 values. The variation of R^2 for different periods of the nonlinear system can be seen in Table 3.2.

Table 3.2: Coefficients of determination for regression analysis of SDI versus other IMs for various periods of the structure

	T = 0.5 sec	T = 1 sec	T = 2 sec	T = 3 sec	T = 4 sec	T = 5 sec
PGA	0.322	0.171	0.0032	0	0	0
PGV	0.832	0.802	0.660	0.539	0.453	0.401
CAV	0.651	0.614	0.504	0.422	0.359	0.319
Sd	0.444	0.602	0.705	0.801	0.862	0.930

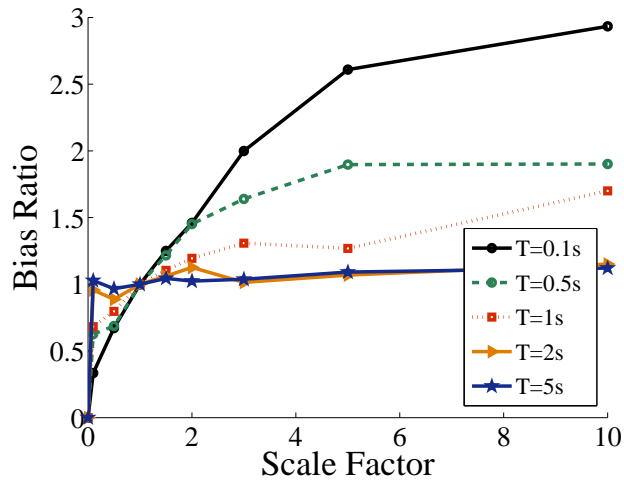
Table 3.2 shows that CAV and PGV have some linear correlation to SDI values, whereas any relationship with PGA rapidly diminishes as the period increases. Based on the method of binning used and definition of bias in Equation 3.1, greater correlation between IMs can result in similar bias quantities. The higher correlation between CAV and PGV versus SDI agrees with the results presented in section 3.3.1. Koliopoulos et al. [38] showed that there is a strong correlation between CAV and Housner Intensity which confirms the high values of correlation coefficient between SDI and CAV. Unlike other IMs, the correlation coefficients of Sd and SDI increase with increase of period which explains the decreased bias values for larger periods in Figure 3.8(d).

The correlation between SDI and PGV originates from the shape of the elastic spectral velocity (S_v) and the so-called constant velocity region of the spectrum. There is a linear relationship between PGV and S_v in the form of $S_v = \alpha_v \cdot PGV$, where α_v is the Newmark factor [40]. Similarly, there is a relationship between Sd and S_v in the form of $S_v \simeq \omega \cdot Sd$. Therefore the mean ratio of SDI values for two bins is approximately equal to the ratio of the PGV values. The constant velocity region of the S_v spectrum only exists approximately in the period range of 0.5 to 3 sec; therefore, low correlation between PGV and SDI exists outside of this range.

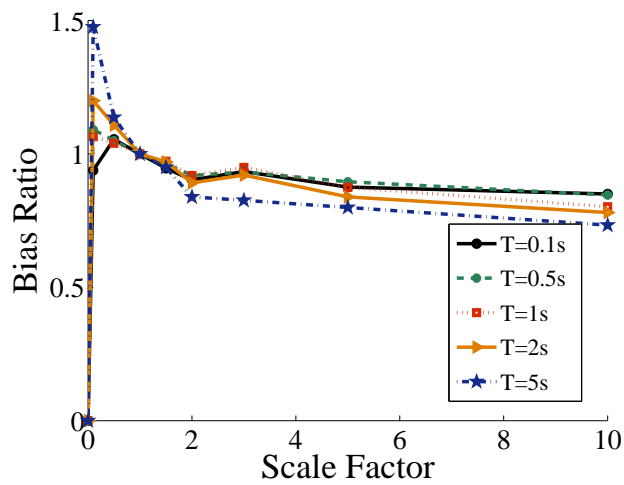
3.3.6 Comparison between scaling based on SDI with existing scaling procedures

In this section, the bias values based on two methods proposed in the literature [15], $Sa(T_1)$ and geometric-mean scaling, are shown. The binning methodology and bias definition defined in section 3.2.3 were both used for obtaining the bias. The first method is binning based on $Sa(T_1)$, which uses the spectral acceleration values at the pre-yielding period of the structure for intensity of the ground motion. Figure 3.14(a) shows the bias graph based on $Sa(T_1)$. Comparison between this graph and Figure 3.8(d) shows close similarity in bias values and trends, as would be expected based on the relationship between $Sd(T_1)$ and $Sa(T_1)$ (through ω^2).

The second method presented here is scaling based on geometric mean of Sd at different periods. To be consistent with Huang et al. [15], periods of 0.3, 0.6, 1, 2, and 4 sec were used to compute the geometric mean values. Figure 3.14(b) shows the bias results based on the geometric mean scaling method. The general trend indicates a slightly negative bias, which means an over-estimation of the nonlinear displacement due to the scaled records. For small periods, the geometric mean scaling method induces some positive bias, particularly with scale factors less than one. The results are consistent with the bias graph based on SDI and Sd . For small periods, the geometric means are similar to SDI values with a long period elongation, as described in section 3.2.4. Therefore the geometric mean scaling method can effectively reduce the estimated bias. For longer periods ($T = 2$ sec and $T = 5$ sec) the nonlinear system responds with a relatively small period of elongation as compared to the initial period. Therefore, SDI values will tend to toward the Sd values, which induces almost no bias as seen in Figure 3.8(d). However, the geometric mean method also considers spectral values at periods smaller than the pre-yielding period of the structure, which are not very relevant to the response of the structure (except when one considers MDOF systems). In fact, the Sd values themselves are a very good intensity measuring parameter for structures with long periods.



(a) binning based on $Sa(T_1)$



(b) Binning based on geomean method

Figure 3.14: Bias ratio for elasto-plastic systems using established scaling techniques

3.3.7 Bias ratio based on binning from synthetic earthquakes

The work presented in this research utilized only recorded ground motions for investigation of bias thus far. However, it is helpful to know if the same findings hold true when synthetic ground

motions are used. The bias results for an elasto-plastic oscillator are plotted in Figure 3.15(a) and Figure 3.15(b) for binning based on CAV and Sd, respectively. Results from binning based on CAV have an approximate bias of 0.9 except for the scale factor equal to 0.1. This is similar to what was observed when as-recorded motions were used. When the binning for is oscillator is based on Sd then bias becomes very pronounced for the short period 0.1 sec as seen in Figure 3.15(b). The overall findings are similar to those for the as-recorded motions in that CAV controls the bias better than does Sd. However, it is interesting to note that at periods greater than 0.1 sec (i.e., 0.5 sec and 1.0 sec) the bias in the Sd plot is considerably less than it was for the as-recorded motions - See Figure 3.8(d) - whereas the bias values for the longer periods of 2 sec and 5 sec are very similar to the as-recorded.

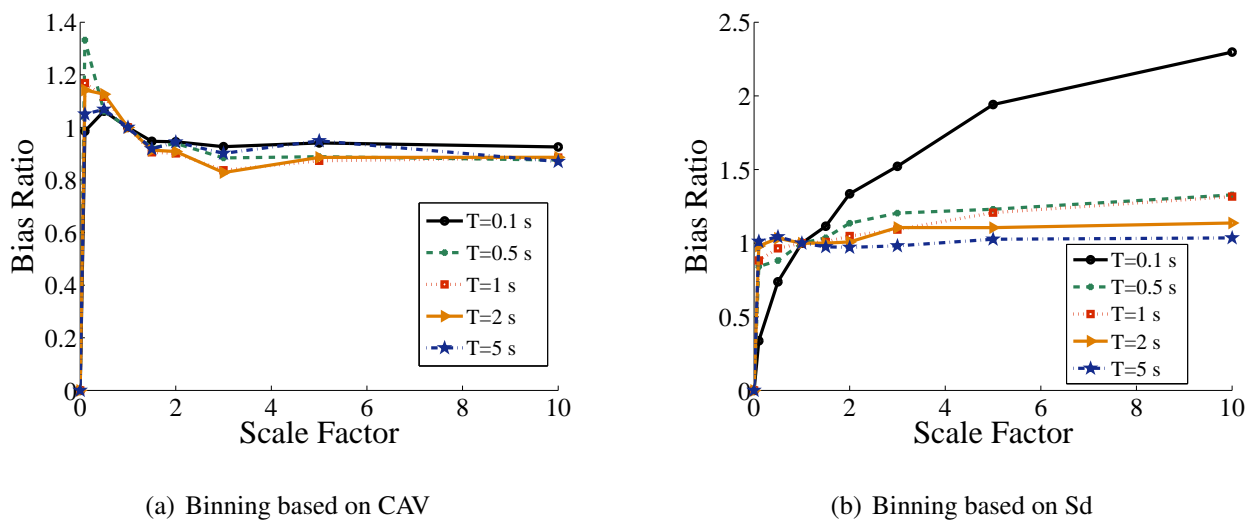


Figure 3.15: Bias ratios for elasto-plastic system using synthetic ground motions.

Figure 3.16 shows the bias results for the elasto-plastic system when SDI is used as the binning parameter. For all periods, the SDI approach stabilizes the bias factor very close to 1.0 for all periods of the structure. While this is not an extensive presentation of bias results for synthetic ground motions, it provides confidence that the overall trends of as-recorded and synthetic ground

motions are largely similar.

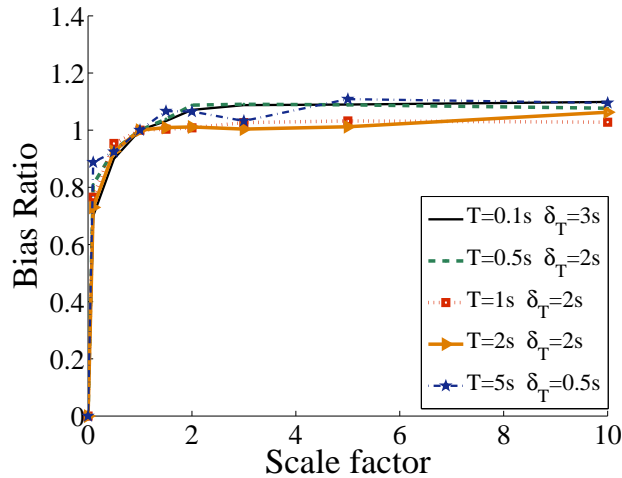


Figure 3.16: Bias for elasto-plastic system for synthetic motions binned on SDI

3.4 Effect of bias on fragility analysis

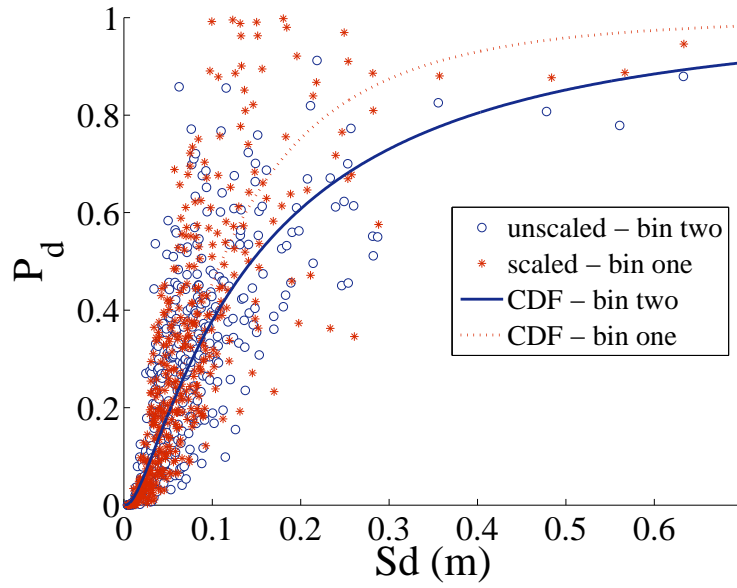
A fragility curve describes the probability of exceeding a limit state as a function of a ground motion intensity parameter. To investigate the effects of scaling on fragility curve estimates the frame structure was analyzed. The bins of ground motions were assembled where bin one was scaled to the same IM magnitudes as those ground motions placed in bin two. Bin two represents the unscaled case and bin one represents the scaled case. Presented here are the fragility curves for either Sd or SDI being selected as the IM. For the sake of demonstration a moderate scale factor of 3.0 is used for bin one in both cases.

Structural capacity was assumed to be in terms of maximum displacement (or drift) and log-normally distributed. For the moderate damage state for a structure, the mean value and coefficient of variation of the capacity were assumed to be $3 \times \sigma_y$ (σ_y assumed to be the yielding displacement of the frame) and 0.4, respectively [65]). The log-normal distribution parameters were obtained

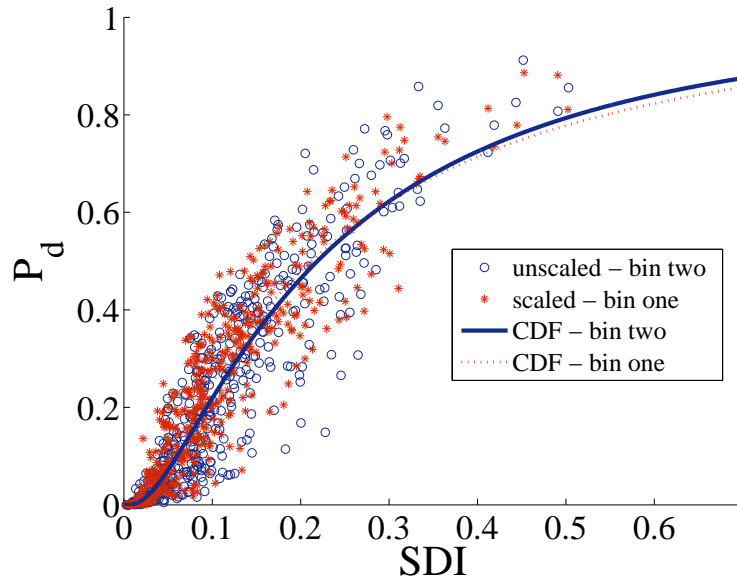
from the mean and coefficient of variation and the probability of failure were computed based on the maximum displacement associated with each ground motion. Fragility curves were obtained by fitting a CDF function (cumulative probability distribution function) on the damage data using the least squares error method presented by Porter et al. [28].

Figure 3.17(a) shows the effect of bias induced by scaling on the fragility curve of the frame when S_d is used as the IM. The vertical axis represents probability of damage (P_d) for the structure and the horizontal axis represents intensity of the records in terms of S_d . Figure 3.17(a) clearly shows a positive bias which over-estimates the probability of damage of the structure and also changes the parameter estimates of the CDF. For example, at $S_d = 0.3$ m the unscaled probability of meeting or exceeding the moderate damage state is approximately 0.7 where the value for the scaled bin is closer to 0.85.

To measure the effectiveness of using the SDI metric in fragility analysis record selection, the same fragility graph is presented in Figure 3.17(b). However, instead of S_d , the SDI metric has been used for record selection. The fragility curves from both the scaled and unscaled bins are nominally identical which is a vast improvement over the use of S_d . In addition to a better control over the bias, one may also observe a lower dispersion and consequently narrower confidence interval when SDI is used as opposed to S_d . Thus, Figure 3.17 shows that SDI is a very good predictor for the maximum deformation of a nonlinear structure as compared to S_d . The importance of this statement becomes more evident considering that maximum drift of the structure is a commonly used metric for performing fragility analysis.



(a) Binning based on S_d (bias value equal to 1.37)



(b) Binning based on SDI (bias value equal to 1.08)

Figure 3.17: Fragility estimate comparisons for a simple frame

3.5 Closure

The probabilistic assessment of the seismic response of a structure often requires the assembly of a suite of ground motions along with many nonlinear analyses of that structure. The lack of a sufficient number of high-intensity as-recorded ground motions often leads to the analysts using some kind of amplitude scaling approach to get around this shortcoming. This study looks specifically at the impact that such an approach has on the inherent bias in the nonlinear structural response estimates and looks at a way to minimize this bias. The bias was quantified in the mean in this research, and was computed by the ratio of the mean response under scaled ground motions versus response under ground motions naturally at the target intensity. The following are some conclusions - along with limitations - associated with this study. For all conclusions, it should be noted the focus was on the selection of common nonlinear systems that respond primarily in a single degree of freedom. In addition, although a typical response metric for structures, the maximum displacement response was the only metric examined in this study. Consistency of the results with force and energy response terms are appropriate topics for future study.

Amplitude-scaling of recorded ground motions can induce considerable bias in the nonlinear response of structures which in turn can significantly affect any probabilistic inferences made. The biases observed when amplitude scaling ground motions are the result of the nonlinear behavior of the structure as well as characteristics of earthquakes. Bias can vary based on magnitude of scaling, period of structure, nonlinear behavior of the structure, and the metric used to scale the ground motions. General trends are toward increasing bias as the scale factor increases, the period increases when PGA is used for binning, or as the period decreases when S_a or S_d are used for binning.

Among the traditional IMs that can be used for the record selection procedure, scaling based on CAV and PGV can result in considerably less bias compared to PGA and S_d . Results obtained

from spectrally-matched ground motions show that the period elongation of the structure in combination with the spectral shape of the ground motion are key factors that affect measured bias. As concluded in other studies, therefore, consideration of any additional period in computing spectral ordinates is beneficial in better predicting response. This is especially true of short- to medium-period structures that show greater nonlinear seismic response and therefore exhibit degradation of the fundamental period.

An IM parameter known as the average spectral displacement (SDI) is proposed to be able to account for bias due to both period elongation and spectral shape. When compared with other typical IMs, SDI was the most consistent at minimizing response bias. As a direct relative to the historical Housner intensity, the added benefit of this parameter is it is easy to compute and does not require any additional structural-specific information (other than the fundamental period). With an assumed period elongation, it is demonstrated that SDI can be used to directly estimate the magnitude of the nonlinear bias. This is important because no nonlinear analysis is therefore required to obtain an accurate estimate of the bias that would be induced in the system from amplitude scaling. While not all the results are included in the research, the ability to predict bias using SDI (or the minimize bias when binning based on SDI) is relatively insensitive to the period elongation selected as long as a fixed elongation of 1 to 2 sec is used or the commonly assumed upper-bound of $2T_1$ is employed.

The findings of this study are important as they relate to common guidelines (such as ASCE 7/16) that use spectral matching of ground motions to the conditional mean spectrum (CMS). While the suggested period ranges to match the CMS are usually between $0.2T_1$ to $1.5T_1$ or $2T_1$ based on higher mode effects and nonlinear softening, this study only directly addressed the elongation due to nonlinear action. As mentioned in [24], while scaling is sometimes questioned, empirical evidence suggests that CMS spectral matching is not to produce nonlinear displacements comparable to unscaled ground motions.

The biases in nonlinear response using several of the existing ground motion selection and scaling procedures currently in the literature were quantified. The geometric mean approach of Huang et al. [15] is effective in minimizing bias, as would be expected given the consideration of multiple periods in the scaling procedure. Amplitude scaling was similarly applied to synthetic ground motions generated using a stochastic procedure. Similar trends in the biased response of the nonlinear oscillators were observed using this secondary ground motion set, further indicating that the spectral shape and nonlinear period elongation are the key components of bias, rather than a parameter specific to naturally occurring strong motion generation and propagation. It should be noted that only one method of synthetic ground motion generation was examined, however.

Not quantified directly in this study, the magnitude of the bias may be magnitude/intensity dependent. For example, when viewing bias as the relationship between two point clouds of nonlinear responses (not the bias ratio), the limits of the probability density function of nonlinear responses in each bin is actually representative of the ground motion intensities selected. Not accounting for this in the bias computation has no effect on the mean bias (as studied here), but may have some impact when considering the variability in bias due to amplitude scaling.

For the basic frame considered in this study, the SDI parameter shows great promise in reducing if not nearly eliminating the bias in fragility estimates. Although not an objective of this study, using SDI as the selected IM shows additional potential in reducing the dispersion associated with fragility estimates. This finding is worth of further study and is related to the SDI being a better predictor of nonlinear response than commonly employed intensity-independent IMs and those that use only the initial elastic period, i.e., $Sa(T_1)$ or $Sd(T_1)$.

The frame structure presented in section 3.2.2 acts as a more realistic nonlinear SDOF as opposed to MDOF structure due to the relatively large stiffness of the beam. Therefore the effect of higher modes is not captured through this model, and further bias quantification studies are warranted

for different MDOF configurations. Each MDOF period and period elongation would need to be estimated to properly predict the bias based on SDI. This is complicated by the fact that modal participation changes with nonlinear period elongation. However, as previously mentioned, the period elongation of the structure is the primary cause for induced bias when amplitude scaling ground motions. In a MDOF system with spaced first mode (i.e., not high correlation with 1st and 2nd modes), the period elongation will occur primarily in the first mode as the higher modes do not experience the same degree of nonlinear response. Consequently, the bias induced by amplitude scaling of ground motions will be less in the mean for nonlinear MDOF systems than SDOF systems.

CHAPTER 4: PARAMETER SCREENING FOR PERFORMANCE BASED ASSESSMENT ANALYSIS OF HIGHWAY BRIDGES

4.1 Introduction

There are many parameters participate analytical bridge models which are going to be considered as for this study. From the experimental test we know that there values may vary for different models and also for different moment along the life span of the structure and the statistical models that describe the variation for each parameter can be obtained. A study needed to be performed to indicate whether or not this variation has any significant impact on the response of the structure. The results from aforementioned study will indicate that if variation of each parameter should be considered or if it may be neglected. Different studies using different techniques such as sensitivity analysis and screening studies of the parameters have been performed previously to balance the accuracy of PBA with computational efficiency and evaluate the importance of the parameters in fragility analysis. Mackie and Stojadinovic (2001) [58] performed the sensitivity analysis of bridge fragility and probabilistic seismic demand model to abutment parameters such as longitudinal stiffness, transverse stiffness, and participating mass. Gardoni et al. (2002 [85] & 2003 [86]) have investigated the probabilistic capacity and demand models for reinforced concrete columns with application for RC bridge structures based on experimental observations. In their approach with the aid of stepwise deletion procedure with respect to posterior COV of the model parameters, the important parameters of the model were selected. Nielson and DesRoches (2007) [87] performed seismic evaluation of a typical configuration for a MSSS girder bridge. They performed a two-level fractional factorial screening design to obtain the main effects of the parameters using 14 parameters. From the analysis of variance they concluded that the seismic response of the structure is sensitive to damping ratio, loading direction, mass of the structure, stiffness of the bearings

are the most important parameters in the seismic response of bridge structure. Choi et al (2008) [88] obtained fragility functions for corroding reinforced concrete (RC) columns and carried out sensitivity analysis of the fragility on the reliability function of the RC column with respect to the gradient of first order reliability index. Consequently the important parameters were computed using method of measure of importance with respect to reliability function of the fragility of the system developed by Der Kiureghian and Ke (1995) [89]. Pan et al. (2007) [90] investigated the seismic fragility analysis of typical highway bridges in NY State. In their studies uncertainties associated with the estimation of material strength, bridge mass, friction coefficient of expansion bearings, and expansion-joint gap size were considered. Sensitivity analysis of the seismic response to variations in superstructure mass, gap size, concrete compressive strength, reinforcing bar yield stress, friction coefficient of expansion bearing, and abutment wallsoil stiffness were obtained for PGA=1.0 g. Based on their study the friction coefficient of bearings, reinforcement yield strength, superstructure weight, gap size and concrete compressive strength are the important parameters that needed to be included probabilistically in the fragility analysis analytical model. Pedget and DesRoches (2007) [93] investigated the significant parameters on seismic response of MSSS Steel Girder Bridge with potential retrofitting scenarios. Important parameters were obtained using two level fractional factorial design of experiment. The important parameters were selected and the effect of elimination of the lesser important parameters on the structure fragility analysis were investigated. Based on their results, the geometrical uncertainties for various bridge classes such as height of the columns and number of spans as well as randomness in the ground motion are more important compared to model parameter variation such as damping ratio and stiffness of elastomeric bearings. Pan et al. (2009) [91] & (2010) [92] used parametric study to obtain significant parameters in variation of the response of the MSSS Steel Girder bridge structure. Between multiple candidates they determined that uncertainties associated with the yield strength of the steel, the superstructures weight, gap size of the expansion joints, the friction coefficient of bearings and the concrete compressive strength should be considered during the fragility anal-

ysis of the bridge system. All the mentioned studies were carried out using limited number of parameters that can be recognize in analytical model of the bridge structure. Moreover no comprehensive study has been performed to evaluate the effect of parameter selection and reduction on the fragility analysis of the highway bridges. A more scientific measurement of effectiveness for parameter reduction needed to be defined and investigated for fragility analysis results.

A number of methods are available to assist in the identification of significance of parameters or factors. These methods are generally called screening or sensitivity studies. One of the more traditional methods is an approach called “one-factor at- a-time” (Wu and Hamada, (2000) [63]). For this method all but one of the factors are held at a constant value. I.e. one factor is investigated by itself therefore by changing its value the impact of this variable on the response of the model is going to be observed and measured. This this procedure needed to be repeated for each parameter of interest. This is an iterative and inefficient approach to the problem. Also it is hard to monitor the correlation between variables using this method.

There is an extension of the “one-factor-at-a-time” that needs the derivatives of response Function. The derivatives of the response of the structure, such as drift, deformation, forces etc., are functions of the various parameters in the model and define the slopes of the response functions. The gradient of these response functions is an indicator of the sensitivity of response with respect to each parameter. This method is very powerful but, it requires that sensitivity equations for the various parameters of interest be implemented into a finite element code and which is not feasible for very complex systems like fully 3D bridge modeling. A method which is very popular in statistical studies and have been used widely in industrial engineering researches for screening the parameters called design of experiments (DOE) approach. This is a statistical approach which study the importance of each parameter and also is more computationally efficient compared to previously mentioned methods.

One of the DOE methods is full factorial experiment. Full factorial experiment is a comprehensive study of all possible combinations of the parameters values. A more simplistic DOE method exist that called two level experimental design. In a two level design, each parameter is considered at two values, both upper and lower, traditionally. For each combination of parameter levels, the experiment is analyzed and the responses of interest are monitored. Combination of parameters needed to be considered for this setup is the 2^k combinations where k is the number of parameters being considered. In our case it means 2^k bridge models needed to be created and, consequently parameters of interest from time history response of each bridge be monitored. This method can be used for monitoring limited number of parameters but this method becomes very computationally expensive when a large number of parameters needed to be monitored.

One of the DOE methods is Plackett-Burman design. The power of Plackett-Burman design is laid on the efficiency of this method. It can identify the important parameters that contribute the most in the response of the structure more efficiently. To illustrate why the efficient is important in our case we should mention that a two level experimental design with 15 parameters for a bridge requires of generating 32768 models and finding the seismic response of them given the various ground motion scenarios however using Plackett-Burman screening design can be performed with as low as 15 bridge models. Table 4.1 shows the list of various parameters that needed to be included in fragility seismic analysis of multi-span continuous concrete girder bridge. Plackett-Burman screening design can be used here to identify the importance of sources of uncertainty. Consequently only important parameters that contribute the most in response of structure needed to be defined probabilistically in the modeling of the bridge structure (using probability distribution function) and the rest of the parameters can be treated as deterministic.

Table 4.1: Sources of uncertainty in performance based seismic assessment of bridges

	Source of Uncertainty	Included in previous researches?	Can be easily imple- mented?
1	Discretization level for the structure	No	partially
2	centerline deck model	No	No
3	treatment of girders and decks (frame and shell)	Simplistic	Yes
4	assumed dead load (including foundation and abutments)	Yes	Yes
5	Damping ratio	No	Yes
6	Time step for analysis	Yes	Yes
7	Gap size between deck and abutment back wall	No	Yes
8	Stiffness of impact elements	Yes	Yes
9	Translational stiffness of foundations	Yes	Yes
10	Rotational stiffness of foundations	Simplistic	Yes
11	Use of lumped foundation springs as opposed to piles, p-y, soils elements	No	No
12	Yield force for foundation springs - translational	No	Yes
13	Deck element modeling (linear or nonlinear)	No	No
14	Deck elements stiffness	No	Yes
15	Concrete strength	Yes	Yes

	Source of Uncertainty	Included in previous researches?	Can be easily imple- mented?
16	Concrete ultimate strain	No	Yes
17	Concrete module of elasticity	No	Yes
18	Concrete material model in Opensees	No	Maybe
19	Discretization of concrete section for column and bent cap	No	Maybe
20	Reinforcing steel model in Opensees	No	Maybe
21	Yield strength of reinforcing steel	Yes	Yes
22	Modulus of elasticity for reinforcing steel	No	Yes
23	Strain hardening ratio for reinforcing steel	No	Yes
24	Actual column/bent cap dimension	No	partially
25	Torsional stiffness of columns and bent cap elements	No	Maybe
26	Number of integration points for these ele- ments	No	Yes
27	Use of displacement controlled versus load controlled types of elements in modeling	No	Depends on Con- vergence issue
28	Distribution of the mass along the column height	No	Yes
29	Elastomeric pad shear stiffness	Yes	Yes
30	Coefficient of friction between bearing pads and bent cap	Yes	Yes
31	Size of elastomeric pad	No	partially

	Source of Uncertainty	Included in previous researches?	Can be easily imple- mented?
32	Type of the material for elastomeric pad	No	No
33	Gap between steel retention dowel and slot in girder	Yes	Yes
34	Steel dowel strength	No	Yes
35	Abutment stiffness in active direction	Yes	Yes
36	Abutment stiffness in passive direction	Yes	Yes
37	Abutment stiffness in transverse direction	Yes	Yes
38	Yield displacement of abutment soil	No	Maybe
39	Ultimate strength of abutment piles	No	Maybe
40	Number of ground motions in each suite	No	Not sure
41	characteristics of ground motions in each suite	No	Not sure
42	Direction of ground motion	No	No
43	Deformation capacity of each element type	Partially	No

For parameter screening analysis, first the type of bridge and level of detail in modeling needed to be indicated. In Table 4.1 there are 43 parameters but not all of them might be included in modeling of the bridge, i.e. the bridge might not have elastomeric bearing. Also implementation of some of these parameters might not be feasible as stated in Table 4.1. The remaining parameters that can be included in the analytical model of the bridge needed to be defined variable in an appropriate range. For each parameter of interest 3 values needed to be considered. Mean value, lower limit

and upper limit. The Plackett-Burman matrix needed to be constructed. Table 4.2 is an example of Plackett-Burman design matrix for 8 parameters that have been presented for demonstration propose only.

Table 4.2: Plackett-Burman design matrix for 8 parameters and 8 runs

	F1	F2	F3	F4	F5	F6	F7	F8
R1	+	-	-	-	-	-	-	-
R2	+	+	+	+	-	+	-	-
R3	+	-	+	+	+	-	+	-
R4	+	-	-	+	+	+	-	+
R5	+	+	-	-	+	+	+	-
R6	+	-	+	-	-	+	+	+
R7	+	+	-	+	-	-	+	+
R8	+	+	+	-	+	-	-	+

In Table 4.2, F_j is the j^{th} parameter(like steel material stiffness, bearing stiffness, concrete ultimate strength and etc.) and R_i is the i^{th} run result which is the structure's response of interest (i.e. bearing displacement, maximum deformation of the top node of structure, maximum stress or etc.). If M_{ij} is the element of Plackett-Burmann design matrix, the "+" means that the F_j parameter value is set to its upper limit whereas "-" means F_j value is set to its lower limit for i^{th} run. The normalized effect of F_j can be found from the following formulation:

$$E(F_j) = \left[\sum_{i=1}^N 2M_{ij}R_j \right] / E_0N \quad (4.1)$$

Where E_0 is the response of interest when all F_j parameters are set to their mean values and N is the number of parameters participating in the Plackett-Burman design. Sorting the $E(F_j)$ values for various parameters from maximum to minimum shows which parameter has the most effect on the response of interest and effect of which one can be neglected in the analysis. The procedure above describes the procedure for performing sensitivity analysis using Plackett-Burman technique for single objective. However since the results from this analysis needed to be used in PBA of the bridge structure and since various EDP's and capacity parameters are involved in PBA procedure therefore the effect of F_j parameters needed to be assessed for different responses of the structure and overall effect of F_j needed to be evaluated. For multiple objectives the overall effect of F_j can be evaluated as below:

$$E(F_j) = \left[\sum_{k=1}^M E_k F_j / M \right] \quad (4.2)$$

Where M is the maximum number of objectives (i.e. curvature ductility of the columns, deformation of bearings, and abutments, other EDP's or parameters that participate in measuring the PBA of the structure). Sorting $E(F_j)$ values can indicate the effect of each parameter on the overall response of the structure.

4.2 Methodology

This section is dedicated to the methodology utilized for parameter screening analysis of the bridge structure. At first the logic behind selection of the bridge have been discussed. The selected bridge general layout and dimensions as well as structure 3D finite element modeling properties is included. Nonlinear properties for bridge elements i.e. foundation, abutments, piles, bent cap beam, columns and deck impact elements which have been incorporated in the finite element modeling

have been described. The procedure utilized for experimental design including Plackett-Burman design matrix and parameters upper and lower bounds, ground motion selection for seismic analysis and response analysis of the structure have been included consequently. At the end, the method for evaluation of the effect of screening analysis and parameter reduction in PBA and fragility analysis have been included.

4.2.1 Selection of the bridge structure

The analytical model of the structure is an inseparable element for the seismic performance based analysis. Despite the fact that 3 dimensional modeling is more complex and consuming compared to conventional 2D analysis, since seismic excitations affect the structure in multiple directions, 3D analysis can generate more realistic results for the response of the bridge subjected to seismic excitation. For this reason 3 dimensional analysis is considered for this research. The selection of the bridge is performed with respect to population of the existing bridge structures in the United States. Table 4.3 and Table 4.4 shows the bridge classification based on their structure type for CSUS and California State regions (NBI 2012). Based on these tables there are various types of bridges constructed in these seismically active regions and including all characteristics of these bridges if not impossible is very time consuming in this study. It should be noted that the intent of this study is to solve the existing well-known issues of PBA procedure, reduce the uncertainty in the procedure and examine the broaden method for its effectiveness in fragility analysis of the highway bridges. Therefore for this study a bridge that is more frequently constructed in CSUC region (that are two high seismic hazard zones in United States) have been selected.

Table 2.2 shows the distribution of bridges in USCS region Based on Nielson et al. 2007 [68]. The most frequent bridge in table 2.2 is the multi-span simply supported concrete girder bridge which represent 18.9% of all of the bridge in USCS region. MSSS concrete girder bridges have mostly

Table 4.3: Classification of bridge structures for CSUS region

Structure type	Population	Percentage of population
Slab	19820	10.341
Stringer /Multi-Beam or Girder	70646	36.86
Tee Beam	13099	6.834
Box Beam or Girders (Multiple)	18878	9.84
Box Beam or Girders (Single or Spread)	3487	1.81
Truss-Thru	1945	1.014
others(25% of population are culverts)	63780	33.27

Table 4.4: Classification of bridge structures for California State

Structure type	Population	Percentage of population
Slab	5784	23.311
Stringer /Multi-Beam or Girder	3823	15.40
Tee Beam	3028	12.203
Box Beam or Girders (Multiple)	7569	30.50
Box Beam or Girders (Single or Spread)	259	1.04
Arch-Deck	308	1.241
others(14% of population are culverts)	4041	16.28

constructed during 1970-1980 with limited consideration of seismic resistance design and detailing. These characteristics makes MSSS concrete girder bridge a good candidate for this research. The characteristics of selected MSSS concrete bridge have been presented in the following section.

4.2.2 Configuration of multi-span simply supported concrete girder bridge.

In this section the modeling details of the MSSS concrete girder bridge have been provided. In the beginning it should be noted that in the bridge structure layout, detailing and modeling is performed mainly based on the information provided by Nielson 2005 [30], Choi 2002 [69] and Ma and Deng (2000) [76]. A layout for a Multi-Span Simply Supported Concrete (MSSS Concrete) girder bridge is shown in Figure 4.1. The bridge structure has three spans. The left, middle and right span lengths are 12.2 m, 24.4 m and 12.2 m respectively. The total length of the bridge is 48.8 m. The width of the span deck is 15.01 m. The bridge deck is constructed from eight AASHTO type concrete prestressed girders. The left and right span girders are AASHTO type I girders whereas the middle span girder type is AASHTO Type III. The end girders are supported by the abutments on one side and on the other side are supported by the bent beams. Both sides of the middle span girders are supported on the bent cap beams. The bearings for this bridge are elastomeric pads with two steel dowels (25.4 mm dowel diameter). The bearing elastomeric pads under the type I girders are 406 mm long by 152 mm wide and have 25.4 mm thickness. The type III girders use pads which are 559 mm long by 203 mm wide and 25.4 mm thick. Figure 4.1 shows the general configuration of the MSSS concrete bridge used in this study. In Figure 4.1 the fixed bearings and expansion bearings can be recognized by triangles and circles respectively.

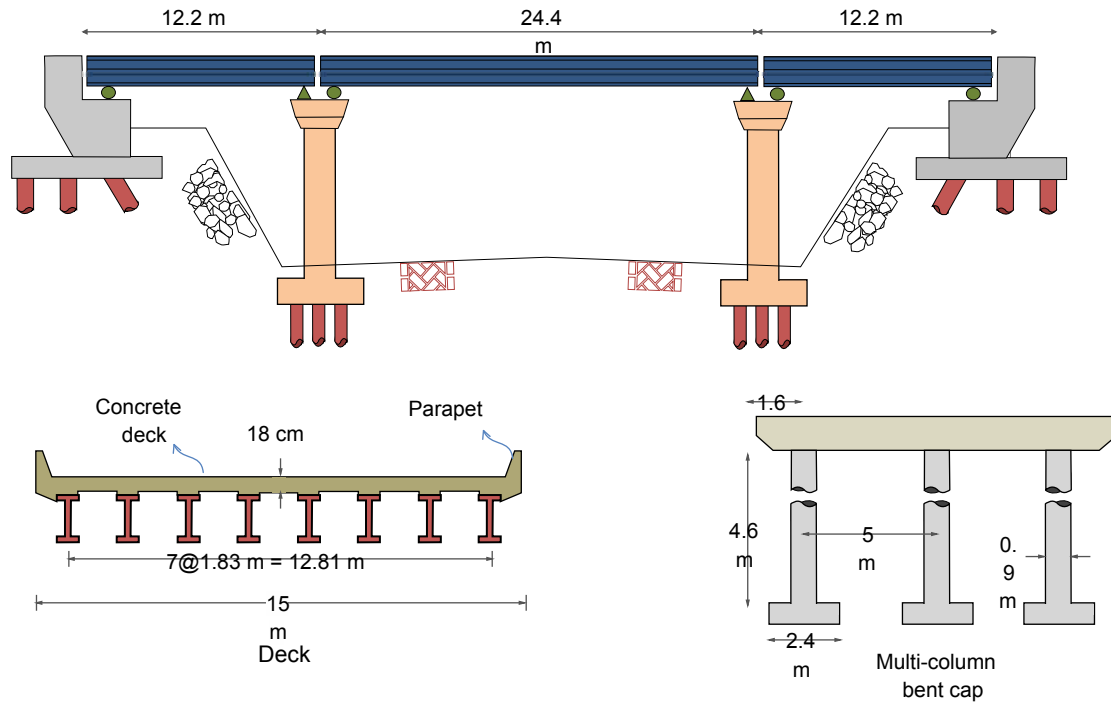


Figure 4.1: MSSS Concrete Girder Bridge Configuration

The substructure of the bridge is consisted of multi column bent caps. The multi-column bent caps constructed from reinforced concrete and are 1066 mm wide and 1219 mm deep. The columns are circular reinforced concrete and have 4600 mm height and 914 mm diameter. The reinforcing detailing of the bent cap and column as well as bridge important super structure and sub-structure detailing can be found in Figure 4.2. As it can be seen in Figure 4.2 the bent beams have 15#29 and 4#16 reinforcing bars and #16 bars for transverse shear stirrups per 305 mm. The column longitudinal and shear transverse reinforcing stirrups are 12#29 bars and #13 per 305 mm respectively. The concrete strength is assumed to be 20.7 MPa. Also reinforcing steel assumed to have yield strength of 414 MPa (Hwang et al. (2000) [77]). For the bridge structure the deep foundation have been used. The pile caps dimensions assumed to be 2438 mm square with 1092 mm thickness. The pile cap is connected to the concrete column on the top and to the eight piles at

the bottom. The abutments of the bridge assumed to be pile-bent girder seats type with 2.4 m tall back wall.

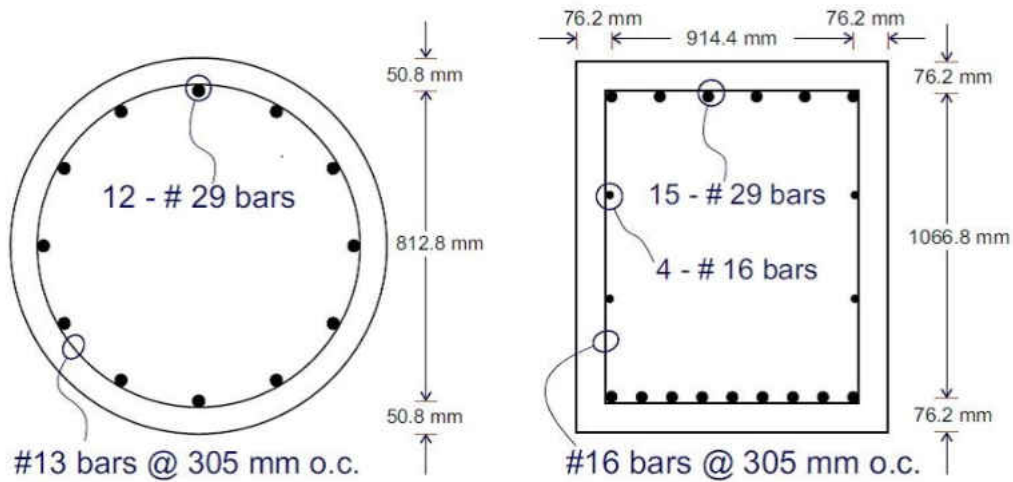


Figure 4.2: Reinforcing layouts for concrete beam and bent cap

4.2.3 Nonlinear properties of MSSS Concrete Girder Bridge

There are various component that participate in the bridge structure nonlinear response to seismic hazards, therefore the accuracy of the modeling of different components has direct influence on the output response of the structure. For this study different components of the structure including the deck elements, multi-columns bent caps, abutments, different bearing types and foundation have been included in the modeling of the MSSS concrete bridge. Nonlinear behavior of each component accurately have been modeled using recommendations from the literature. Also to make the screening design of the parameters feasible and control the stiffness and nonlinear properties of the components, various parameters have been implemented in modeling of each component. In

the following sections, more detailed information for elements description and properties can be found.

4.2.3.1 Deck elements

Figure 4.3 shows a schematic view of the concrete deck and girders for MSSS bridge. Due to the stiffness of the bridge superstructure compared to the sub-structure, the bridge deck does not play an important role in the seismic response of the nonlinear structure. Additionally, using the expansion elastomeric bearings in the bridge model result in a reasonable level of isolation between the response of the superstructure and substructure. Therefore the nonlinear response of the bridge is not very sensitive to the deck stiffness properties selection. However the mass of the superstructure participate significantly in seismic response of the bridge and needed to be considered deliberately. For this study the beam column linear elements have been used for modeling the deck elements assuming that these elements will remain elastic under seismic loading. For the composite section of the concrete deck and girders, the assumed properties have been reported in table 4.5.

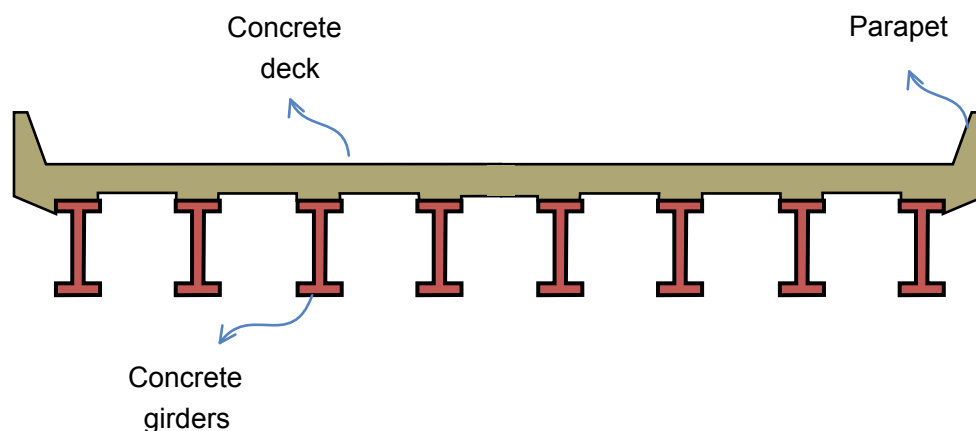


Figure 4.3: Reinforcing layouts for concrete beam and bent cap

Table 4.5: Typical deck stiffness and mass properties for MSSS concrete girder bridge

End Spans					Main Span				
E (MPa)	Iz (m4)	Iy (m4)	Area (m2)	Weight (kN/m)	E (MPa)	Iz (m4)	Iy (m4)	Area (m2)	Weight (kN/m)
2.78E+04	0.11	75.83	3.94	92.85	1.10	103.76	5.40	127.34	92.83

4.2.3.2 Multi-column bent caps

The multicolumn and bent cap system are essential load carrying elements in sub-structure of MSSS concrete girder box. They are connected to the concrete girders at the top using fixed and expansion bearing and on the bottom they are connected to concrete foundation of the sub-structure. The main role of the bent cap is to provide support for the concrete girders. In this study the bent beam and concrete columns are modeled using nonlinear beam-column element (*nonlinearBeamColumn*) in the *OpenSees* software. Figure 4.4 shows the detailed modeling of multi-column bent cap discretization. Multiple displacement beam column element have been used for modeling each column. Also for each displacement beam column element couple of integration points have been for computation of element load vector from section load vector. Connection between the bent cap and foundation with the column assumed to be rigid.

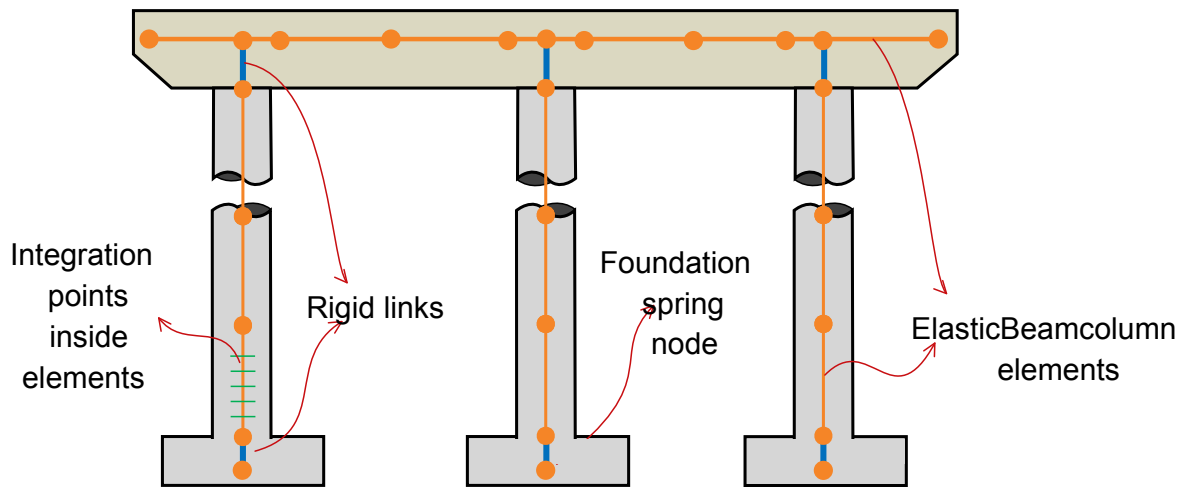


Figure 4.4: schematic discretization of the multi-column bent cap

For the confined and un-confined concrete, *concrete01* material have been used from the *OpenSees* material library. The typical values for confined, un-confined and steel material can be found in Table 4.6.

Table 4.6: typical parameters value for concrete and steel material

Parameter	Typical parameter value
Unconfined concrete strength (Mpa)	33.52
Confined concrete strength (Mpa)	41.23
Confined concrete ultimate strength (Mpa)	8.36
Confined concrete ultimate strain	-0.05
Steel hardening ratio	0.02
Reinforcing steel yield strength (Mpa)	496.24
Reinforcing steel modulus of elasticity (Gpa)	202.10
Concrete modulus of elasticity (Gpa)	274.11
Confined concrete modulus of elasticity (Gpa)	313.09

The section properties of the bent cap and concrete column have been modeled using fiber sections. Width and depth of the bent cap assumed to be 1066 mm and 1220 mm respectively. The bent cap have been discretized to 12 by 12 fibers in the direction of the depth and width respectively. For the bent cap a quadratic section generator have been used to define the concrete cover and concrete core. Steel reinforcements also have been defined using straight layers in *Opensees*. Appropriate torsion of the bent beam have been assigned to the section. The column radius assumed to be 457 mm and been discretized to 12 by 10 fibers in circumferential and radial direction respectively. The unconfined concrete cover assumed to be 38 mm. The section properties for the column also have been generated using circular patch for concrete cover and concrete core. The steel reinforcing have been modeled using circular fiber layers in the *Opensees* software. Appropriate torsion proportional to section properties of the bent beam have been assigned to the section using torsional section aggregator.

4.2.3.3 Abutments

The pile bent type abutment have been used in this study because they are frequently used as an integral part of the MSSS concrete girder bridge (Hwang et al. (2000) [77]). Three types of resistant have been defined for bent pile abutment of the bridge. Vertical stiffness which sustain the vertical loads. Longitudinal and transverse resistance which sustain horizontal loads due to traffic, wind, seismic and etc. The abutment will transfer vertical and horizontal loads to the soil partially with the piles and partially with the abutment wall. Figure 4.5 shows the schematic view of the pile cap abutment.

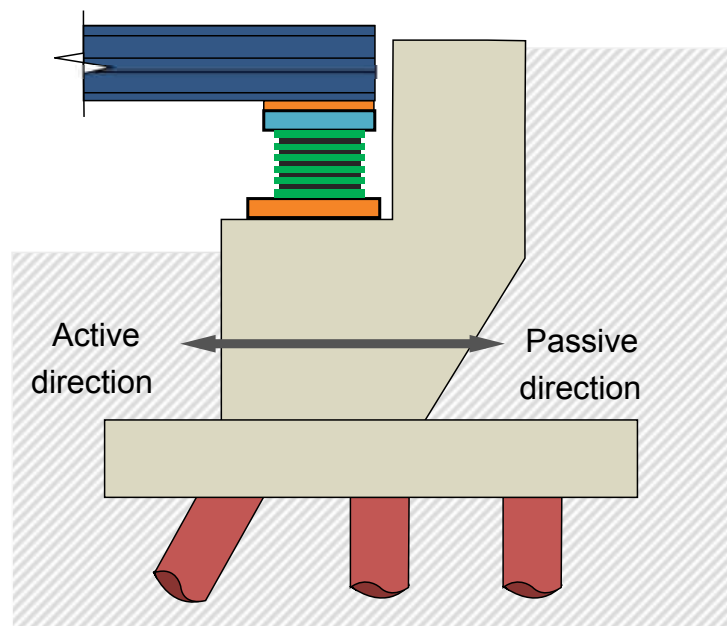


Figure 4.5: Abutment behavior in longitudinal direction

The longitudinal resistance of the abutment in the passive direction (toward the backfill soil) have been defined using the resistance of the backfill soil in passive direction and resistance of the piles. In the active direction -since the abutment is being detached from the backfill soil - only resistance

of the pile participate in the active resistance of the abutment. In the transverse direction, the shear component between the abutment wall and the soil backfill can be neglected relative to the soil-pile stiffness participation. Consequently for the transverse direction only stiffness due to interaction between the soil and abutment pile have been used as abutment transverse stiffness. The nonlinear properties of the stiffness of the abutment have been developed and used in this study. Based on the Caltrans (2006) [78] suggestions, the design pile-stiffness value is 7 KN/mm/pile, soil stiffness is 20.2 KN/mm/m and the ultimate passive soil pressure is 0.37 MPa. A qual-linear behavior needed to be used for the stiffness of the abutment soil portion in passive direction due to degradation of the stiffness of the abutment soil with increase of longitudinal deformation of the back wall. First and second yielding displacement take place at 10% and 35% of the deformation corresponding ultimate soil pressure Caltrans (2006) [78]. The other parameters of the qual-linear model have been obtained using Caltrans (2006) [78] recommendation and model and have been obtained from Nielson 2005 [30]. The stiffness of pile in longitudinal passive, active and transverse direction assumed to be similar. Based on Choi (19) the pile stiffness can be modeled using tri-linear model. Stiffness of pile assumed to be 7 KN/mm/pile and the ultimate strength of pile assumed to be 119 KN/pile based on (Caltrans 1990). For more detailed modeling information of the abutment pile stiffness refer to Choi (19).

The stiffness of the abutment soil in passive direction have been developed with *Opensees* Uniaxial *hysteretic* material parallel with the *elasticPPgap* material and been limited for passive deformations using *ENT* material. The stiffness of pile in active, passive and transverse direction are the same and have been modeled using Uniaxial *hysteretic* material. Figures 4.6 and 4.7 shows nonlinear behavior of the abutment developed in *Opensees* software in longitudinal and transverse direction.

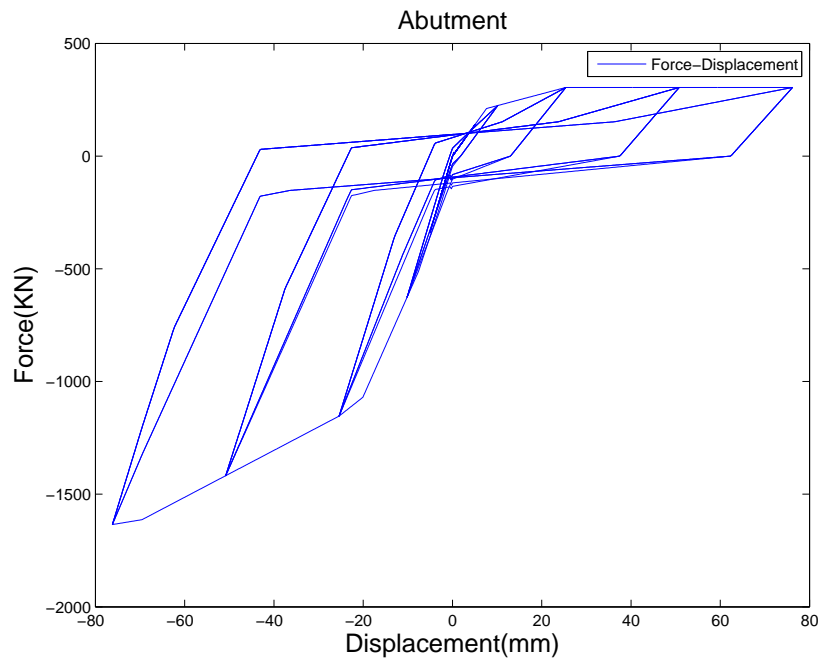


Figure 4.6: Nonlinear properties of the abutment in longitudinal direction

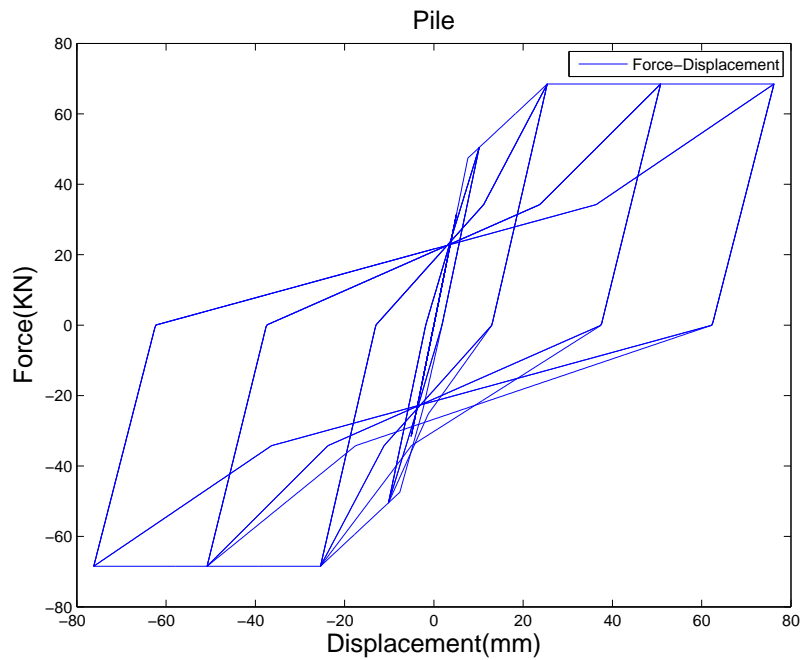


Figure 4.7: Nonlinear properties of the abutment in transverse direction

4.2.3.4 Impact elements

Based on the Muthukumar (2003) [79] the ponding between the deck elements can be modeled using the bilinear spring elements. Figures 4.8 and 4.9 shows the schematic and nonlinear stiffness model for impact elements recommended by Muthukumar (2003) [79].

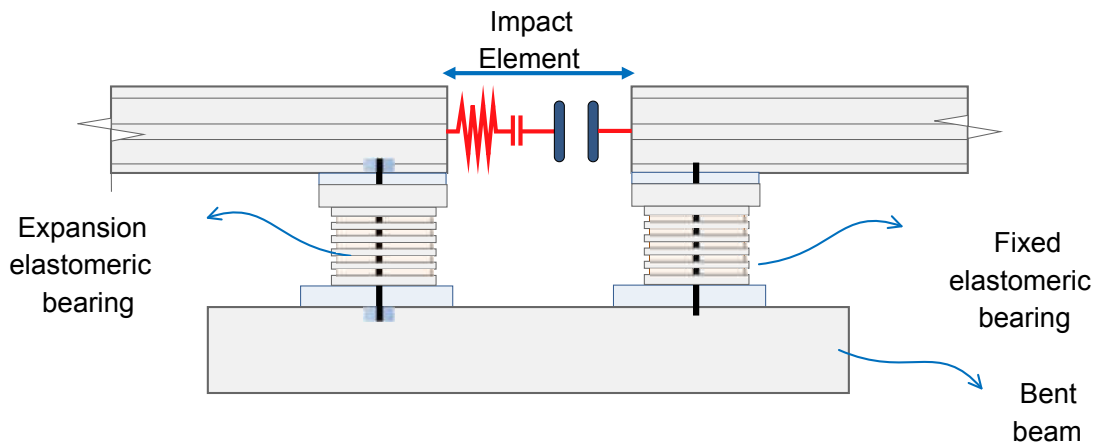


Figure 4.8: Modeling of impact elements for pounding between bridge deck elements

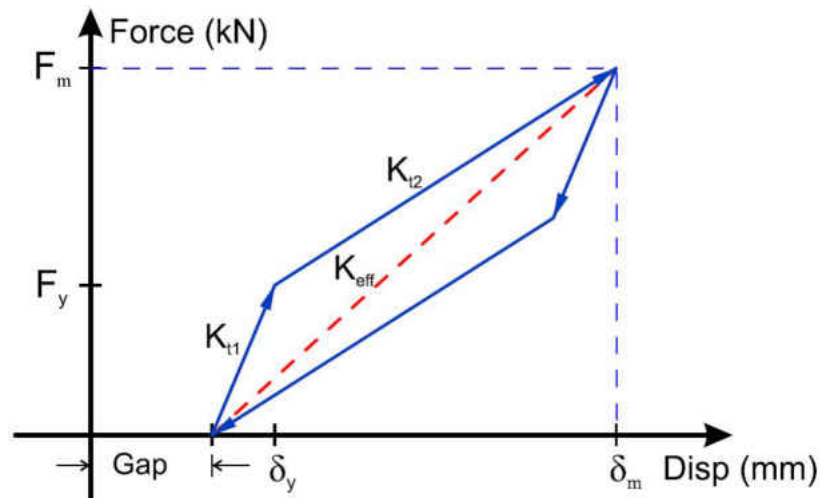


Figure 4.9: Analytical model of Impact between decks (Muthukumar, 2003)

The properties of the impact element can be obtained using $K_{t1}, K_{eff}, \delta_y, \delta_m$ and the gap size between the deck elements. The typical values for $K_{t1}, K_{eff}, \delta_y, \delta_m$ recommended to be 1116

KN/mm, 456 KN/mm for 1.9 m width of the deck, 2.54 mm and 25.4 mm respectively (Muthukumar (2003) [79]).

Impact elements for this study have been modeled using *Opensees ElasticPPGap* materials. The initial gap is assumed to be 38 mm. Figure 4.10 shows the impact elements nonlinear properties obtained from *Opensees* analysis and have been implemented as deck contact elements in the model.

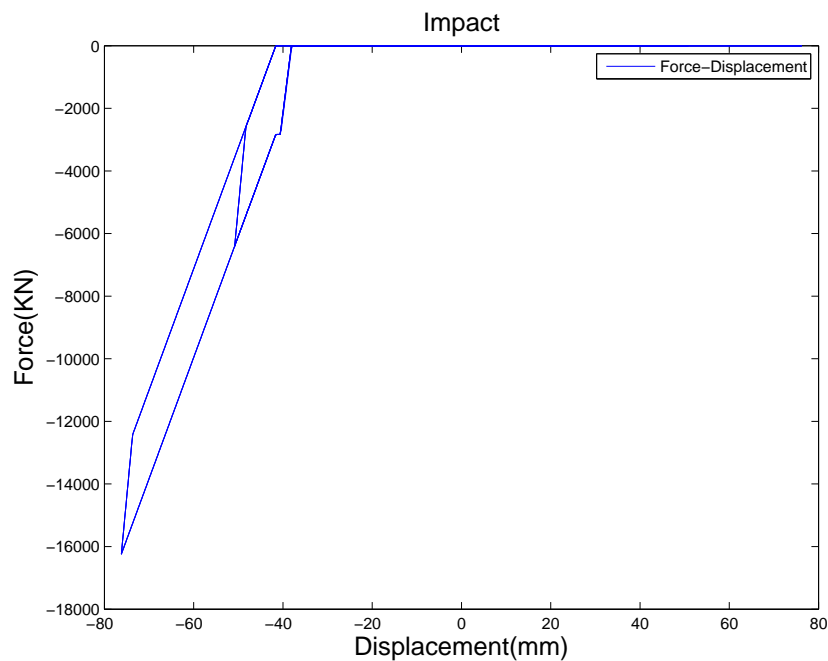


Figure 4.10: Typical hysteretic behavior of impact element between decks

4.2.3.5 Fixed and expansion elastomeric bearing

Elastomeric bearings have been frequently used for concrete girder bridges. It is consisted of a rubber bearing that transfer the loads between the surface of bent cap and girders and a steel dowels that can carry the horizontal load from the girder of the superstructure to the bent cap. The

properties of these bearing assumed to be the same in longitudinal and transverse direction. The nonlinear characteristic of the elastomeric pad is dependent on various parameters. The parameters are the shear stiffness of the elastomeric rubber which is a function of size of the pad and normal stress on the pad itself, the steel dowel stiffness and yielding strength and the gap between the steel dowels and elastomeric pad. Pad elements have been modeled using parallel *ElasticPPGap* materials in *Opensees* with initial stiffness of 3.35KN/mm and yield strength proportional to the applied vertical load and shear stiffness of the elastomeric pad ($F_y=N$) which accounts for the sliding of the bearing element on the surface of the bent cap or abutment concrete. The steel dowel element have been modeled using *hysteretic* material. The typical initial stiffness of the dowel assumed to be 92KN/mm. Also for the gap between the dowel retention and the pad the gap element have been used in series with the parallel *hysteretic* and *steel01* material. For the expansion bearing the only difference is the size of the gap between the steel dowel and the elastomeric pad. For the fixed bearing type the typical gap size is 3.1 mm assuming a small tolerance needed for the steel dowel installation in the elastomeric pad. However for the expansion elastomeric bearing the typical gap value have been assumed to be 25.4 mm. All the assumption have been made for the elastomeric bearings are in accordance with the Choi 2002 [69] and Hwang et al. 2000 [70]. The details for nonlinear analytical models of the bridge bearing can be found in Nielson 2005 [30]. Figures 4.11 and 4.12 shows the nonlinear behavior for the fixed and expansion elastomeric bearings with the assumed variables listed above.

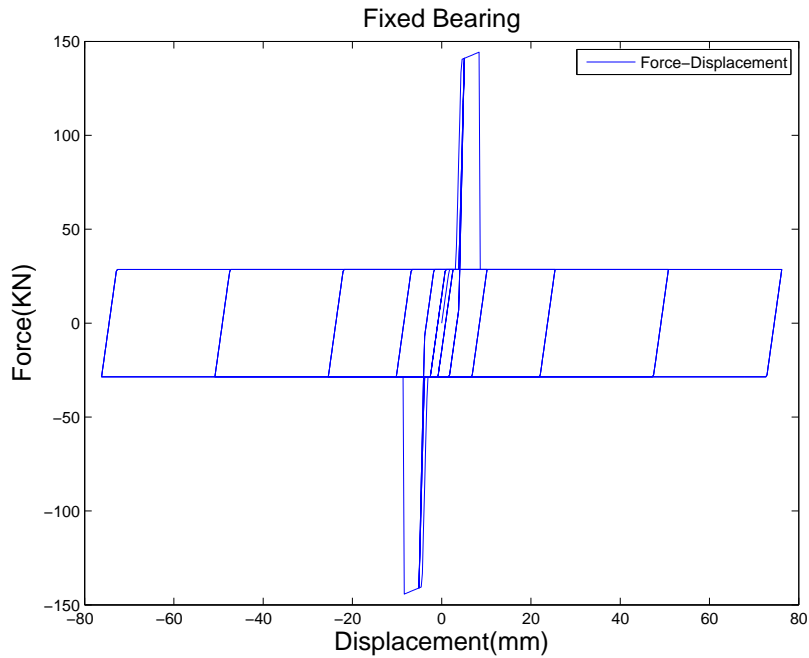


Figure 4.11: Typical nonlinear properties of the fixed elastomeric bearing

4.2.3.6 Foundation

The foundation are the primarily units that transfer the bridge internal forces to the sub structure soil. Most of the MSSS bridges uses a group of pile as a deep foundation (Hwang et al. 2000 [70]) to take advantage from the frictional resistance participation from the soil-pile interface and also the increased vertical and horizontal soil bearing capacity in the deeper ground sub-surface. Deep foundation also have been used for reduction of differential settlement for the bridge structure. A pile foundation unit which is consisted from piles and the pile cap that ties the piles to each other can be seen in figure 4.13.

In this study the stiffness of the piles unit is obtained with respect to two types of stiffness. First

the horizontal stiffness of the pile and second the vertical stiffness of the pile due to the soil-pile interaction. Other contributors for the foundation including pile cap stiffness and piles rotational stiffness have been neglected due to limited model stiffness participation (Ma and Deng, 2000 [76]) however the vertical stiffness of the pile will contribute to the rotational stiffness of the piles unit because of the eccentricity of the piles vertical load projection on to the pile cap surface. For the piles layout the model suggested by Nielson 2005 [30] have been adopted. The piles unit layout can be seen in figure 4.14.

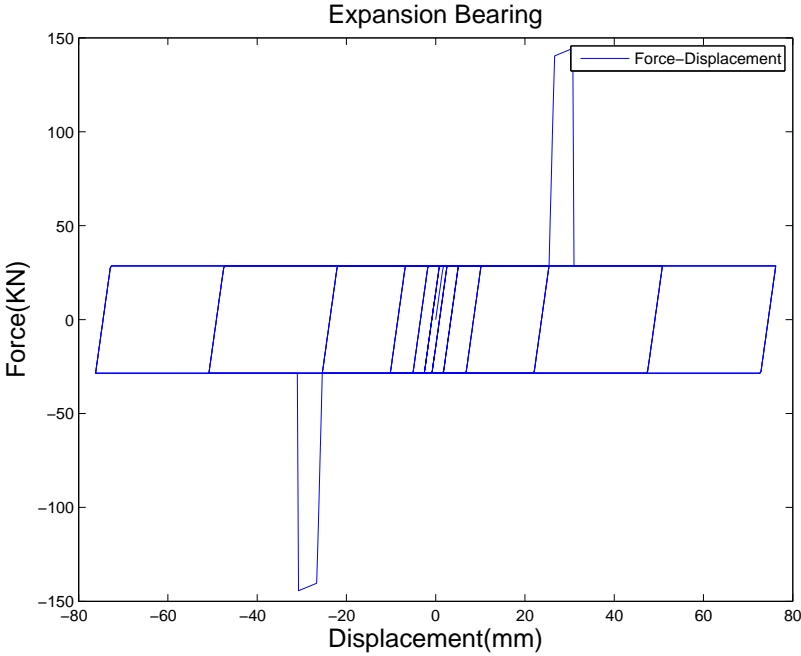


Figure 4.12: Typical nonlinear properties of the expansion elastomeric bearing.

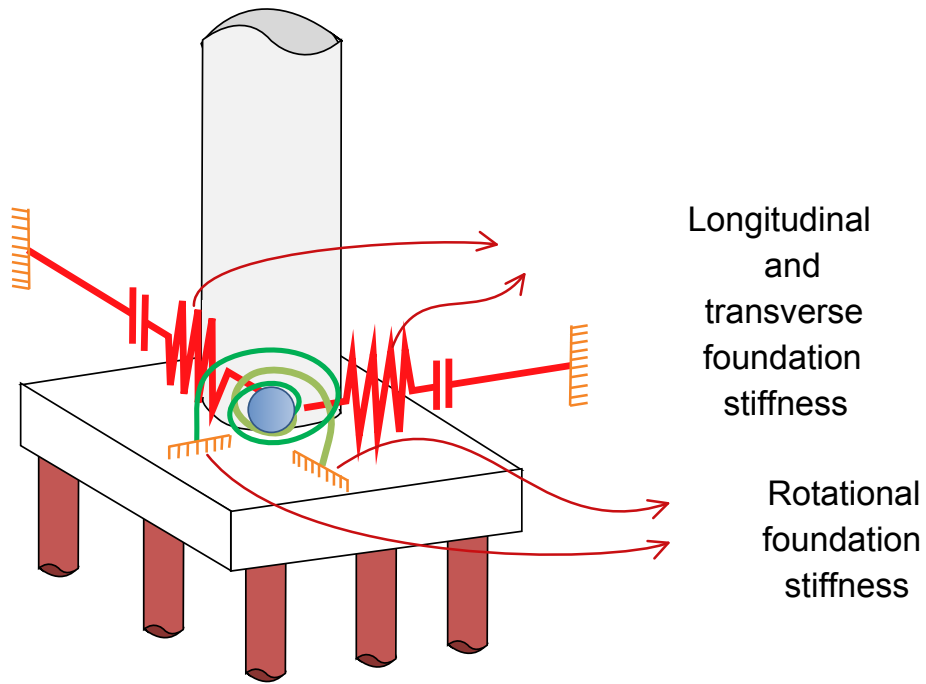


Figure 4.13: Schematic and model properties view of the MSSS bridge deep foundation

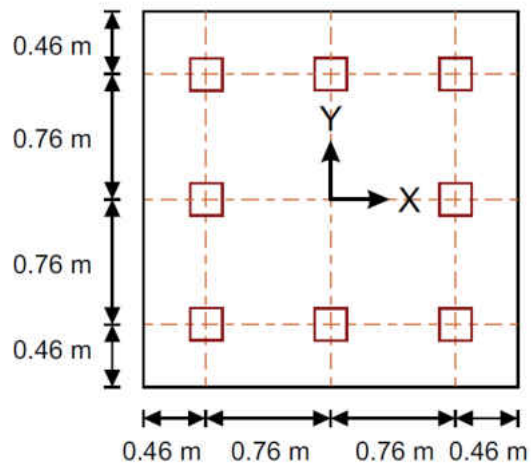


Figure 4.14: MSSS bridge deep foundation unit layout

For each single pile the vertical and horizontal stiffness assumed to be 175 KN/mm and 7 KN/mm/pile. The overall rotational and horizontal stiffness of the deep foundation unit can be obtained from formulation suggested by Ma and Deng (2000) [76] and have been implemented in the Openses model. It should be noted that the translational foundation behavior assumed to be tri-linear however the rotational foundation spring assumed to be linear in the model. The nonlinear behavior of the horizontal stiffness of the foundation can be found in figure 4.15.

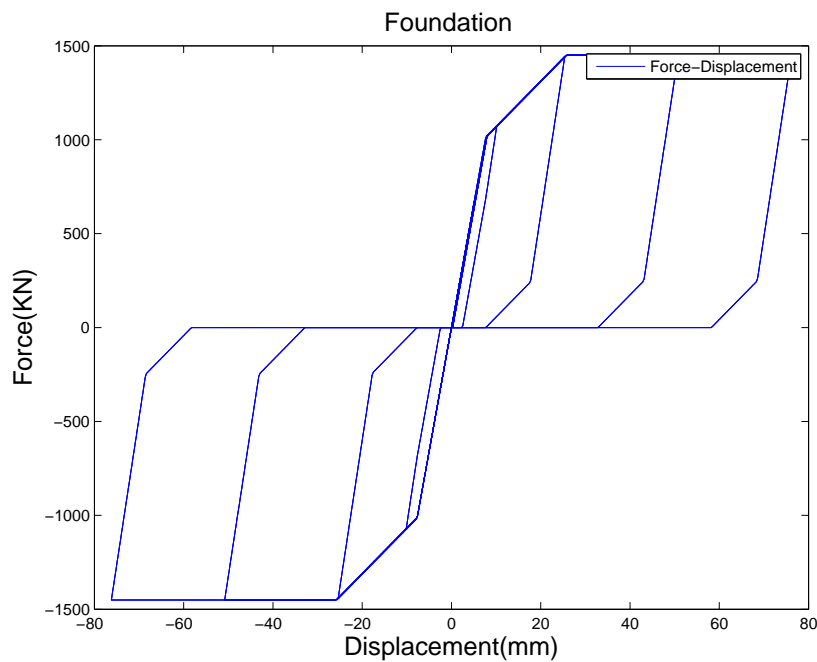


Figure 4.15: Typical horizontal behavior of nonlinear stiffness of deep foundation

4.2.4 parameter screening analysis of the bridge structure

In section 4.1, 43 parameters that control the characteristic of the bridge structure had been identified. However from these parameters, only 30 of them have been implemented to the model used for this study. Implementation of the rest of these parameters either have not been feasible (i.e.

use of lumped foundation springs as opposed to piles p-y, soils elements due to computational expenses for soil structure interaction model) or it was not possible to define a parameter that can independently control that specific characteristic of the structure. The reason is, combination of parameters which controls a specific input characteristic needed a special treatment in design of experiment and the effect of their interaction on their primary effects needed to be considered. This special consideration can highly increase the computational time which is in contradiction with our initial objective for using Plackett-Burman design in DOE to minimize the computational expenses. Table 4.7 shows the final selection of the sources of uncertainty parameters that have been implemented in the structural model. The second column is showing the upper bound and lower bound of each parameter value. For most cases these bounds are obtained from Nielson and DesRoches (2007) [68] For cases where no data were available $\pm 50\%$ range around the parameter deterministic (median) value have been used for the parameter range. The median values are previously used in other researches mentioned in section 4.2.2 or obtained based on the bridge design code requirements.

As it can be seen from table 4.7 most of these parameters are controlling nonlinear characteristics of the bridge structure. The upper bounds and lower bounds are determining the extremes for variation scenarios of each parameter. It should be noted that these values are not based on the variables distributions of uncertainty. Therefore the outcome of the seismic response of each realization of the structure is highly influenced based on the defined variable range.

Table 4.7: Definition and values for participant parameters in screening study

Parameters	Parameters abbreviation	lower bound	median	upper bound
Coefficient of friction_elastomeric pad (multiplying factor)	cof_ep	0.50	1.00	1.50
Deck stiffness (multiplying factor)	deckstiffac	0.50	1.00	1.50

Parameters	Parameters abbreviation	lower bound	median	upper bound
Damping ratio	dr	0.02	0.05	0.08
Gap at dowels (expansion bearings only) (mm)	dwl_gap	0.00	25.40	50.80
Gap between steel retention dowel and slot in girder for fixed elastometric bearing (mm)	dwl_gap2	0.00	3.18	6.35
Dowel strength for a single dowel multiply by two (KN)	dwl_str	46.18	57.78	69.26
Confined concrete ultimate strain	ecult	-0.04	-0.05	-0.06
Torsional stiffness of column elements (KN.m/rad)	Etor	1557.96	3115.91	4673.87
Concrete strength (Mpa)	fc	26.41	33.52	40.62
Confined concrete ultimate strength (multiplying factor)	fcult	-1.08	-1.21	-1.32
Steel strength (Mpa)	fys	438.22	496.25	555.28
Gap at left abutment (mm)	gap1	36.00	38.00	40.00
Gap at right abutment (mm)	gap2	36.00	38.00	40.00
Gap at left hinge (mm)	gap3	20.00	25.50	31.00
Gap at right hinge (mm)	gap4	20.00	25.50	31.00
Stiffness of Impact elements in longitudinal direction (KN/mm)	impactK1	557.61	1126.38	1672.84
Stiffness of Impact elements in transverse direction (KN/mm)	impactK2	191.77	387.37	575.30
Number of integration points for bentcap elements	intbent	4.00	5.00	6.00
Number of integration points for column elements	intcolumn	4.00	5.00	6.00
Multiplication factor for deck mass (percentage)	ms	0.90	1.00	1.10
Vertical stiffness of foundation piles (KN/mm/pile)	rot_fnd	105.08	212.26	315.23
Lateral stiffness of abutment piles (KN/mm/pile)	st_aba	4.90	9.91	14.71
Soil stiffness of abutment (KN/mm/m)	st_abp	10.27	20.75	30.82
Shear modulus of elastomeric pad (multiplying factor)	st_ep	0.50	1.00	1.50
Modulus of elasticity for reinforcing steel (Gpa)	steelEs	180.09	202.10	220.11

Parameters	Parameters abbreviation	lower bound	median	upper bound
Strain hardening ratio for reinforcing steel	steelhr	0.01	0.02	0.03
Pile translational yielding strength factor	transpilefyfactor	0.50	1.00	1.50
Lateral stiffness of foundation piles (KN/mm/pile)	trns_fnd	3.50	7.08	10.51
Ultimate strength of abutment pile (multiplying factor)	Ultpilefac	0.50	1.00	1.50
Yield displacement of abutment soil (fraction of ultimate displacement of abutment soil)	Uyas0	0.08	0.10	0.12

4.2.5 Selection of ground motions for screening study

Our results in chapter 3 shows that selection of the records based on SDI is more appropriate deformation of the structure is being recorded as the monitored response of the structure. In addition, record selection based on SDI can reduce the bias whenever ground motion scaling needed to be considered due to lack of enough ground motions in the database. Since the 3D analysis of the structure have been considered for this study, at least two orthogonal components of the ground motions needed to be applied to the structure in the horizontal directions. Therefore 40 pairs of orthogonal ground motions have been selected based on their SDI values. Similar to PGA or PGV, the SDI values exist for each component of ground motions. To compute the overall intensity of the ground motion the rms (root mean square) of two components have been used as a measuring metric for intensity of the ground motions. Using rms values is a common method for computing the overall intensity of the ground motion from each single component metrics (reference). Previously selected and studied suit of 1130 pairs of ground motions in chapter 3 is used as a ground motions pool record selection. The records have been selected randomly given the constrain of evenly distribution of their intensities in the total SDI spectrum of the ground motion pool. Table 4.8 is showing the selected earthquakes for DOE studies and their relevant magnitude and site characteristic. This table is produced based on the data obtained from PEER NGA database 2012 [22]. Figures 4.16 and 4.17 show the distribution of moment M versus shear wave velocity V_{S30} and moment magnitude M versus rupture distance R_{rup} for the selected ground motions.

Table 4.8: Selected pairs of ground motions for bridge parameter screening study

NGA #	SDI (m)	D5-95(s)	Event	Year	Station	Mag	Mech-anism	R_{jb} (km)	R_{rup} (km)	V_{S30} (m/s)	Low freq(Hz)
31	0.04	13.1, 10.6	Parkfield	1966	Cholame - Shandon Array #8	6.19	Strike-Slip	12.9	12.9	256.8	0.25

NGA #	SDI (m)	D5-95(s)	Event	Year	Station	Mag	Mechanism	R_{jb} (km)	R_{rup} (km)	V_{s30} (m/s)	Low freq(Hz)
93	0.02	20.4, 18.3	San Fernando	1971	Whittier Narrows Dam	6.61	Reverse	39.5	39.5	298.7	0.12
160	0.17	9.7, 9.7	Imperial Valley-06	1979	Bonds Corner	6.53	Strike-Slip	0.5	2.7	223	0.12
170	0.11	14.9, 8.3	Imperial Valley-06	1979	EC County Center FF	6.53	Strike-Slip	7.3	7.3	192.1	0.12
266	0.06	19.0, 15.4	Victoria-Mexico	1980	Chihuahua	6.33	Strike-Slip	18.5	19	274.5	0.25
268	0.02	11.5, 10.5	Victoria-Mexico	1980	SAHOP Casa Flores	6.33	Strike-Slip	39.1	39.3	338.6	0.25
368	0.19	8.0, 9.1	Coalinga-01	1983	Pleasant Valley P.P. - yard	6.36	Reverse	7.7	8.4	257.4	0.25
369	0.07	9.1, 11.6	Coalinga-01	1983	Slack Canyon	6.36	Reverse	26	27.5	684.9	0.25
527	0.11	6.5, 6.1	N. Palm Springs	1986	Morongo Valley	6.06	Reverse-Oblique	3.7	12.1	345.4	0.1
551	0.01	19.1, 18.7	Chalfant Valley-02	1986	Convict Creek	6.19	Strike-Slip	29.4	31.2	338.5	0.25
552	0.01	9.1, 11.5	Chalfant Valley-02	1986	Lake Crowley - Shehorn Res.	6.19	Strike-Slip	22.1	24.5	338.5	0.62
556	0.008	11.1, 12.3	Chalfant Valley-02	1986	McGee Creek - Surface	6.19	Strike-Slip	28.2	30.1	359.2	0.12
727	0.14	12.1, 12.3	Superstition Hills-02	1987	Superstition Mtn Camera	6.54	Strike-Slip	5.6	5.6	362.4	0.38
728	0.10	15.2, 20.2	Superstition Hills-02	1987	Westmorland Fire Sta	6.54	Strike-Slip	13	13	193.7	0.12
752	0.15	14.7, 11.5	Loma Prieta	1989	Capitola	6.93	Reverse-Oblique	8.7	15.2	288.6	0.25
776	0.18	20.1, 20.6	Loma Prieta	1989	Hollister - South & Pine	6.93	Reverse-Oblique	27.7	27.9	370.8	0.12
953	0.25	8.5, 8.5	Northridge-01	1994	Beverly Hills - 14145 Mulhol	6.69	Reverse	9.4	17.1	355.8	0.25
963	0.18	8.9, 9.0	Northridge-01	1994	Castaic - Old Ridge Route	6.69	Reverse	20.1	20.7	450.3	0.12
991	0.05	10.8, 10.2	Northridge-01	1994	LA - Cypress Ave	6.69	Reverse	29	30.7	446	0.25
1004	0.26	8.7, 7.9	Northridge-01	1994	LA - Sepulveda VA Hospital	6.69	Reverse	0	8.4	380.1	0.12

NGA #	SDI (m)	D5-95(s)	Event	Year	Station	Mag	Mechanism	R_{jb} (km)	R_{rup} (km)	V_{s30} (m/s)	Low freq(Hz)
1077	0.09	10.8, 8.8	North-ridge-01	1994	Santa Monica City Hall	6.69	Reverse	17.3	26.4	336.2	0.14
1087	0.27	10.3, 12.1	North-ridge-01	1994	Tarzana - Cedar Hill A	6.69	Reverse	0.4	15.6	257.2	0.1
1116	0.11	13.3, 9.4	Kobe-Japan	1995	Shin-Osaka	6.9	Strike-Slip	19.1	19.1	256	0.12
1158	0.13	11.7, 10.1	Kocaeli-Turkey	1999	Duzce	7.51	Strike-Slip	13.6	15.4	276	0.24
1163	0.04	35.1, 36.4	Kocaeli-Turkey	1999	Hava Alani	7.51	Strike-Slip	58.3	60	424.8	0.09
1180	0.06	52.7, 54.6	Chi-Chi-Taiwan	1999	CHY002	7.62	Reverse-Oblique	25	25	235.1	0.04
1185	0.03	80.3, 84.5	Chi-Chi-Taiwan	1999	CHY012	7.62	Reverse-Oblique	59	59	198.4	0.04
1197	0.26	8.2, 6.2	Chi-Chi-Taiwan	1999	CHY028	7.62	Reverse-Oblique	3.1	3.1	542.6	0.15
1201	0.17	30.1, 24.4	Chi-Chi-Taiwan	1999	CHY034	7.62	Reverse-Oblique	14.8	14.8	378.8	0.04
1203	0.12	25.8, 32.7	Chi-Chi-Taiwan	1999	CHY036	7.62	Reverse-Oblique	16.1	16.1	233.1	0.06
1205	0.10	31.8, 20.9	Chi-Chi-Taiwan	1999	CHY041	7.62	Reverse-Oblique	19.4	19.8	492.3	0.05
1231	0.47	25.6, 18.0	Chi-Chi-Taiwan	1999	CHY080	7.62	Reverse-Oblique	0.1	2.7	680	0.12
1246	0.09	49.5, 51.4	Chi-Chi-Taiwan	1999	CHY104	7.62	Reverse-Oblique	18	18	223.2	0.06
1260	0.05	32.9, 29.2	Chi-Chi-Taiwan	1999	HWA007	7.62	Reverse-Oblique	52.6	56.3	255.6	0.03
1508	0.22	22.0, 24.0	Chi-Chi-Taiwan	1999	TCU072	7.62	Reverse-Oblique	0	7	468.1	0.06
1509	0.26	11.8, 21.4	Chi-Chi-Taiwan	1999	TCU074	7.62	Reverse-Oblique	0	13.5	549.4	0.16
1517	0.48	14.5, 23.2	Chi-Chi-Taiwan	1999	TCU084	7.62	Reverse-Oblique	0	11.2	680	0.25
1536	0.11	34.6, 31.8	Chi-Chi-Taiwan	1999	TCU110	7.62	Reverse-Oblique	11.6	11.6	212.7	0.05
1553	0.04	52.2, 51.4	Chi-Chi-Taiwan	1999	TCU141	7.62	Reverse-Oblique	24.2	24.2	209.2	0.06
2752	0.04	15.4, 18.5	Chi-Chi-Taiwan-04	1999	CHY101	6.2	Strike-Slip	21.6	21.7	258.9	0.19

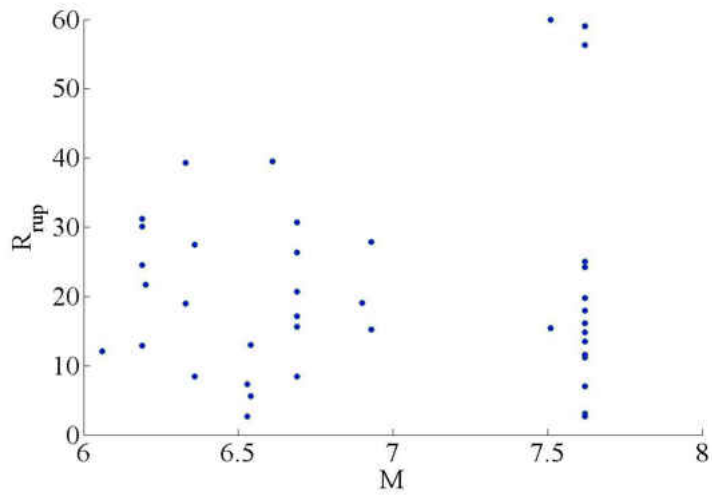


Figure 4.16: Relationship between R_{rup} and Moment magnitude for the selected pairs of ground motions

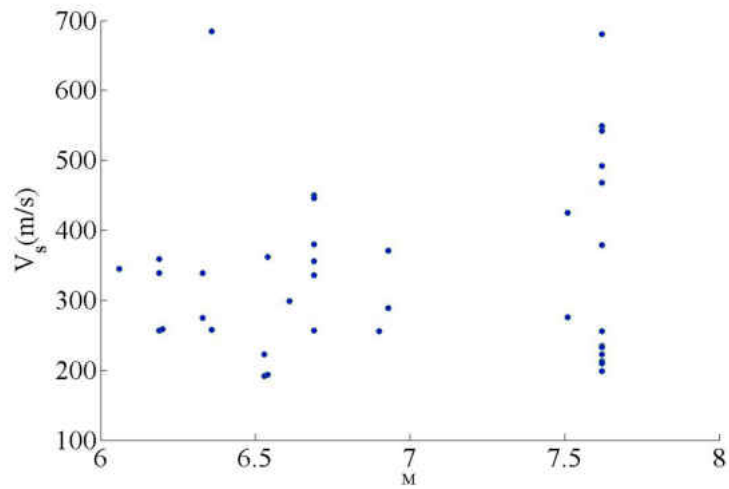


Figure 4.17: Relationship between V_{S30} and Moment magnitude for the selected pairs of ground motions

It should be noted that in the calculation of SDI the period of the first mode of vibration of the bridge in each direction have been considered. The first mode of vibration assumed to remain the same with variation of bridge DOE input parameters for simplicity. The period of the first mode of vibration of the structure in longitudinal and transverse direction is 0.39 s and 0.31 s. The results from the chapter 3 shows that period elongation between 1 s to 2 s can be assumed for nonlinear structures therefore the period elongation of the nonlinear bridge is assumed to be 1 s for each direction.

4.2.6 Plackett-Burman design

Plackett-Burman design have been used in parameter screening to investigate the effect of each parameter and find the most influential parameter effect. Table 4.9 shows the two level Plackett-Burman matrix. In table 4.9, (-) and (+) shows the upper bound and lower bound of each input parameter consequently. Values for the upper bound and lower bound have been defined in table 4.7. Total number of 32 runs have been used which is the minimum number of runs of Plackett-Burman design of 32 parameters. Increasing the number of runs can increase the accuracy of the main effect estimation and can reduce the secondary effect of parameters in the response. However since the purpose of selecting this design was to reduce the computational time, therefore the number of runs have been decided to be kept as the minimum. It should be noted that this design is repeated for all 40 pairs of ground motions that have been selected in section 4.2.5.

Table 4.9: Plackett-Burman design matrix

Parameters abbreviation	R u n 1	R u n 2	R u n 3	R u n 4	R u n 5	R u n 6	R u n 7	R u n 8	R u n 9	R u n 10	R u n 11	R u n 12	R u n 13	R u n 14	R u n 15	R u n 16	R u n 17	R u n 18	R u n 19	R u n 20	R u n 21	R u n 22	R u n 23	R u n 24	R u n 25	R u n 26	R u n 27	R u n 28	R u n 29	R u n 30	R u n 31	R u n 32			
fc	+	+	-	+	-	+	+	+	-	+	+	-	-	-	+	-	-	+	+	-	-	+	+	-	+	-	-	+	-	-	+	-			
fys	-	+	-	-	-	-	-	+	-	+	-	+	-	+	+	+	-	+	-	-	+	+	+	+	-	-	+	-	+	+	+	+	-		
cof_ep	+	-	-	+	-	-	+	+	+	-	-	+	+	-	+	-	+	+	-	-	+	+	-	-	+	+	+	-	-	+	-	-	-		
st_ep	+	+	-	-	-	-	+	-	-	+	+	-	+	-	+	-	+	-	+	+	-	-	+	-	+	+	+	+	+	-	-	+	-		
dwl_str	-	-	-	-	+	+	+	-	-	+	-	+	+	+	+	-	+	-	+	-	+	-	+	+	+	-	+	+	-	+	+	-	-		
dwl_gap	-	+	-	-	-	+	-	-	+	+	+	+	+	-	-	-	+	-	+	-	+	-	+	-	+	+	+	-	+	+	-	+	+		
st_abp	+	-	-	-	-	-	+	+	-	-	+	+	+	+	-	+	-	-	-	+	-	+	+	-	-	+	-	+	-	+	+	+	+		
st_aba	+	-	-	+	+	+	-	+	+	+	-	+	-	+	-	-	-	+	-	+	+	-	+	+	-	+	-	+	-	-	-	-	-		
rot_fnd	+	-	-	-	-	+	+	-	+	-	-	+	-	+	-	+	+	+	+	+	+	-	-	+	+	-	+	-	+	+	+	+	+		
trns_fnd	+	-	-	-	+	+	-	+	-	+	+	+	-	-	+	+	+	-	-	-	-	-	-	-	+	+	+	+	-	-	-	-	+	+	
ms	+	+	-	+	+	-	-	+	-	-	+	-	+	+	-	-	+	+	+	+	-	-	-	+	-	-	+	-	-	+	-	+	+		
dr	-	-	-	-	-	+	-	+	+	-	+	-	+	+	+	+	+	+	+	+	-	-	+	-	+	-	+	-	+	+	-	-	-		
gap1	-	-	-	+	-	-	-	-	+	-	+	-	-	+	+	+	+	+	+	-	+	+	-	+	-	+	-	+	+	-	-	+	+		
gap2	-	+	-	+	+	+	+	+	+	+	+	+	+	+	+	-	-	-	-	-	-	-	-	+	-	+	-	+	+	-	-	+	+		
gap3	+	-	-	-	+	-	-	+	+	-	+	+	+	+	-	-	-	+	+	-	-	+	-	-	+	-	+	+	-	+	+	-	+	+	
gap4	+	+	-	-	+	-	-	+	+	-	-	-	+	-	+	+	-	-	+	-	+	-	+	+	+	-	-	+	-	+	-	+	+		
impactK1	-	+	-	+	+	-	+	-	-	-	-	+	-	-	-	+	+	+	+	-	-	+	+	+	-	+	+	+	-	-	-	-	+	+	
impactK2	+	-	-	+	+	-	-	-	-	+	+	+	+	-	+	+	+	-	+	+	+	+	+	+	-	-	-	-	-	+	-	-	-	-	
transpilefactor	+	-	-	+	-	+	+	-	-	+	+	-	+	-	+	-	+	-	+	-	+	-	+	+	+	-	+	+	+	+	+	+	+	-	
deckstiffac	+	+	-	+	-	-	+	-	+	+	-	-	+	+	-	+	+	-	-	-	-	-	-	+	+	+	+	-	+	-	+	-	+	-	
fcult	-	+	-	+	-	-	-	+	+	+	+	+	-	-	-	-	+	-	-	+	-	+	-	+	+	+	-	-	+	+	+	+	+	+	
ecult	+	+	-	-	+	+	-	-	-	-	+	-	-	+	-	-	+	+	-	-	+	+	+	+	-	+	+	-	-	+	+	-	+	+	
steelEs	-	+	-	-	+	-	+	-	+	-	+	+	-	+	+	-	-	+	-	-	+	+	+	+	-	+	+	-	-	-	-	-	+	-	
steelhr	+	+	-	-	-	+	+	+	+	+	+	-	-	-	-	+	+	-	+	+	+	+	+	-	-	-	+	-	-	-	-	-	-	+	+
Etor	-	-	-	+	+	+	+	-	+	+	+	-	+	-	-	+	-	+	-	+	-	+	+	-	+	-	-	-	-	-	-	-	+	+	+
intcolumn	-	-	-	+	+	-	+	+	-	+	-	-	-	+	+	-	+	-	+	-	+	-	+	-	-	-	-	+	-	+	+	+	+	+	+
intbent	-	-	-	-	+	-	+	+	+	+	+	-	-	-	-	+	-	+	+	+	-	-	+	-	+	+	+	-	+	+	+	-	+	+	-
dwl_gap2	-	+	-	+	-	+	-	-	-	+	-	+	+	+	+	+	+	-	+	+	+	-	-	-	-	-	+	-	-	+	+	+	+	+	+
Uyas0	+	+	-	+	+	+	-	-	+	-	-	-	-	-	+	+	-	-	-	-	-	-	-	-	-	-	+	+	+	+	+	+	+	+	-
Utlpilefac	-	-	-	+	-	+	-	+	-	-	-	-	+	-	-	-	-	-	-	+	+	+	+	+	+	+	+	+	+	+	+	+	+	+	+

4.2.7 ANOVA table and computation of p-values

Based on the matrix that have been presented in Table 2, various variation of the bridge structure have been generated. Also all 40 pairs of ground motions have been applied to each bridge realization and parameters of interest for the response of the bridge have been monitored and recorded. These parameters are very informative in measurement of performance of the bridge structure and participate in fragility curve development due to vulnerable nature of their element/material (Mackie and Stojadinovic (2004) [42], Mackie and Stojadinovic (2001) [58], Mackie et al. (2011) [60] and Nielson and DesRoches (2007) [68]). Table 4.10 shows the monitored structure response parameters and their abbreviation.

Each one of these response parameters are consisted of multiple responses themselves (lets call them sub-parameters hereafter). For example curvature ductility of the columns are recorded for 6 column in longitudinal and transverse direction. For the abutments also multiple nodes have been defined for each end span of the bridge and the same situation exist of other response parameters. However it was possible to find the effect of input parameters on each sub-parameter, more comprehensive method needed to be used in addition to DOE techniques to find the combined effect of the monitored parameter from the sub-parameters. In similar researches, the maximum value of the sub-parameter have been selected and been used in the ANOVA analysis (Nielson and DesRoches (2007) [68]). Instead, in this research RMS of maximum value of sub parameters have been computed to achieve a single value to quantify the response of each bridge monitored parameter. The intension was to account for participation of different elements of the bridge components in the response of the structure. These 9 monitored responses have been analyzed individually and for each response parameter the main effect and ANOVA table have been computed with respect to the design of experiment matrix. The significant level used for this analysis of variance assumed to be 0.05 which is a well-accepted value for DOE analysis purpose (DC Montgomery 2010 [80]). Since

earthquakes with different intensities will not affect the structure in the same way, a standardized technique have been utilized so that the response of the structures for various intensity of the excitations become comparable with each other. In addition to 32 runs corresponding to experimental design, another realization of the bridge structure with the median of the parameters (instead of upper and lower bounds) have been analyzed and monitored responses have been recorded for each earthquake. This run can be called run0. Consequently the monitored response parameters for run1 through run32 have been divided by the response recorded from run0. The standardized response can be used for computation of ANOVA table and obtaining main effect without the necessity of usage of blocking for different intensities of the ground motions.

Table 4.10: Monitored response components of bridge structure

Abbreviation	Description
Duc_ac	Curvature ductility of concrete columns in transverse direction
Duc_lg	Curvature ductility of concrete columns in longitudinal direction
Fxb-tr	Deformation of fixed bearings in transverse direction
Fxb-lg	Deformation of fixed bearings in longitudinal direction
Exb-tr	Deformation of expansion bearings in transverse direction
Exb-lg	Deformation of expansion bearings in longitudinal direction
Ab-pass	Deformation of abutments in longitudinal passive action
Abd-ac	Deformation of abutments in longitudinal active action
Abd-tr	Deformation of abutments in transverse direction

The important outcome of the ANOVA table are the p-values for each parameter. Usually the parameters with p-value less than 0.05 considered to be effective on the variation of the response. However contrary conclusion is not correct for the parameter with a higher p-value. The simple explanation of the p-value in this study is the small p-value indicate that the variation of the response with the input parameter variation (upper and lower bound) is meaningful than would be

expected by chance. Having found the significant parameters with p-values less than 0.05 in the response, the main effect of each parameters were obtained and consequently based on the ranking of the main effects, 3 parameters that have the highest effects in their group were selected for each monitored response of the bridge.

4.2.8 Effect of the parameters screening on fragility analysis

The primary goal of using parameter screening and DOE approach in this study was to reduce the number of parameters needed to be implemented in the finite element model of the structure and consequently PBA of the highway bridges. However one might ask about the effect of reduction of number of probabilistically treated parameters in the bridge model and its impact on the fragility analysis results. Therefore in this section three different extreme cases of the parameter treatment in the probabilistic response analysis of the bridge have been selected for further investigation. The first corresponds to deterministic treatment of variables in the demand model of the bridge structure. The second case uses partially probabilistic approach which means only the important parameters obtained from the parameters screening studies is implemented in the demand analysis. The third case is fully probabilistic approach, for that all the parameters have been treated as probabilistic in the bridge demand model. Therefore for the first case only the earthquake and the incident angle will be treated probabilistic, For the second case influential parameters obtained from the screening of the bridge responses will be will be treated probabilistically in addition to the earthquake and its incident angle and for the third case all the parameters considered for the screening of the variables will be included in the bridge model probabilistically. For the parameters that will be considered deterministic, the mean value of the assigned probability will be used as a fixed (deterministic) value in the model. A conventional fragility analysis method from the Nielson and DesRoches (2007) [68] have been adopted for fragility analysis. First the joint probability distribution of the input parameters have been generated from the marginal distributions of the

parameters. For each case multiple bridge realization have been generated using Latin-Hypercube sampling method (Ayyub and Lai, 1989 [81]). This method will draw samples with uniform probability of occurrence from the joint probability function of the input parameters and based on each sample (vector of input parameters) have been drawn, a realization of the bridge will be generated. From 550 pairs of ground motions considered in chapter 3 the top 300 pairs in terms of SDI intensity have been selected for making the ground motion pool. Also the incident angle of the ground motion have been assumed to be uniformly random. The maximum response of each structure subjected to various ground motions is recorded in multiple locations as listed in table 3. From the response of the structure and the intensity of the records applied to the structure, probabilistic seismic demand model (PSDM) will be computed using Equation 4.3.

$$\ln(S_d) = a + b * \ln(SDI) \quad \& \quad \beta_{d|SDI} \quad (4.3)$$

In Equation 4.3 S_d and $\beta_{d|SDI}$ are the mean and dispersion of the demand conditioned on the SDI intensity. Parameters a and b also can be obtained from the regression analysis on the demand values (i.e. *Duc.lg*, *Fxb.tr* and etc.) obtained for their corresponding ground motion intensity (SDI) in logarithmic space. Also from the regression analysis dispersion of the demand parameter conditioned on the intensity measuring variable (i.e. SDI) value will be computed for various demand variables. For performing the fragility analysis, the capacity model needed to be defined. The limit states description used in this study are in accordance with the FEMA, 2003 guidelines. The FEMA 2003 indicated 4 levels of limit states for the capacity. These limit states are Slight damage, Moderate damage, Extensive damage and complete damage. Description of these limit states have been listed below:

- Slight: Minor cracking and spalling to the abutment, cracks in shear keys at abutments,

minor spalling and cracks at hinges, minor spalling at the column (damage requires no more than cosmetic repair) or minor cracking to the deck.

- Moderate: Any column experiencing moderate (shear cracks) cracking and spalling (column structurally still sound), moderate movement of the abutment (<2 in), extensive cracking and spalling of shear keys, any connection having cracked shear keys or bent bolts, keeper bar failure without unseating, rocker bearing failure or moderate settlement of the approach.
- Extensive: Any column degrading without collapse shear failure (column structurally unsafe), significant residual movement at connections, or major settlement approach, vertical offset of the abutment, differential settlement at connections, shear key failure at abutments.
- Complete: Any column collapsing and connection losing all bearing support, which may lead to imminent deck collapse, tilting of substructure due to foundation failure.

For fragility analysis the quantitative limit states are required. However the limit states mentioned above are descriptive rather than quantitative. In this study the quantitative measurement corresponds to each level of FEMA 2003 limit state description mentioned above have been used based on the suggested values from Nielson and DesRoches 2007 [68]. The tables 4.23 and 4.22 shows the capacity model assumed for this study.

Having obtained the limit states and demand models, component fragility functions for each limit states needed to be calculated.

$$P[C_i - D < 0 | IM] = \Phi \left(\frac{\ln(S_{d|SDI}/S_{c_i})}{\beta_{d|SDI}^2 + \beta_{c_i}^2} \right) \quad (4.4)$$

Where C corresponds to the capacity of the structure (or limit states) and i corresponds to the the i^{th} limit states.

Final objective of this section of the research is to perform a comprehensive comparison between deferent cases. The effect of including parameters uncertainty in the model on the fragility curves needed to be evaluated. To show the amount of uncertainty that have been captured using design of experiment selected parameters in case 2, the following method is presented:

Various sources of uncertainties participate in the fragility analysis. The aleatory uncertainties from the randomness of the ground motion variability, epistemic uncertainties from accuracy of the modeling used to represent the structure dynamics and epistemic uncertainties that is originated from the lack of knowledge for material variations and etc. However in comparison between case 2 and case 1, its assumed that participation of all the uncertainties in the fragility analysis are the same except for the epistemic uncertainty that comes from the variations of the input parameters. Based on Baker and Cornell (2008) [83], the uncertainty in the fragility curve can be modeled as uncertainty in the mean estimate of the demand model. This representation of uncertainty in the mean estimate of demand model is suitable for this study since the mean and dispersion of capacity models adopted for case 1 to case 3 does not account for variability of the parameters. From Baker and Cornell (2008) [83], the aleatory and epistemic uncertainty in the demand model can be written as:

$$\begin{aligned}
 \text{Aleatory uncertainty: } & \text{Var}[\ln(S_d|SDI)] = \beta_{A;d|SDI}^2 \\
 \text{Epistemic uncertainty: } & \text{Var}[\mu_{\ln(S_d|SDI)}] = \beta_{E;d|SDI}^2 \tag{4.5} \\
 \text{where } & \beta_{d|SDI} = \sqrt{\beta_{A;d|SDI}^2 + \beta_{E;d|SDI}^2}
 \end{aligned}$$

Considering the $\beta_{d|SDI}$ can be obtained using regression analysis on the structure component responses and the $\beta_{E;d|SDI}^2 = 0$ for case 1(since no input parameters variation is defined for case 1), the epistemic uncertainty of case 2 can be obtained from equation 4.6 assuming the equal aleatory

uncertainty for case 1 and case 2.

Consequently the fragility median estimate and epistemic uncertainty $\pm\sigma$ bounds can be obtained using equations 4.7 and 4.8 where $\hat{P}[C_i - D < 0|IM]$ and $P_{\pm\sigma}[C_i - D < 0|IM]$ are the mean estimate and bounds of the fragility for i^{th} limit state.

$$\beta_{E;d|SDI(case 2)} = \sqrt{\beta_{d|SDI(case 2)}^2 - \beta_{A;d|SDI(case 1)}^2} \quad (4.6)$$

$$\hat{P}[C_i - D < 0|IM] = \Phi \left(\frac{\ln(S_{d|SDI}/S_{c_i})}{\beta_{d|SDI}^2 + \beta_{c_i}^2 + \beta_{E;d|SDI}^2} \right) \quad (4.7)$$

$$P_{\pm\sigma}[C_i - D < 0|IM] = \Phi \left(\frac{\ln(S_{d|SDI}/S_{c_i}) \pm \beta_{E;d|SDI}}{\beta_{d|SDI}^2 + \beta_{c_i}^2 + \beta_{E;d|SDI}^2} \right) \quad (4.8)$$

Figure 4.18 shows the schematic view of the uncertainty bounds of fragility curve and describes the implementation of equation 4.8. The actual PDF functions that describe the variation of the mean estimate is included for SDI of 0.29 m, 0.69 m and 0.99 m. However the distribution of the mean estimate of the demand is normal, the distribution of the probability of exceeding a damage state does not follow a normal distribution and its distribution shape is dependent on the intensity of the ground motion. Therefore the epistemic uncertainty captured by defining parameters variation in case 2 compared to case 1 can be presented as the fragility mean estimate and mean estimate $\pm\beta_{E;d|SDI(case 2)}$.

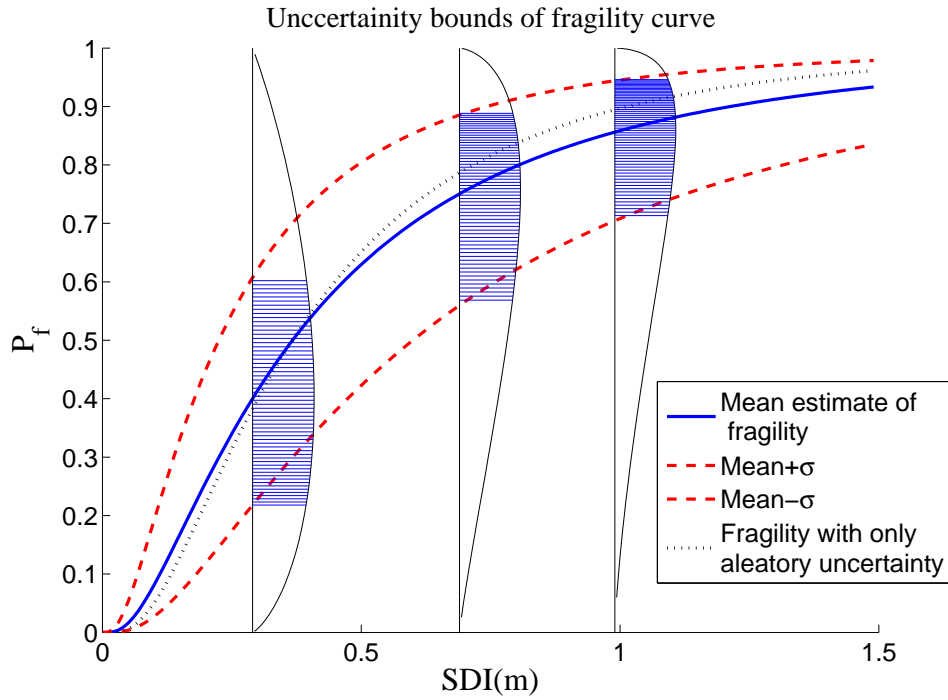


Figure 4.18: Schematic uncertainty bounds of fragility curve

4.3 Results

4.3.1 Parameters screening of the MSSS bridge seismic response

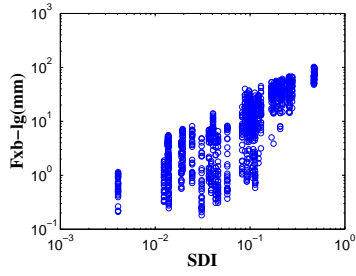
40 pairs of orthogonal components of ground motion have been defined in section 4.2.5. Also 32 variation of bridges have been generated for the original Plackett-Burman design and 33th realization have been used for standardization of the response. The parameters for which the main effects have been analyzed can be seen in table 4.7. This table also shows the parameters upper and lower bound as well as their mean values. 9 different component responses of the bridge (table 4.10) have been recorded for post analysis and screening studies. Consequently the rms of maximum of each response component have been computed. Figure 4.19(b) through 4.19(i)

shows the relation between each rms of monitored response components and intensity of the ground motions applied to the bridge structure. It should be noted that these responses are not standardized with the method described at section 4.2.8. In figure 4.19, 40 intensities corresponding to selected orthogonal components of the ground motions can be seen. For each pairs of ground motion, variation of the response on the vertical axis is shown. Therefore 32 responses corresponding to each intensity of the ground motion are location along the vertical axis for all the components of the bridge structure in this figure.

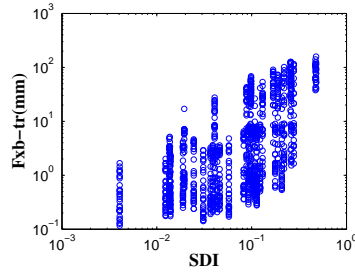
Multiple important results from the variation in the response of the structure can be perceived from figure 4.19. The mean and distribution of the bridge component responses are highly dependent on the intensity of the ground motions. The logarithmic scale implies that a higher ground motions intensity can exponentially increase the response of the structure. Investigating the response related to each ground motion indicates that the variation of the responses for different realization of the bridge structures generated based on Plackett-Burman design matrix is also significant. Also the coefficient of variation for responses corresponding to each intensity is varying for all the components of the structure. As an example, for curvature ductility of the column in longitudinal direction, COV are 0.46 and 0.85 for SDI of 0.27 m and 0.09 m respectively. This matter need a close attention since for a SDOF linear structure, the COVs for both cases should be same. For a MDOF nonlinear structure the modal participation and time variant stiffness of the structure makes the prediction of the response very difficult. Another matter of interest is the very high sensitivity of the component responses to the variation of the input parameters. For example in figure 4.19(d), the response of the expansion bearing varies in the range of 1.24 to 39.74 mm when SDI is 0.13 m. Also in figure 4.19(f) the abutment deformation in longitudinal direction varies between 0.43 mm to 5.93 mm for SDI equal to 0.02 m. This broad variation of the responses of a component subjected to an identical pair of ground motion is originated from the extreme cases defined for the parameters upper and lower bounds. However these extreme cases push the

structure to generate upper and lower limits of the response, in reality existent of a such realization of the bridge generated from upper and lower bounds of parameters is very unlikely from the probabilistic point of view.

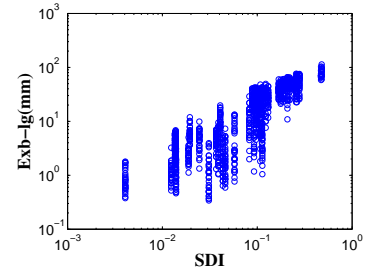
Comparison between figures 4.19(a) to 4.19(d) shows that the response of fixed and expansion elastomeric bearings are very similar in dispersion. However the magnitude of response of the fixed bearing is less than expansion bearing since the gap between the steel dowel and deck is implemented for the expansion bearing. As a results, the fixed bearing has more stiffness compared to the expansion bearing. Also the maximum response of fixed bearing in the longitudinal and transverse directions are similar due to the symmetrical stiffness of the bearings in both direction. The same conclusion is not valid for the expansion bearing. The minimum response of the expansion bearing is smaller in magnitude for the transverse direction compared to longitudinal direction since the bearing gap is only implemented in the longitudinal direction to facilitate the movement of the superstructure on the bent cap. Comparison between figures 4.19(e) to 4.19(g) identifies the general behaviors of the abutment in different directions. These figures shows that deformations of the abutment in active and passive longitudinal directions are significantly higher than transverse direction. Also in figures 4.19(h) and 4.19(i), curvature ductility of the columns are less than 1 for most cases. I.e. for SDI values less than 0.2 m, the curvature of the columns are less than the yielding curvature. Whereas for SDI more than 0.2, the longitudinal and transverse curvature ductility in the mean exceeds 0.7 therefore the combined ductility of the orthogonal directions exceeds the yielding ductility in the mean.



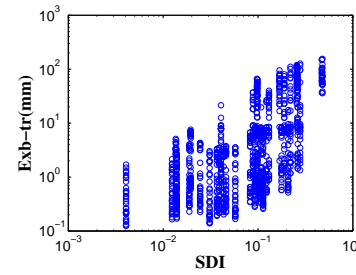
(a) Fixed bearings in longitudinal direction (mm)



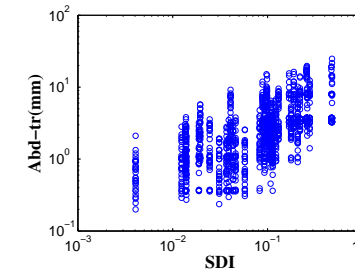
(b) Fixed bearings in transverse direction (mm)



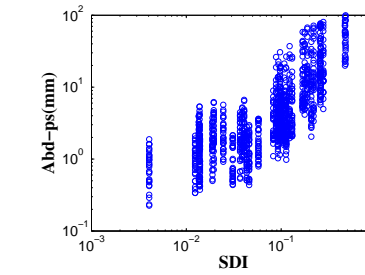
(c) Expansion bearings in longitudinal direction (mm)



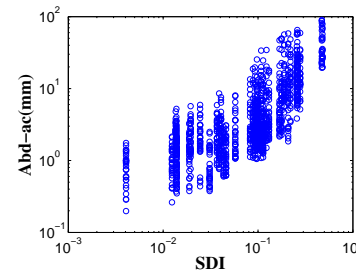
(d) Expansion bearings in transverse direction (mm)



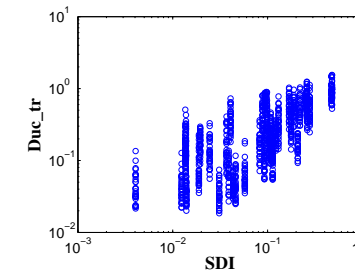
(e) Abutments in transverse direction (mm)



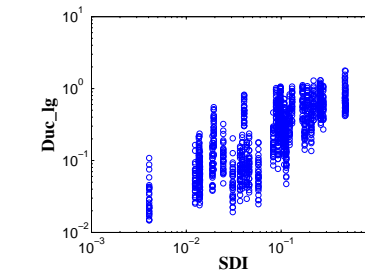
(f) Abutments in longitudinal passive action (mm)



(g) Abutments in longitudinal active action (mm)



(h) Curvature ductility of concrete columns in transverse direction



(i) Curvature ductility of concrete columns

Figure 4.19: Variation of structure monitored responses versus SDI intensity of the earthquake in log-space

Tables 4.11 to 4.19 show the p-values and main effects that have been computed using *MATLAB*

n-way ANOVA function. Only parameters that have p-values less than 0.05 have been listed and the parameters are sorted based on their main effect absolute values. Complete *ANOVA* tables can be reviewed in appendix A.

Tables 4.11 to 4.13 show the influential input parameters for the response of abutments in longitudinal and transverse direction. For the abutment in active direction, lateral stiffness of the abutment piles is the most important parameter. The negative sign of the main effect indicates that decreasing of the stiffness of the piles can increase the deformation of the abutment in active direction. The gap at the dowel for expansion bearings and mass of the superstructure are at the 2nd and 3rd rank for response of the abutment in active direction. In the passive and transverse direction also the abutment deformation is influenced by active stiffness of abutment piles, gap between the deck elements, damping ratio of the bridge model, gap at the dowel for fixed bearings and ultimate strength of abutment piles. Most of the important parameters in abutment deformation are either participate in the analytical modeling of the abutment unit or participate in the modeling of the bridge components attached to the abutment. Influential parameters on the response of columns can be seen from tables 4.14 and 4.15. The important participant parameters in curvature ductility of the columns are damping ratio, yield strength of the longitudinal reinforcing rebars, Steel modulus of elasticity, and rotational stiffness of the foundation units. Increasing the rotational stiffness of the foundation and steel module of elasticity can increase the curvature ductility of the columns whereas an inverse trend can be realized for other parameters. I.e decreasing the damping ratio or yield strength of the steel rebars can decrease the curvature ductility of the columns. Tables 4.16 to 4.19 are dedicated to bearing important parameters. For deformation of expansion and fixed bearings, friction coefficient of the bearing, elastomeric pad shear stiffness, deck mass, damping ratio, stiffness of the impact elements and gap for the fixed bearing dowels are the influential parameters. Of course the friction coefficient and shear stiffness of the pad that participate in the stiffness of the element have negative effect values. The same trend can be seen for damping ratio

which participate in all the elements dynamic behavior as a global stiffness proportional damping. Increasing the gap at the fixed bearing dowels also can increase the bearings deformation. For the abutment and expansion bearings in active direction, the mass of the superstructure appear with positive sign which indicate that increasing the mass can increase the deformation of the structure components. It should be noted that the mass provide moment of inertia for the super structure as well as gravity load for the elements retaining the superstructure. The effect of mass for curvature ductility of the columns in longitudinal and transverse directions are -0.072 and 0.074 respectively. These values are very small compared to the top ranked effects for the column seismic response. This can be explained with the appropriate level of isolation which is provided by bearings between the superstructure and substructure.

By studying the results from tables 4.11 to 4.19 one can realize that the effect of input parameter rapidly reduce from the top to the bottom of the tables. For example in table 4.13 the effect of soil stiffness of the abutment piles is 5.51 times more than stiffness of impact elements. It means the soil stiffness of the abutment piles have 5.51 times more influence on the deformation of abutment in the transverse direction compared to the stiffness of impact elements. For this reason only the first three parameters for each monitored response have been selected as influential parameters for future studies in PBA and bridge fragility analysis. Table 4.20 shows the selected parameter for MSSS concrete girder bridge.

Table 4.11: Sorted main effects and their correspondence p-values for deformation of abutments in longitudinal active direction

Parameter	P-Value	Effect
st_aba	0.000	-1.859
dwl_gap	0.000	0.986
ms	0.000	0.875
Utpilefac	0.000	-0.703
gap3	0.000	-0.655
ecult	0.000	0.443
st_abp	0.000	-0.422
fcult	0.000	0.373
dr	0.000	-0.361
steelhr	0.003	-0.206
impactK1	0.003	-0.203
deckstiffac	0.003	-0.203
dwl_str	0.004	0.201
impactK2	0.004	-0.200
dwl_gap2	0.022	-0.159

Table 4.12: Sorted main effects and their correspondence p-values for deformation of abutments in longitudinal passive direction

Parameter	P-Value	Effect
st_aba	0.000	-1.829
Ultpilefac	0.000	-0.761
gap3	0.000	-0.681
ms	0.0000	0.538
st_abp	0.000	-0.492
dwl_gap	0.000	0.390
dr	0.000	-0.288
dwl_str	0.000	0.282
ecult	0.000	0.268
steelhr	0.000	-0.256
dwl_gap2	0.000	-0.240
impactK1	0.000	-0.222
fcult	0.001	0.212
Etor	0.001	-0.212
deckstiffac	0.005	-0.182
cof_ep	0.007	0.174
st_ep	0.011	-0.165
gap2	0.032	-0.140

Table 4.13: Sorted main effects and their correspondence p-values for deformation of abutments in transverse direction

Parameter	P-Value	Effect
st_aba	0.000	-1.711
dwl_gap2	0.000	-0.480
dr	0.000	-0.445
impactK2	0.000	-0.312
Utpilefac	0.000	-0.295
gap3	0.000	-0.291
trns_fnd	0.000	-0.287
gap1	0.000	-0.231
gap4	0.001	-0.222
ms	0.001	0.211
dwl_str	0.020	0.151
cof_ep	0.020	0.151
rot_fnd	0.030	-0.141

Table 4.14: Sorted main effects and their correspondence p-values for curvature ductility of concrete columns in longitudinal direction

Parameter	P-Value	Effect
dr	0.000	-0.573
fys	0.000	-0.291
steelEs	0.000	0.179
deckstiffac	0.000	0.147
rot_fnd	0.000	-0.141
dwl_gap	0.000	-0.102
intbent	0.000	0.087
ms	0.001	-0.072
dwl_gap2	0.001	-0.071
cof_ep	0.005	0.063
dwl_str	0.041	0.046
fc	0.049	0.044

Table 4.15: Sorted main effects and their correspondence p-values for curvature ductility of concrete columns in transverse direction

Parameter	P-Value	Effect
dr	0.000	-0.398
rot_fnd	0.000	0.312
fys	0.000	-0.229
cof_ep	0.000	0.223
transpilefyfactor	0.000	0.218
deckstiffac	0.000	0.137
st_aba	0.000	-0.111
steelEs	0.000	0.110
st_ep	0.000	-0.102
steelhr	0.000	-0.090
intcolumn	0.000	0.085
impactK2	0.000	-0.075
ms	0.000	0.075
trns_fnd	0.000	0.068
dwl_gap	0.001	-0.065
dwl_str	0.014	0.047
fc	0.014	0.047
st_abp	0.015	0.047
Utpilefac	0.021	-0.045
ecult	0.025	-0.043
gap2	0.030	-0.042
dwl_gap2	0.040	-0.040
gap4	0.044	-0.039

Table 4.16: Sorted main effects and their correspondence p-values for deformation of expansion bearings in longitudinal direction

Parameter	P-Value	Effect
cof_ep	0.000	-0.439
ms	0.000	0.258
impactK1	0.000	-0.238
st_ep	0.000	-0.237
dr	0.000	-0.185
impactK2	0.001	-0.111
dwl_gap	0.001	0.109
gap3	0.010	0.083
dwl_str	0.041	-0.066

Table 4.17: Sorted main effects and their correspondence p-values for deformation of expansion bearings in transverse direction

Parameter	P-Value	Effect
cof_ep	0.0000	-1.63175
intbent	0.0000	1.373738
ms	0.0000	-0.81965
trns_fnd	0.0000	0.745686
st_ep	0.0001	-0.70422
fcult	0.0089	0.468148
ecult	0.0473	0.354693

Table 4.18: Sorted main effects and their correspondence p-values for deformation of fixed bearings in longitudinal direction

Parameter	P-Value	Effect
dwl_gap2	0.000	0.760
cof_ep	0.000	-0.599
st_ep	0.000	-0.395
dr	0.000	-0.351
impactK1	0.000	-0.339
ms	0.000	0.245
gap3	0.006	0.175
dwl_str	0.007	-0.175
dwl_gap	0.008	-0.170
steelEs	0.021	0.148
st_aba	0.046	0.128

Table 4.19: Sorted main effects and their correspondence p-values for deformation of fixed bearings in transverse direction

Parameter	P-Value	Effect
dwl_gap2	0.000	1.178
cof_ep	0.000	-1.014
dr	0.000	-0.565
ms	0.000	0.552
st_ep	0.000	-0.458
dwl_str	0.000	-0.307
steelhr	0.000	0.306
steelEs	0.000	0.294
trns_fnd	0.026	-0.178
fcult	0.037	0.167

Table 4.20: Significant Parameters for MSSS Concrete Girder Bridge

Response parameters	emerging as top three significant variables
Coefficient of friction for elastomeric pad	4
Gap at dowels for expansion bearings	1
Gap between steel retention dowel and slot in girder for fixed elastometric bearing	4
Modulus of elasticity for reinforcing steel	1
Damping ratio	5
Steel strength	1
Gap at the hinges	1
Deck mass	2
Stiffness of Impact elements in longitudinal direction	1
Shear modulus of elastomeric pad	4
Rotational stiffness of foundation piles	1
Ultimate strength of abutment pile	1
Lateral stiffness of abutment piles	3

As it can be seen, some input parameters appear multiple times as top three highest main effects for each monitored response. As a result in table 4.20 only 13 parameters exist. The second column of table 4.20 counts the number of times that the parameter emerged as the top three important variable for each monitored response. As an example damping ratio appears at the top three rows for 5 different responses of the bridge therefore one can assume it is one of the most influential parameters in all the monitored responses of the bridge.

These 13 parameters have been selected based on the monitored response of 9 components of the structure which are important for vulnerability analysis of the bridge. However considering other elements response in the screening analysis might change the ranking of the parameters main effect. The results from the DOE approach is also sensitive to the selected parameter bounds in the screening analysis and the ground motions that have been applied to the structure. Despite increasing the number of ground motions in the DOE analysis can significantly increase the computational

time yet it can yield more accurate results.

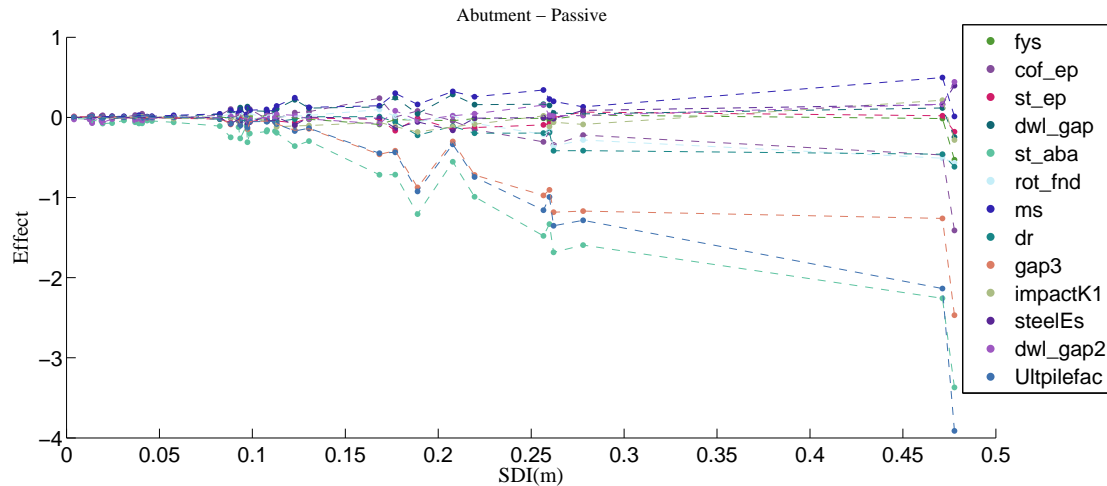


Figure 4.20: Effect of screening design parameters on abutments in longitudinal passive direction (in)

Another interesting result which can be acquired from the screening study of the MSSS concrete bridge is comparing the variation of main effects for different ground motion intensities. Figure 4.20 shows the variation of the main effects (non-normalized) of abutment in longitudinal passive direction for different intensity of the ground motions. Only selected monitored parameters from screening studies are included in the graph (table 4.20). Studying the variation of the effects in figure 4.20 can yield a better understanding for the response of a specific component of the structure given the variation of the parameters and ground motion intensities. The soil stiffness of abutment piles, Ultimate strength of the abutment piles soil and gap between the decks are the first three parameters with highest effects. For this component all these parameters have negative effects as it can be seen. The effect is consistently negative for these parameters for various ground motions intensity. Top three parameters in response of abutment in passive direction are followed by mass of the superstructure, soil stiffness of the abutment, and gap at the dowel for expansion bearings. The soil stiffness of the abutment is not selected since it is not appeared as the top three

parameters however mass of the superstructure and gap at the dowel for expansion bearing can be seen in figure 4.20. The mass of the superstructure has the positive effects for most of the ground motions intensities whereas the gap at the dowel for expansion bearing can be realized with orange color and has negative effects. Observation of the variations of the effects with respect to ground motions intensity reveals the parameters that have consistent sign for their effect for most of the intensities of ground motion have p-values less than 0.05. For example in figure B.6 for curvature ductility of columns in longitudinal direction, the gap at dowel for expansion bearing is changing sign for different ground motions intensities and its p-value (table A.4) is measured as 0.74. The same statement can be said for impact elements stiffness. Because of the lack of enough space in this documents, figures B.4 to B.9 for other monitored responses are included in Appendix B. It should be noted that in these graphs only the selected parameters from the DOE approach are included. These graphs contain important information regarding the participation of monitored parameters in the response of components of the structure.

4.3.2 Fragility analysis of MSSS Bridge using parameters screening results

The same bridge that have been used for screening of the parameters have been used for fragility analysis. As mentioned in section 4.2.8, three cases have been considered for this study. Table 4.21 shows the structure input parameters and assumptions made for their probability density function. The last column indicates in which cases the parameter have been modeled probabilistically.

Table 4.21: Fragility analysis parameter definition and parameters case participation

Parameter definition	Parameter abbreviation	Probability density function type	PDF Value 1	PDF Value 2	Case participation
Coefficient of friction_elastomeric pad (multiplying factor)	cof_ep	uniform	0.50	1.50	Cases 2&3
Deck stiffness (multiplying factor)	deckstiffac	uniform	0.50	1.50	Case 3
Damping ratio	dr	normal	0.05	0.01	Cases 2&3
Gap at dowels (expansion bearings only) (mm)	dwl_gap	uniform	0.00	50.80	Cases 2&3
Gap between steel retention dowel and slot in girder for fixed elastomeric bearing (mm)	dwl_gap2	uniform	0.00	6.35	Cases 2&3
Dowel strength for a single dowel multiply by two (KN)	dwl_str	uniform	46.18	69.26	Case 3
Confined concrete ultimate strain	ecult	lognormal	0.04	0.01	Cases 3
Torsional stiffness of column elements(KN.m/rad)	Etor	Uniform	1557.96	4673.87	Case 3
Concrete strength (Mpa)	fc	normal	33.46	4.27	Case 3
Confined concrete ultimate strength (multiplying factor)	fcult	uniform	1.08	1.32	Case 3
Steel strength (Mpa)	fys	lognormal	463.00	37.00	Cases 2&3
Gap at left abutment (mm)	gap1	normal	38.10	1.09	Cases 3
Gap at right abutment (mm)	gap2	normal	38.10	1.09	Cases 3
Gap at left hinge (mm)	gap3	normal	25.50	3.30	Cases 2&3
Gap at right hinge (mm)	gap4	normal	25.50	3.30	Cases 2&3
Stiffness of impact elements in longitudinal direction(KN/mm)	impactK1	uniform	557.61	1672.84	Cases 2&3
Stiffness of impact elements in transverse direction(KN/mm)	impactK2	uniform	191.77	575.30	Case 3
Number of integration points for bentcap elements	intbent	uniform	3.00	5.00	Case 3
Number of integration points for column elements	intcolumn	uniform	3.00	5.00	Case 3
Multiplication factor for deck mass (percentage)	ms	uniform	0.80	1.20	Cases 2&3

Parameter definition	Parameter abbreviation	Probability density function type	PDF Value 1	PDF Value 2	Case participation
Vertical stiffness of foundation piles (KN/mm/pile)	rot_fnd	uniform	105.08	315.23	Cases 2&3
Lateral stiffness of abutment piles (KN/mm/pile)	st_aba	uniform	4.90	14.71	Cases 2&3
Soil stiffness of abutment (KN/mm/m)	st_abp	uniform	10.27	30.82	Cases 3
Shear modulus of elasotmeric pad(multiplying factor)	st_ep	uniform	0.50	1.50	Cases 2&3
Modulus of elasticity for reinforcing steel(Gpa)	steelEs	lognormal	200.10	10.35	Cases 2&3
Strain hardening ratio for reinforcing steel	steelhr	uniform	0.01	0.03	Case 3
Pile translational yielding strength factor	transpilefyfactor	uniform	0.50	1.50	Case 3
lateral stiffness of foundation piles (KN/mm/pile)	trns_fnd	uniform	3.50	10.51	Cases 3
Ultimate strength of abutment pile (multiplying factor)	Utpilefac	uniform	0.70	1.30	Cases 2&3
Yield displacement of abutment soil (fraction of ultimate displacement of abutment soil)	Uyas0	uniform	0.08	0.12	Case 3
Earthquake number	EQ_num	uniform	1.00	300.00	Cases 1, 2 & 3
Incident angle of ground motion	EQ_dir	Uniform	0.00	360.00	Cases 1, 2 & 3

Many of the distributions and values assigned to the various modelling parameters are recommendations from the literatures. Steel strength, concrete strength, bearing friction, damping ratio and deck gaps can be found in Ellingwood B, Hwang H. 1985 [71], Hwang and Jaw 2007 [72], Dutta 1999 [73] and Fang et al.1999 [74], Bavirisetty 2000 [75] and Choi E,2000 [69] respectively. For the other modelling parameters, where the distribution informations are not available a uniform distributions were used. To be consistent with the assumption used in the screening of the parameters the lower and upper levels assumed to be 50% and 150% around the recommended deterministic values. Using the parameters indicated in table 4.21 the joint probability density function of the

parameters have been developed and 100 sample of the bridge have been generated with the same probability of occurrence. This study only accounts for uncertainty associated with materials and earthquake properties and the effect of geometrical uncertainties (i.e. span length, column height, number of spans and etc.) have not been included in the probabilistic model of the structure. Limit states for different state of the damage and various bridge components can be seen in tables 4.23 and 4.22.

Table 4.22: Extensive and complete limit states for bridge components

Components	Extensive		Complete	
	Median	COV	Median	COV
Concrete Column Curvature Ductility	3.52	0.63	5.24	0.64
Elastomeric Bearing Fixed-longitudinal(mm)	136.10	0.58	186.60	0.64
Elastomeric Bearing Fixed-transverse(mm)	142.20	0.72	195.00	0.66
Elastomeric Bearing Expansion-longitudinal(mm)	136.00	0.58	186.60	0.64
Elastomeric Bearing Expansion-transverse(mm)	142.20	0.72	195.00	0.66
Abutment-Passive(mm)	1000.00	0.00	1000.00	0.00
Abutment-Active(mm)	77.20	8.50	1000.00	0.00
Abutment-Transvers(mm)	77.20	8.50	1000.00	0.00

Table 4.23: Slight and moderate limit states for bridge components

Components	Slight		Moderate	
	Median	COV	Median	COV
Concrete Column Curvature Ductility	1.29	0.58	2.10	0.50
Elastomeric Bearing Fixed-longitudinal(mm)	28.90	0.60	104.20	0.54
Elastomeric Bearing Fixed-transverse(mm)	28.80	0.78	90.90	0.67
Elastomeric Bearing Expansion-longitudinal(mm)	28.90	0.60	104.20	0.54
Elastomeric Bearing Expansion-transverse(mm)	28.80	0.78	90.90	0.67
Abutment-Passive(mm)	37.00	0.46	146.00	0.46
Abutment-Active(mm)	9.70	0.70	37.90	9.02
Abutment-Transverse(mm)	9.75	0.70	37.90	9.02

Based on the maximum response of the structure component of interests (table 4.10), the probabilistic seismic demand models (PSDMs) have been developed using equation 4.3. For the columns, the curvature ductility PSDMs is developed using the maximum combined curvature of the columns during the earthquake. For that the rms of the curvature ductility in longitudinal and transverse direction have been computed and the maximum value have been recorded for each column. As stated before the SDI values are being measured in meter wherever have been used in this study. The PSDMs models for various components of the structure can be seen in tables 4.25 4.26 and 4.27. To investigate of the number of sampling for fragility analysis is statistically significant, demand model parameters are evaluated for variation of number of samples. The coefficient of variation for demand parameters is obtained for variation of number of samples. In figure 4.22(a), the variation of columns demand parameters are shown versus the number of samples obtained from the case 3 demand analysis. This figure shows the fluctuation of parameters is significant for sample number less than 60 and the variation stabilizes when number of samples

are more than 60. Figure 4.22(a) shows the COV of the parameters estimate versus the number of samples. Assuming that 0.02 is an acceptable level for COV, sampling size of 80 is statically significant. Figures F.1 and F.2 show the variation of demand models parameters to the number of sampling. Figures F.3 and F.4 shows the variation of coefficient of variation to the number of sampling. As it can be seen the number of 100 samples is a statistically significant sample size for fragility analysis for all the components of the bridge structures.

Figure 4.21 shows the comparison between PSDMs for the columns curvature ductility obtained from Case 1, Case2 and Case3. The remaining demand models graphs can be found in the appendix D. Based on the limit states and PSDMs computed for the model, the fragility curves for component bridge elements have been obtained. Figures D.1 to D.8 shows the fragility results for the component bridge element for Case 1, Case 2 and Case 3. In these figures LS1, LS2, LS3 and LS4 corresponds to slight, moderate, extensive and complete limit states respectively.

In case 1, the bridge analytical model does not account for any epistemic uncertainty from the parameters. Therefore the vulnerability results from case 1 only represent the aleatory uncertainty inherited from randomness in the ground motion. Case 3 also includes all the parameters uncertainty in the bridge finite element model. Case 2 represent the aleatory uncertainty as well as a portion of epistemic uncertainty from the parameters selected based on DOE outcome. If the DOE outcome would be reliable, fragility graphs for case 2 should be similar to case 3 because the parameters included in the sampling technique accounts for most of the variability of the bridge response.

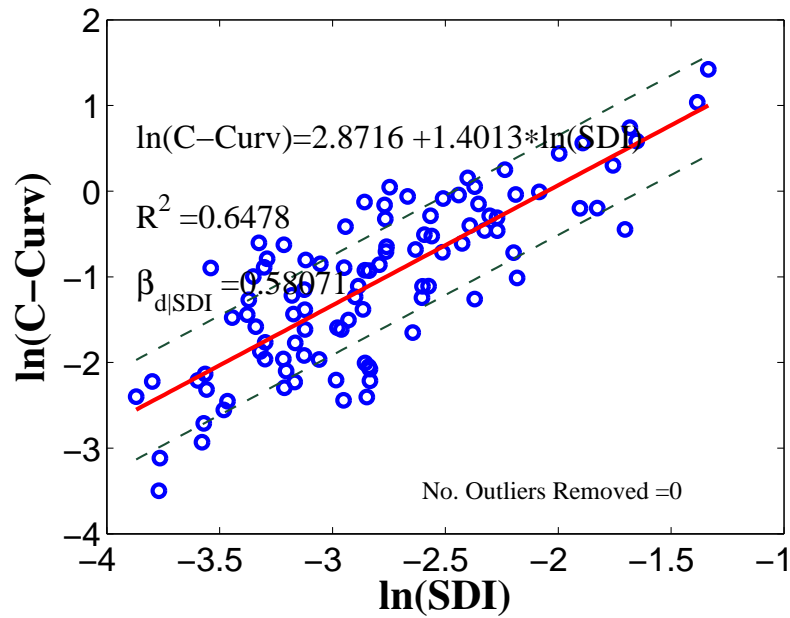
For all the cases in figures D.1 to D.8 the abutment is the least vulnerable component of the bridge as it never reaches the complete limit state and the probability of failure of the component is equal to zero for LS4. In contrast the columns and the expansion elastomeric bearings are the most vulnerable parts of the bridge. I.e. in figure D.4a for SDI of 0.5 m, the probability of exceeding

extensive damage is 75% for of the elastomeric bearing in longitudinal direction which is 30% for the same limit state for the fixed bearing (figure D.2a). The reason is the implementation of the gap in the elastomeric bearing for increasing the ability of movement of the bearing given the same capacity model assumed for extensive damage state. However the fragility analysis of the MSSS concrete bridge can yield interesting results for seismic performance of bridge components the intent of this research is to track and treat the uncertainties inherited from the input parameters. Therefore a method need to be used to show the effectiveness of parameters reduction obtained from DOE approach on the fragility curves.

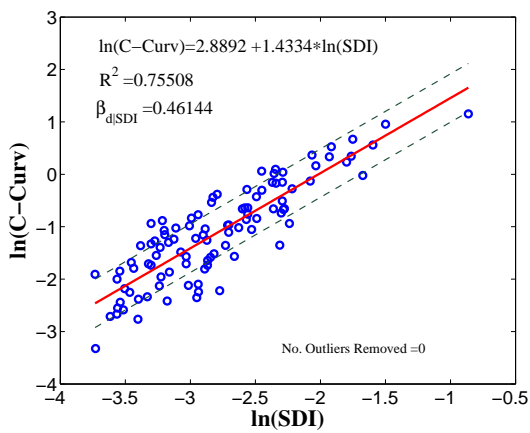
Table 4.24: Slight and moderate limit states for bridge components

Components	$\beta_{E;S_d SDI}$ (Case2)	$\beta_{E;S_d SDI}$ (Case3)
Concrete Column Curvature Ductility	0.35	0.34
Elastomeric Bearing Fixed-longitudinal	0.41	0.42
Elastomeric Bearing Fixed-transverse	0.67	0.69
Elastomeric Bearing Expansion-longitudinal	0.38	0.39
Elastomeric Bearing Expansion-transverse	0.63	0.57
Abutment-Passive	0.40	0.41
Abutment-Active	0.38	0.39
Abutment-Transverse	0.41	0.41

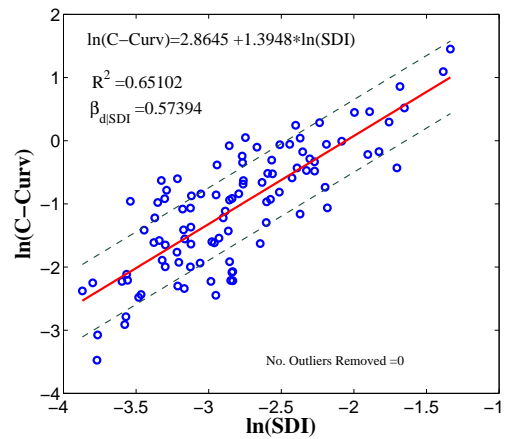
To show the inherent epistemic uncertainty in case 1 which is captured by implementing input parameters variability in the fragility analysis, the $\pm\sigma$ bounds are obtained from equation 4.8. Table 4.24 shows obtained $\beta_{E;S_d|SDI}$ values for different component of the bridge where columns 2 and 3 show $\beta_{E;S_d|SDI}$ when epistemic uncertainty is obtained using case 2 and case 3. Using the $\beta_{E;S_d|SDI}$ values, the $\pm\sigma$ uncertainty bounds are drawn around the fragility curves.



(a) Case 2



(b) Case 1

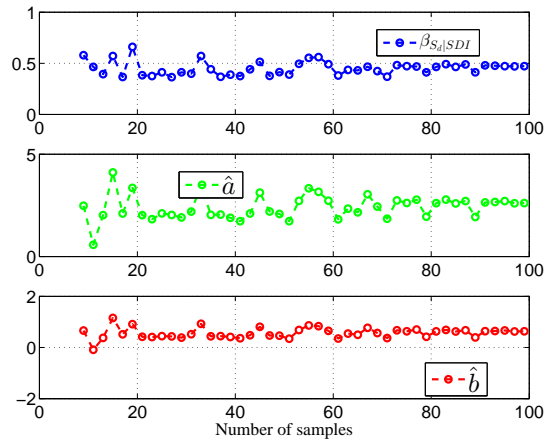


(c) Case 3

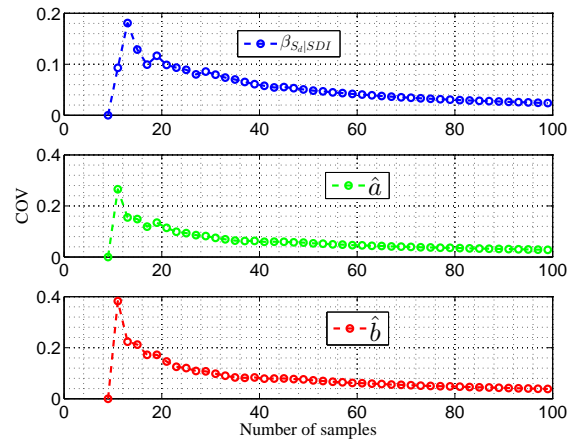
Figure 4.21: Bridge PSDMs for bridge columns curvature ductility

The difference between bounds of uncertainty for component fragility results of case 2 and case 3 is an indicator of the performance for screening study. One can conclude that if the subset of

parameters can induce the same level of variation in the response of the structure as all the parameters then the bounds of epistemic uncertainty in case 2 and case 3 should be close. Therefore for components that the bounds of case 2 and 3 are similar, the subset of the parameters can be used as opposed to all the parameters in fragility analysis. Figure 4.23 shows examples for difference between uncertainty bounds of case 2 and case 3 around the mean estimate of the fragility. Figure 4.23(a) shows mean estimate fragility of expansion elastomeric bearing element in transverse direction and its associated uncertainty bounds for limit state 2. The blue lines belong to case 2 and the red lines belong to case 3. These fragility curves have been obtained using mean estimate and dispersion of case 1 demand model and $\beta_{E;S_d|SDI}$ of case 2 and 3. The difference between the dispersion of case 2 and case 3 can be seen in table 4.24 where $\beta_{E;S_d|SDI}$ for case 3 and case 2 are 0.57 and 0.63 respectively. Assuming that the aleatory uncertainties originated from randomness of ground motions are the same for both cases, the higher value for $\beta_{E;S_d|SDI}$ means more dispersion for the PDF of exceeding the limit state. Also higher value for $\beta_{E;S_d|SDI}$ means wider bounds around the mean estimate of fragility. Figure 4.23(a) shows that the selected parameters with DOE approach are the influential parameters for deformation of expansion bearing in transverse direction. The same argument can be used for the columns curvature ductility where $\beta_{E;S_d|SDI}$ for case 2 and 3 are 0.34 and 0.34 respectively. Figure 4.23(c) shows the fragility mean estimate and bounds for abutment in passive direction for limit state 1. As it can be seen the dispersion of the two fragility is almost the same, therefore the mean estimate and the bounds are fairly close. This matter shows that for the expansion bearing in transverse direction, the selected parameters from DOE approach are the main parameters that participate in the response of elastomeric bearing in transverse direction. For lack of space uncertainty bounds for other components are included in Appendix E.



(a) Variation of the COV for the columns demand model parameters



(b) Variation of the COV for the columns demand model parameters

Figure 4.22: Variation of the demand model parameters to the number of samples

Figures E.1 to E.4 are showing the epistemic uncertainty bounds around mean estimate of fragility for case 2 and case 3. Comparison between figures E.1 with E.3 and E.2 with E.4 shows that the uncertainty bounds of case 2 and 3 are very similar for all the components.

Table 4.25: PSDMs for MSSS Concrete Girder Bridge Components (Case 1)

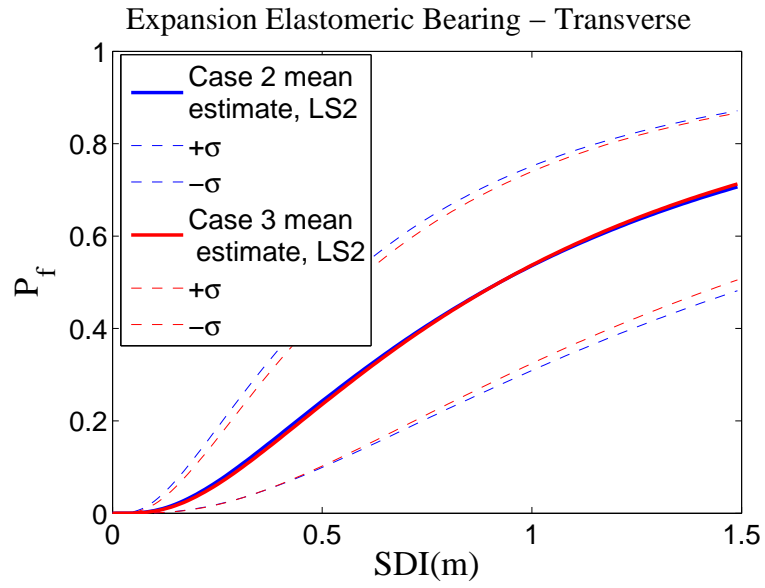
Components			abbreviation	PSDM	$\beta_{d SDI}$	R^2
Concrete	Column	Curvature	C_Curv	$\ln(\text{C-Curv})=2.88 + 1.43.\ln(\text{SDI})$	0.46	0.76
Ductility						
Elastomeric	Bearing	Fixed-longitudinal	fxb-x	$\ln(\text{fxb-x})=5.77 + 1.43.\ln(\text{SDI})$	0.54	0.61
Elastomeric	Bearing	Fixed-transverse	fxb-z	$\ln(\text{fxb-z})=4.56 + 1.19.\ln(\text{SDI})$	0.53	0.58
Elastomeric	Bearing	Expansion-longitudinal	exb-x	$\ln(\text{exb-x})=6.66 + 1.54.\ln(\text{SDI})$	0.51	0.74
Elastomeric	Bearing	Expansion-transverse	exb-z	$\ln(\text{exb-z})=4.60 + 1.22.\ln(\text{SDI})$	0.54	0.59
Abutment-Passive			abut-psl	$\ln(\text{abut-psl})=3.56 + 0.85.\ln(\text{SDI})$	0.35	0.65
Abutment-Active			abut-acl	$\ln(\text{abut-acl})=2.63 + 0.66.\ln(\text{SDI})$	0.27	0.65
Abutment-Transverse			abut-tr	$\ln(\text{abut-tr})=2.84 + 0.92.\ln(\text{SDI})$	0.39	0.64

Table 4.26: PSDMs for MSSS Concrete Girder Bridge Components (Case 2)

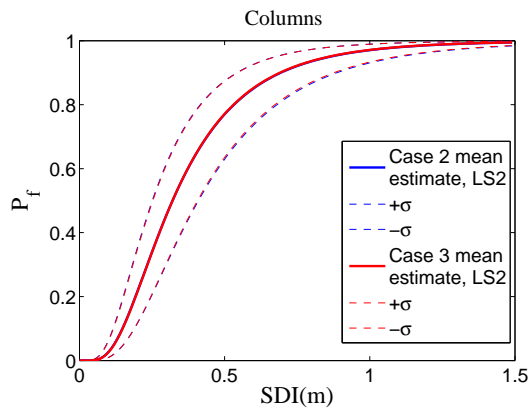
Components	abbreviation	PSDM	$\beta_{d SDI}$	R^2
Concrete Column Curvature	C.Curv	$\ln(\text{C-Curv})=2.87 + 1.40\ln(\text{SDI})$	0.58	0.65
Elastomeric Bearing Fixed-longitudinal	fxb-x	$\ln(\text{fxb-x}(\text{mm}))=5.85 + 1.48\ln(\text{SDI})$	0.69	0.60
Elastomeric Bearing Fixed-transverse	fxb-z	$\ln(\text{fxb-z}(\text{mm}))=5.70 + 1.58\ln(\text{SDI})$	0.86	0.52
Elastomeric Bearing Expansion-longitudinal	exb-x	$\ln(\text{exb-x}(\text{mm}))=6.53 + 1.51\ln(\text{SDI})$	0.64	0.64
Elastomeric Bearing Expansion-transverse	exb-z	$\ln(\text{exb-z}(\text{mm}))=5.69 + 1.58\ln(\text{SDI})$	0.83	0.53
Abutment-Passive	abut-psl	$\ln(\text{abut-psl}(\text{mm}))=3.82 + 0.92\ln(\text{SDI})$	0.53	0.49
Abutment-Active	abut-acl	$\ln(\text{abut-acl}(\text{mm}))=2.63 + 0.63\ln(\text{SDI})$	0.47	0.36
Abutment-Transverse	abut-tr	$\ln(\text{abut-tr}(\text{mm}))=3.03 + 0.94\ln(\text{SDI})$	0.57	0.46

Table 4.27: PSDMs for MSSS Concrete Girder Bridge Components (Case 3)

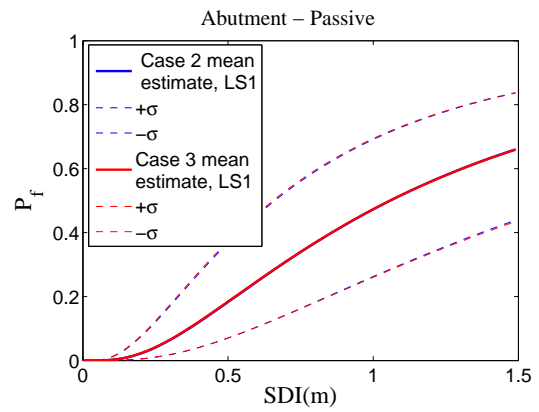
Components	abbreviation	PSDM	$\beta_{d SDI}$	R^2
Concrete Column Curvature Ductility	C.Curv	$\ln(\text{C-Curv})=2.86 + 1.39.\ln(\text{SDI})$	0.573	0.65
Elastomeric Bearing Fixed-longitudinal	fxb-x	$\ln(\text{fxb-x})=5.84 + 1.48.\ln(\text{SDI})$	0.68	0.59
Elastomeric Bearing Fixed-transverse	fxb-z	$\ln(\text{fxb-z})=5.61 + 1.55.\ln(\text{SDI})$	0.86	0.5
Elastomeric Bearing Expansion-longitudinal	exb-x	$\ln(\text{exb-x})=6.61 + 1.54.\ln(\text{SDI})$	0.64	0.64
Elastomeric Bearing Expansion-transverse	exb-z	$\ln(\text{exb-z})=4.95 + 1.35.\ln(\text{SDI})$	0.83	0.49
Abutment-Passive	abut-psl	$\ln(\text{abut-psl})=3.80 + 0.92.\ln(\text{SDI})$	0.53	0.48
Abutment-Active	abut-acl	$\ln(\text{abut-acl})=2.60 + 0.63.\ln(\text{SDI})$	0.5	0.37
Abutment-Transverse	abut-tr	$\ln(\text{abut-tr})=2.98 + 0.93.\ln(\text{SDI})$	0.56	0.46



(a) Elastomeric Bearing Expansion-transverse



(b) Columns Curvature Ductility



(c) Abutment-Passive

Figure 4.23: Fragility bounds of uncertainty of case2 and case 3

4.4 Closure

Sensitivity of component responses of MSSS concrete girder bridge to large number of input parameters are investigated. Plackett-Burman experimental design which is one of the design of experiment techniques is utilized due to the efficiency and ability of capturing the main effects of the parameters in the response of the structure. The results from the sensitivity analysis reveals seismic response of various components of the bridge are sensitive to number of parameters. Superstructure mass, damping ratio, soil stiffness of the abutment piles, gap between the deck elements, and gap at the dowels for fixed and expansion bearings and ultimate strength of the abutment pile are the parameters that participate the most in the variation of the response of the abutments. For the columns, damping ratio, yield strength of the reinforcement steel, steel module of elasticity and rotational foundation stiffness are the influential parameters whereas the bearings responses are sensitive to damping ratio and super structure mass, gap at the fixed bearing dowels, pre-yielding stiffness of the impact elements, shear stiffness and friction coefficient of the elastomeric pad. Using these selected parameters from screening study the fragility analysis was performed for the MSSS concrete girder bridge. Fragility results using three cases of aleatory uncertainty, aleatory and epistemic uncertainty using selected subset of parameters and aleatory and epistemic uncertainty by implementing all the parameters in the analytical model of the structure were compared. Comparison between the results shows that instead of all the parameters, the subset of parameters selected based on screening study can be implemented in the analytical model of the structure without compromising the dispersion of the response induced by epistemic uncertainty of the parameters. This can be interpreted as validation of the screening study and parameter reduction technique for fragility analysis. Noting that eliminating the lesser important parameters from the fragility analysis considerably reduce the computational expenses of the analysis.

CHAPTER 5: UNCERTAINTY TREATMENT FOR COMPONENT BRIDGE ELEMENTS

5.1 Introduction

One of the concerns in the fragility analysis is the correlation between demand and capacity. Conventionally this matter wasn't considered in the fragility methodology. The reason lie in the lack of sophisticated models for the capacity that shares the same input parameters domain with the demand model. For example all the capacity models used in the fragility analysis in chapter 4 were adopted from Padgett and DesRoches (2008) [84] and Nielson and DesRoches (2007) [68]). The adopted capacity model is consists of PDF functions for each component of the structure given the various limit states. However in reality, the distribution of capacity model is a function of variability of parameters domain including variables that participate in the demand model. Availability of models that quantify the likelihood of damage or reaching a specific damage state for a specified component of the bridge is very limited due to the requirement for comprehensive analytical and experimental studies. This chapter tries to improve the conventional methodology for the fragility analysis to address this issue and to measure the variation in the fragility function for the conventional and newly presented methodology.

5.2 Methodology

5.2.1 Uncertainty treatment of the fragility analysis

By taking a closer look at the demand and capacity models that are incorporated in the conventional fragility model an overlap can be recognized between their parameters domain. Traditional

analytical definition of fragility curve was presented as 5.1 where LS and D are representative of the demand and capacity of the component bridge element. A more general definition of fragility can be obtained from the equation 5.2 which can account for the correlation between the demand and capacity of the bridge elements.

$$F_i = \sum_S \sum_{LS} P[D = d|LS]P[LS|IM = s] \quad (5.1)$$

$$F_i = P[C_i - D < 0|IM] \quad (5.2)$$

Where F_i is the probability of exceeding the i^{th} limit state and C_i and D are the capacity and demand of the component element correspondingly for i^{th} limit state. In the Peer performance based assessment framework the demand analysis is performed assuming that the probability distribution of the demand is lognormal. The same approach is used for finding the probability distributions of the capacity of the structures. Then for each component of the structure the probability of exceeding one limit state can be obtained from the following:

$$P[C_i - D < 0|IM] = \Phi \left(\frac{\ln(S_{d|IM}/S_c)}{\beta_{d|IM}^2 + \beta_c^2} \right) \quad (5.3)$$

Equation 5.3 implies that the demand and capacity of the structure are independent from each other. In reality some of the parameters involved in defining the capacity of a structure is the same as the parameters that define the demand domain. Therefore capacity domain inherent the same uncertainty incorporated in the demand domain.

The fragility curve when the correlation coefficient between demand and capacity is known can be

evaluated in closed-form from:

$$P[C_i - D < 0|IM] = \Phi \left(\frac{\ln(S_{d|SDI}/S_c)}{\beta_{d|SDI}^2 + \beta_c^2 - 2\rho_{d|SDI,c}\beta_{d|SDI}\beta_c} \right) \quad (5.4)$$

Where $\rho_{S_{d|SDI}.S_{d|SDI}}$ is the correlation coefficient between demand and capacity given the intensity of the ground motion. Figure 5.1 shows the effect of the correlation on fragility curve assuming that the correlation is independent of the ground motion intensity. The more correlation decrease the variance of the fragility PDF function. The $\rho_{S_{d|SDI}.S_{d|SDI}}$ is very hard to be evaluated in closed form given the complexity of the nonlinear bridge structure. Therefore another alternative for peer framework methodology needed to be presented to consider the dependence of demand and capacity. Three types of parameters can be recognized in the demand and capacity domain. The parameters that participate in both demand and capacity (\vec{X}), The parameters that only participate in demand domain (\vec{Y}) and the parameters that only participate in the capacity domain (\vec{Z}). Therefore probability of exceedance for i^{th} limit state conditioned on the intensity of the ground motion can be rewritten as follows:

$$P[C_i(\vec{X}, \vec{Z}) - D(\vec{X}, \vec{Y}) < 0|IM] \quad (5.5)$$

Material properties, variability in structure geometry, fabrication error, gap between steel retention dowel and slot in girder, soil characteristics and etc. can be classified as \vec{X} variables. Ground motion uncertainties including incident angel can be classified as \vec{Y} variable. Uncertainties that do not affect demand of the structure like confidence interval value that assumed by the designer, deformation capacity of elements or components of the bridge structure and etc. can be assumed as \vec{Z} variables.

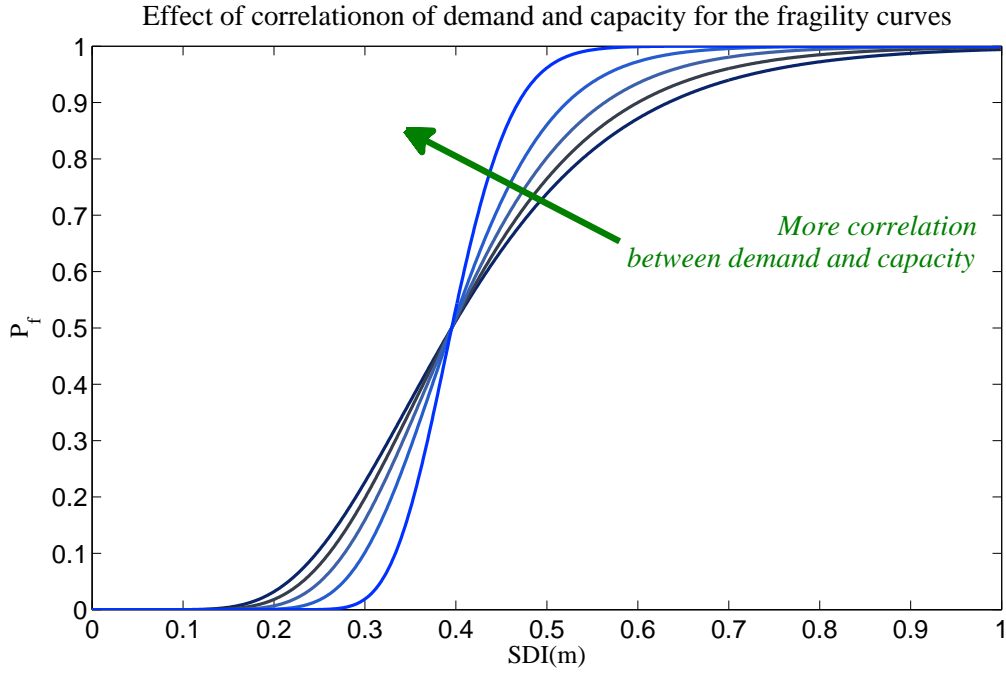


Figure 5.1: Effect of correlation between demand and capacity on the fragility curve

Probability of exceedance for i^{th} limit state needed to be evaluated numerically. Monte Carlo simulation is very time consuming and computationally inefficient for a full 3D structure model. In that case Latin hypercube sampling technique can be taken into the account. From the joint probability distribution of \vec{X} different realizations of \vec{x} variables needed to be selected. Assuming that \vec{x} is the j^{th} realization of \vec{X} vector consequently for the j^{th} sample drawn from the all possible samples existed rearranging Equation 5.5 leads to:

$$P[C_i(\vec{Z}) - D(\vec{Y}) < 0 | IM, \vec{X} = \vec{x}_j] \quad (5.6)$$

In 5.6 demand and capacity associated with i^{th} damage state are independent, therefore the same methodology used in peer framework for PBA of structures can be used for evaluation of this

probability. Assuming demand and capacity are log normally distributed, component demand and capacity models conditioned on the ground motion intensity and variable \vec{x}_j can be obtained. 5.6 now can be rearranged as follows:

$$P[C_i - D < 0 | IM, \vec{X} = \vec{x}_j] = \Phi \left(\frac{\ln(S_{d|\vec{x}_j, IM} / S_{c|\vec{x}_j})}{\beta_{d|\vec{x}_j, IM}^2 + \beta_{c, \vec{x}_j}^2} \right) \quad (5.7)$$

Equation 5.8 shows the probability of exceeding i^{th} damage state :

$$P[C_i - D < 0 | IM] = \int_{\vec{X}} \Phi \left(\frac{\ln(S_{d|\vec{x}_j, IM} / S_{c|\vec{x}_j})}{\beta_{d|\vec{x}_j, IM}^2 + \beta_{c, \vec{x}_j}^2} \right) P(\vec{X}) d\vec{X} \quad (5.8)$$

Because of the complexity of the problem, obtaining the closed form solution for this integral is not feasible. Therefore to consider the correlation between capacity and demand a two levels sampling technique is taken into the account.

The first step is drawing samples with equal probability from joint probability density function of \vec{X} . Assuming that \vec{x}_j is the j^{th} realization of \vec{X} vector. The conditional probability $P[C_i - D < 0 | IM, \vec{X} = \vec{x}_j]$ follows lognormal distribution for a given level of IM (Cornell et al., (2002) [57]; Song and Ellingwood, (1999) [1]). Cornell et al. (2002) [57] suggested that the median of demand of the structure component can be presented as following:

$$S_{d|\vec{x}_j, IM} = aIM^b \quad (5.9)$$

Where a and b can be obtained from a regression analysis over structural response of interest. Also $\beta_{d|\vec{x}_j, IM}$ is dispersion of the data for a given level of IM which can be obtained from the regression analysis. For the capacity analysis $S_{c|\vec{x}_j}$ and $\beta_{c|\vec{x}_j}$ are the mean and dispersion of the logarithm of

the capacity for i^{th} limit state (e.g. mean and dispersion of log of column lateral deformation that cause moderate damage to the column). Figure 5.2 will provides a more clear representation of the two layer sampling technique for component fragility analysis.

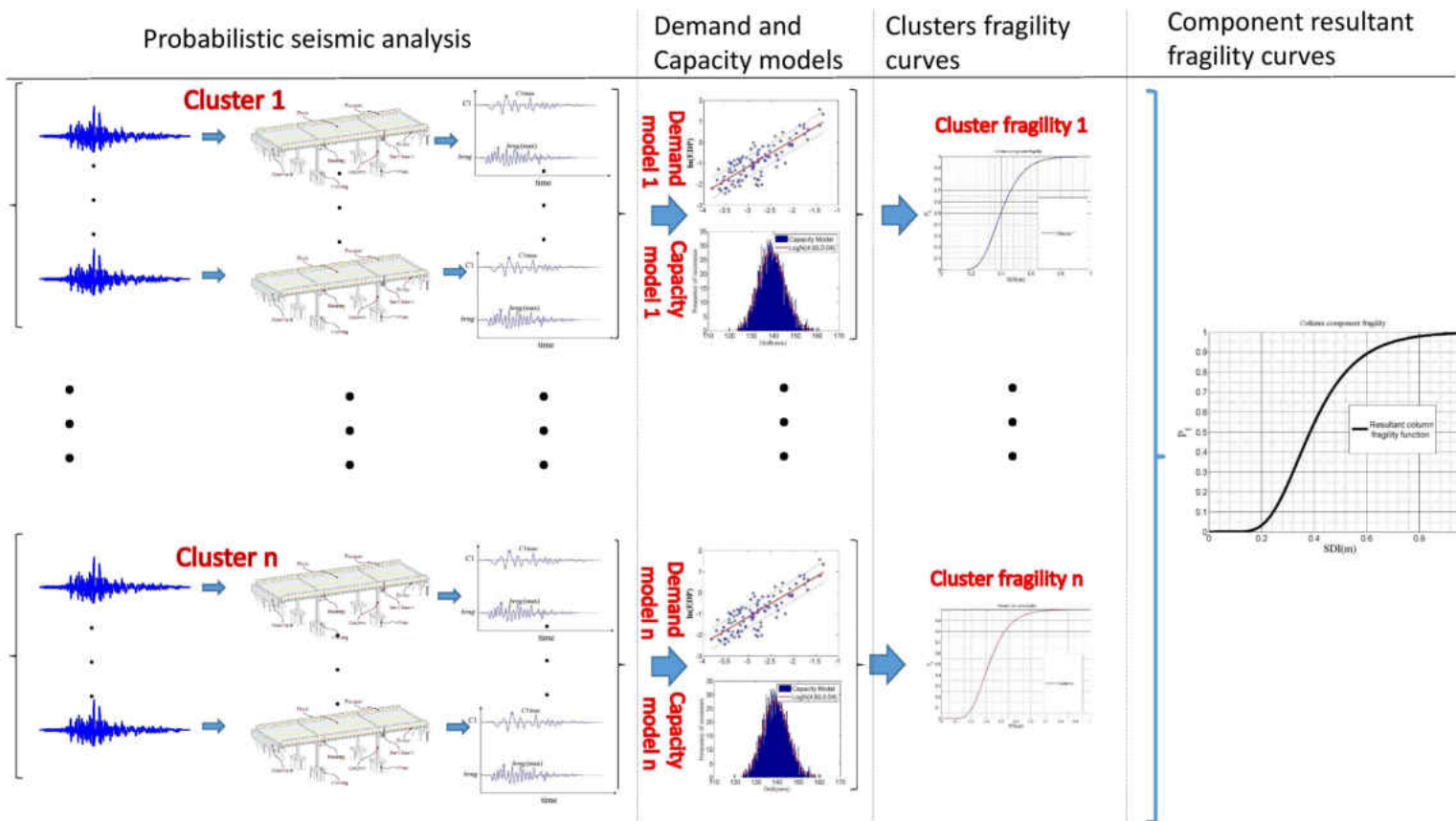


Figure 5.2: Schematic description of the two layers sampling technique for fragility analysis

5.2.2 Description of the capacity model

The equation 5.8 can completely capture the correlation in the demand and capacity for the fragility model when the continuous functions for demand and capacity with their associated probability of occurrence are available. However in reality these functions needed to be obtained from discrete component response outputs .Therefore the feasibility of implementation of this formulation needed to be demonstrated. To examine fragility analysis using equation 5.8, first a constitutive model for the capacity is required .As mentioned before, empirical capacity models for the bridge components are very rare. One of the models that can be used for this study is the buckling of the longitudinal reinforcement adopted from Berry and Eberhard (2005) [82]. The buckling of longitudinal reinforcement represent the level of damage where safety implication is significant and the element needed to be replaced [82]. This capacity model is equivalent with extensive to complete damage limit states defined in chapter 4. In their model, column drift is used as a predictor for reinforcement buckling and the equation of damage prediction is obtained using regression analysis on the experimental data. Also the effect of variation of the parameters that represent the geometry and reinforcement of the circular concrete column is considered. Some of these parameters in the capacity parameters domain is the same as the demand parameters domain defined for MSSS concrete girder bridge column which makes this model suitable for this study. Equation 5.10 shows the model for reinforcement bucking of the circular column:

$$\frac{\Delta_{bb_calc}}{L}(\%) = 3.25(1 + K_e \rho_{eff} \frac{f_y d_b}{f'_c D})(1 - \frac{P}{A_g f'_c})(1 + \frac{L}{10D}) \quad (5.10)$$

The variables in equation 5.10 are defined below:

$\frac{\Delta_{bb_calc}}{L}$: drift ratio (percent) at bar buckling

$K_e = 150$: constant for spiral reinforced concrete columns

ρ_{eff} : volumetric percent of transverse reinforcement

d_b : longitudinal bar diameter

D : column diameter

$\frac{P}{A_g f_c}$: axial load ratio

L : equivalent column cantilever length

There is also an associated coefficient of variance for the drift ratio which accounts for the different sources of error originated from experimental and analytical uncertainty. Based on the Berry and Eberhard (2005) [82] COV of 0.25 is recommended for circular columns.

The comparison between parameters domain of MSSS concrete girder bridge demand and rebar buckling capacity model can specify the parameter classification defined in equation 5.6. The percentage of transverse reinforcement, longitudinal bar diameter, column diameter and gross cross section area assumed deterministic in the demand mode, therefore in the capacity model they need to be substituted with a fixed value. Steel and concrete strength needed to be modeled probabilistically because they are modeled probabilistic in the demand model. Axial load is also a function of the superstructure mass which needed to be considered probabilistically to be compatible with the demand model. The variation of effective length of the column on the other hand does not participate in the demand model but since the column is not cantilever neither fixed at both ends therefore the error in estimation of the effective length needed to be considered.

5.2.3 Component fragility analysis of the MSSS concrete bridge column

For this section the MSSS bridge model which is similar to Case 2 defined in section 4.2.8 is adopted here. The intention is to use the complete bridge structure for the demand analysis but only generate the component fragility curves of the column given the fact that the constitutive

models for abutments, bearings and impact elements are not available. The same capacity model which is described in section 5.2.2 is utilized for the capacity evaluation of the bridge column. Based on the scope of equation 5.5, for probabilistic analysis, three vectors of the parameters were extracted from parameter domain of demand and capacity. \vec{X} which are the parameters that participate in both demand and capacity model, \vec{Y} and \vec{Z} are the parameters that only participate in the demand and capacity model respectively. Table 5.1 shows the parameter domain definition for the fragility analysis of the bridge column. The last column of table 5.1 indicates to which vector (\vec{X} , \vec{Y} or \vec{Z}) each parameter belongs.

The two layers sampling technique is used for generating the bridge realizations. First using the Latin-Hypercube technique, N samples with equal probability of occurrence needed to be drawn from JPDP function of \vec{X} , consequently for each $\vec{X} = \vec{x}$, K samples needed to be drawn from \vec{Y} and \vec{Z} JPDPs. The bridge realizations needed to be generated using the combination of \vec{X} and \vec{Y} (total of $N * K$ bridge realizations). To facilitate the explanation of the process, the cluster number is defined as i^{th} when the bridge realization is generated from \vec{x}_i and \vec{y}_j ($i = 1, 2, \dots, N$ and $j = 1, 2, \dots, K$). Therefore N clusters of samples exist where each cluster is consisted of K bridge realizations. For the i^{th} cluster, the capacity model needed to be obtained using \vec{x}_i and \vec{z}_j . Having generated the bridge realizations, N different demand models needed to be evaluated. If the variation of the capacity model for each bridge realization had not been taken into the account, one might proceed and find the probability of failure of each cluster using the cluster demand and capacity model and consequently compute the fragility function using 5.15 however including the capacity model variability in the analysis would increase the complexity of the analysis.

As mentioned before, The COV for the model assumed to be 0.25. This variation accounts for the variation of the column drift due to experimental errors as well as variation in the parameters domain. It means the PDF of the capacity is dependent on variation of \vec{X} . Using this COV and its standard deviation counterpart for obtaining PDF of capacity result in double counting of the

effect of variation of \vec{X} which is already included in the Latin-Hypercube sampling. To overcome this obstacle, effect of variation of the \vec{X} needs to be excluded from the dispersion of the capacity. The following procedure is utilized to prevent the double counting of uncertainties and eliminate the correlation of demand and capacity in the dispersion of EDP model.

Bar buckling EDP can be defined using a median estimate of the drift and standard errors. Equation 5.11 shows the drift model where $\Delta_{bb_{calc}}^{\hat{}}$, ε_{Ψ} and ε_{err} represent the median estimate of the drift, model errors due to variation of the \vec{X} and \vec{Z} parameters and model errors due to other aleatory and epistemic uncertainties.

$$\Delta_{bb_{calc}} = \Delta_{bb_{calc}}^{\hat{}} \cdot \varepsilon_{\Psi} \cdot \varepsilon_{err} \quad (5.11)$$

Assuming the log-normal distribution for the bar-buckling drift, equation 5.11 can be rearranged to:

$$\ln(\Delta_{bb_{calc}}) = \ln(\Delta_{bb_{calc}}^{\hat{}}) + \theta_1 + \theta_2 \quad (5.12)$$

Where θ_1 and θ_2 are $\ln(\varepsilon_{\Psi})$ and $\ln(\varepsilon_{err})$ and are mean zero and normally distributed. Consequently the dispersion of the drift can be obtained from equation 5.13 where β denotes the dispersion.

$$\beta_{\ln(\Delta_{bb_{calc}})} = \sqrt{\beta_{\theta_1}^2 + \beta_{\theta_2}^2}$$

Solving for the β_{θ_2} ;

$$\beta_{\theta_2} = \sqrt{\beta_{\ln(\Delta_{bb_{calc}})}^2 - \beta_{\theta_1}^2} \quad (5.13)$$

Therefore instead of $\beta_{\ln(\Delta_{bb_{calc}})}$, β_{θ_2} which accounts for the variation of the parameters other than \vec{X} and \vec{Z} needs to be utilized for defining the PDF function of the capacity. It should be noted that in equation 5.13, $\beta_{\ln(\Delta_{bb_{calc}})}$ can be evaluated using equation 5.14.

$$\beta_{\ln(\Delta_{bb_{calc}})} = \sqrt{\ln(COV^2 + 1)} \quad (5.14)$$

For each bridge realization a median estimate of the capacity and its corresponding dispersion exist. The resultant capacity model for each realization cluster needs to be obtained from the combining the capacity PDFs of realizations of \vec{X} .

The fragility curves corresponds to N different pairs of demand and capacity models can be computed using equation 5.3 and the overall fragility curve for the column component can be obtained using equation 5.15.

$$fragility = \sum_{i=1}^K \Phi \left(\frac{\ln(S_{d|\vec{x}_i, SDI} / S_{c|\vec{x}_i})}{\beta_{d|\vec{x}_i, SDI}^2 + \beta_{c, \vec{x}_i}^2} \right) / N \quad (5.15)$$

Table 5.1: Fragility analysis parameter definition and vector classification

Parameter definition	Parameter abbreviation	Probability density function type	PDF Value 1	PDF Value 2	Vector classification
Coefficient of friction_elastomeric pad (multiplying factor)	cof_ep	uniform	0.50	1.50	Y
Damping ratio	dr	normal	0.05	0.01	Y
Shear modulus of elastomeric pad(multiplying factor)	st_ep	uniform	0.50	1.50	Y
Gap at dowels (expansion bearings only) (mm)	dwl_gap	uniform	0.00	50.80	Y

Parameter definition	Parameter abbreviation	Probability density function type	PDF Value 1	PDF Value 2	Vector classification
Gap between steel retention dowel and slot in girder for fixed elastometric bearing (mm)	dwl_gap2	uniform	0.00	6.35	Y
Gap at left hinge (mm)	gap3	normal	25.50	3.30	Y
Gap at right hinge (mm)	gap4	normal	25.50	3.30	Y
Stiffness of Impact elements in longitudinal direction(KN/mm)	impactK1	uniform	557.61	1672.84	Y
Lateral stiffness of abutment piles (KN/mm/pile)	st_aba	uniform	4.90	14.71	Y
Modulus of elasticity for reinforcing steel(Gpa)	steelEs	lognormal	200.10	10.35	Y
lateral stiffness of foundation piles (KN/mm/pile)	trns_fnd	uniform	3.50	10.51	Y
Ultimate strength of abutment pile (multiplying factor)	Ultpilefac	uniform	0.70	1.30	Y
Concrete strength (Mpa)	fc	normal	33.45	4.28	X
Steel strength (Mpa)	fys	lognormal	463.00	37.00	X
multiplication factor for deck mass	ms	uniform	0.80	1.20	X
Factor of length for the column	L.f	normal	0.60	0.12	Z

5.3 Results

Using the parameter distributions defined in table 5.1, 6, 40 and 40 samples are drawn from \vec{X} , \vec{Y} and \vec{Z} respectively. Therefore 240 total realizations of the bridge are generated. Since 6 samples are drawn from the \vec{X} , consequently 6 different demand models and fragility curves are obtained. Each demand model and its corresponding fragility curve are generated from one cluster of samples. Prior to evaluation of the capacity model for each cluster, the uncorrelated capacity dispersion (β_{θ_2}) needs to be calculated.

For numerical evaluation of β_{θ_2} , first the $\beta_{\ln(\Delta_{bb_{calc}})}$ needed to be evaluated. 40000 realization of (\vec{X} , \vec{Z}) were generated and the mean and dispersion of $\Delta_{bb_{calc}}$ were calculated. Figure 5.3(a) shows the histogram and log-normal PDF function fitted on the column drifts. Figure 5.3(b) shows the increase in the dispersion of the capacity model with inclusion of \vec{X} , \vec{Z} . The median and dispersion of the drift are 139.56 mm and 28.78 mm respectively. therefore the β_{θ_1} is 0.20 Also assuming COV of 0.25, $\beta_{\ln(\Delta_{bb_{calc}})}$ is equal to 0.24 . Consequently β_{θ_2} is equal to 0.13 from equation 5.13 . Therefore the COV of 0.13 were used for the variation of the bar buckling drift model for each bridge realization.

To make the comparison of the newly proposed fragility method with the conventional fragility analysis possible, it is assumed that 40 samples drawn from each \vec{Y} and \vec{Z} will be repeated with the same order for all the clusters. Table 5.2 shows parameter realization for the fragility analysis which is used in this section. Having obtained the bridge realizations, the probabilistic response analysis of MSSS bridge is performed. Consequently for each cluster, demand and capacity model is obtained.

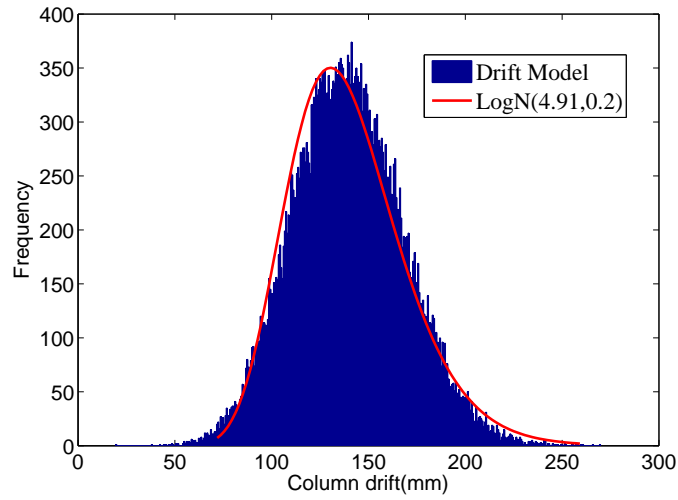
Table 5.2: Two levels sampling technique for bridge generation

Bridge realization no.	Cluster no.	Parameters realization									
1	1	$x_{1,1}$	$x_{2,1}$	$x_{3,1}$	$y_{1,1}$	$y_{1,1}$	$y_{2,1}$.	.	$y_{11,1}$	$z_{1,1}$
2	1	$x_{1,1}$	$x_{2,1}$	$x_{3,1}$	$y_{1,1}$	$y_{1,2}$	$y_{2,2}$.	.	$y_{14,2}$	$z_{1,2}$
.	1
.	1
.	1
40	1	$x_{1,1}$	$x_{2,1}$	$x_{3,1}$	$y_{1,1}$	$y_{1,40}$	$y_{2,40}$.	.	$y_{14,40}$	$z_{1,40}$
41	2	$x_{1,2}$	$x_{2,2}$	$x_{3,2}$	$y_{1,1}$	$y_{1,1}$	$y_{2,1}$.	.	$y_{14,1}$	$z_{1,1}$
42	2	$x_{1,2}$	$x_{2,2}$	$x_{3,2}$	$y_{1,1}$	$y_{1,2}$	$y_{2,2}$.	.	$y_{14,2}$	$z_{1,2}$
.	2
.	2
.	2
80	2	$x_{1,2}$	$x_{2,2}$	$x_{3,2}$	$y_{1,1}$	$y_{1,40}$	$y_{2,40}$.	.	$y_{14,40}$	$z_{1,40}$
.
.
.
201	6	$x_{1,6}$	$x_{2,6}$	$x_{3,6}$	$y_{1,1}$	$y_{1,1}$	$y_{2,1}$.	.	$y_{14,1}$	$z_{1,1}$
202	6	$x_{1,6}$	$x_{2,6}$	$x_{3,6}$	$y_{1,1}$	$y_{1,2}$	$y_{2,2}$.	.	$y_{14,2}$	$z_{1,2}$
.	6
.	6
.	6
240	6	$x_{1,6}$	$x_{2,6}$	$x_{3,6}$.	$y_{1,40}$	$y_{2,40}$	$y_{1,1}$.	$y_{14,40}$	$z_{1,40}$

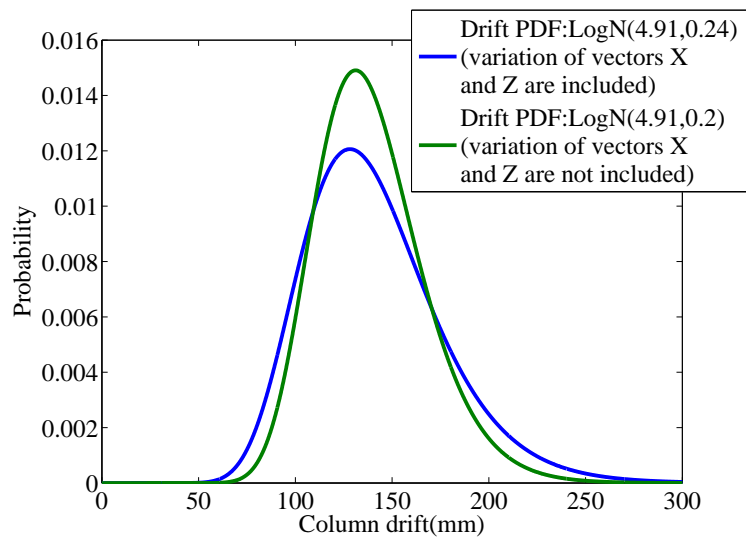
Figure 5.4 shows the capacity and demand models obtained for clusters 1, 3, and 5 for illustration purposes. Based on the adopted bar buckling model, for each bridge realization a mean and dispersion of the capacity model is obtained. The cluster's overall capacity models is generated from fitting a lognormal distribution to the combination of the individual capacity models. In figures 5.4(a), 5.4(c), and 5.4(e), the demand models are different but their variation are limited. The reason can be described as the ground motion pool applied to the clusters are identical (aleatory uncertainty). Therefore the variation is only originated from epistemic uncertainty of geometry and material domain. The next step is combining the clusters fragility curves using equation 5.15. Figure 5.5(b) shows the fragility curves obtained from different clusters (colored curves) and the resultant fragility curve obtained by integrating different clusters probability of failure given the intensity of the ground motion. The variation between clusters fragility curve is significant considering the fact that these variations are not originated from aleatory uncertainties of applied ground motions. Having combined the clusters fragility curves, the same procedure is repeated with the same parameters domain using conventional fragility method. To perform the conventional fragility analysis, the same 40 realizations of \vec{Y} and \vec{Z} used for the clusters in table 5.2 is utilized. For the realizations of \vec{X} also 40 random samples was drawn from the 6 different realization which can be seen in table 5.2. Also for the conventional method the COV of the capacity for each bridge realization assumed to be 0.25 which was the original recommendation of Berry, Michael and Eberhard (2005) [82]. Figure 5.5(b) shows the fragility curve obtained from both conventional and newly proposed methodology. This difference implies that conventional formulation for fragility which doesn't incorporate the correlation between demand and capacity can produce biased results. The difference between two curves can be described with the correlation coefficient term ($\rho_{S_{d|SDI}, S_{d|SDI}}$) of the fragility CDF function. The correlation coefficient in this case between demand and capacity is measured as $\rho_{S_{d|SDI}, S_{d|SDI}} = 0.286$. The value of 0.25 is a common assumption for the correlation coefficient in development of fragility analysis between the researchers. Although this for this case the correlation coefficient was obtained easily,

in general the measurement of the effect of the correlation is not very simple. In the proposed method the variation of the dispersion for the correlation coefficient between demand and capacity is considered given the intensity of the ground motion whereas the conventional method does not account for that. Since the sampling of new and conventional method is very similar, the mean of the demand models are also similar therefore the correlation value becomes the only participant factor in the variation of fragility curve in this comparison. However if a more general sampling were taken into the account, i.e. the aleatory uncertainty were different for clusters, the proposed fragility curve would be different from the conventional fragility in the median as well as dispersion. Therefore only adding the correlation term cannot represent the uncertainties originated from the correlation of the demand and capacity for the fragility analysis.

To summarize the results from this section, when empirical capacity models are available which shares the same parameters with the demand model, using presented formulation is recommended. However obtaining a more accurate results with the improved methodology is accompanied with computational expense trade-off. I.e. the conventional method for the above example could be performed using 40 realization of the bridge however the new methodology requires 240 realization. Also where the sophisticated capacity models are not available or the computational resources are limited, a correlation factor between 0.2-0.3 can be assumed between demand and capacity.

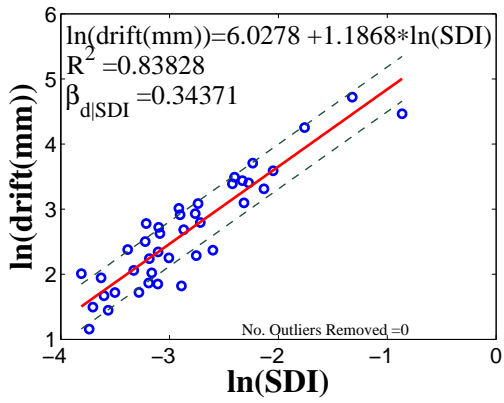


(a) Demand model for cluster 1

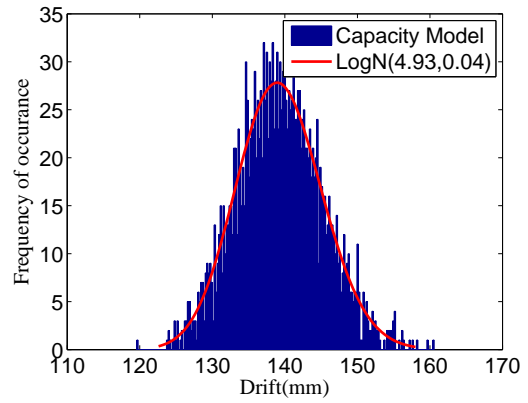


(b) Demand model for cluster 1

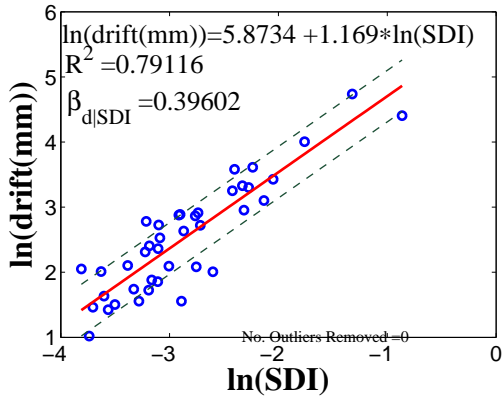
Figure 5.3: Correlation elimination from the bar buckling model's dispersion



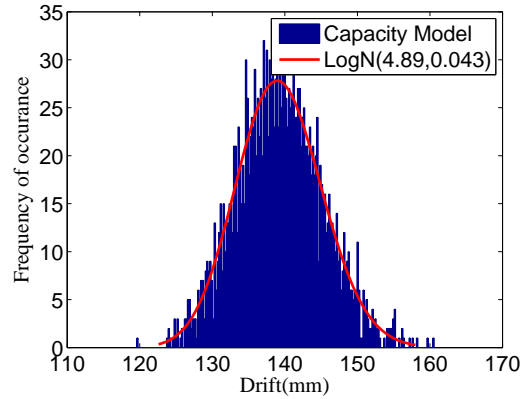
(a) Demand model for cluster 1



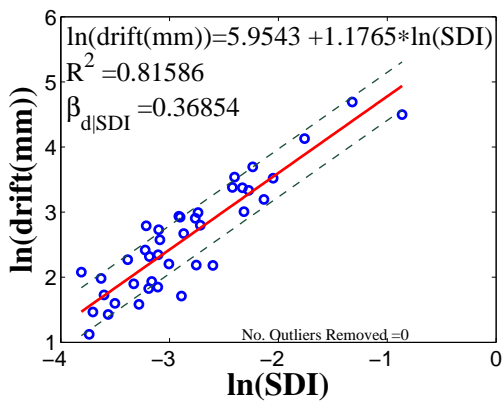
(b) Capacity model for cluster 1



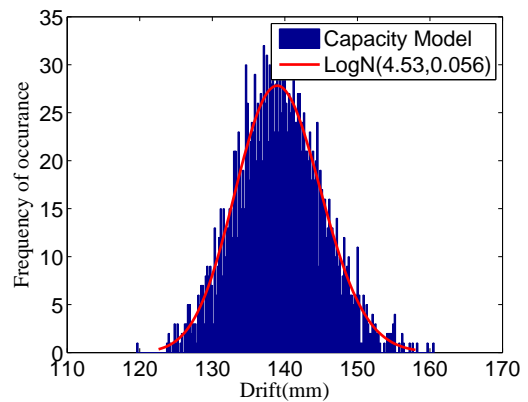
(c) Demand model for cluster 3



(d) Capacity model for cluster 3

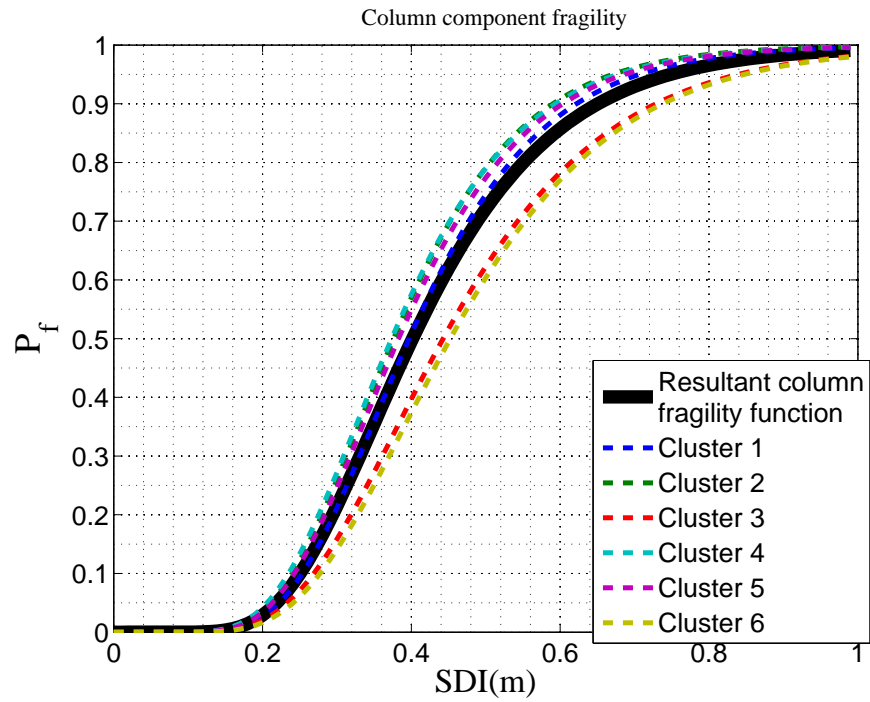


(e) Demand model for cluster 5

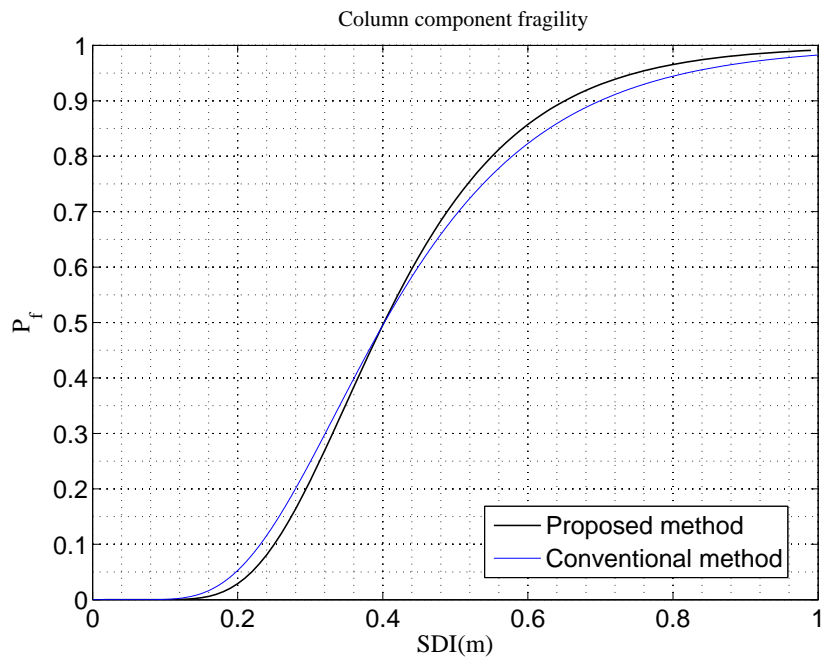


(f) Capacity model for cluster 5

Figure 5.4: Variation of the demand and capacity model for different clusters in multi layers sampling



(a) Resultant fragility curve for the bridge column



(b) Comparison between proposed and conventional method for fragility analysis

Figure 5.5: Improved fragility analysis

CHAPTER 6: CONCLUSIONS AND FUTURE WORKS

6.1 Conclusions

The stochastic nature of earthquakes provided motivation for deviating from a load- and resistance-factor design approach toward a performance-based design (PBD) approach for structures. At first the progress of this new approach seemed to be promising and different frameworks were proposed for different classes of structures, i.e., steel moment frame, concrete, masonry, composite, and bridge structures.

In recent years, PBD has been implemented in different design codes. Despite the hope that PBD would be the dominant design method in near future, it hasn't seen widespread adoption by the practicing engineering for multiple reasons and is only being applied for very limited cases where more accurate designs is needed. Some of the obstacles for adoption of performance-based seismic design are summarized below. The first reason is limited awareness of probabilistic knowledge in practice engineers and lack of dedication for transition from deterministic design to probabilistic design. The second reason is the relatively expensive procedure needed for PBD of structures. When the structure can be designed in deterministic approach with limited number of iteration whereas many realization of the structure, seismic load and etc. are needed for probabilistic approach. Multiple parts of PBD and performance-based assessment (PBA) are still under research and development. The hazard analysis for various sites, materials and structural variability, various structural and non-structural components behavior and capacity, definition of component and system limit states and etc. are some examples of these parts therefore broad information either does not exist or is not easily accessible for engineers and researchers. Even if all these information was accessible, verification of the outcome if not impossible, is very challenging. PBD is consisted of multiple procedures and each procedure is divided to multiple steps. The only guarantee for the

design outcome is verification of all the steps in the procedures of PBD.

Seismic PBA of the structures is the most important step in performance based seismic design procedure. Aforementioned obstacles have a direct impact on the outcomes of PBA which are the structure's loss models. Inaccessibility of information for the PBA was replaced with defining the uncertainties. Multiple sources of uncertainties are typically included in the fragility curves, including but not limited to the randomness of the ground motions, material, fabrication and constructions errors, modeling and computational errors, and estimation of limit states. Including all these sources of uncertainties made the procedure of PBA even more cumbersome than before and the problem was shifted by researchers toward accurate evaluation and implementation of the uncertainties in the PBA domain. Sensitivity of the fragility analysis to the variation of these uncertainties was another issue of the interest where no study was available on whether the lack of information in one step of PBA procedure might be neglected or severely might change the assessment outcome.

The objective of the research presented in this dissertation is to identify and reduce the uncertainties inherited in fragility analysis of highway bridges. This research found and addressed multiple sources of uncertainties in seismic PBA of bridge structures. The main area of focus for this research was on the ground motion selection uncertainties, material and modeling uncertainties and performance-based procedure and formulation errors.

The uncertainties in the ground motions is originated from prediction errors for amplitude and frequency content of future earthquake and also representation of all the characteristics of the ground motion with a single variable known as ground motion intensity. For an accurate PBA, a ground motion catalog which includes a wide spectrum of ground motion intensities and frequency content is needed. Unfortunately the distribution of the ground motions are more skewed toward smaller intensity ground motions since the high intensity earthquakes are very rare and happen

with a large return period. Therefore ground motion scaling is a widely used method for obtaining an appropriate ground motions suite for analysis.

Ground motion scaling is commonly known to cause bias and changes in the response of structures that would not have been observed in unscaled motions of the same intensity. Many methods of scaling have been proposed to overcome the scaling bias. However, no previous studies investigated the origin of the bias in the ground motions. This research explains the source of the bias in as-recorded and synthetic ground motions scaling and evaluated the variation of the bias based on different scaling scenarios and frequently used SDOF structures. Considering the maximum deformation is the most prevalent metric for measurement of performance of the bridge components, the bias is measured for maximum response of the structure to scaled and unscaled bins of ground motions with equal intensity. The results confirm the existence of bias for amplitude scaling of ground motions and shows the bias varies depending on structure's nonlinear properties, pre- and post-yielding periods of the structure, and metric of measurement of intensity of the ground motion. The results also show that the bias exists for synthetic ground motions as well as as-recorded ground motions. A ground motion intensity metric was introduced that can predict the bias induced by other scaling techniques.

This metric is called spectral displacement intensity or SDI. SDI can be obtained from linear response analysis of SDOF structure however it is capturing the effect of nonlinear deformation in its value. Results confirm that using SDI can significantly reduce the bias when it is used as the metric for measuring the intensity of the ground motions. The SDI value can also be used as predictor of the deformation in nonlinear SDOF structures.

The results of this study are limited to SDOF systems and more investigation is needed to be performed for the effect of bias for MDOF systems as various mode shapes and their participation in the response form the maximum deformation of the structure. Here it worth mentioning that

all the prevalent ground motions intensity measures are based on SDOF systems where none of them account for the nonlinear characteristic of the structure whereas SDI incorporate the period elongation of nonlinear structures and therefore is superior to the other IMs.

The reduction of epistemic uncertainties in fragility assessment of structure was investigated in this research. Assuming that the bridge structure is a function, the output of this function are component responses, i.e., deformations, rotations or drifts, section responses like curvature, and strain. The inputs of the function are the material properties, geometrical characteristics of the structure, and static and dynamic loads applied to the structure. Therefore variation of each input parameter has the potential to change the response of the structure. More accurate probabilistic models might be obtained with implementation of more input parameters. However the amount of computational resources increases exponentially with the number of parameters when probabilistic response of the structure is needed. Therefore a more elegant allocation of resources is needed to the parameters that have the priority over the others in the responses of the structure. The DOE one of the many tools available for investigation of the effect of large number of parameters on a complex system. Many researchers previously utilized the DOE for parameter screening for fragility analysis of bridge structures, however the number of parameters they implemented in the model was limited. Also no further investigation was performed for validation of the outcome of screening design on fragility analysis. For this research 32 input parameters that describe entire characteristics for MSSS concrete bridge were implemented in the model. Parameters such as concrete and steel strength, soil strength and foundation stiffness, strength of the piles and soil lateral strength for the pile unit and abutments active, passive, and transverse behavior were included. The Plackett-Burman method was used for screening studies of the parameters.

Based on the effect of parameters and their associated p-values, 13 parameters were selected to be treated as probabilistic in the bridge model and the rest of the parameters were substituted with their mean values. Valuable informations can be concluded from investigating the effects of the

parameters obtained from the DOE for the seismic behavior of the structure. For example super-structure mass, damping ratio, soil stiffness of the abutment piles, gap between the deck elements, and gap at the dowels for fixed and expansion bearings and ultimate strength of the abutment pile are the parameters that participate the most in the variation of the response of the abutments. For the columns, damping ratio, yield strength of the reinforcement steel, steel module of elasticity and rotational foundation stiffness are the influential parameters whereas the bearings responses are sensitive to damping ratio and super structure mass, gap at the fixed bearing dowels, pre-yielding stiffness of the impact elements, shear stiffness and friction coefficient of the elastomeric pad.

Further investigation was performed to find the effect of the response variation reduction on the fragility analysis.

Three cases we defined for fragility analysis. Case 1 where only accounts for aleatory uncertainties from randomness in the ground motions. Case 2 where aleatory and a portion of epistemic uncertainties introduced by the 11 selected parameters are considered and case 3 which in addition to aleatory uncertainty the epistemic uncertainties from all the parameters are included in the fragility analysis of the bridge structure. The fragility results show a small difference between the cases. The case 1 has the least dispersion for the demand model whereas case 3 has the most dispersion. The mean estimate of the demand models for all cases are relatively close. Uncertainty bounds was evaluated from epistemic uncertainty for case 2 and case 3 and was drawn around the mean estimate of the demand model for case 1. The bounds show that the epistemic uncertainty which was captured by implementation of 13 parameters in case 2 and 30 parameters in case 3.

For most of the cases the bounds are fairly close for case 2 and 3 which indicate that the subset of parameters selected using DOE generated the same variability as 30 parameters in case 3 for the responses of the structure. However for expansion bearing in the transverse direction, the bounds of case 2 are slightly wider than case 3 . Reason can be described by statistical error produced by sampling technique knowing that including distribution of more parameters in case 3 should

induce equal to more dispersion in the demand model compared to the dispersion of a subset of parameters used in case 2. Plackett-Burman screening design assumes the response of the system varies linearly with variation of input parameters. This simplistic approach requires less computation for finding the main effects of the parameters. Also Plackett-Burman screening design is unable to predict the higher effect of parameters variation on the response of the structure since it does not account for interaction of the variables in the response of structure. In fact one of the main reason for using Plackett-Burman design is due to limit number of runs needed for obtaining the main effect whereas more elaborated DOE methods cannot efficiently be utilized. Even with this simplistic technique, comparison between the results reveals that instead of all the parameters, the subset of parameters selected based on screening study can be implemented in the analytical model of the structure without compromising the dispersion of the response induced by epistemic uncertainty of the parameters. This can be interpreted as validation of the screening study and parameter reduction technique for fragility analysis. Noting that eliminating the lesser important parameters from the fragility analysis considerably reduce the computational expenses of the analysis.

Finally, the errors produced by utilization of conventional and simplistic approach for obtaining the fragility curves were investigated. In the conventional approach correlation between demand and capacity either wasn't considered or was assumed as a fixed correlation coefficient based on the experience of the modeler in the fragility function. Previously no method was utilized to obtain the exact fragility formulation for correlated demand and capacity no effort have been made to measure the proper correlation coefficient value between these two. Therefore this research proposed a closed form formulation for mean estimate of the fragility curve that accounts for the correlation between demand and capacity. Since the closed form formulation could not be utilized for the complex bridge structure, the feasibility of implementation of this formulation needed to be verified. Therefore a model was adopted for column limit states which had uncertainty in the

mean of capacity model. Further investigation conclude that the capacity model uncertainty is mixed with the demand model uncertainty. This matter shows that the proposed formulation solely cannot treat the correlation between demand and capacity and another layer of treatment is needed for considering the correlation. To proceed with the proposed method first, the demand model's uncertainty was removed from the capacity uncertainty. Consequently the fragility curves obtained with the proposed method and treated capacity model. The outcome was compared with the conventional methods where correlation was not considered between demand and capacity. Obtaining the fragility curve itself indicates that the proposed method can practically be used for fragility analysis. However the computational expense of the proposed method is higher than the conventional method, the proposed method can yield more accuracy for the probability of exceeding the damage state. The results from this portion of the research also shows considering the correlation between demand and capacity can change the dispersion of the fragility CDF function whereas the variation of the mean of the fragility CDF function is limited. A further step were taken to estimate the correlation coefficient between demand and capacity for the studied case. The correlation coefficient evaluated as 0.286 which is within the common range assumed by other researchers.

While the main focus of the investigations were on PBA for highway bridges, the finding of this research can be implemented for other types of structures and other seismic assessment methods. For example, ground motion scaling is widely used for nonlinear time-history analysis and as a result, the scaling induced bias exist for ordinary structural seismic design which was implemented in the various prevalent codes from long time ago. The Plackett-Burman screening design method also can be used for different types of structures where seismic response of the structure is dependent on multiple parameters and limited resources are available to measure the importance of each parameter in the response. The fragility formulation proposed which consider the correlation between demand and capacity can be implemented for various types of structures since the

conventional PBA method is being used for bridge structures as well as other structures.

6.2 Future works

Despite the effort was made to track and treat the sources of uncertainty in this dissertation, more research and investigation needed to be performed to improve the outcome of fragility analysis for complex structures. In general two types of uncertainty were identified by researchers, the aleatory which is not originated from lack of informations and epistemic uncertainty which can be reduced with increasing the knowledge. The aleatory uncertainties needed to properly be considered in the fragility analysis and all the efforts needed to be made to increase the informations on different sources of epistemic uncertainty for reduction of the overall uncertainty in the outcome of PBA. These effort needed to be made for multiple parts of fragility analysis. For the ground motions selection part, a better estimation of period elongation is needed to be introduced for nonlinear structures. Also more investigation is needed for measuring the bias induced with two orthogonal component of ground motions and identification of the differences in the period elongation as opposed to when a single component of ground motions is applied to the structure. For fragility analysis part, more sophisticated empirical models for evaluation of the capacity of components of the structure are needed which shares the same parameters domain with the demand model. Also quantifiable limit state functions are needed for various components of the structures. Better method needed to be developed and implemented for estimation of the demand model. Utilization of nonlinear regression might result in a more accurate model rather than linear demand model. Also the type of distribution of demand and capacity model given the intensity of ground motion is another matter of the interest. The effect of assumed distribution shapes for the demand and capacity models in the outcome of fragility analysis needed to be investigated. I.e. there is no guarantee for the log normal distribution shape of the demand and capacity model thus available

numerical method can easily be taken into account for evaluation of the demand and capacity PDF and consequently the probability of exceeding the capacity given the demand model can be obtained.

APPENDIX A: ANOVA TABLES FOR DESIGN OF EXPERIMENT

This section is dedicated to analysis of variance tables obtained from design of experiment .The meaning of each row of the ANOVA table have been discussed below :

- The first column shows the source of the variability.
- The second column shows the sum of squares (SS) due to each source.
- The third column shows the degrees of freedom (df) associated with each source which in Plackett-Burman design is 1.
- The fourth column shows the mean squares (MS), which is the ratio SS/df .
- The fifth column shows the F statistics, which are the ratios of the mean squares.
- The sixth column shows the p-values for the F statistics.

It should be noted that these tables have been obtained using MATLAB®.

Table A.1: ANOVA table for deformation of abutments in longitudinal active direction

Parameters	Sum Sq.	d.f.	Mean Sq.	F	Prob>F
fc	0.511151	1	0.511151	0.325519	0.568412
fys	2.475099	1	2.475099	1.576229	0.20954
cof_ep	0.413659	1	0.413659	0.263433	0.607862
st_ep	1.896995	1	1.896995	1.208072	0.271926
dwl_str	13.01496	1	13.01496	8.288376	0.004058
dwl_gap	311.6737	1	311.6737	198.4846	6.06E-42
st_abp	57.10173	1	57.10173	36.36436	2.15E-09
st_aba	1106.965	1	1106.965	704.9536	0.00E+00
rot_fnd	1.888645	1	1.888645	1.202755	0.272983
trns_fnd	2.875288	1	2.875288	1.831083	0.176245
ms	245.0902	1	245.0902	156.082	7.79E-34
dr	41.74901	1	41.74901	26.58722	2.93E-07
gap1	1.910876	1	1.910876	1.216912	0.27018
gap2	1.3926	1	1.3926	0.886856	0.346513
gap3	137.5952	1	137.5952	87.62542	3.55E-20
gap4	0.07977	1	0.07977	0.0508	0.821713
impactK1	13.2552	1	13.2552	8.441371	0.003732
impactK2	12.8481	1	12.8481	8.182116	0.004301
transpilefactor	0.304683	1	0.304683	0.194033	0.659657
deckstiffac	13.20086	1	13.20086	8.406763	0.003804
fcult	44.73935	1	44.73935	28.49157	1.12E-07
ecult	63.06438	1	63.06438	40.16159	3.26E-10
steelEs	1.257447	1	1.257447	0.800786	0.371031
steelhr	13.65156	1	13.65156	8.693786	0.003252
Etor	4.948212	1	4.948212	3.151193	0.076115
intcolumn	0.169792	1	0.169792	0.108129	0.742339
intbent	0.992253	1	0.992253	0.631901	0.42681
dwl_gap2	8.147789	1	8.147789	5.188795	0.022901
Uyas0	2.491977	1	2.491977	1.586977	0.207994
Ultpilefac	158.5191	1	158.5191	100.9505	6.80E-23
Error	1961.262	1249	1.570266	□	□
Total	4225.487	1279	□	□	□

Table A.2: ANOVA table for Deformation of abutments in longitudinal passive direction

Parameters	Sum Sq.	d.f.	Mean Sq.	F	Prob>F
fc	3.912655	1	3.912655	2.855902	0.091289
fys	0.003927	1	0.003927	0.002866	0.957311
cof_ep	9.765501	1	9.765501	7.127976	0.007687
st_ep	8.748531	1	8.748531	6.385676	0.011627
dwl_str	25.52135	1	25.52135	18.62839	1.71E-05
dwl_gap	48.70882	1	48.70882	35.55325	3.23E-09
st_abp	77.50697	1	77.50697	56.57342	1.03E-13
st_aba	1071.333	1	1071.333	781.9812	5.46E-9
rot_fnd	0.007353	1	0.007353	0.005367	0.941612
trns_fnd	0.189407	1	0.189407	0.138251	0.710089
ms	92.75312	1	92.75312	67.70181	4.73E-16
dr	26.62374	1	26.62374	19.43304	1.13E-05
gap1	0.280469	1	0.280469	0.204718	0.651017
gap2	6.315083	1	6.315083	4.609468	0.031988
gap3	148.526	1	148.526	108.4112	2.11E-24
gap4	0.981582	1	0.981582	0.716471	0.397466
impactK1	15.87015	1	15.87015	11.58385	0.000686
impactK2	4.691396	1	4.691396	3.424316	0.064479
transpilefactor	1.054371	1	1.054371	0.7696	0.38051
deckstiffac	10.67184	1	10.67184	7.789522	0.005335
fcult	14.47431	1	14.47431	10.565	0.001183
ecult	23.12934	1	23.12934	16.88243	4.24E-05
steelEs	5.109851	1	5.109851	3.729752	0.053677
steelhr	21.10772	1	21.10772	15.40682	9.14E-05
Etor	14.38504	1	14.38504	10.49984	0.001225
intcolumn	2.663168	1	2.663168	1.943884	0.163495
intbent	0.060774	1	0.060774	0.04436	0.83322
dwl_gap2	18.48803	1	18.48803	13.49468	0.000249
Uyas0	0.000976	1	0.000976	0.000712	0.978716
Ultpilefac	185.3202	1	185.3202	135.2678	9.26E-30
Error	1711.16	1249	1.370024	□	□
Total	3549.365	1279	□	□	□

Table A.3: ANOVA table for Deformation of abutments in transverse direction

Parameters	Sum Sq.	d.f.	Mean Sq.	F	Prob>F
fc	0.730003	1	0.730003	0.542835	0.461399
fys	0.091993	1	0.091993	0.068407	0.793714
cof_ep	7.298464	1	7.298464	5.427185	0.019984
st_ep	0.677524	1	0.677524	0.503811	0.477963
dwl_str	7.333484	1	7.333484	5.453226	0.01969
dwl_gap	2.668684	1	2.668684	1.984451	0.159171
st_abp	2.762048	1	2.762048	2.053877	0.152069
st_aba	937.1773	1	937.1773	696.8911	#####
rot_fnd	6.321523	1	6.321523	4.700725	0.030338
trns_fnd	26.38444	1	26.38444	19.61964	1.03E-05
ms	14.19286	1	14.19286	10.5539	0.00119
dr	63.39393	1	63.39393	47.14014	1.04E-11
gap1	17.12841	1	17.12841	12.7368	0.000372
gap2	0.690759	1	0.690759	0.513653	0.473696
gap3	27.051	1	27.051	20.1153	7.96E-06
gap4	15.74005	1	15.74005	11.7044	0.000644
impactK1	2.41E-06	1	2.41E-06	1.79E-06	0.998933
impactK2	31.21524	1	31.21524	23.21185	1.63E-06
transpilefactor	3.475838	1	3.475838	2.584655	0.108157
deckstiffac	1.13771	1	1.13771	0.846008	0.357862
fcult	0.293902	1	0.293902	0.218547	0.640231
ecult	0.366808	1	0.366808	0.27276	0.601579
steelEs	0.339651	1	0.339651	0.252566	0.615362
steelhr	0.5793	1	0.5793	0.430771	0.511732
Etor	3.150073	1	3.150073	2.342414	0.126148
intcolumn	1.813555	1	1.813555	1.348571	0.24575
intbent	0.853224	1	0.853224	0.634463	0.425875
dwl_gap2	73.77326	1	73.77326	54.85827	2.38E-13
Uyas0	0.009171	1	0.009171	0.00682	0.934197
Ultpilefac	27.92867	1	27.92867	20.76794	5.69E-06
Error	1679.652	1249	1.344797	□	□
Total	2954.231	1279	□	□	□

Table A.4: ANOVA table for Curvature ductility of concrete columns in longitudinal direction

Parameters	Sum Sq.	d.f.	Mean Sq.	F	Prob>F
fc	0.624992	1	0.624992	3.887339	0.048872
fys	27.12116	1	27.12116	168.6888	2.85E-36
cof_ep	1.257547	1	1.257547	7.821718	0.005241
st_ep	0.036579	1	0.036579	0.227513	0.633457
dwl_str	0.674739	1	0.674739	4.196758	0.04071
dwl_gap	3.300759	1	3.300759	20.53013	6.43E-06
st_abp	0.270125	1	0.270125	1.680129	0.195147
st_aba	0.086896	1	0.086896	0.540479	0.462372
rot_fnd	6.374958	1	6.374958	39.65111	4.20E-10
trns_fnd	0.31166	1	0.31166	1.938467	0.164083
ms	1.649555	1	1.649555	10.25994	0.001394
dr	104.9652	1	104.9652	652.8651	#####
gap1	0.288319	1	0.288319	1.793292	0.180769
gap2	0.115307	1	0.115307	0.717189	0.39723
gap3	0.016941	1	0.016941	0.105371	0.745531
gap4	0.000985	1	0.000985	0.006127	0.937624
impactK1	0.009733	1	0.009733	0.060536	0.805691
impactK2	0.176431	1	0.176431	1.097366	0.295047
transpilefactor	0.589811	1	0.589811	3.668522	0.055677
deckstiffac	6.936034	1	6.936034	43.1409	7.46E-11
fcult	0.208409	1	0.208409	1.29627	0.255114
ecult	0.049122	1	0.049122	0.305527	0.580537
steelEs	10.24718	1	10.24718	63.73567	3.20E-15
steelhr	0.220967	1	0.220967	1.374378	0.241285
Etor	0.110458	1	0.110458	0.687028	0.407336
intcolumn	0.000572	1	0.000572	0.003558	0.952448
intbent	2.405777	1	2.405777	14.96351	0.000115
dwl_gap2	1.633214	1	1.633214	10.1583	0.001472
Uyas0	0.308017	1	0.308017	1.915808	0.166567
Ultpilefac	0.298949	1	0.298949	1.859407	0.172939
Error	200.8096	1249	0.160776	□	□
Total	371.1	1279	□	□	□

Table A.5: ANOVA table for Curvature ductility of concrete columns in transverse direction

Parameters	Sum Sq.	d.f.	Mean Sq.	F	Prob>F
fc	0.717119	1	0.717119	6.003251	0.014416
fys	16.79937	1	16.79937	140.6334	8.13E-31
cof_ep	15.92037	1	15.92037	133.2749	2.29E-29
st_ep	3.338398	1	3.338398	27.94689	1.47E-07
dwl_str	0.717982	1	0.717982	6.010476	0.014357
dwl_gap	1.347372	1	1.347372	11.27932	0.000807
st_abp	0.706981	1	0.706981	5.918383	0.015123
st_aba	3.914689	1	3.914689	32.77122	1.30E-08
rot_fnd	31.09238	1	31.09238	260.2851	2.48E-53
trns_fnd	1.486367	1	1.486367	12.44289	0.000435
ms	1.781097	1	1.781097	14.91018	0.000119
dr	50.61916	1	50.61916	423.7505	2.64E-81
gap1	0.430685	1	0.430685	3.605411	0.057822
gap2	0.5665	1	0.5665	4.742372	0.029615
gap3	0.016551	1	0.016551	0.138554	0.709786
gap4	0.486019	1	0.486019	4.068633	0.0439
impactK1	0.262047	1	0.262047	2.193687	0.138829
impactK2	1.805922	1	1.805922	15.11799	0.000106
transpilefyfactor	15.14966	1	15.14966	126.8231	4.35E-28
deckstiffac	6.000999	1	6.000999	50.23644	2.27E-12
fcult	0.003789	1	0.003789	0.031719	0.858675
ecult	0.604312	1	0.604312	5.058905	0.024673
steelEs	3.867175	1	3.867175	32.37346	1.58E-08
steelhr	2.5913	1	2.5913	21.69267	3.54E-06
Etor	0.207225	1	0.207225	1.734751	0.188047
intcolumn	2.305873	1	2.305873	19.30326	1.21E-05
intbent	0.055296	1	0.055296	0.462906	0.496395
dwl_gap2	0.504285	1	0.504285	4.221545	0.040121
Uyas0	0.021862	1	0.021862	0.183017	0.668867
Ultpilefac	0.637594	1	0.637594	5.337524	0.021033
Error	149.1994	1249	0.119455	□	□
Total	313.1578	1279	□	□	□

Table A.6: ANOVA table for Deformation of expansion bearings in longitudinal direction

Parameters	Sum Sq.	d.f.	Mean Sq.	F	Prob>F
fc	0.717119	1	0.717119	6.003251	0.014416
fys	16.79937	1	16.79937	140.6334	8.13E-31
cof_ep	15.92037	1	15.92037	133.2749	2.29E-29
st_ep	3.338398	1	3.338398	27.94689	1.47E-07
dwl_str	0.717982	1	0.717982	6.010476	0.014357
dwl_gap	1.347372	1	1.347372	11.27932	0.000807
st_abp	0.706981	1	0.706981	5.918383	0.015123
st_aba	3.914689	1	3.914689	32.77122	1.30E-08
rot_fnd	31.09238	1	31.09238	260.2851	2.48E-53
trns_fnd	1.486367	1	1.486367	12.44289	0.000435
ms	1.781097	1	1.781097	14.91018	0.000119
dr	50.61916	1	50.61916	423.7505	2.64E-81
gap1	0.430685	1	0.430685	3.605411	0.057822
gap2	0.5665	1	0.5665	4.742372	0.029615
gap3	0.016551	1	0.016551	0.138554	0.709786
gap4	0.486019	1	0.486019	4.068633	0.0439
impactK1	0.262047	1	0.262047	2.193687	0.138829
impactK2	1.805922	1	1.805922	15.11799	0.000106
transpilefactor	15.14966	1	15.14966	126.8231	4.35E-28
deckstiffac	6.000999	1	6.000999	50.23644	2.27E-12
fcult	0.003789	1	0.003789	0.031719	0.858675
ecult	0.604312	1	0.604312	5.058905	0.024673
steelEs	3.867175	1	3.867175	32.37346	1.58E-08
steelhr	2.5913	1	2.5913	21.69267	3.54E-06
Etor	0.207225	1	0.207225	1.734751	0.188047
intcolumn	2.305873	1	2.305873	19.30326	1.21E-05
intbent	0.055296	1	0.055296	0.462906	0.496395
dwl_gap2	0.504285	1	0.504285	4.221545	0.040121
Uyas0	0.021862	1	0.021862	0.183017	0.668867
Ultpilefac	0.637594	1	0.637594	5.337524	0.021033
Error	149.1994	1249	0.119455	□	□
Total	313.1578	1279	□	□	□

Table A.7: ANOVA table for Deformation of expansion bearings in transverse direction

Parameters	Sum Sq.	d.f.	Mean Sq.	F	Prob>F
fc	7.758015	1	7.758015	0.760036	0.383485
fys	0.040348	1	0.040348	0.003953	0.949879
cof_ep	852.0331	1	852.0331	83.4718	2.54E-19
st_ep	158.6957	1	158.6957	15.54707	8.49E-05
dwl_str	36.43746	1	36.43746	3.569697	0.059074
dwl_gap	0.919644	1	0.919644	0.090096	0.764106
st_abp	3.188378	1	3.188378	0.312358	0.576337
st_aba	3.648592	1	3.648592	0.357444	0.550037
rot_fnd	10.48891	1	10.48891	1.027575	0.310925
trns_fnd	3.830887	1	3.830887	0.375303	0.540239
ms	177.9352	1	177.9352	17.43192	3.18E-05
dr	214.986	1	214.986	21.06171	4.90E-06
gap1	1.182966	1	1.182966	0.115893	0.73359
gap2	0.109384	1	0.109384	0.010716	0.917568
gap3	7.924933	1	7.924933	0.776388	0.378418
gap4	2.675026	1	2.675026	0.262066	0.608795
impactK1	6.83695	1	6.83695	0.669801	0.413277
impactK2	2.844813	1	2.844813	0.2787	0.597648
transpilefactor	1.674362	1	1.674362	0.164033	0.685539
deckstiffac	2.071907	1	2.071907	0.20298	0.652404
fcult	0.461224	1	0.461224	0.045185	0.831699
ecult	0.77874	1	0.77874	0.076291	0.782433
steelEs	70.13207	1	70.13207	6.870683	0.008869
steelhr	40.25823	1	40.25823	3.94401	0.047257
Etor	0.62495	1	0.62495	0.061225	0.804611
intcolumn	19.77387	1	19.77387	1.937202	0.16422
intbent	0.118922	1	0.118922	0.011651	0.914063
dwl_gap2	603.8898	1	603.8898	59.16174	2.93E-14
Uyas0	3.917	1	3.917	0.38374	0.535721
Ultpilefac	5.721463	1	5.721463	0.560519	0.454192
Error	12749.09	1249	10.20744	□	□
Total	14990.05	1279	□	□	□

Table A.8: ANOVA table for Deformation of fixed bearings in longitudinal direction

Parameters	Sum Sq.	d.f.	Mean Sq.	F	Prob>F
fc	1.849499	1	1.849499	1.40266	0.236504
fys	0.112649	1	0.112649	0.085433	0.770114
cof_ep	114.6883	1	114.6883	86.97961	4.82E-20
st_ep	49.87308	1	49.87308	37.82375	1.04E-09
dwl_str	9.788122	1	9.788122	7.423312	0.006528
dwl_gap	9.279026	1	9.279026	7.037214	0.008085
st_abp	0.029716	1	0.029716	0.022536	0.880693
st_aba	5.264469	1	5.264469	3.992574	0.045918
rot_fnd	3.427959	1	3.427959	2.599765	0.107132
trns_fnd	1.185688	1	1.185688	0.899226	0.343173
ms	19.24217	1	19.24217	14.59326	0.00014
dr	39.39793	1	39.39793	29.87939	5.55E-08
gap1	0.155514	1	0.155514	0.117942	0.731336
gap2	0.273514	1	0.273514	0.207433	0.648866
gap3	9.804614	1	9.804614	7.43582	0.006483
gap4	0.017349	1	0.017349	0.013157	0.908697
impactK1	36.79379	1	36.79379	27.90442	1.50E-07
impactK2	4.444804	1	4.444804	3.37094	0.066593
transpilefactor	0.084866	1	0.084866	0.064363	0.799771
deckstiffac	0.105304	1	0.105304	0.079863	0.77753
fcult	0.079345	1	0.079345	0.060175	0.80626
ecult	3.214231	1	3.214231	2.437673	0.118705
steelEs	7.00315	1	7.00315	5.31119	0.021352
steelhr	4.213662	1	4.213662	3.195642	0.074077
Etor	0.22263	1	0.22263	0.168843	0.681213
intcolumn	1.597676	1	1.597676	1.211678	0.271212
intbent	0.344923	1	0.344923	0.26159	0.60912
dwl_gap2	184.7972	1	184.7972	140.1502	1.01E-30
Uyas0	0.058349	1	0.058349	0.044252	0.83342
Ultpilefac	1.957144	1	1.957144	1.484298	0.223333
Error	1646.888	1249	1.318565	□	□
Total	2156.195	1279	□	□	□

Table A.9: ANOVA table for Deformation of fixed bearings in transverse direction

Parameters	Sum Sq.	d.f.	Mean Sq.	F	Prob>F
fc	4.392888	1	4.392888	2.144765	0.143309
fys	0.695626	1	0.695626	0.33963	0.560148
cof_ep	329.2254	1	329.2254	160.7396	9.74E-35
st_ep	67.2096	1	67.2096	32.81414	1.27E-08
dwl_str	30.06874	1	30.06874	14.68064	0.000134
dwl_gap	0.081071	1	0.081071	0.039582	0.842333
st_abp	1.390301	1	1.390301	0.678795	0.410159
st_aba	6.914885	1	6.914885	3.376095	0.066386
rot_fnd	1.522815	1	1.522815	0.743493	0.38871
trns_fnd	10.11039	1	10.11039	4.936253	0.026478
ms	97.44422	1	97.44422	47.57576	8.39E-12
dr	102.1191	1	102.1191	49.85818	2.74E-12
gap1	0.569472	1	0.569472	0.278037	0.598085
gap2	1.401871	1	1.401871	0.684444	0.408219
gap3	0.260209	1	0.260209	0.127043	0.721578
gap4	2.537895	1	2.537895	1.239091	0.26586
impactK1	2.889781	1	2.889781	1.410894	0.235134
impactK2	0.401701	1	0.401701	0.196125	0.657944
transpilefactor	3.920311	1	3.920311	1.914036	0.166763
deckstiffac	5.806905	1	5.806905	2.835139	0.092473
fcult	8.90635	1	8.90635	4.348399	0.037246
ecult	5.195266	1	5.195266	2.536515	0.111493
steelEs	27.66672	1	27.66672	13.50788	0.000248
steelhr	29.89382	1	29.89382	14.59523	0.00014
Etor	3.574799	1	3.574799	1.745345	0.186705
intcolumn	6.864577	1	6.864577	3.351532	0.067381
intbent	2.360228	1	2.360228	1.152348	0.283266
dwl_gap2	444.0117	1	444.0117	216.7824	2.29E-45
Uyas0	6.598683	1	6.598683	3.221713	0.072909
Ultpilefac	0.195665	1	0.195665	0.095531	0.757312
Error	2558.19	1249	2.048191	□	□
Total	3762.421	1279	□	□	□

**APPENDIX B: VARIATION OF MSSS CONCRETE BRIDGE
MONITORED PARAMETERS EFFECT WITH RESPECT TO GROUND
MOTION INTENSITY**

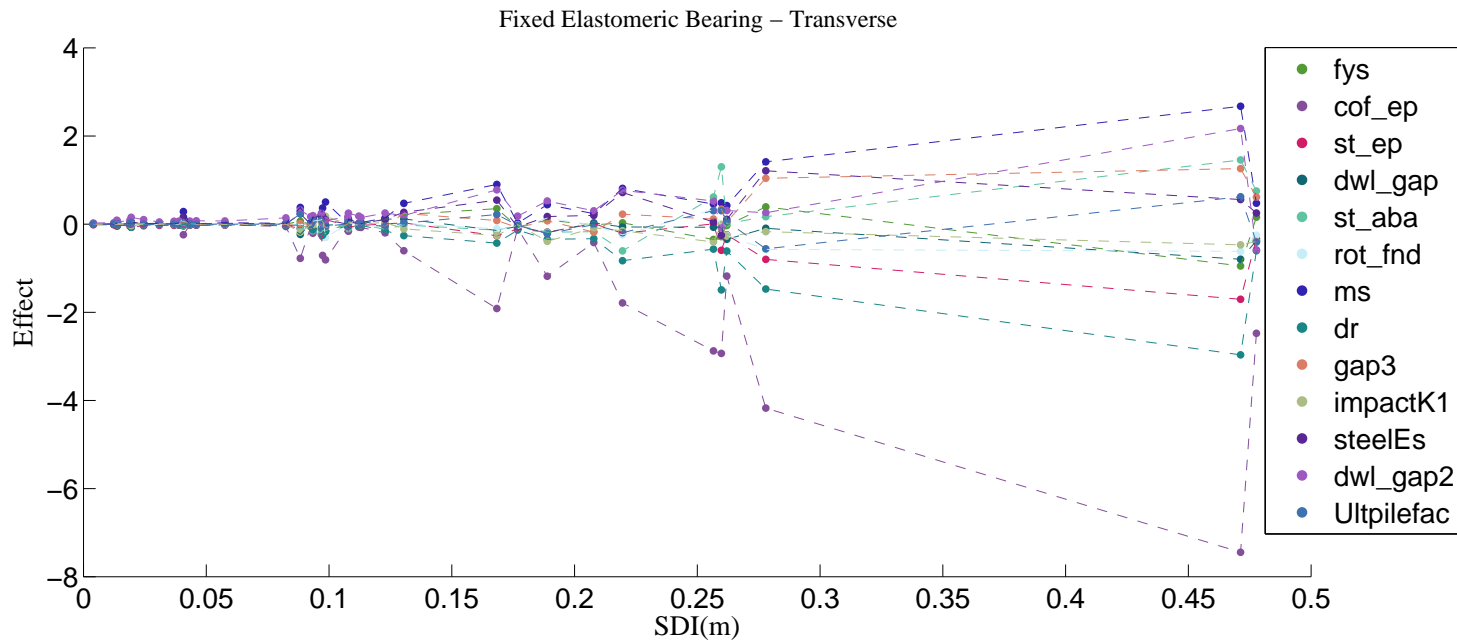


Figure B.1: Effect of screening design parameters on fixed bearings in transverse direction (in)

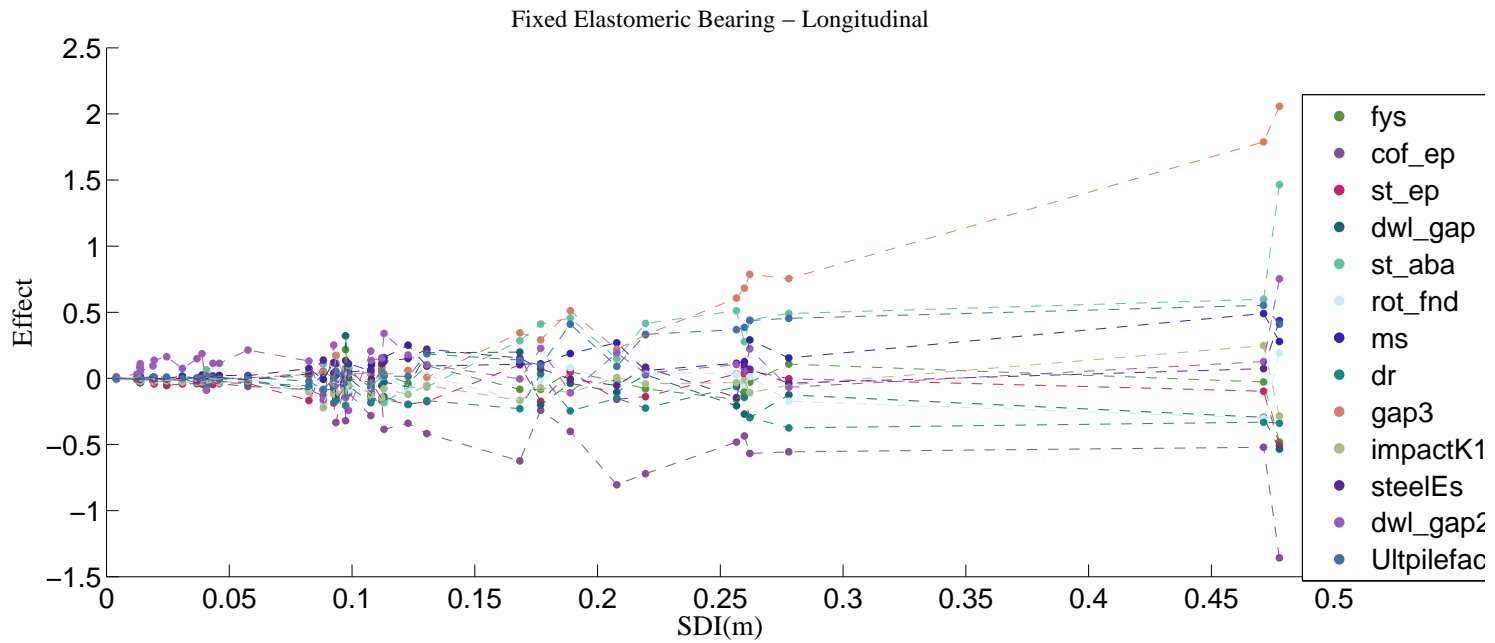


Figure B.2: Effect of screening design parameters on fixed bearings in longitudinal direction (in)

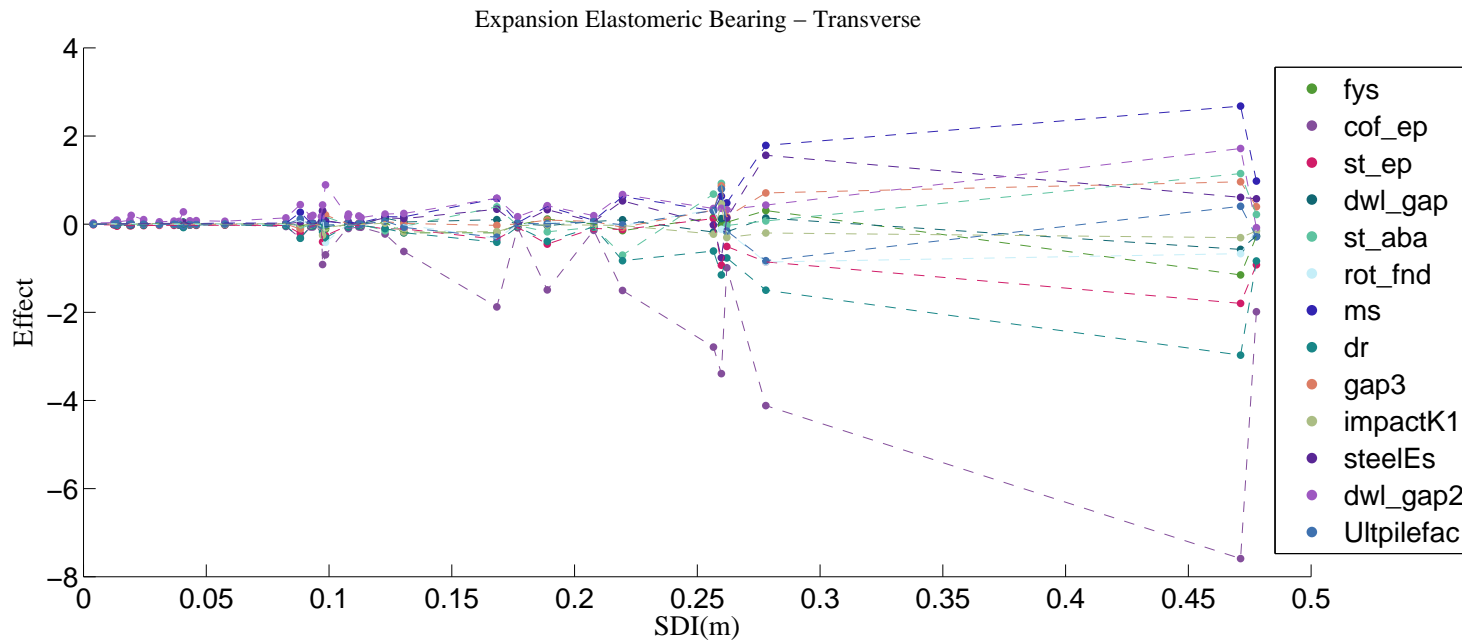


Figure B.3: Effect of screening design parameters on expansion bearings in transverse direction (in)

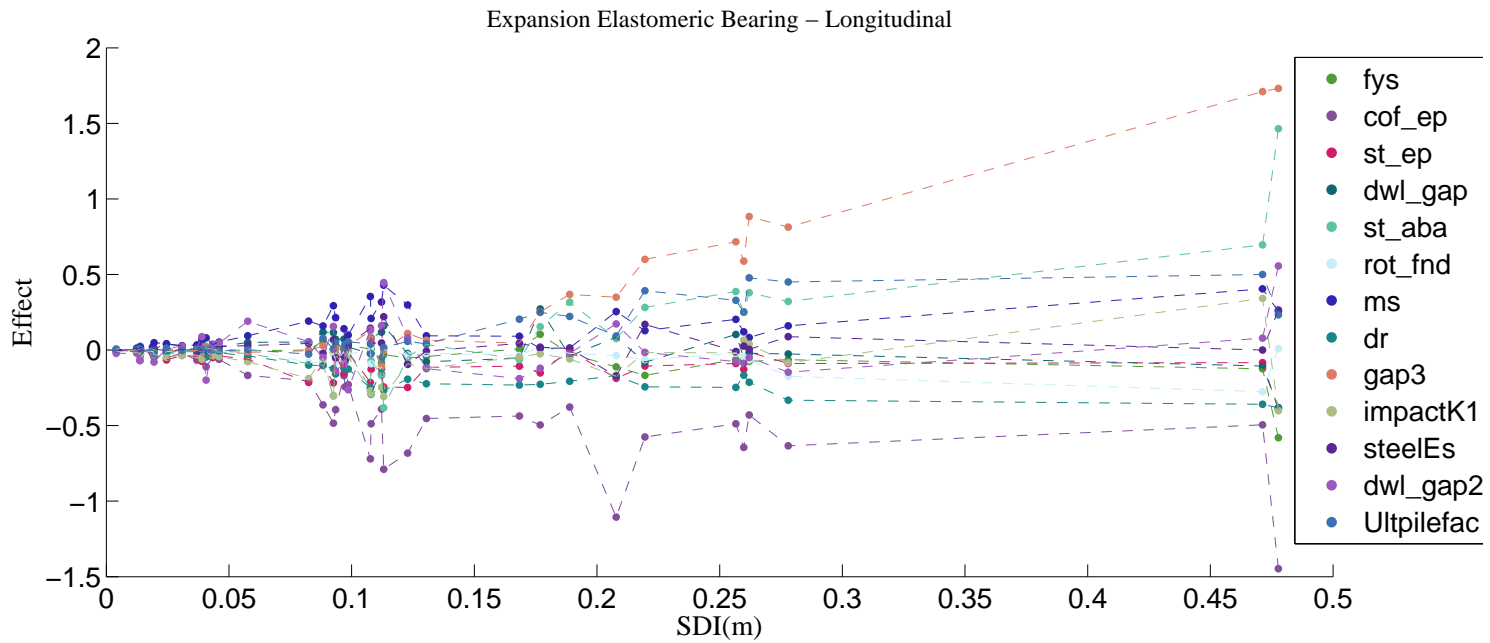


Figure B.4: Effect of screening design parameters on expansion bearings in longitudinal direction (in)

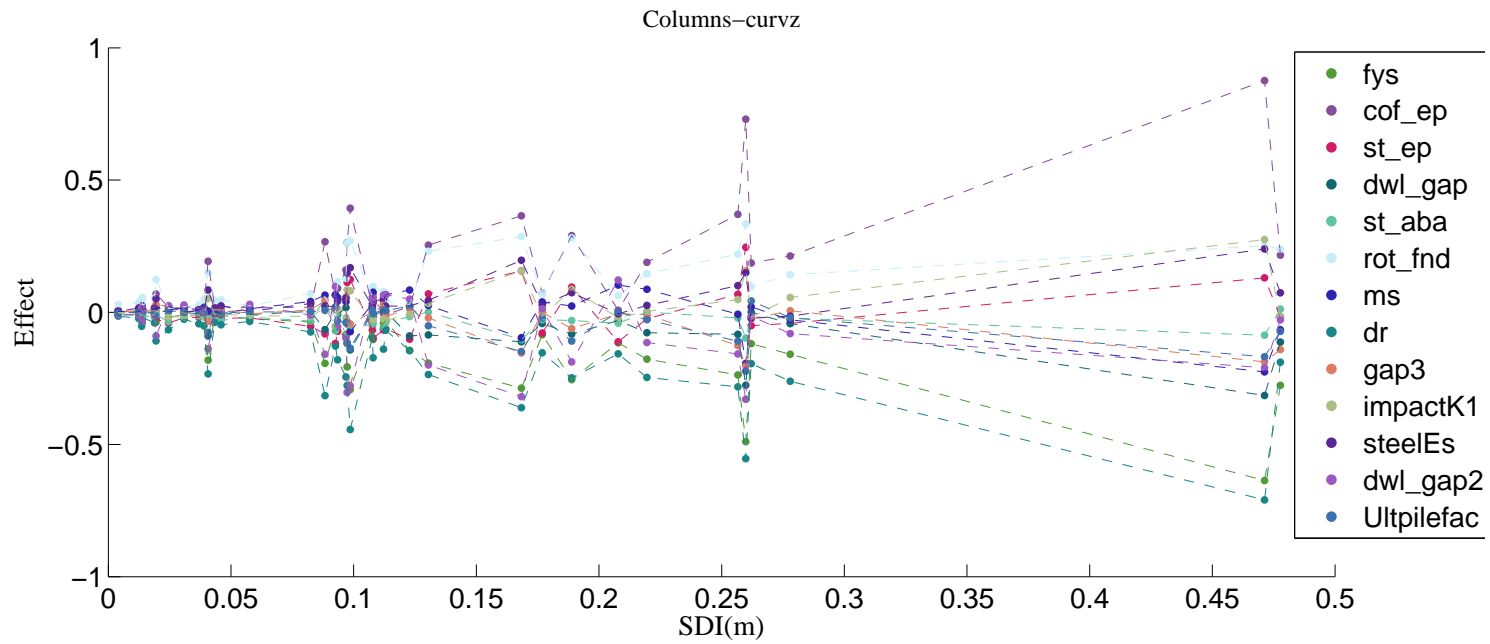


Figure B.5: Effect of screening design parameters on curvature ductility of concrete columns in transverse direction

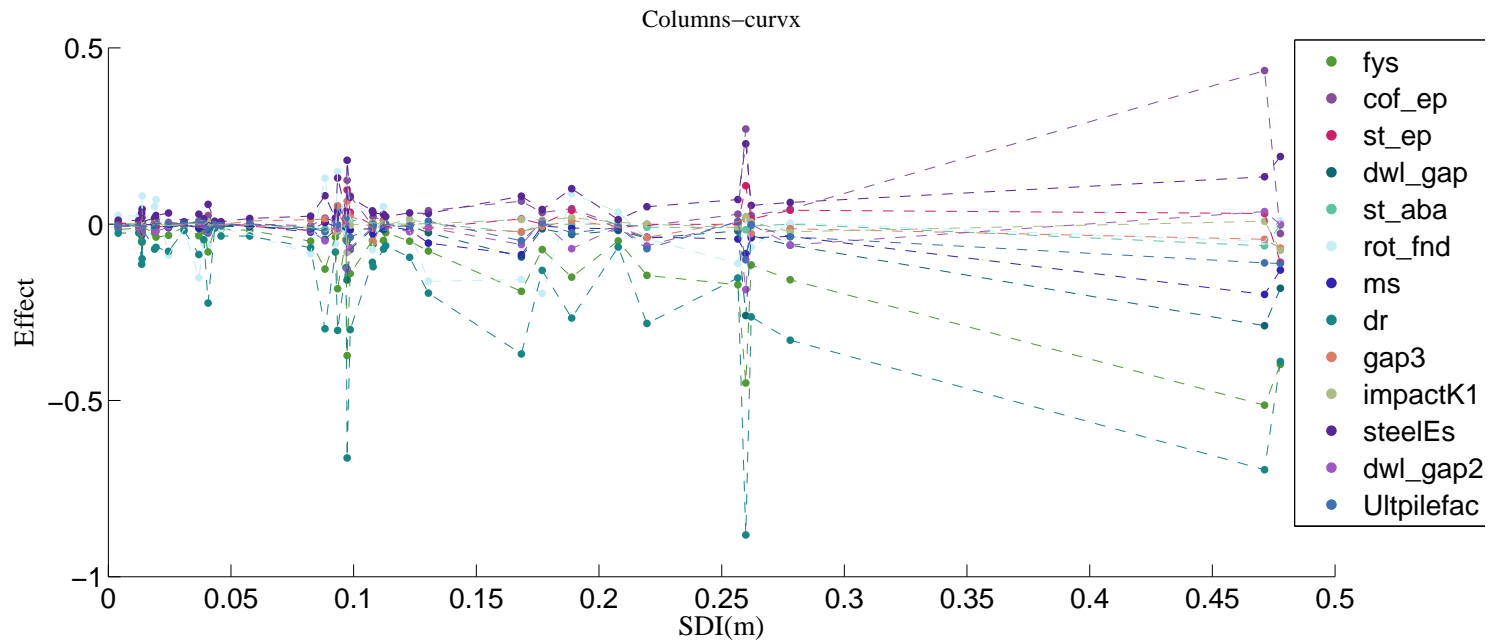


Figure B.6: Effect of screening design parameters on curvature ductility of concrete columns in longitudinal direction

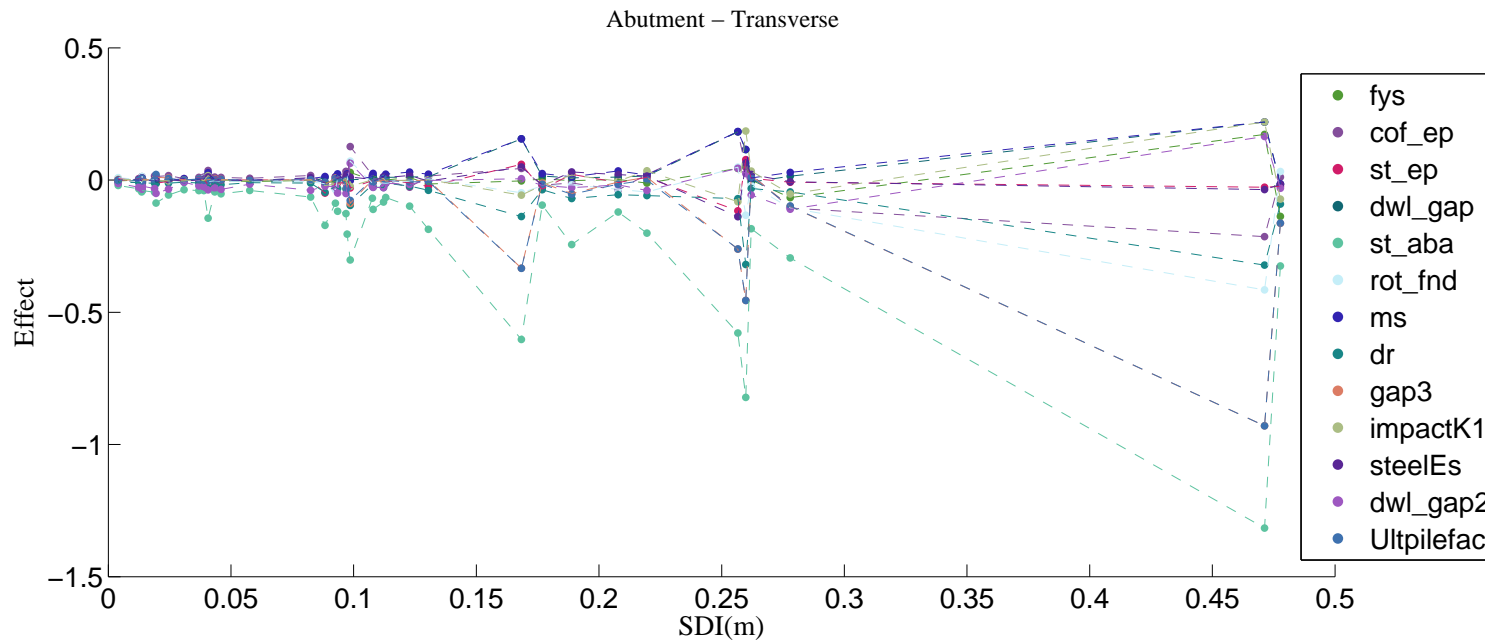


Figure B.7: Effect of screening design parameters on abutments in transverse direction (in)

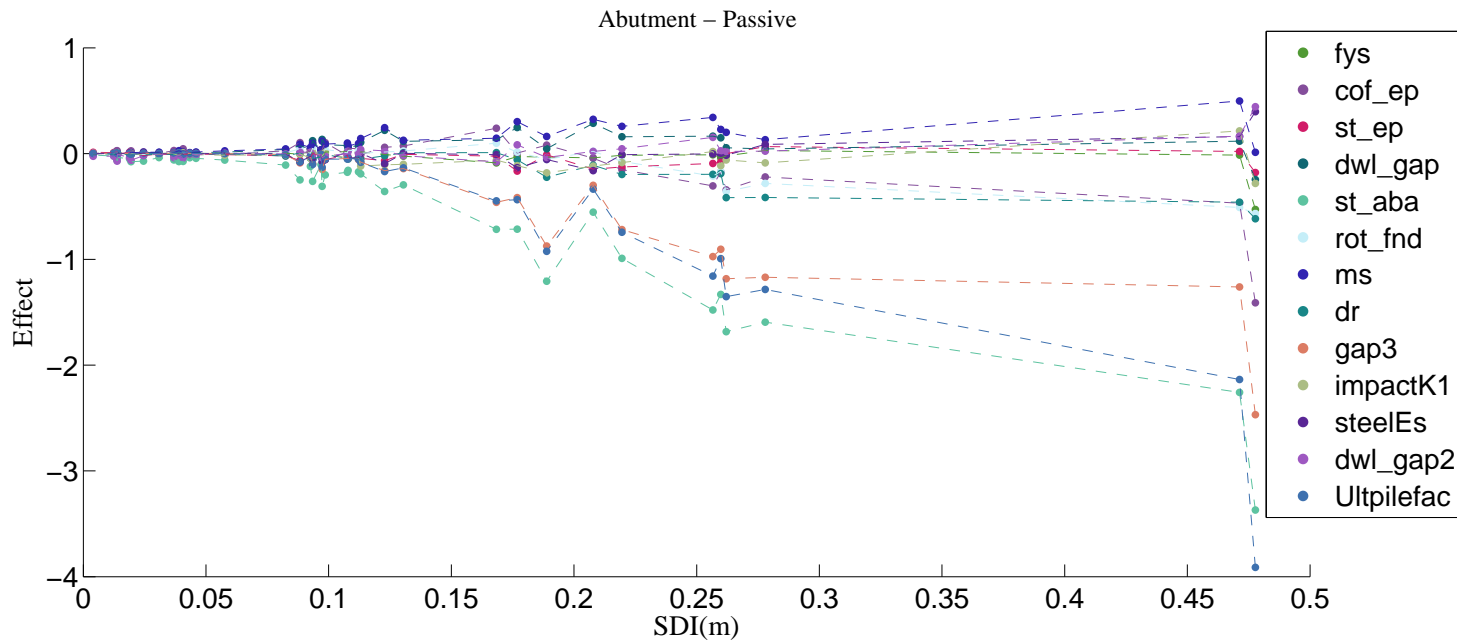


Figure B.8: Effect of screening design parameters on abutments in longitudinal passive direction (in)

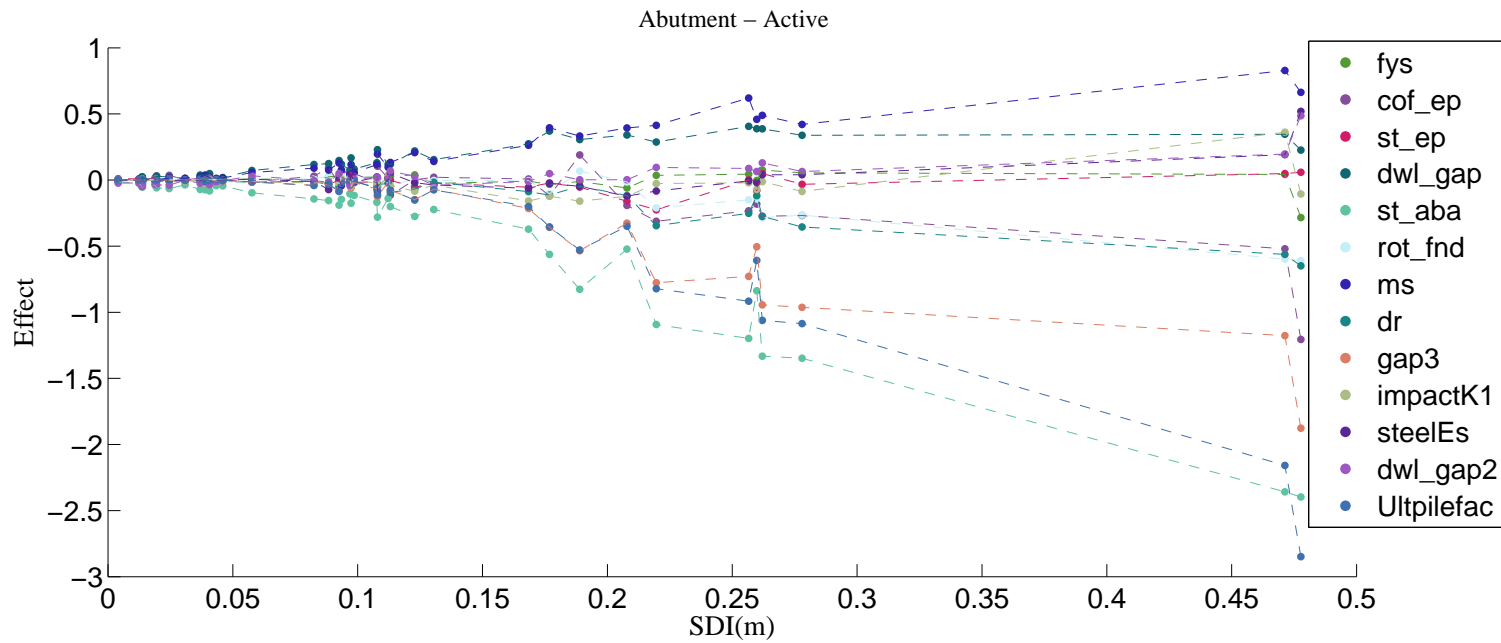
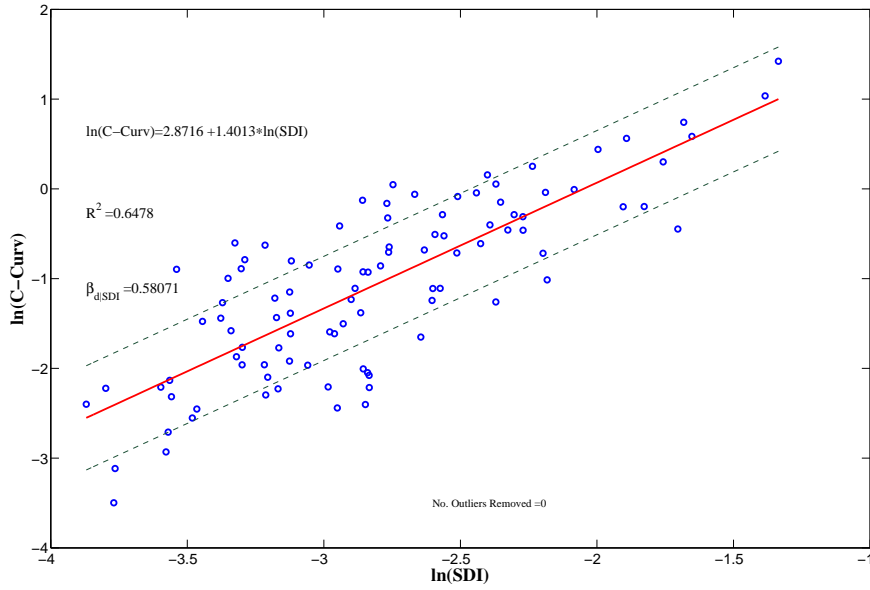
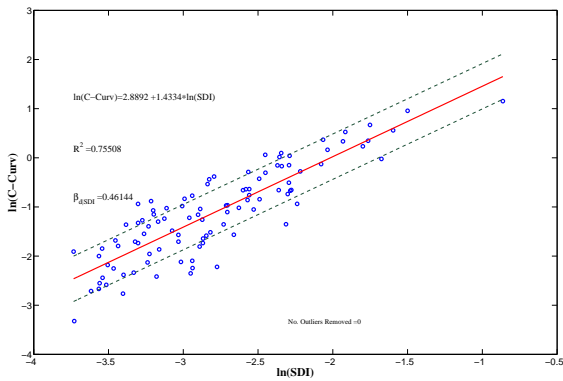


Figure B.9: Effect of screening design parameters on abutments in longitudinal active direction (in)

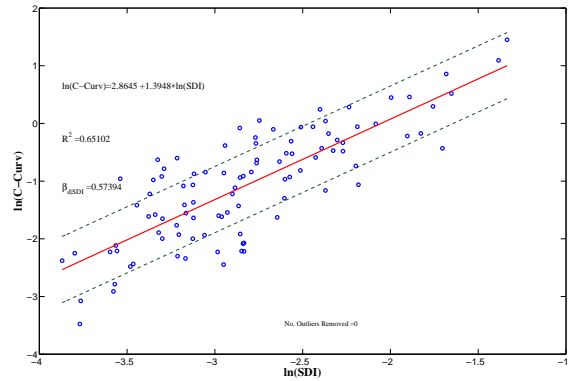
**APPENDIX C: PDSM MODELS FOR MSSS CONCRETE BRIDGE
COMPONENTS**



(a) Case 2



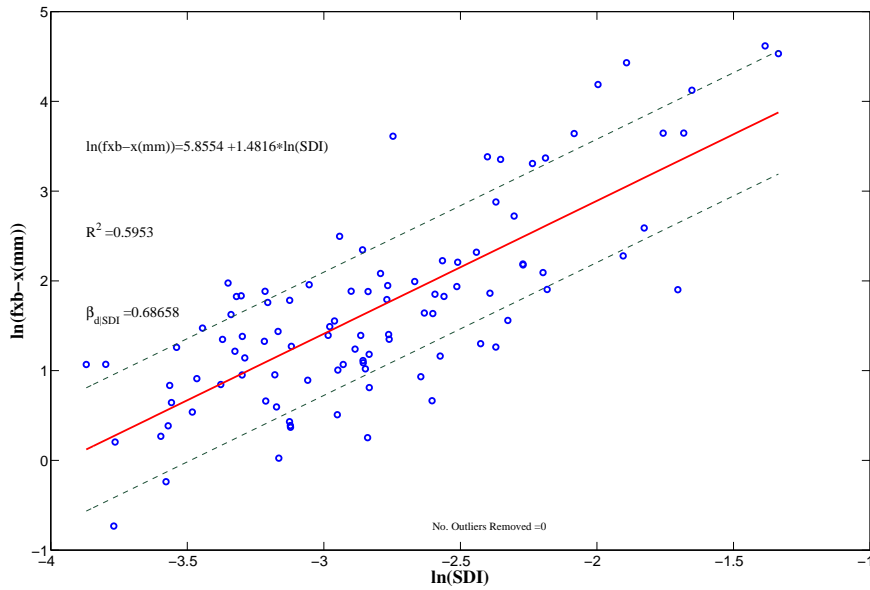
(b) Case 1



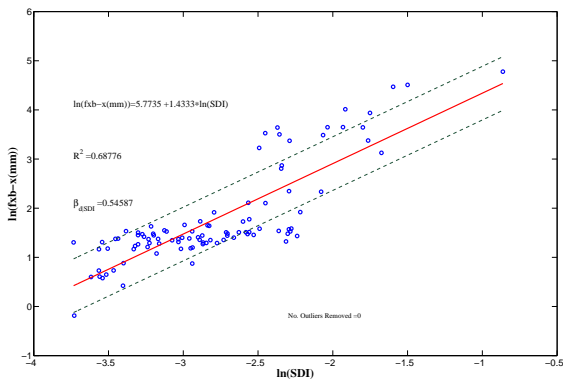
(c) Case 3

Figure C.1: Bridge component demand model for bridge columns

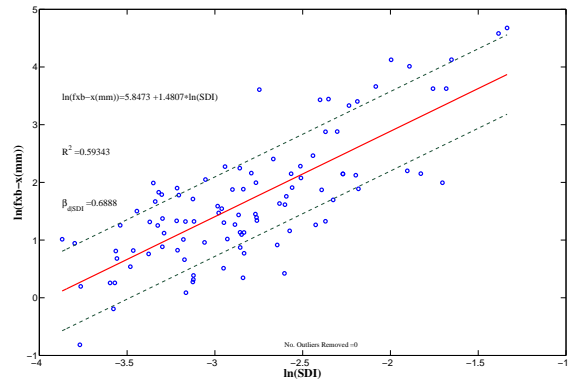
The PSDMs for the MSSS concrete components are included in this section. Each figure include the PSDMs obtained from regression for each class of analysis defined in section 4.2.8.



(a) Case 2

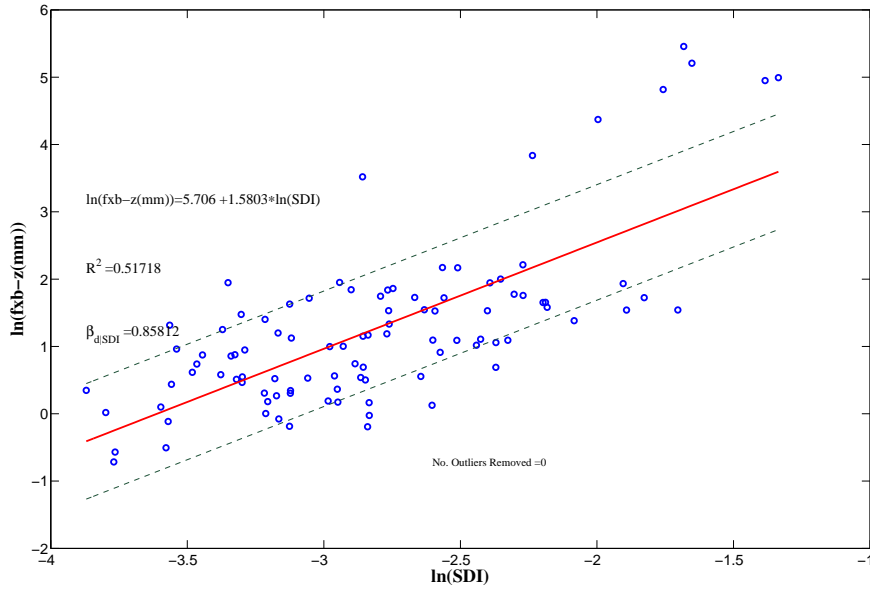


(b) Case 1

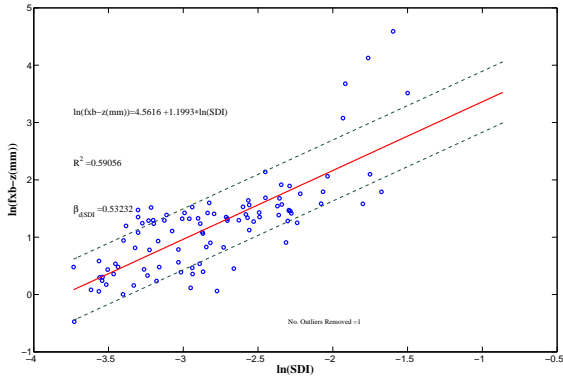


(c) Case 3

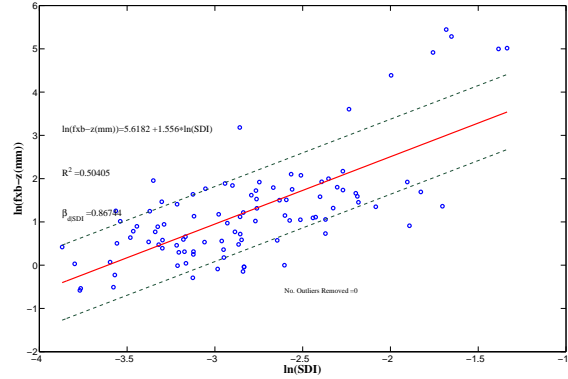
Figure C.2: Bridge component demand model for fixed elastomeric bearing in longitudinal direction



(a) Case 2

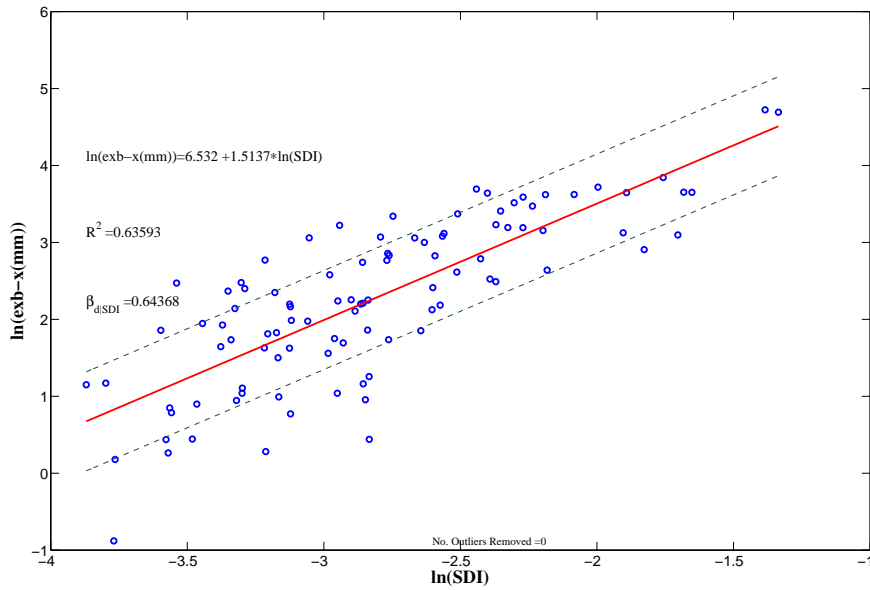


(b) Case 1

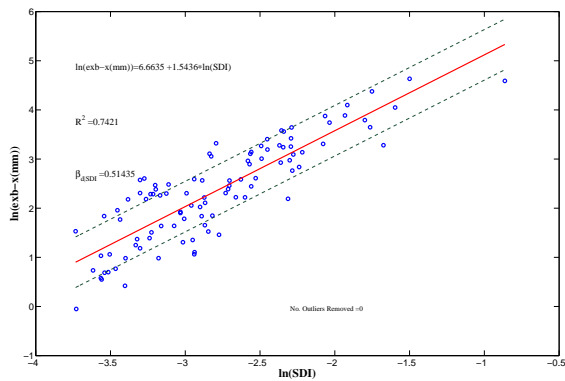


(c) Case 3

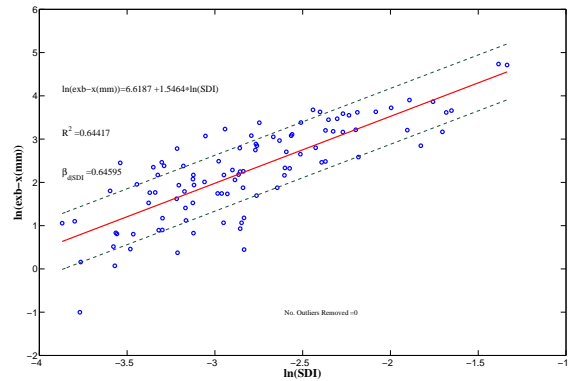
Figure C.3: Bridge component demand model for fixed elastomeric bearing in transverse direction



(a) Case 2

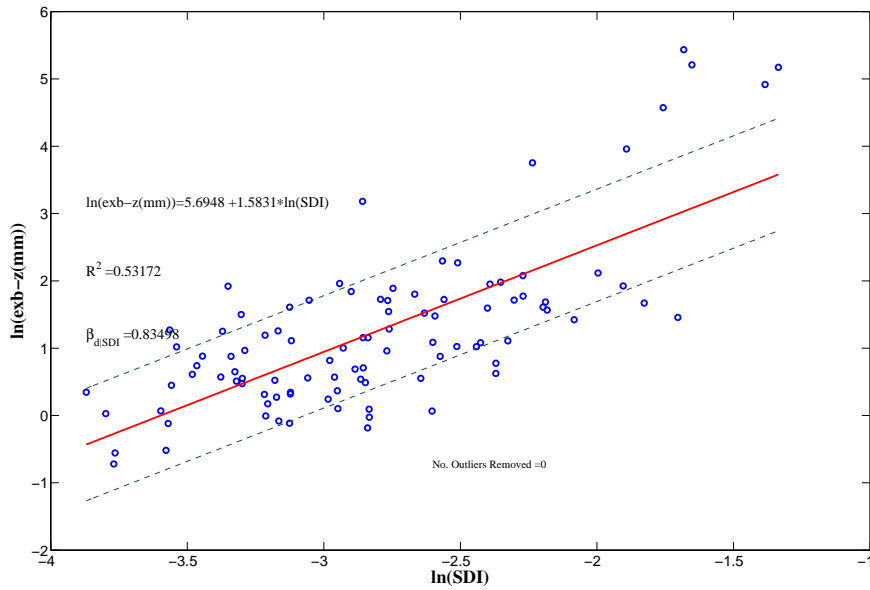


(b) Case 1

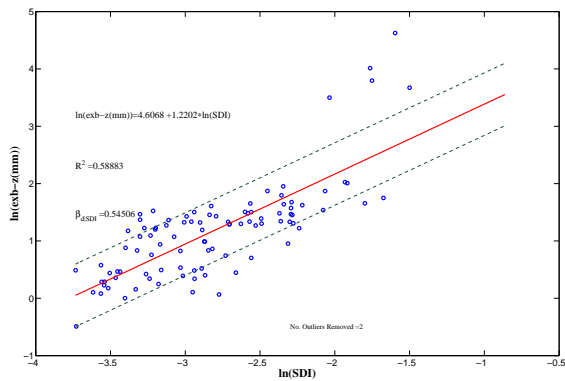


(c) Case 3

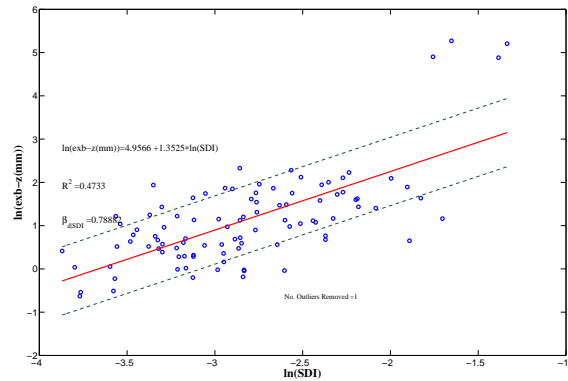
Figure C.4: Bridge component demand model for expansion elastomeric bearing in longitudinal direction



(a) Case 2

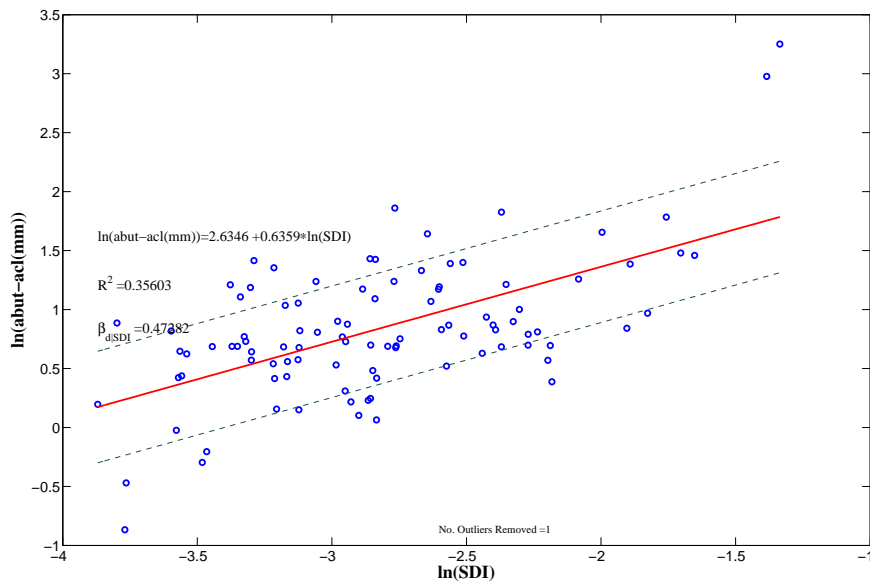


(b) Case 1

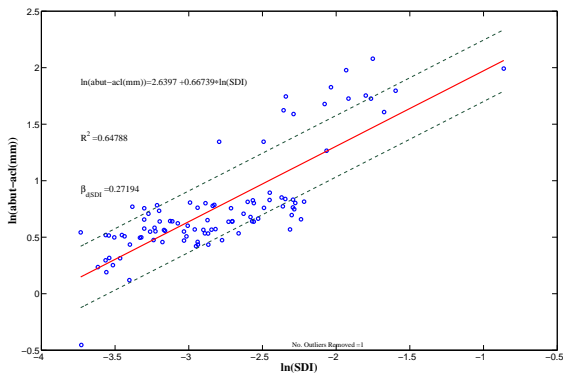


(c) Case 3

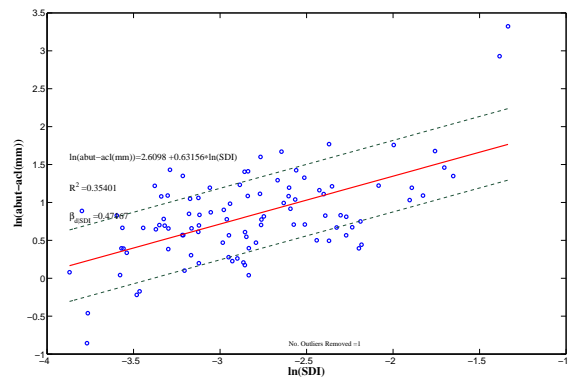
Figure C.5: Bridge component demand model for expansion elastomeric bearing in transverse direction



(a) Case 2

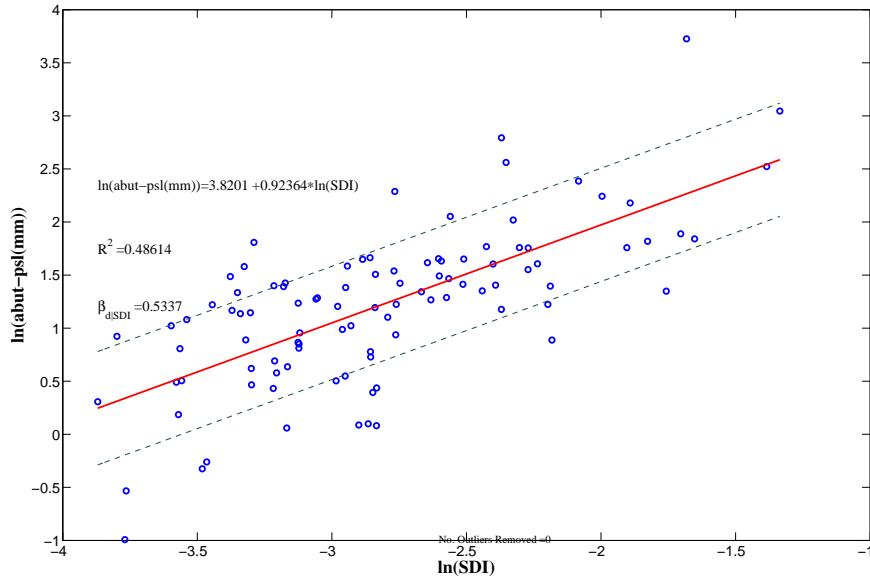


(b) Case 1

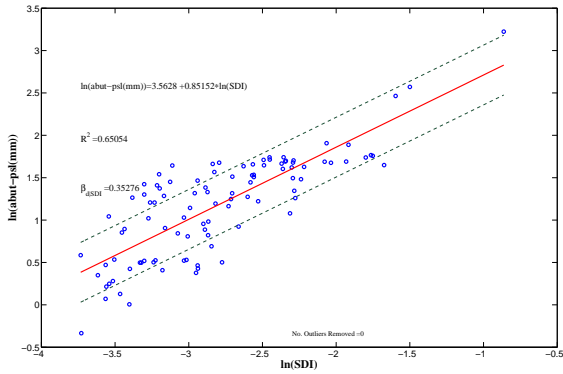


(c) Case 3

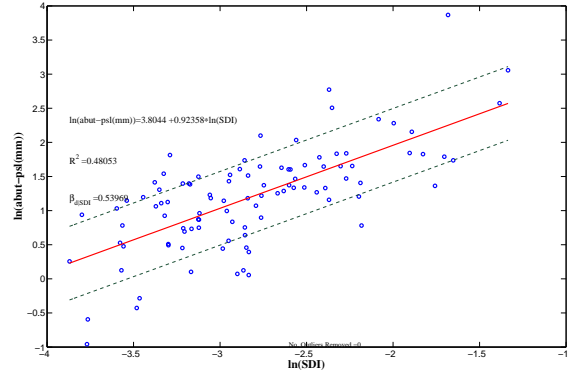
Figure C.6: Bridge component demand model for abutments in active longitudinal direction



(a) Case 2

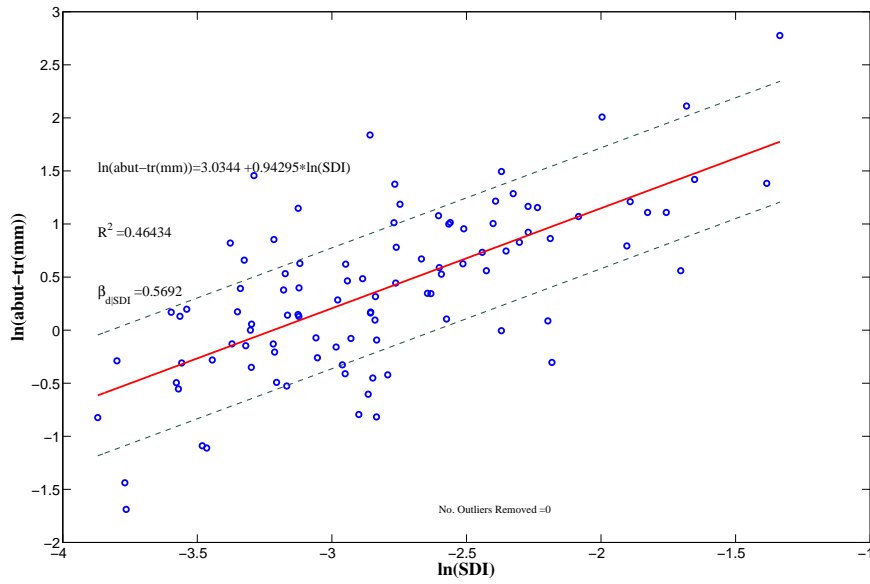


(b) Case 1

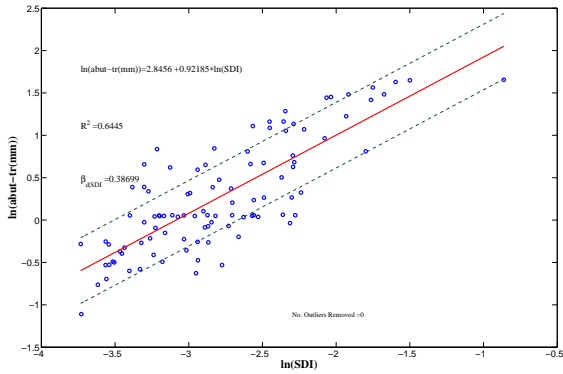


(c) Case 3

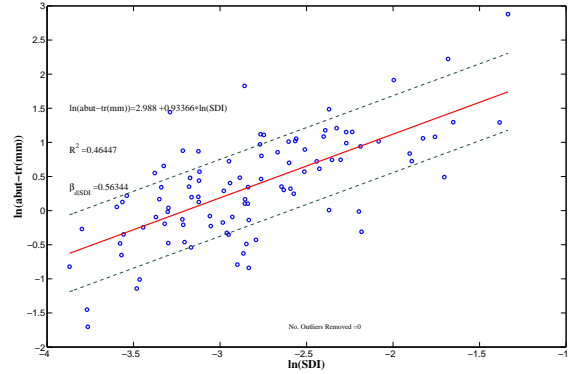
Figure C.7: Bridge component demand model for abutments in passive longitudinal direction



(a) Case 2



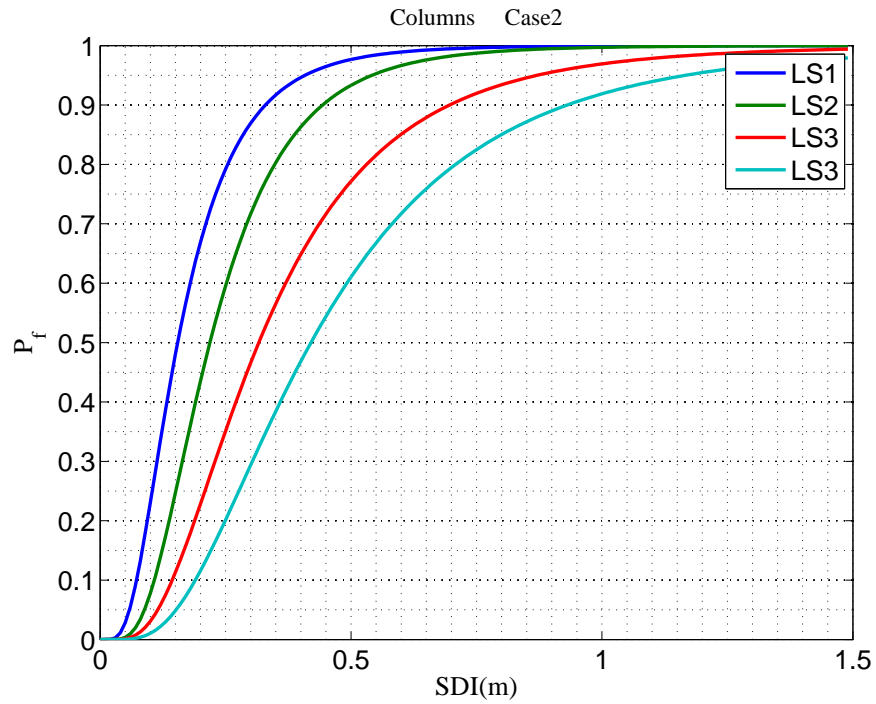
(b) Case 1



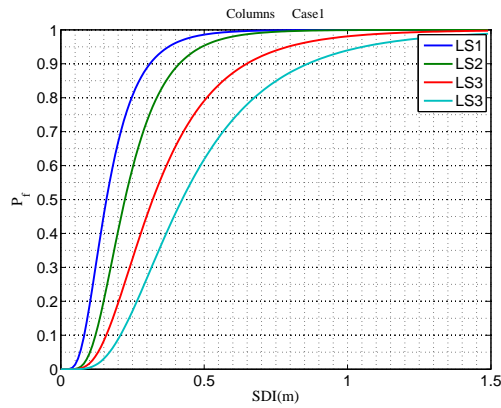
(c) Case 3

Figure C.8: Bridge component demand model for abutments in passive longitudinal direction

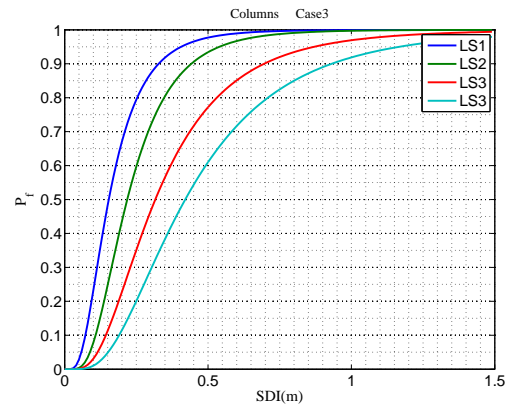
**APPENDIX D: FRAGILITY RESULTS OF MSSS CONCRETE GIRDER
BRIDGE**



(a) Case 2

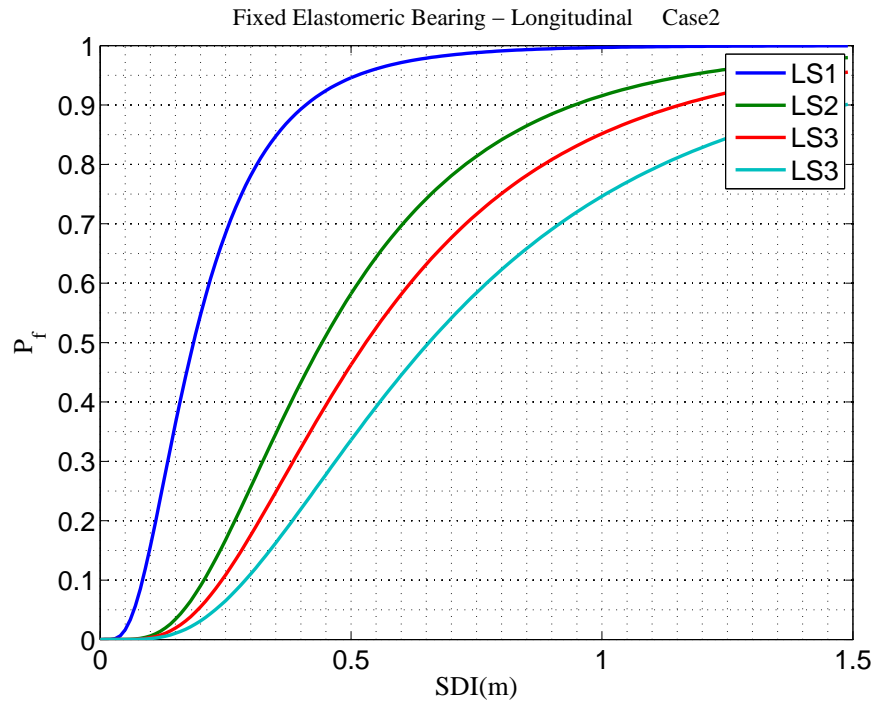


(b) Case 1

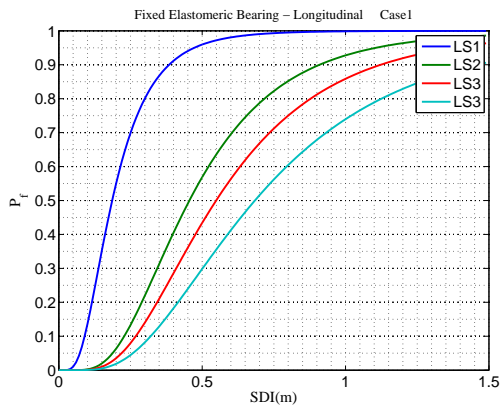


(c) Case 3

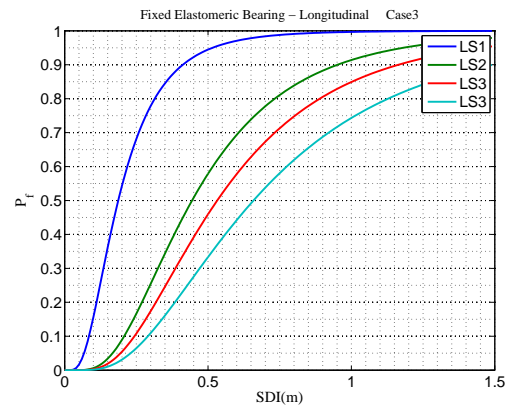
Figure D.1: Bridge columns component fragility curves



(a) Case 2

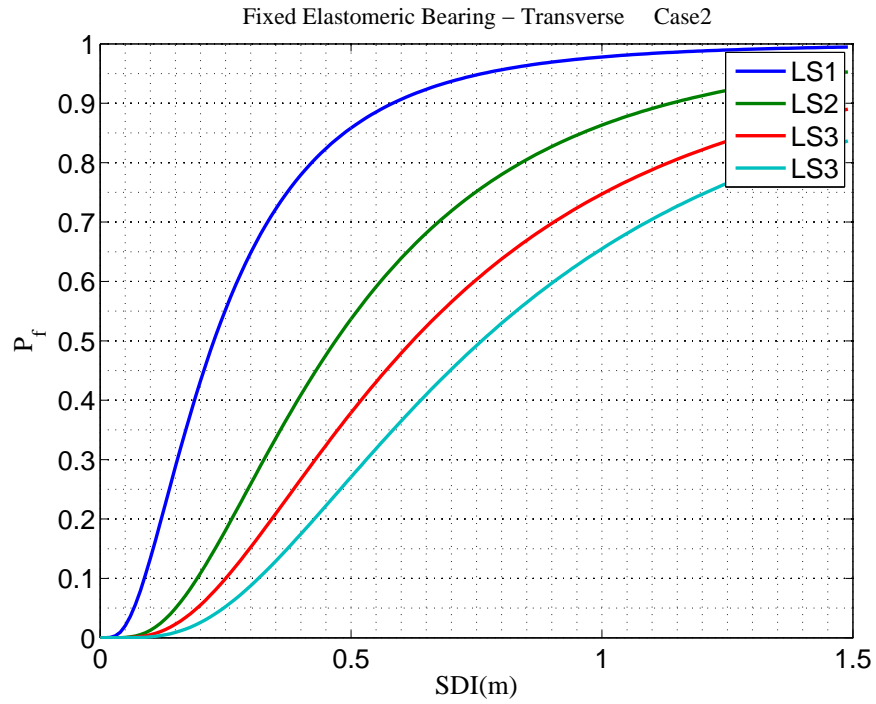


(b) Case 1

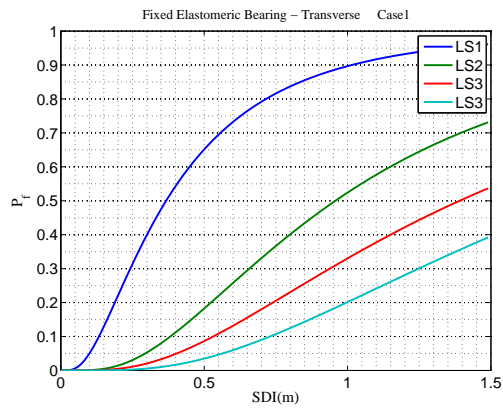


(c) Case 3

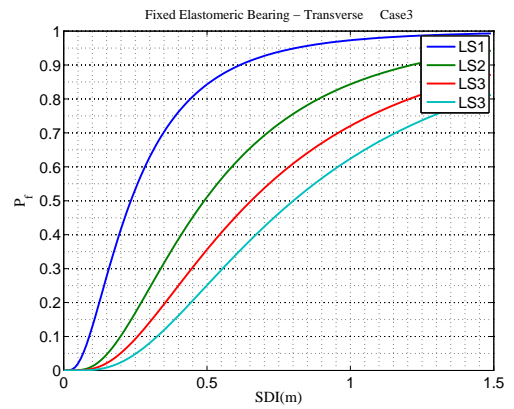
Figure D.2: Bridge component fragility curves for fixed elastomeric bearing in longitudinal direction



(a) Case 2

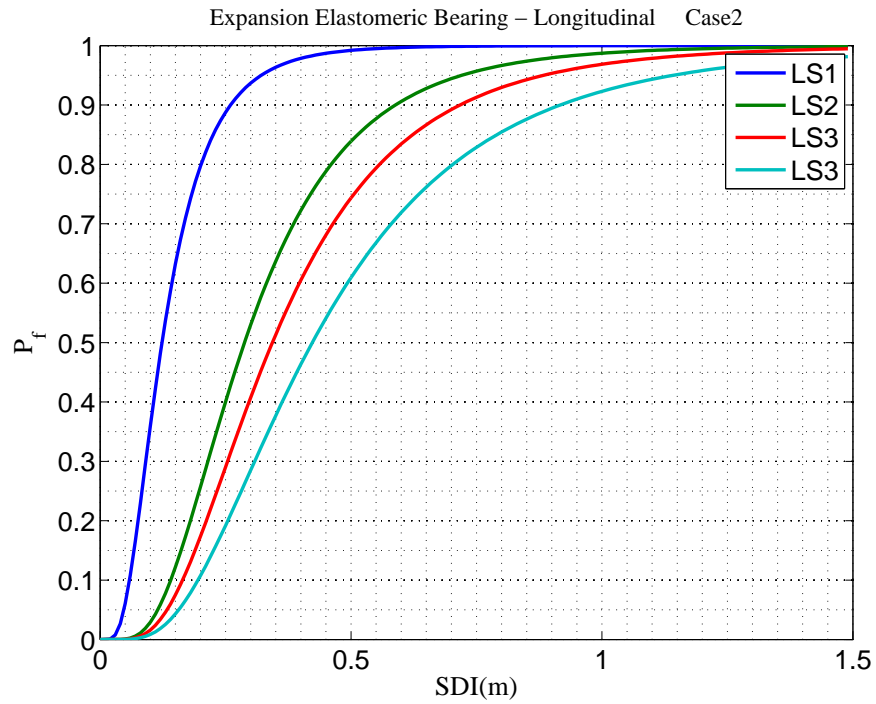


(b) Case 1

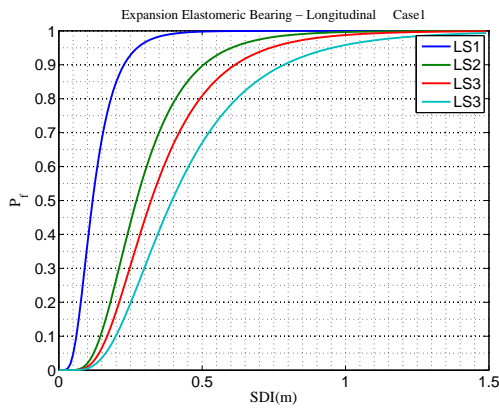


(c) Case 3

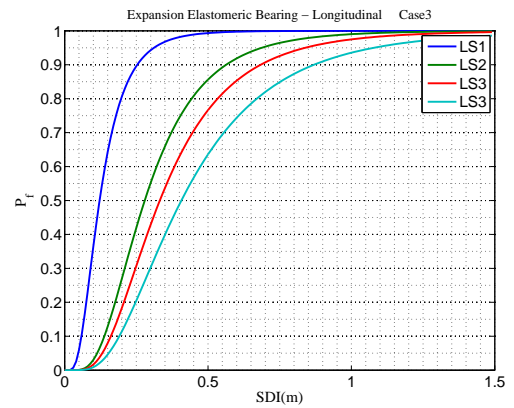
Figure D.3: Bridge component fragility curves for fixed elastomeric bearing in transverse direction



(a) Case 2

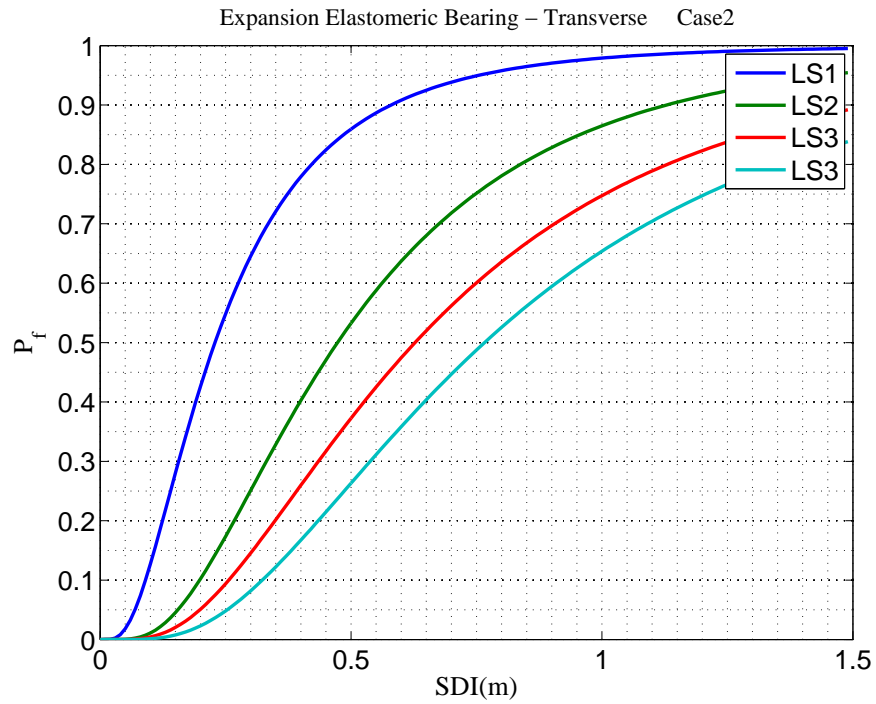


(b) Case 1

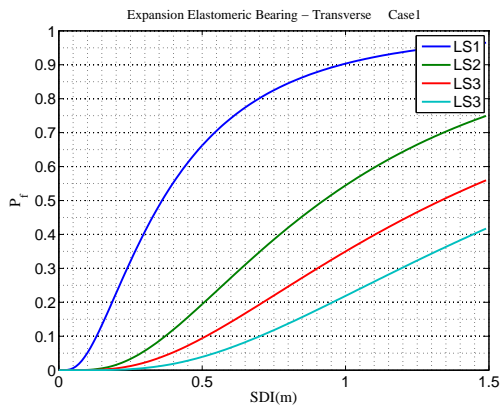


(c) Case 3

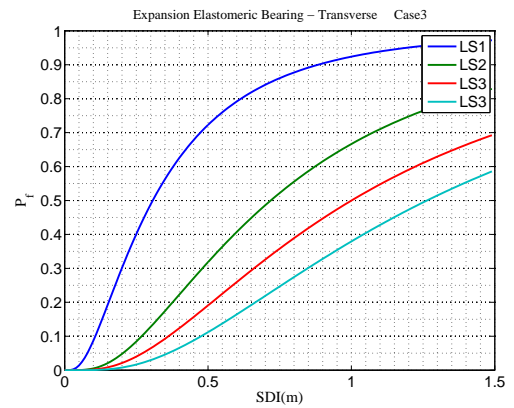
Figure D.4: Bridge component fragility curves for expansion elastomeric bearing in longitudinal direction



(a) Case 2

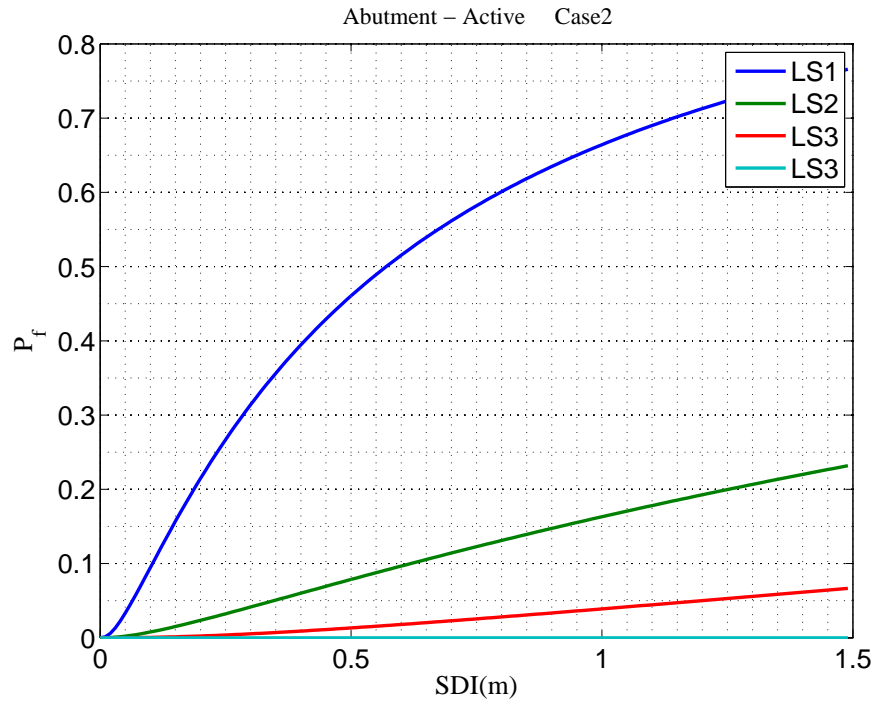


(b) Case 1

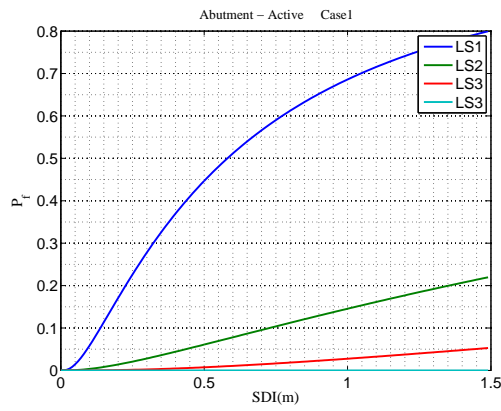


(c) Case 3

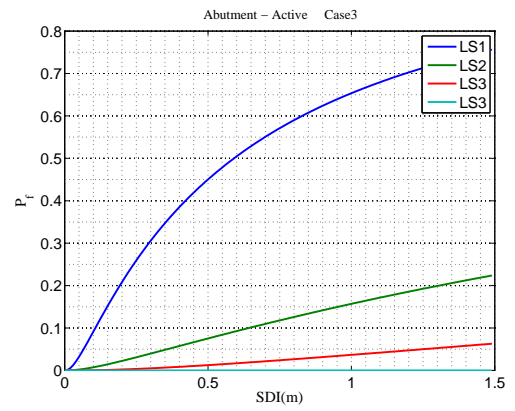
Figure D.5: Bridge component fragility curves for expansion elastomeric bearing in transverse direction



(a) Case 2

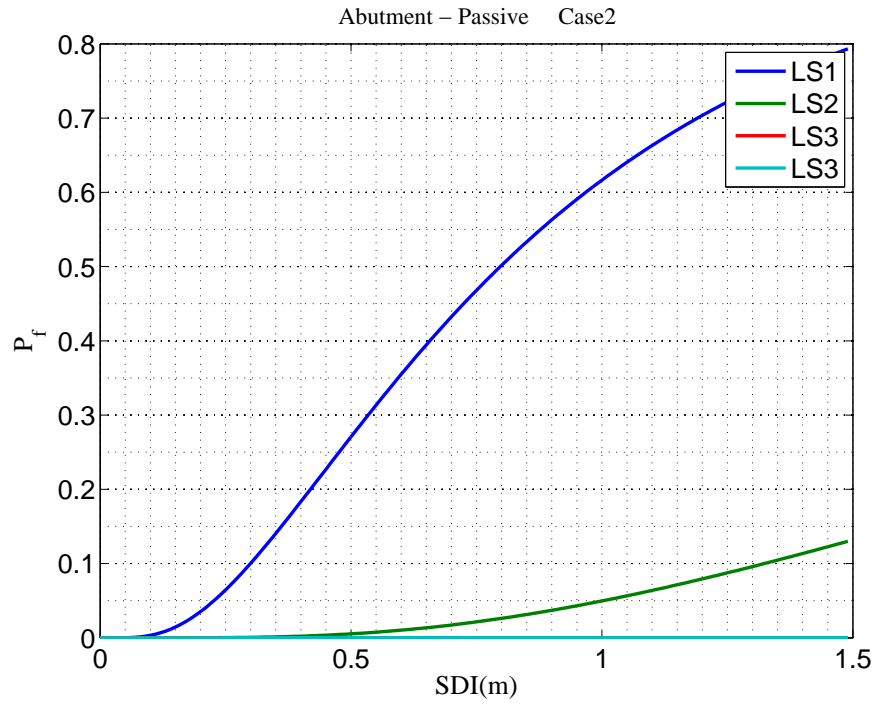


(b) Case 1

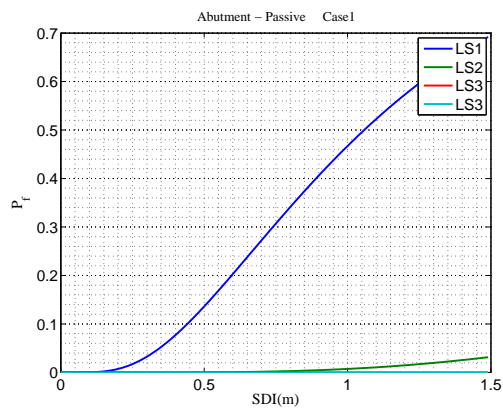


(c) Case 3

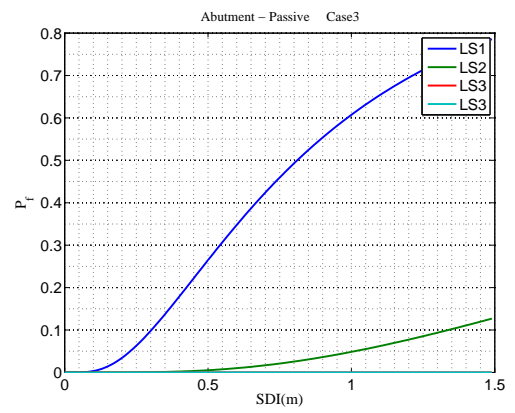
Figure D.6: Bridge component fragility curves for abutment in longitudinal active direction



(a) Case 2

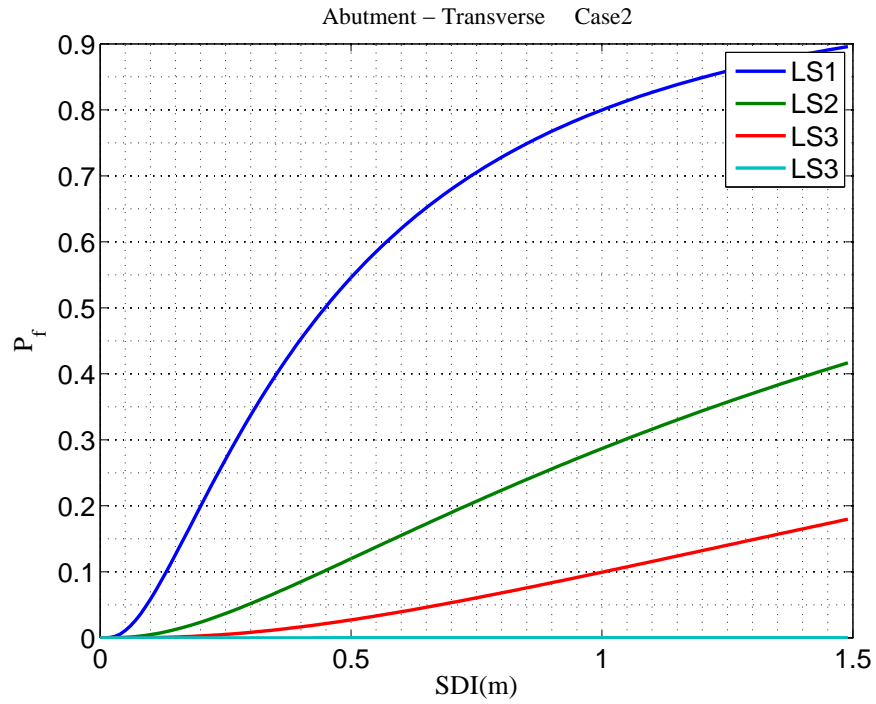


(b) Case 1

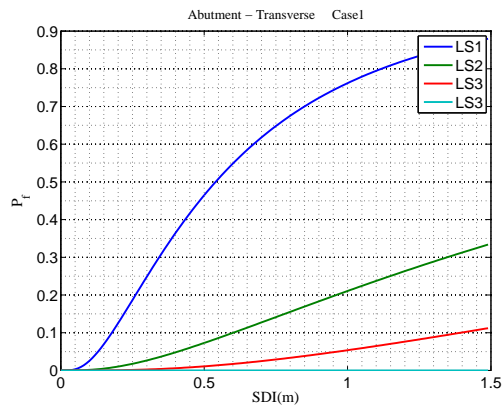


(c) Case 3

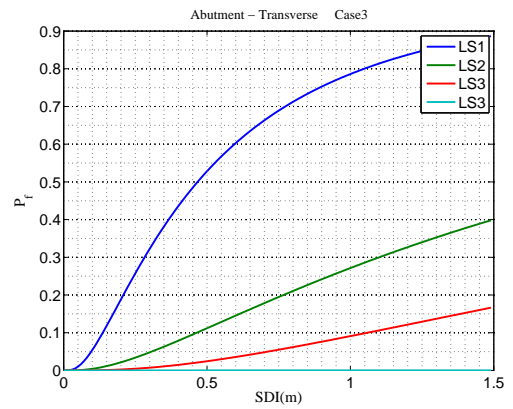
Figure D.7: Bridge component fragility curves for abutment in longitudinal passive direction



(a) Case 2



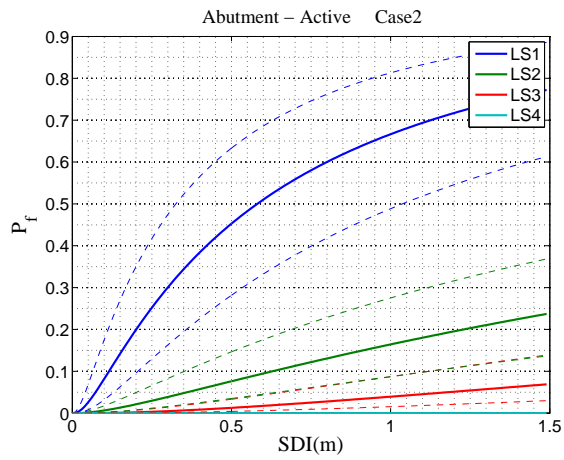
(b) Case 1



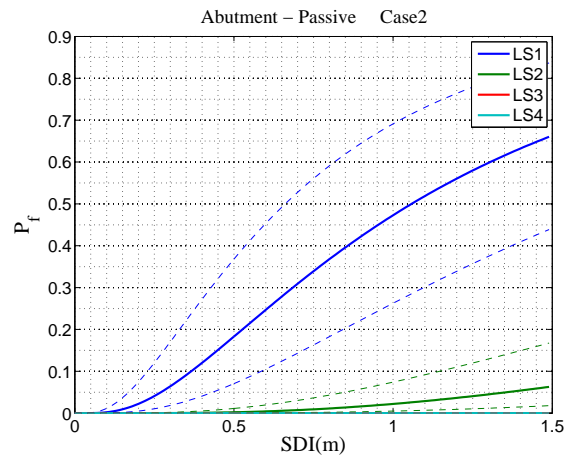
(c) Case 3

Figure D.8: Bridge component fragility curves for abutment in transverse direction

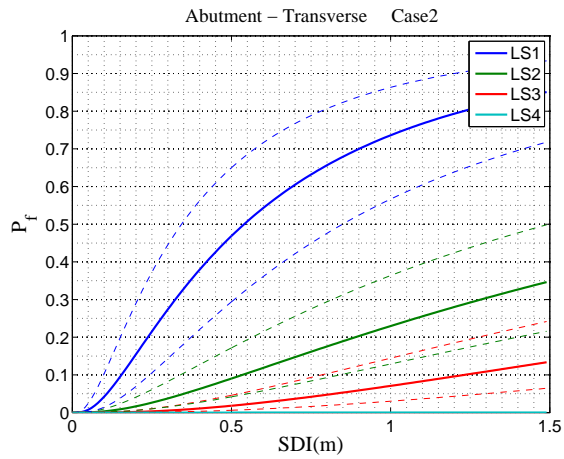
**APPENDIX E: EPISTEMIC UNCERTAINTY BOUNDS OF FRAGILITY
FOR MSSS CONCRETE GIRDER BRIDGE**



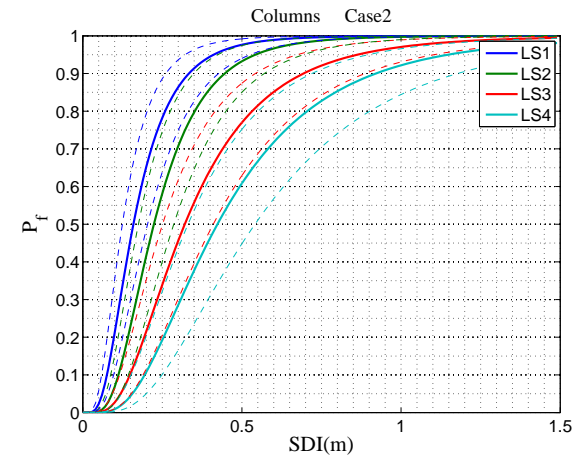
(a) Abutment in longitudinal active direction



(b) Abutment in longitudinal passive direction

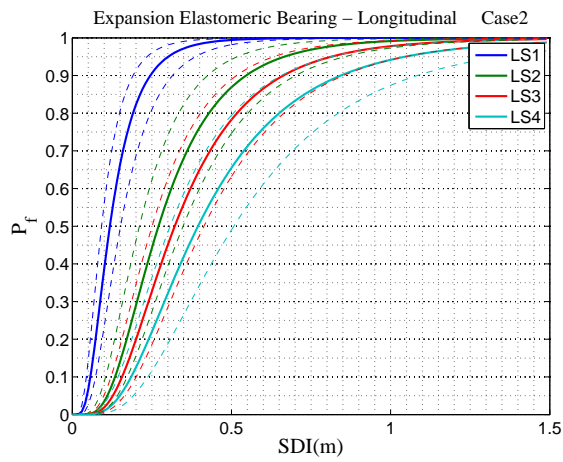


(c) Abutment in transverse direction

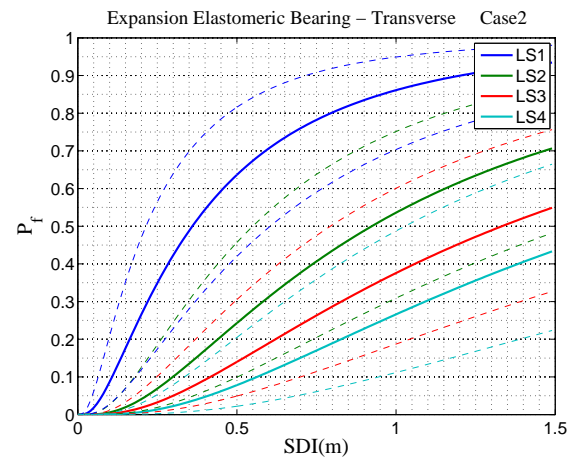


(d) Columns

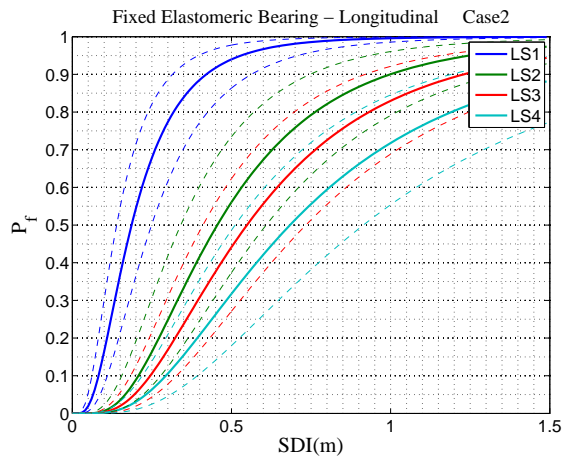
Figure E.1: Captured epistemic uncertainty in the fragility analysis for case 2



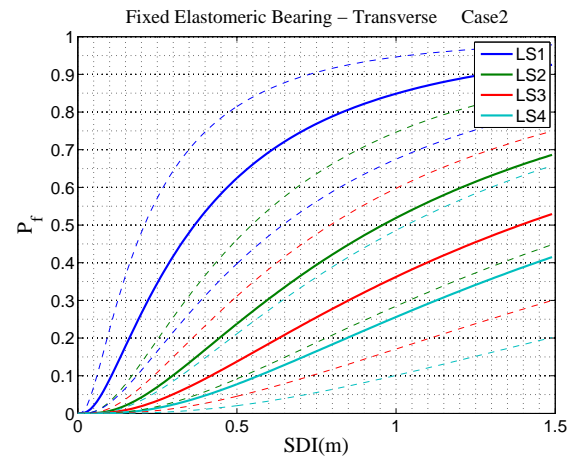
(a) Expansion elastomeric bearing in longitudinal direction



(b) Expansion elastomeric bearing in transverse direction

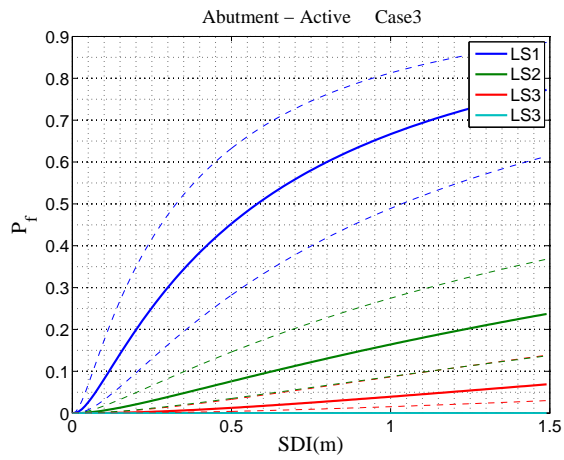


(c) Fixed elastomeric bearing in longitudinal direction

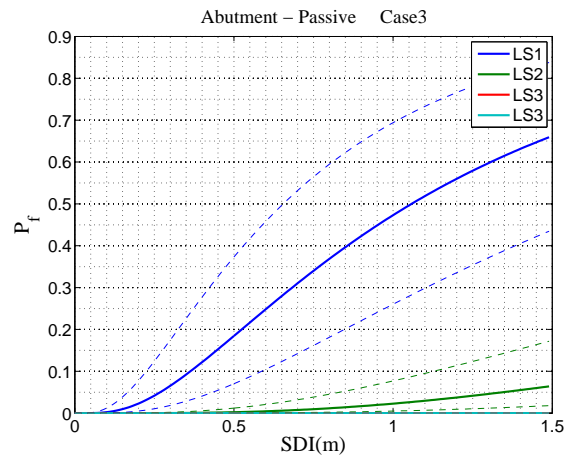


(d) Fixed elastomeric bearing in transverse direction

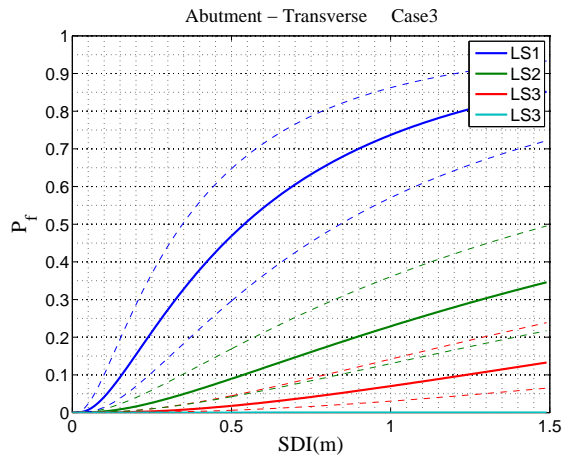
Figure E.2: Captured epistemic uncertainty in the fragility analysis for case 2



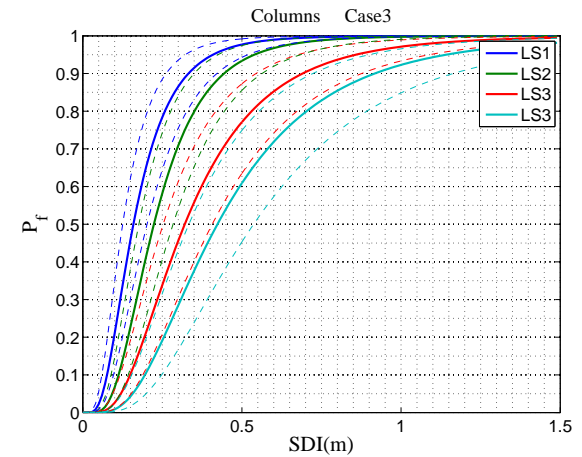
(a) Abutment in longitudinal active direction



(b) Abutment in longitudinal passive direction

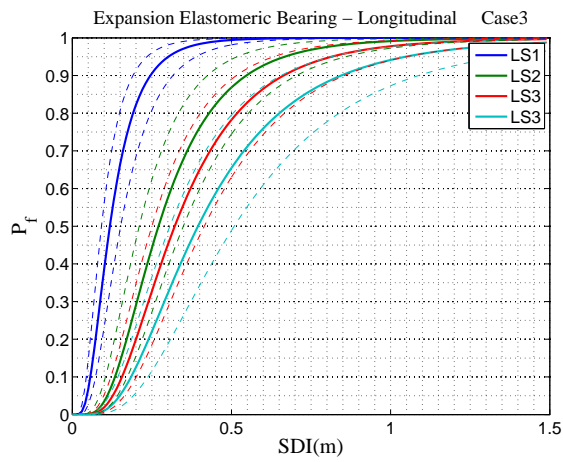


(c) Abutment in transverse direction

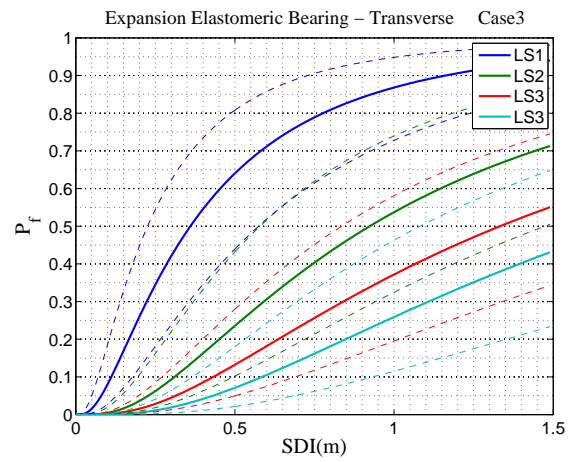


(d) Columns

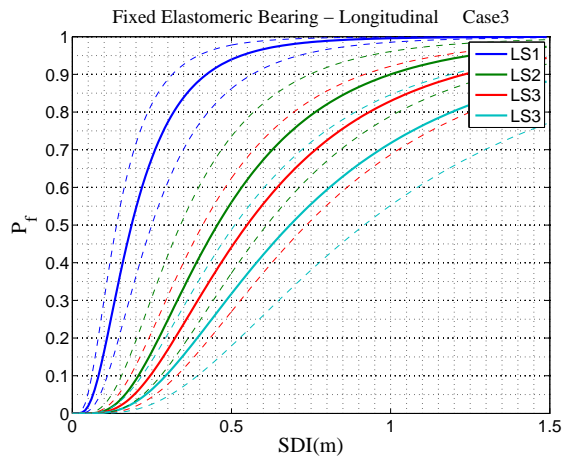
Figure E.3: Captured epistemic uncertainty in the fragility analysis for case 3



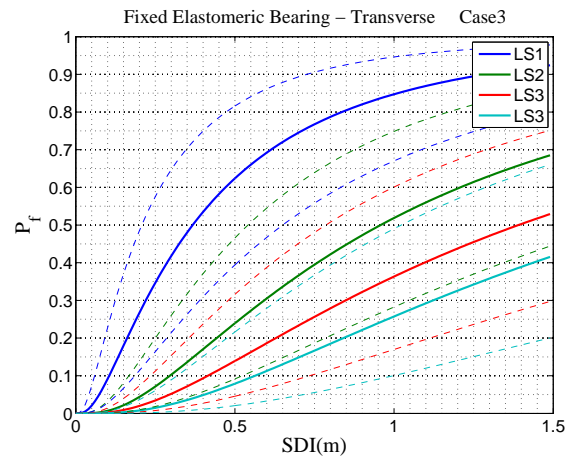
(a) Expansion elastomeric bearing in longitudinal direction



(b) Expansion elastomeric bearing in transverse direction



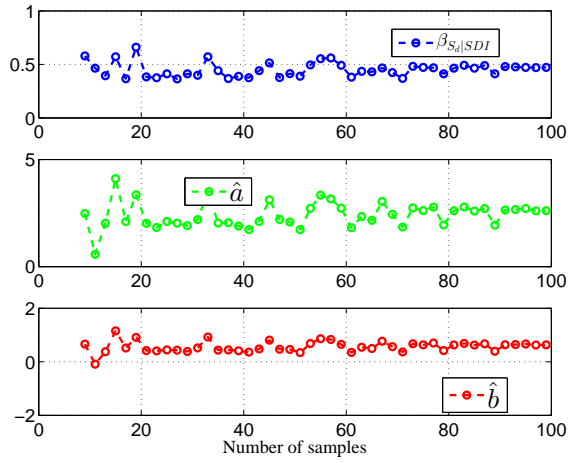
(c) Fixed elastomeric bearing in longitudinal direction



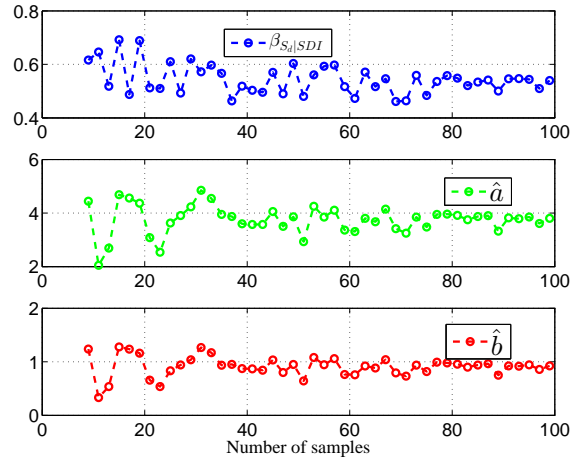
(d) Fixed elastomeric bearing in transverse direction

Figure E.4: Captured epistemic uncertainty in the fragility analysis for case 3

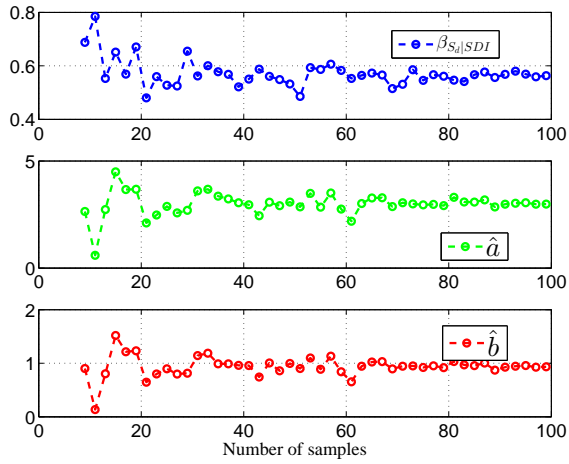
**APPENDIX F: MEASUREMENT OF STATISTICAL SIGNIFICANTS OF
NUMBER OF SAMPLES FOR DEMAND MODEL PARAMETERS**



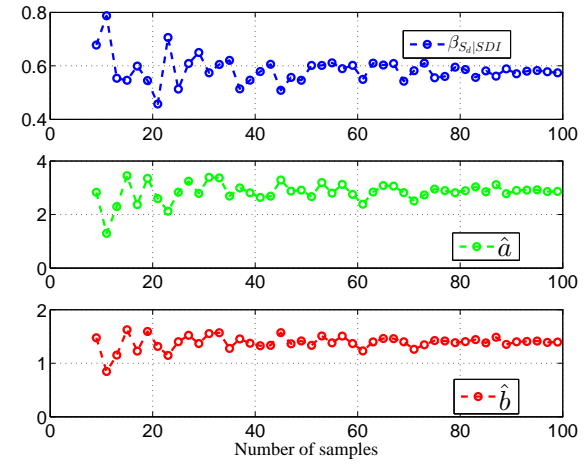
(a) Columns



(b) Fixed Elastomeric Bearing - Longitudinal

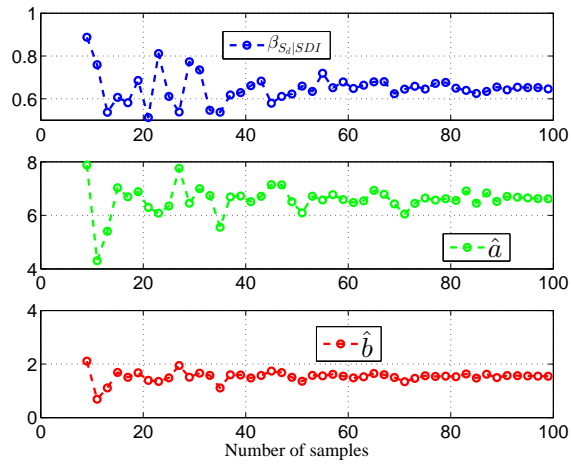


(c) Fixed Elastomeric Bearing - Transverse

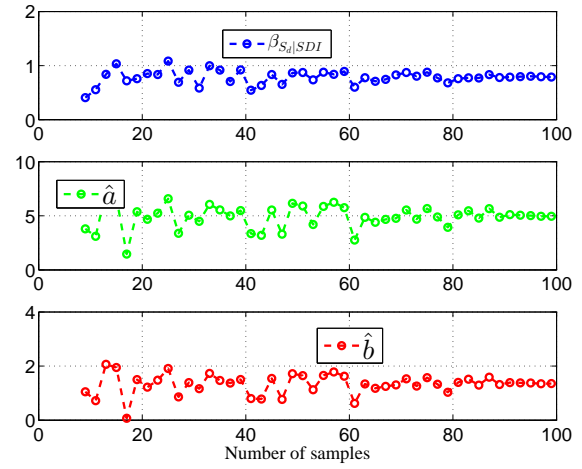


(d) Expansion Elastomeric Bearing - Longitudinal

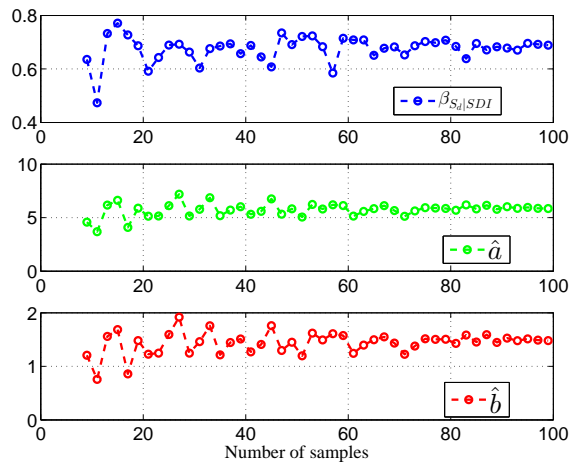
Figure F.1: Variation of the demand model parameters to the number of samples



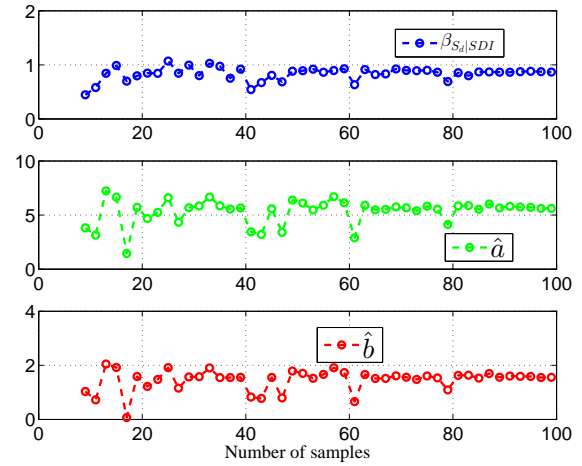
(a) Expansion Elastomeric Bearing - Transverse



(b) Abutment - Passive

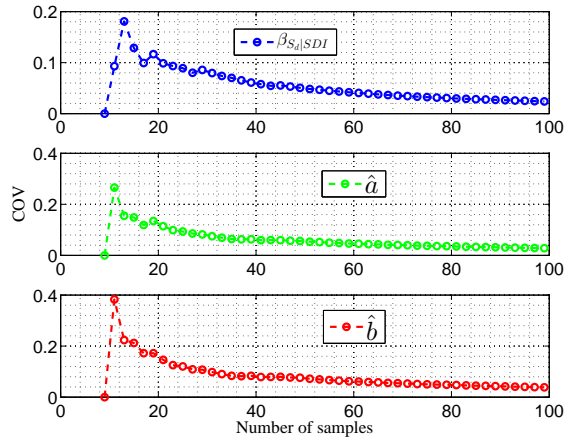


(c) Abutment - Active

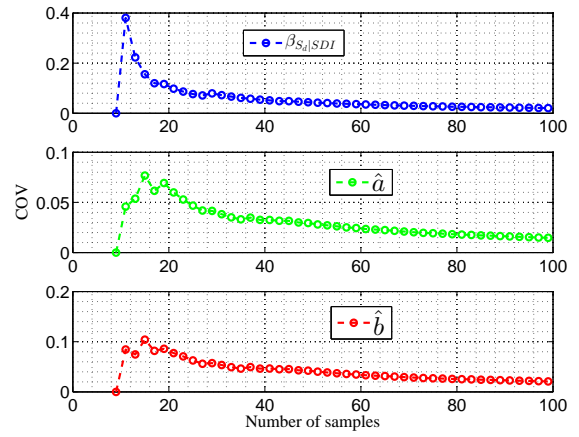


(d) Abutment - Transverse

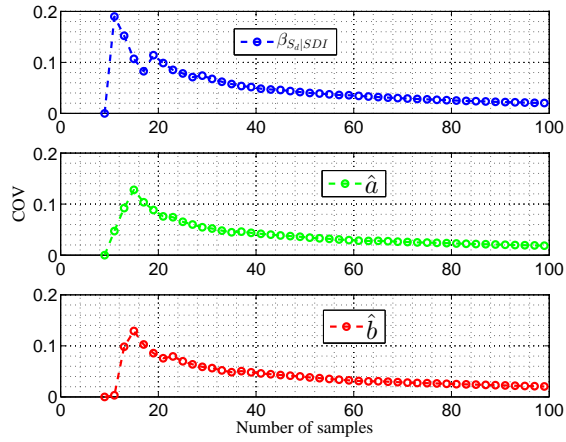
Figure F.2: Variation of the demand model parameters to the number of samples



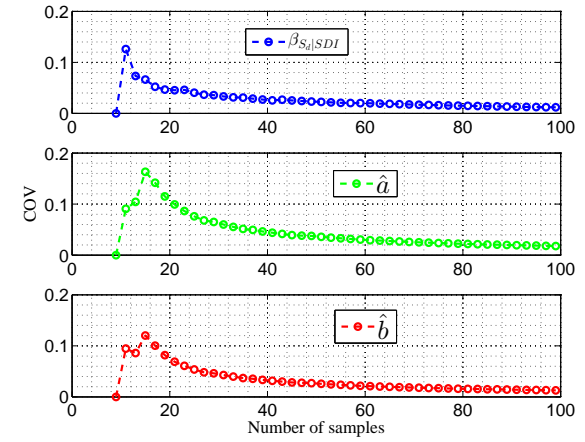
(a) Columns



(b) Fixed Elastomeric Bearing - Longitudinal

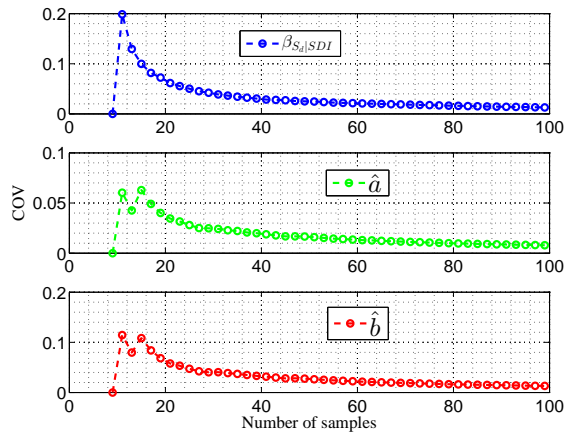


(c) Fixed Elastomeric Bearing - Transverse

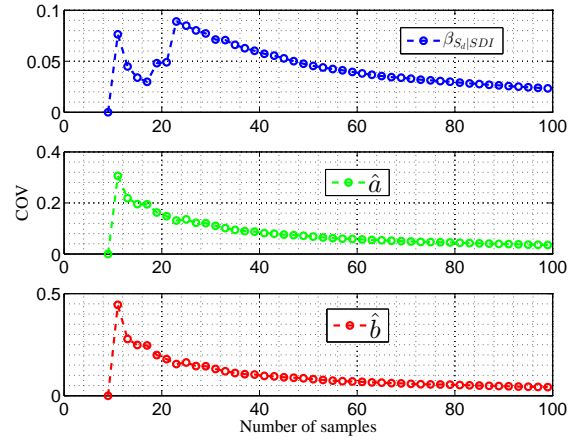


(d) Expansion Elastomeric Bearing - Longitudinal

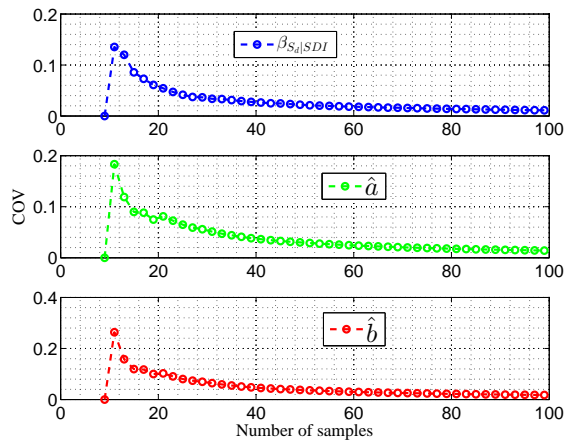
Figure F.3: Variation of the COV for the demand model parameters to the number of samples



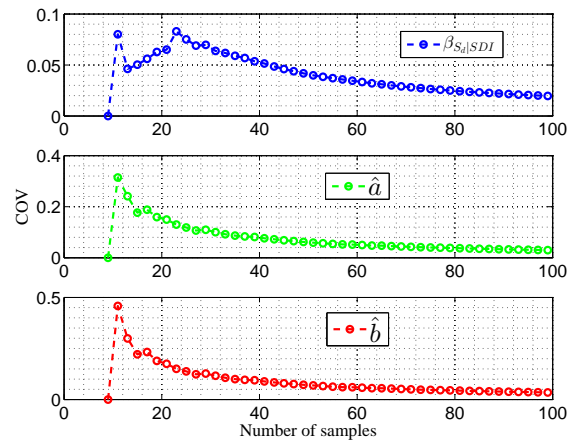
(a) Expansion Elastomeric Bearing - Transverse



(b) Abutment - Passive



(c) Abutment - Active



(d) Abutment - Transverse

Figure F.4: Variation of the COV for the demand model parameters to the number of samples

LIST OF REFERENCES

- [1] Song, J. and Ellingwood, B. R. (1999). *Seismic reliability of special moment steel frames with welded connections: II* Journal of Structural Engineering, 125(4), 372.
- [2] Federal Emergency Management Agency (FEMA) (1997) ,*NEHRP guidelines for the seismic rehabilitation of buildings. Report No. FEMA-273*, Federal Emergency Management Agency, Washington, DC.
- [3] Federal Emergency Management Agency (FEMA) (2000). *Pre-standard and commentary for the seismic rehabilitation of buildings. Report No. FEMA-356*, Federal Emergency Management Agency, Washington, DC.
- [4] Katsanos E, Sextos A, Manolis G. *Selection of earthquake ground motion records: A state-of-the-art review from a structural engineering perspective*. Soil Dynamics and Earthquake Engineering 2010; 30:157169.
- [5] Shome, N., Cornell, C. A., Bazzurro, P., and Carballo, J. E. (1998). *Earthquakes, records and nonlinear responses*. Earthquake Spectra 14:3, 469500.
- [6] Luco, N., and Bazzurro, P. (2007).*Does amplitude scaling of ground motion records result in biased nonlinear structural drift responses?* Earthquake Engineering and Structural Dynamics 36, 18131835
- [7] Grigoriu M. *To scale or not to scale seismic ground-acceleration records*. Journal of Engineering Mechanics 2011;137(4):284293.
- [8] Hancock, J., Bommer, J. J., Stafford, P. (2008). *Numbers of scaled and matched accelerograms required for inelastic dynamic analyses*. Earthquake Engineering and Structural Dynamics 37, 1585607.
- [9] Hancock, J., Watson-Lamprey, J., Abrahamson, N. A., Bommer, J. J., Markatis, A., McCoy, E., and Mendis, R. (2006). *An improved method of matching response spectra of recorded earthquake ground-motion using wavelets* , Journal of Earthquake Engineering 10(special issue 1), 6789.

- [10] Watson-Lamprey J, Abrahamson NA. *Selection of ground motion time series and limits on scaling* . Soil Dynamics and Earthquake Engineering 2006; 26:477482.
- [11] Sewell RT. (1989). *Damage effectiveness of earthquake ground motion: characterization based on the performance of structures and equipment* . Ph.D. Dissertation, Department of Civil Engineering, Stanford University, Stanford, CA.
- [12] Iervolino I, Cornell CA.(2005). *Record selection for nonlinear seismic analysis of structures*. Earthquake Spectra 21:3, 685713.
- [13] Baker JW. (2005). *Vector-valued ground motion intensity measures for probabilistic seismic demand analysis* . Ph.D.Dissertation, Department of Civil and Environmental Engineering, Stanford University, Stanford, CA.
- [14] Luco N, Bazzurro P. (2004). *Effects of earthquake record scaling on nonlinear structural response*. Report on PEER-LL Program Task 1G00 Addendum (Sub-Task 1 of 3), Richmond, CA, 2004.
- [15] Huang Y. N., Whittaker A. S., Luco N., and Hamburger R. O. (2011). *Scaling Earthquake Ground Motions for Performance-Based Assessment of Buildings* . Journal of Structural Engineering 137: 3, 11.
- [16] Zhang J, Huo Y, Brandenberg S, Kashigandi P. *Effects of structural characterizations on fragility functions of bridges subject to seismic shaking and lateral spreading*. Earthquake Engineering and Engineering Vibration 2008; 7.4(1):369382.
- [17] Baker J.W. and Cornell C.A., (2005). *A Vector-Valued Ground Motion Intensity Measure Consisting of Spectral Acceleration and Epsilon* . Earthquake Engineering & Structural Dynamics, 34 :10, 1193-1217.
- [18] Douglas J, Aochi H. (2008). *A survey of techniques for predicting earthquake ground motions for engineering purposes* . Surveys in Geophysics; 29,187220.
- [19] Shantz T. *Selection and scaling of earthquake records for nonlinear dynamic analysis of first model dominated bridge structures*. Proceedings of the 8th U.S. National Conference on Earthquake Engineering, San Francisco CA., 2006.

- [20] Rezaeian, S. & Der Kiureghian, A. (2010). *Simulation of synthetic ground motions for specified earthquake and site characteristics*, Earthquake Eng. Struct. Dyn. 39, 1155-1180.
- [21] Rezaeian, S. & Der Kiureghian, A. (2012). *Simulation of orthogonal horizontal ground motion components for specified earthquake and site characteristics*, Earthquake Eng. Struct. Dyn. 41, 3353-3353
- [22] PEER Ground Motion Database (2011). Pacific Earthquake Engineering Research Center (PEER). from: http://peer.berkeley.edu/peer_ground_motion_database/
- [23] PEER Ground Motion Selection and Modification Working Group. *Evaluation of ground motion selection and modification methods: Predicting median interstory drift response of buildings*. Technical Report PEER 2009/01, Pacific Earthquake Engineering Research Center, Berkeley, CA 2009.
- [24] Baker JW. *Conditional mean spectrum: Tool for ground-motion selection*. Journal of Structural Engineering 2011; 137(3):322-331
- [25] Miranda E. and Bertero V. V. (1994). *Evaluation of strength reduction factors for earthquake resistant design*. Earthquake Spectra 10, 357-379
- [26] Bradley B. *A ground motion selection algorithm based on the generalized conditional intensity measure approach*. Soil Dynamics and Earthquake Engineering 2012; 40:486-491.
- [27] Iervolino I, Galasso C, Cosenza E. *Rexel: computer aided record selection for code-based seismic structural analysis*. Bulletin of Earthquake Engineering 2010; 8:339-362.
- [28] Porter, K., Kennedy, R., and Bachman, R. (2007). *Creating Fragility Functions for Performance-Based Earthquake Engineering*. Earthquake Spectra, 23(2), 471-489.
- [29] Database PGM. *Pacific earthquake engineering research center (peer) 2011*. URL [http://peer.berkeley.edu/peer_ground_motion_database/..](http://peer.berkeley.edu/peer_ground_motion_database/)
- [30] Nielson, Bryant G., *Analytical Fragility Curves for Highway Bridges in Moderate Seismic Zones*, 2005-11-23, Dissertation, Georgia Institute of Technology.

- [31] Ketchum, M., Chang, V., and Shantz, T. (2004). *Influence of Design Ground Motion Level on Highway Bridge Costs*. Report No. Lifelines 6D01, University of California, Pacific Earthquake Engineering Research Center, Berkeley CA.
- [32] Cornell, C. Allin, and Helmut Krawinkler. "Progress and challenges in seismic performance assessment." PEER Center News 3.2 (2000): 1-3.
- [33] Housner G. *Spectrum intensity of strong-motion earthquakes*. Proceedings of the Symposium on Earthquake and Blast Effects on Structures, University of California Los Angeles, 1952; 2036.
- [34] Shome, N. and Cornell, C. A. (1999). *Probabilistic seismic demand analysis of nonlinear structures*. Report No. RMS 35, Stanford University, Department of Civil and Environmental Engineering, Stanford, CA.
- [35] Kadas K, Yakut A, Kazaz I. *Spectral ground motion intensity based on capacity and period elongation*. Journal of Structural Engineering 2011; 137(3):401409.
- [36] Vamvatsikos, D. and Cornell, C. A. (2002). *Incremental dynamic analysis*. Earthquake Engineering and Structural Dynamics 31(3): 491512.
- [37] Jalayer, F. (2003). Direct probabilistic seismic analysis: *Implementing nonlinear dynamic assessments*. Ph.D. thesis, Stanford University.
- [38] Koliopoulos PK, Margaris BN, Klimis NS. *Duration and energy characteristics of greek strong motion records*. Journal of Earthquake Engineering 1998; 2(1):390417.
- [39] Krawinkler, H. and Ibarra, L. (2003). *Collapse probability of frame structures with deteriorating properties*. In *Performance-based engineering for earthquake resistant reinforced concrete structures* : A volume honoring Shunsuke Otani, Eds. T.Kabeyasawa and Shiohara, H., pp. 325 338.
- [40] Newmark N, Hall W. *Earthquake spectra and design*. Earthquake Engineering Research Institute, 1982.

- [41] Mackie, K. and Stojadinovic, B. (2003). *Seismic demands for performance-based design of bridges*. Report No. 2003/16, University of California, Pacific Earthquake Engineering Research Center, Berkeley CA.
- [42] Mackie, Kevin, and Bozidar Stojadinovic. "Fragility curves for reinforced concrete highway overpass bridges." 13th World Conference on Earthquake Engineering. 2004.
- [43] USGS (2004). Earthquake Hazards Program Website. <http://earthquake.usgs.gov/>, Date Accessed: August 15, 2005.
- [44] USGS (2012). Earthquake Hazards Program Website. <http://earthquake.usgs.gov/>.
- [45] California Geological Survey. Regional Geologic Mapping Program <http://www.conservation.ca.gov/cgs/rghm/psha/ofr9608/Pages/Index.aspx/>.
- [46] USGS (2002). Earthquake Hazard in the Heart of the Homeland. Fact Sheet FS-131-02, U.S. Geological Survey.
- [47] Basoz, N., and A. S. Kiremidjian. *Risk assessment of bridges and highway systems from the Northridge earthquake*. Second National Seismic Conference on Bridges and Highways. 1997.
- [48] Shinozuka, Masanobu, et al. *Nonlinear static procedure for fragility curve development*. Journal of Engineering Mechanics 126.12 (2000): 1287-1295.
- [49] Gardoni, Paolo, Armen Der Kiureghian, and Khalid M. Mosalam. *Probabilistic capacity models and fragility estimates for reinforced concrete columns based on experimental observations*. Journal of Engineering Mechanics 128.10 (2002): 1024-1038.
- [50] Yu, O., Allen, D. L., and Drnevich, V. P. (1991). *Seismic Vulnerability Assessment of Bridges on Earthquake Priority Routes in Western Kentucky*. 3rd US Conference on Lifeline Earthquake Engineering, Los Angeles, CA, USA. ASCE.
- [51] Jernigan, J. B. and Hwang, H. (2002). *Development of Bridge Fragility Curves*. 7th US National Conference on Earthquake Engineering, Boston, Mass. EERI.

- [52] FEMA (2003). *HAZUS-MH MRI: Technical Manual*, Vol. Earthquake Model. Federal Emergency Management Agency, Washington DC
- [53] FEMA 445 [2006]. *Next-generation performance-based seismic design guidelines* Federal Emergency Management Agency (FEMA).
- [54] Mander, J. B. and Basoz, N. (1999). *Seismic Fragility Curve Theory for Highway Bridges*. 5th US Conference on Lifeline Earthquake Engineering, Seattle, WA, USA. ASCE.
- [55] Fajfar, Peter, Toma Vidic, and Matej Fischinger. *Seismic demand in medium and long period structures*. Earthquake Engineering & Structural Dynamics 18.8 (1989): 1133-1144.
- [56] Fajfar, Peter. *A nonlinear analysis method for performance-based seismic design*. Earthquake spectra 16.3 (2000): 573-592.
- [57] Cornell, A. C., Jalayer, F., and Hamburger, R. O. (2002). *Probabilistic Basis for 2000 SAC Federal Emergency Management Agency Steel Moment Frame Guidelines*. Journal of Structural Engineering, 128(4), 526532.
- [58] Mackie, K. and Stojadinovic, B. (2001). *Probabilistic Seismic Demand Model for California Bridges*. Journal of Bridge Engineering, 6(6), 468480.
- [59] Shinozuka, M., Feng, M. Q., Kim, H., Uzawa, T., and Ueda, T. (2003). *Statistical Analysis of Fragility Curves*. Technical Report MCEER-03-0002, MCEER 2003.
- [60] Mackie, Kevin R., Kyle J. Cronin, and Bryant G. Nielson. *Response sensitivity of highway bridges to randomly oriented multi-component earthquake excitation*. Journal of Earthquake Engineering 15.6 (2011): 850-876.
- [61] Mackie KR, Stojadinovic B. *R-Factor parameterized bridge damage fragility curves*. Journal of Bridge Engineering 2007, in press.
- [62] Mackie, K. R., and B. Stojadinovi. *Performancebased seismic bridge design for damage and loss limit states*. Earthquake Engineering & Structural Dynamics 36.13 (2007): 1953-1971.

- [63] Wu, C.-F. J. and Hamada, M. (2000). *Experiments: Planning, Analysis, and Parameter Design Optimization*. John Wiley & Sons, Inc., New York.
- [64] Bignell, John L., et al. *Seismic Evaluation of Vulnerable Highway Bridges with Wall Piers on Emergency Routes in Southern Illinois* 13th World Conference on Earthquake Engineering. 2004.
- [65] Choi, E., DesRoches, R., and Nielson, B. (2004). *Seismic Fragility of Typical Bridges in Moderate Seismic Zones* Engineering Structures, 26(2), 187-199.
- [66] Hwang, H. and Huo, J. R. (1998). *Probabilistic Seismic Damage Assessment of Highway Bridges* 6th US National Conference on Earthquake Engineering, Seattle, WA. EERI.
- [67] Naeim, Farzad, and Marshall Lew. *On the use of design spectrum compatible time histories*. Earthquake Spectra 11.1 (1995): 111-127.
2nd ed. John Wiley & Sons; 1999.
- [68] Nielson, Bryant G., and Reginald DesRoches. *Analytical seismic fragility curves for typical bridges in the central and southeastern United States*, Earthquake Spectra 23.3 (2007): 615-633.
- [69] Choi E. *Seismic analysis and retrofit of mid-America bridges* Ph.D. Thesis, Georgia Institute of Technology, 2002.
- [70] Hwang H, Liu JB, Chiu Y-H. *Seismic fragility analysis of highway bridges* MAEC RR-4, Center for Earthquake Research Information, 2000.
- [71] Ellingwood B, Hwang H. *Probabilistic descriptions of resistance of safety-related structures in nuclear plants* Nuclear Engineering and Design 1985; 88:169-178.
- [72] Hwang H, Jaw JW. *Probabilistic damage analysis of structures* Journal of Structural Engineering 1990; 116: 1992-2007.
- [73] Dutta A. *On energy based seismic analysis and design of highway bridges*. Ph.D. Thesis, State University of New York at Buffalo, 1999.

- [74] Fang JQ, Li QS, Jeary AP, Liu DK. *Damping of tall buildings: its evaluation and probabilistic characteristics*. Structural Design of Tall Buildings 1999; 8:145-153.
- [75] Bavisetty R, Vinayagamoorthy M, Duan L. *Dynamic analysis*. In *Bridge Engineering Handbook*, Chen W-F, Duan L (eds). CRC Press: Boca Raton, FL, 2000.
- [76] Ma, Y., and N. Deng. "Deep foundations." *Bridge Engineering Handbook* (2000).
- [77] Hwang, Howard, John B. Jernigan, and Yang-Wei Lin. "Evaluation of seismic damage to Memphis bridges and highway systems". *Journal of Bridge Engineering* 5.4 (2000): 322-330.
- [78] California Dept. of Transportation(CALTRANS). "Seismic design criteria, ver. 1.4. CALTRANS Division of Engineering Services, Office of structure Design, Sacramento , Calif.
- [79] Muthukumar, Susendar. "A contact element approach with hysteresis damping for the analysis and design of pounding in bridges." (2003).
- [80] Montgomery, Douglas C. *Design and analysis of experiments*. John Wiley & Sons, 2008.
- [81] Ayyub BM, Lai K-L. *Structural reliability assessment using latin hypercube sampling*. Proceedings of ICOSSAR89, the 5th International Conference on Structural Safety and Reliability, Part II. ASCE: San Francisco, CA, U.S.A., 1989.
- [82] Berry, Michael P., and Marc O. Eberhard. *Practical performance model for bar buckling*. *Journal of Structural Engineering* 131.7 (2005): 1060-1070.
- [83] Baker, Jack W., and C. Allin Cornell. *Uncertainty propagation in probabilistic seismic loss estimation*. *Structural Safety* 30.3 (2008): 236-252.
- [84] Padgett, Jamie E., and Reginald DesRoches. *Methodology for the development of analytical fragility curves for retrofitted bridges*. *Earthquake Engineering & Structural Dynamics* 37.8 (2008): 1157-1174.
- [85] Gardoni, Paolo, Armen Der Kiureghian, and Khalid M. Mosalam. *Probabilistic capacity models and fragility estimates for reinforced concrete columns based on experimental observations*. *Journal of Engineering Mechanics* 128.10 (2002): 1024-1038.

- [86] Gardoni, Paolo, Khalid M. Mosalam, and ARMEN DER KIUREGHIAN. *Probabilistic seismic demand models and fragility estimates for RC bridges*. Journal of Earthquake Engineering 7.S1 (2003): 79-106.
- [87] Nielson, Bryant G., and Reginald DesRoches. *Influence of modeling assumptions on the seismic response of multi-span simply supported steel girder bridges in moderate seismic zones*. Engineering structures 28.8 (2006): 1083-1092.
- [88] Choe, Do-Eun, et al. *Probabilistic capacity models and seismic fragility estimates for RC columns subject to corrosion*. Reliability Engineering & System Safety 93.3 (2008): 383-393.
- [89] Der Kiureghian, A., and J. B. Ke. *Finite-element based reliability analysis of frame structures*. Proc., 4th Int. Conf. on Structural Safety and Reliability. Vol. 1. New York: International Association for Structural Safety and Reliability, 1985.
- [90] Pan, Y., Anil K. Agrawal, and M. Ghosn. *Seismic fragility of continuous steel highway bridges in New York State*. Journal of Bridge Engineering 12.6 (2007): 689-699.
- [91] Pan, Y., et al. *Seismic fragility of multispan simply supported steel highway bridges in New York State. I: Bridge modeling, parametric analysis, and retrofit design*. Journal of Bridge Engineering 15.5 (2009): 448-461.
- [92] Pan, Y., et al. *Seismic fragility of multispan simply supported steel highway bridges in New York State. II: Fragility analysis, fragility curves, and fragility surfaces*. Journal of Bridge Engineering 15.5 (2010): 462-472.
- [93] Padgett, Jamie Ellen, and Reginald DesRoches. *Sensitivity of seismic response and fragility to parameter uncertainty*. Journal of Structural Engineering 133.12 (2007): 1710-1718.